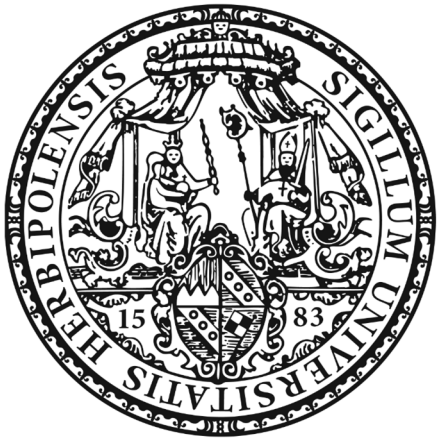

Stem Cell-based Adipose Tissue Engineering

Engineering of Prevascularized Adipose Tissue Constructs *In Vitro* & Investigation on Gap Junctional Intercellular Communication in Adipose-derived Stem Cells

Stammzellbasiertes Tissue Engineering von Fettgewebe

Entwicklung eines prävaskularisierten Fettgewebekonstrukts *in vitro* & Untersuchung der interzellulären Kommunikation über Gap Junctions in Stammzellen aus dem Fettgewebe

DOCTORAL THESIS FOR A DOCTORAL DEGREE

AT THE GRADUATE SCHOOL OF LIFE SCIENCES,

JULIUS-MAXIMILIANS-UNIVERSITÄT WÜRZBURG,

SUBMITTED BY

MIRIAM WIESNER

FROM

WÜRZBURG, GERMANY

WÜRZBURG, 2019

Submitted on: ……

Office stamp

Members of the Promotionskomitee:

Chairperson: Prof. Dr. Thomas Dandekar

Primary Supervisor: Prof. Dr. Torsten Blunk

Supervisor (Second): Prof. Dr. Franz Jakob

Supervisor (Third): Prof. Dr. Heike Walles

Date of Public Defence: ……

Date of Receipt of Certificates: ……

In Liebe und Dankbarkeit für meine Eltern

Table of Contents

Summary **11**

Zusammenfassung **13**

1 Introduction **17**

1.1 Adipose tissue 17

1.1.1 Adipose tissue structure 18

1.1.2 Adipose tissue function 19

1.1.3 Adipogenic differentiation 20

1.1.4 Cell-cell communication in adipose tissue 24

1.1.5 Adipose tissue vascularization 26

1.1.6 Adipose tissue extracellular matrix (ECM) 28

1.2 Adipose tissue engineering 31

1.2.1 Background – clinical need for adipose tissue augmentation 31

1.2.2 The principle of adipose tissue engineering 32

1.2.3 Components and strategies for adipose tissue engineering 33

1.2.3.1 Cell sources for tissue engineering applications 33

1.2.3.2 Three-dimensional scaffolds for tissue engineering applications 35

1.2.3.3 Vascularization strategies for adipose tissue engineering 39

1.2.3.4 Extracellular matrix scaffolds to foster vascularization for adipose tissue engineering 41

1.3 Goals of the thesis 44

1.3.1 *In vitro* development of a prevascularized adipose tissue construct using a decellularized porcine jejunal segment 45

1.3.2 Evaluation of the effect of basic fibroblast growth factor (bFGF) on ASC proliferation and differentiation capacity 45

1.3.3 Investigation on gap junctional intercellular communication in ASCs with regard to its impact on adipogenic differentiation 46

2 Materials **47**

2.1 Instruments 47

2.2 Consumables 48

2.3 Chemicals 49

2.4 Antibodies 51

2.5 Primers 52

2.6 Cells 52

2.7 Cell culture media 53

2.8 Buffers and solutions 54

2.9 Software 55

3 Methods 57
3.1 Isolation of adipose-derived stem cells 57
3.2 Cell culture of ASCs and MVECs 57
3.2.1 Expansion culture 57
3.2.2 Investigation of gap junctional intracellular communication (GJIC) 58
3.3 Adipogenic induction of ASCs in 2D 58
3.4 Isolation and decellularization of a porcine jejunal segment 59
3.5 Custom-made bioreactor system for dynamic culture 59
3.6 Seeding of decellularized jejunal segments with MVECs & ASCs, and co-culture in the bioreactor system 61
3.7 Preparation of hydrogels and 3D culture 61
3.7.1 Preparation of fibrin hydrogels 61
3.7.2 3D cell culture 62
3.8 Biochemical assays 62
3.8.1 Quantitative analysis of DNA content 62
3.8.2 Quantitative analysis of triglyceride content 62
3.9 RNA isolation and real time qRT-PCR analysis 63
3.10 Investigation on cell viability 63
3.10.1 Live/dead staining 63
3.10.2 MTT staining 64
3.11 Histology and immunohistochemistry 64
3.11.1 Histological investigation of adipogenesis in 2D & 3D 64
3.11.2 Immunohistochemical staining 65
3.11.2.1 Laminin, collagen type IV, and CD31 staining on jejunal construct sections 65
3.11.2.2 Cx43 staining in 2D culture 65
3.11.2.3 Ki-67 on 3D samples 66
3.12 Whole mount staining 66
3.13 Quantification of protein content 67
3.13.1 Sodium dodecyl sulfate polyacrylamid gel electrophoresis 67
3.14 Western blot analysis 68
3.15 Flow cytometry 69
3.15.1 Nile red 69
3.15.2 Dye transfer 69
3.16 Statistical analysis 70

4 Results and Discussion 71
4.1 Engineering of prevascularized adipose tissue *in vitro* using decellularized porcine jejunal segments 71
4.1.1 Engineered prevascularized adipose tissue *in vitro* - Experimental design 73

4.1.2 Cell viability ... 73
4.1.3 Adipogenesis in engineered jejunal matrix constructs ... 74
4.1.4 Extracellular matrix development in engineered jejunal matrix constructs ... 76
4.1.5 Visualization of tissue architecture of engineered adipose tissue ... 78
4.1.6 Discussion ... 79
4.2 Investigations on the effects of bFGF on ASC proliferation and differentiation capacity ... 84
4.2.1 Influence of bFGF on ASC cell growth and morphology ... 85
4.2.2 Effect of bFGF preculture vs. continuous application on adipogenic differentiation capacity of ASCs ... 86
4.2.3 Impact of bFGF preculture in conjunction with a 2-day proliferation phase ... 91
4.2.4 Investigation of bFGF preculture in a 3D hydrogel system ... 94
4.2.5 bFGF preculture, cell density, and adipogenesis ... 97
4.2.6 Discussion ... 99
4.3 Establishment of analytical tools for investigations on gap junctional intercellular communication (GJIC) ... 103
4.3.1 Effect of different AGA concentrations on the proliferation of ASCs ... 104
4.3.2 Effect of different AGA concentrations on the adipogenic differentiation ... 105
4.3.3 Establishment of the Cx43 immunohistochemical staining on ASCs ... 109
4.3.4 Discussion ... 113
4.4 Gap junctional intercellular communication in adipose-derived stromal/stem cells is cell density-dependent and positively impacts adipogenic differentiation ... 116
4.4.1 Expression and functionality of gap junctions in ASCs ... 118
4.4.2 Cell density and adipogenesis ... 122
4.4.3 Influence of GJIC inhibition on adipogenesis ... 125
4.4.4 Cx43 expression during adipogenic differentiation ... 128
4.4.5 Discussion ... 130
5 Conclusion and Outlook ... 135
References ... 139
List of Figures ... 160
List of Tables ... 162
List of Abbreviations ... 163
Affidavit ... 167
Statement on Copyright and Self-plagiarism ... 168
Acknowledgement ... 169
Curriculum Vitae ... 170

Summary

In reconstructive and plastic surgery, there exists a growing demand of adequate tissue implants, since currently available strategies for autologous transplantation are limited by complications including transplant failure and donor site morbidity. By developing *in vitro* and *in vivo* autologous substitutes for defective tissue sites, adipose tissue engineering can address these challenges, although there are several obstacles to overcome. One of the major limitations is the sufficient vascularization of *in vitro* engineered large constructs that remains crucial and demanding for functional tissues. Decellularized jejunal segments may represent a suitable scaffolding system with preexisting capillary structures that can be repopulated with human microvascular endothelial cells (hMVECs), and a luminal matrix applicable for the adipogenic differentiation of human adipose-derived stem cells (hASCs). Hence, co-culture of these cells in jejunal segments, utilizing a custom-made bioreactor system, was characterized in terms of vascularization and adipose tissue development. Substantial adipogenesis of hASCs was demonstrated within the jejunal lumen in contrast to non-induced controls, and the increase of key adipogenic markers was verified over time upon induction. The development of major extracellular matrix components of mature adipose tissue, such as laminin and collagen IV, was shown within the scaffold in induced samples. Successful reseeding of the vascular network with hMVECs was demonstrated in long-term culture and co-localization of vascular structures and adipogenically differentiated hASCs was observed. Therefore, these results represent a novel approach for *in vitro* engineering of vascularized adipose tissue constructs that warrants further investigations in preclinical studies.

Another still existing obstacle in adipose tissue engineering is the insufficient knowledge about the applied cells, for instance the understanding of how cells can be optimally expanded and differentiated for successful engineering of tissue transplants. Even though hASCs can be easily isolated from liposuction of abdominal fat depots, yielding low donor site morbidity, huge numbers of cells are required to entirely seed complex and large 3D matrices or scaffolds. Thus, cells need to be large-scale expanded *in vitro* on the premise of not losing their differentiation capacity caused by replicative aging. Accordingly, an improved differentiation of hASCs in adipose tissue engineering approaches remains still desirable since most engineered constructs exhibit an inhomogeneous differentiation pattern. For mesenchymal stem cells (MSCs), it has been shown that growth factor application can lead to a significant improvement of both proliferation and differentiation capacity. Especially basic fibroblast growth factor (bFGF) represents a potent mitogen for MSCs, while maintaining or even promoting their osteogenic, chondrogenic and adipogenic differentiation potential. As there are currently different contradictory information present in literature about the applied bFGF concentration and the explicit effect of bFGF on ASC differentiation,

here, the effect of bFGF on hASC proliferation and differentiation capacity was investigated at different concentrations and time points in 2D culture. Preculture of hASCs with bFGF prior to adipogenic induction showed a remarkable effect, whereas administration of bFGF during culture did not improve adipogenic differentiation capacity. Furthermore, the observations indicated as mode of action an impact of this preculture on cell proliferation capacity, resulting in increased cellular density at the time of adipogenic induction. The difference in cell density at this time point appeared to be pivotal for increased adipogenic capacity of the cells, which was confirmed in a further experiment employing different seeding densities. Interestingly, furthermore, the obtained results suggested a cell-cell contact-mediated mechanism positively influencing adipogenic differentiation. As a consequence, subsequently, studies were conducted focusing on intercellular communication of these cells, which has hardly been investigated to date.

Despite the multitude of literature on the differentiation capacity of ASCs, little is reported about the physiological properties contributing to and controlling the process of lineage differentiation. Direct intercellular communication between adjacent cells via gap junctions has been shown to modulate differentiation processes in other cell types, with connexin 43 (Cx43) being the most abundant isoform of the gap junction-forming connexins. Thus, in the present study we focused on the expression of Cx43 and gap junctional intercellular communication (GJIC) in hASCs, and its significance for adipogenic differentiation of these cells. Cx43 expression in hASCs was demonstrated histologically and on the gene and protein expression level and was shown to be greatly positively influenced by cell seeding density. Functionality of gap junctions was proven by dye transfer analysis in growth medium. Adipogenic differentiation of hASCs was shown to be also distinctly elevated at higher cell seeding densities. Inhibition of GJIC by 18α-glycyrrhetinic acid significantly compromised adipogenic differentiation, as demonstrated by histology, triglyceride quantification, and adipogenic marker gene expression. Flow cytometry analysis showed a lower proportion of cells undergoing adipogenesis when GJIC was inhibited, further indicating the importance of GJIC in the differentiation process. Altogether, these results demonstrate the impact of direct cell-cell communication via gap junctions on the adipogenic differentiation process of hASCs and may contribute to further integrate direct intercellular crosstalk in rationales for tissue engineering approaches.

Zusammenfassung

In der rekonstruktiven und plastischen Chirurgie besteht ein wachsender Bedarf an adäquaten Gewebetransplantaten, da die derzeit verfügbaren Strategien für autologe Transplantationen von Geweben durch Komplikationen wie beispielsweise Transplantatversagen sowie Morbiditäten an der Entnahmestelle beeinträchtigt werden. Das Tissue Engineering kann dieser Problematik jedoch durch die Entwicklung von *in vitro* und *in vivo* gezüchtetem, autologen Gewebeersatz für defekte Gewebestellen begegnen, wobei es dabei noch mehrere Hindernisse zu überwinden gilt. Eine der größten Limitationen ist die ausreichende Vaskularisierung der *in vitro* hergestellten, großen Konstrukte, welche für die Funktion des Gewebes entscheidend ist. Hierfür können dezellularisierte, jejunale Segmente ein geeignetes Gerüstsystem darstellen, deren bereits vorhandene Kapillarstrukturen mit humanen, mikrovaskulären Endothelzellen (hMVECs) und deren luminale Matrix mit humanen Stammzellen aus dem Fettgewebe (hASCs), mit anschließender adipogen Differenzierung, besiedelt werden können. Im Rahmen der vorliegenden Arbeit wurden diese Konstrukte mit Hilfe eines maßgeschneiderten Bioreaktorsystems kultiviert und die Kokultur der Zellen in der jejunalen Matrix hinsichtlich der Fettgewebeentwicklung untersucht. Im Gegensatz zu nicht-induzierten Kontrollen wurde nach adipogener Induktion innerhalb des jejunalen Lumens eine substanzielle Fettgewebebildung der hASCs, sowie ein Anstieg wichtiger adipogener Marker im zeitlichen Verlauf nachgewiesen. Die Bildung wesentlicher extrazellulärer Matrixkomponenten des reifen Fettgewebes, wie beispielsweise Laminin und Kollagen IV, wurde innerhalb der Matrix bei induzierten Proben ebenso beobachtet. Die erfolgreiche Neubesiedlung des Gefäßnetzes mit hMVECs konnte in der Langzeitkultur gezeigt und eine Kolokalisation von Gefäßstrukturen und differenzierten hASCs beobachtet werden. Somit stellen diese Ergebnisse einen vielversprechenden, neuen Ansatz für die *in vitro* Entwicklung von vaskularisierten Fettgewebekonstrukten dar, welcher jedoch noch weitere Untersuchungen in präklinischen Studien erfordert.

Eine weitere Limitation in der Entwicklung von Fettgewebe ist das unzureichende Wissen über die verwendeten Zellen – so zum Beispiel wie Zellen optimal expandiert und differenziert werden können, um einen Gewebeersatz erfolgreich herzustellen. Auch wenn hASCs leicht aus abdominalen Liposuktionen, welche zu einer relativ geringen Morbidität an der Entnahmestelle führen, isoliert werden können, ist eine sehr große Anzahl an Zellen erforderlich, um komplexe und große 3D-Matrizes vollständig mit Zellen zu besiedeln. So müssen Zellen *in vitro* im großen Maßstab expandiert werden, wobei auf die Erhaltung ihrer Differenzierungskapazität und die Vermeidung des replikativen Alterns geachtet werden muss. Da viele der entwickelten Konstrukte des Weiteren ein inhomogenes Differenzierungsmuster aufweisen, ist eine Verbesserung der adipogenen Differenzierung von ASCs im Rahmen von Tissue Engineering Ansätzen wünschenswert. Für mesenchymale Stammzellen (MSCs)

wurde bereits gezeigt, dass die Anwendung von Wachstumsfaktoren zu einer deutlichen Verbesserung der Proliferations- und Differenzierungskapazität führen kann. Insbesondere der Wachstumsfaktor bFGF (basic fibroblast growth factor) stellt ein starkes Mitogen für MSCs dar, wobei er das osteogene, chondrogene und adipogene Differenzierungspotenzial der Zellen aufrechterhält und sogar fördert. Da es in der Literatur derzeit unterschiedliche und teilweise widersprüchliche Informationen über die verwendeten bFGF Konzentrationen und den expliziten Effekt von bFGF auf die Differenzierung von ASCs gibt, wurde der Effekt von bFGF auf die Proliferations- und Differenzierungsfähigkeit mit unterschiedlichen Konzentrationen und zu unterschiedlichen Zeitpunkten in der 2D Kultur untersucht. Die Vorkultur der hASCs mit bFGF vor der adipogenen Induktion hatte einen beachtlichen Effekt auf die Differenzierung, während die Verabreichung von bFGF während der Kultur, die adipogene Differenzierungsfähigkeit der Zellen nicht verbesserte. Darüber hinaus zeigten die Ergebnisse einen Einfluss der Vorkultur auf die Zellproliferation, was zu einer erhöhten Zelldichte zum Zeitpunkt der adipogenen Induktion führte. Der Unterschied in der Zelldichte zu diesem Zeitpunkt schien entscheidend für die gesteigerte Differenzierungskapazität der Zellen zu sein, was sich in einem weiteren Experiment mit unterschiedlichen Aussaatdichten bestätigte. Interessanterweise deuteten die Ergebnisse außerdem darauf hin, dass ein Zell-Zell-Kontakt-vermittelter Mechanismus die adipogene Differenzierung positiv beeinflusst. Daher wurden anschließend Untersuchungen zur interzellulären Kommunikation dieser Zellen durchgeführt, welche bisher kaum erforscht wurde.

Trotz der Vielzahl an Literatur über die Differenzierungsfähigkeit von ASCs ist wenig über die physiologischen Prozesse bekannt, die zur Differenzierung in verschiedene Zelltypen beitragen und diese kontrollieren. So wurde gezeigt, dass die direkte interzelluläre Kommunikation zwischen benachbarten Zellen über Gap Junctions Differenzierungsprozesse moduliert. Connexin 43 (Cx43) stellt dabei die häufigste Isoform der Gap Junction-bildenden Connexine dar. Im Rahmen dieser Arbeit wurde die Expression von Cx43 und die interzelluläre Kommunikation durch Gap Junctions (gap junctional intercellular communication; GJIC) in hASCs, sowie ihre Bedeutung für die adipogene Differenzierung untersucht. Die Cx43 Expression in hASCs wurde histologisch und auf Gen- und Proteinexpressionsebene nachgewiesen und wurde durch die Zellaussaatdichte nachweislich stark beeinflusst. Die Funktionalität der Gap Junctions konnte mit Hilfe eines Assays zur Übertragung von Farbstoffen untersucht werden. Es zeigte sich hierbei eine zelldichteabhängige, adipogene Differenzierungkapazität der hASCs. Die Hemmung der GJIC durch 18α-Glycyrrhetinsäure beeinträchtigte die adipogene Differenzierung deutlich, wie sich durch die Histologie, die Triglyceridquantifizierung und die adipogene Markergenexpression beobachten ließ. Bei Hemmung der GJIC zeigte sich mit Hilfe der Durchflusszytometrie, dass weniger Zellen adipogen differenzieren konnten, was die Bedeutung von GJIC im Differenzierungsprozess hervorhebt. Zusammenfassend

veranschaulichen diese Ergebnisse den Einfluss direkter Zell-Zell-Kommunikation über Gap Junctions auf den adipogenen Differenzierungsprozess von hASCs und könnten somit in Zukunft dazu beitragen, direkte interzelluläre Kommunikation in Tissue Engineering Ansätze zu integrieren.

1 Introduction

1.1 Adipose tissue

Adipose tissue (AT) is one of the largest body compartments and regulates metabolism and energy homeostasis in humans. In times of supernutrition, excess energy is stored by accumulation of triglycerides (TG), while in times of malnutrition or lower nutritional supply, accompanied by an energy deficit, free fatty acids (FFAs) are released from adipose depots to provide energy for organs like liver or muscle[1]. However, AT comprises by far more functions than excess energy storage. For instance, it represents an insulating substance and a mechanical support for other important body structures and furthermore, it functions as one of the largest endocrine organs of the human body[2].

AT is distributed throughout the body and can be generally subcategorized into subcutaneous and intraabdominal adipose tissue[3,4]. In healthy patients, subcutaneous adipose tissue accounts on average for 80% of the total AT. Due to sexual dimorphism this subcutaneous fat is most abundant in the gluteofemoral regions as well as in the mammary area in females, whereas in males, the main subcutaneous depots include the nape of the neck, the area over the deltoid and triceps muscles, and the lumbosacral region[4]. Adipose tissue, which is located around organs, accounts for the remaining 20% and is mainly located in visceral, retroperitoneal and omental regions[4–6].

During the last decades, a growing interest arose concerning AT research, especially because of the increasing incidences of obesity, which became one of the major public health problems in modern industrial countries[4,7]. Obesity, which is a major cause of morbidity and mortality, is defined as an excess of body fat that may negatively affect health[4,8]. According to estimations of the World Health Organization from 2008, over 50% of both men and women in European countries were overweight, and roughly 23% of women and 20% of men were obese. Additionally, 1 in 3 children (~11 years old) is overweight or also obese[9]. Obesity is associated with the development of many comorbidities like type 2 diabetes mellitus, coronary heart disease (CHD), respiratory complications and osteoarthritis. Furthermore, obesity is accompanied by insulin resistance, dyslipidemia, and hypertension, which are often coincident in individuals and termed metabolic syndrome[8,10]. In obese patients with a body mass index (BMI) > 30, more than half of the body weight (up to 70%) is represented by adipose tissue, while in lean and trained individuals body fat represents only 2-3%[4,11,12]. The average amount of fat mass is gender-specific, displaying 10-20% in healthy males and about 20-30% in healthy women[4].

1.1.1 Adipose tissue structure

Two major types of adipose tissue exist in mammals, namely white adipose tissue (WAT) and brown adipose tissue (BAT). In adults BAT is found only in small amounts in distinct depots, while the largest depots occur in human during infancy, being gradually replaced by WAT[2,5,13–15]. However, a transformation of BAT can occur also in adults by cold adaptation or pharmacological treatment[5]. Histologically, brown adipose tissue is highly vascularized and exhibit, unlike WAT, multilocular adipocytes containing a multitude of mitochondria[2,4]. In this tissue, the stored lipid droplets primarily serve as a fuel for the production of heat, provided by non-shivering thermogenesis without producing ATP[2,12]. In recent years, BAT draw scientific attention, as remaining BAT depots were described in adults and a metabolic superiority towards WAT was depicted. Also of interest is the possibility of turning WAT into BAT, which represents a potential therapeutic target for obesity treatment[15–17]. In contrast to BAT, mature adipocytes in white fat tissue contain solely a single large lipid droplet[4]. 90% of the cell is composed of a triglyceride filled lipid-laden vacuole, pushing both cytoplasm and the flattened semilunar nucleus against the edge of the cell, generating the typical unilocular signet-ring shape[4]. The vacuole contains a mixture of neutral fats, fatty acids, phospholipids, and cholesterol, however, TGs represent with approximately 95% the highest amount of the total lipid content[4]. Even if mature adipocytes represent 30-75% of the total tissue mass, they only account for 25% of the total cell population in AT. The other 75% are composed of other cell types including macrophages, fibroblasts, pericytes, blood cells, endothelial cells, and adipose precursor cells, among others, comprised in the so-called “stromal vascular fraction“ (SVF)[1,4,18]. Histologically, adipose tissue is composed of mature lipid filled large adipocytes, nerve tissue and a dense network of extracellular matrix (ECM) and is highly interspersed with microvasculature, so that every adipocyte can be supplied with nutrient and oxygen[19,20]. The ECM surrounding every adipocyte is designated as basal membrane and contains as main components collagen and laminin besides others[20,21]. Adipose tissue has a great ability to respond quickly and dynamically to alterations in nutrient supply by regression or expansion throughout the entire life span, in order to fulfil its major role in whole-body energy homeostasis[6,22]. In times of prolonged caloric excess mature adipocytes react with a hypertrophic expansion resulting in an obese state, and additionally, recruited preadipocytes can cause an hyperplastic growth of the adipose tissue[4,6,23,24]. In the course of this, adipocytes can rapidly reach the diffusional limit of oxygen during growth and therefore hypoxia is an early determinant that limits healthy expansion[6]. A variety of remodeling processes take place in adipose tissue due to cellular plasticity concerning vasculature and ECM to ensure sufficient tissue supply[20,25,26]. While developing adipocytes display multiple lipid vacuoles in their cytoplasm, mature adipocytes own only one, which can drastically expand during prolonged excess of energy. During lipid accumulation adipocytes can change their lipid volume by

several thousand-fold (with maximum volume of 1,000 pL) expanding their diameter in total from 20 µm to 200 µm[4]. During periods of nutrient deprivation stored fat is rapidly turned over and triglycerides are again mobilized to supply other tissues with energy, and adipocytes are shrinking again.

1.1.2 Adipose tissue function

For decades adipose tissue has been considered as an inert mass of stored energy, which accumulates triglycerides in times of high energy intake (excess nutrition) and releases free fatty acids (FFAs) in times of caloric deficit to provide energy for other organs[1,12]. Apart from this obvious function as an excess energy storage and metabolic regulator, it additionally yields some advantageous properties as thermal isolator against heat loss, and provides a cushioning function as mechanical support for other organs[2,4]. Furthermore, since the discovery of leptin in the year 1994 adipose tissue was also recognized as a critical endocrine organ[10,12]. The adipocyte-secreted hormone leptin was pivotal for the awareness that adipose tissue is a highly specialized active endocrine organ as well as one of the largest endocrine organs of the human body[12]. The hormone signals to the brain and other tissues via hypothalamic pathway, maintains energy homeostasis via a negative feedback loop and terminates food intake [10,27,28]. Thus, its secretion is proportional to the adipose tissue mass[27]. In recent years additional effects of leptin on angiogenesis and the immune reaction, among others, were discovered[29,30].

Moreover, in the last decades, it was found that WAT is actively involved in regulation of cellular functions through a complex network of endocrine, paracrine, and autocrine signals. These secreted, multiple bioactive factors termed adipokines (e.g., hormones, complement factors, soluble factors) influence the response of many tissues, including the hypothalamus, pancreas, liver, skeletal muscle, kidneys, endothelium, and immune system, to name but a few. Likewise, they take part in the regulation of processes such as reproduction, immune response, blood pressure control, coagulation, fibrinolysis, and angiogenesis, among others[4]. As adipokine secretion is involved in the regulation of insulin resistance and glucose homeostasis, dysregulation of the secreted factors, primarily occurring in obese individuals, can lead to type 2 diabetes and other comorbidities[4,31]. For instance adiponectin is a major insulin-sensitizing adipokine in liver and muscle, and is one of the most abundantly expressed genes in subcutaneous adipocytes[32–35]. In contrast to other adipokines like leptin, adiponectin secretion is generally negatively correlated with adipose tissue and body weight. Its levels are decreased in cases of obesity, enhancing and amplifying related comorbidities like type 2 diabetes[32,34]. In contrast, high levels of adiponectin are associated with anti-diabetic, anti-inflammatory and anti-

atherogenic effects[34,36]. Besides these two very important adipokines, a great diversity of molecules involved in lipid and glucose metabolism are secreted by adipocytes including factors such as lipoprotein lipase (LPL), apolipoprotein E (apoE), fatty acid binding protein 4 (aP2/FABP4), angiopoietin-like protein 4 (ANGPTL4), cholesteryl ester transfer protein (CETP), glucocorticoids, sex steroids, prostaglandins, adipsin, resistin, among others[4,10,35,36]. Additionally, growth factors are also secreted, e.g., insulin-like growth factor 1 (IGF-1), nerve growth factor (NGF), macrophage colony-stimulating factor (M-CSF), transforming growth factor-β (TGF-β), vascular endothelial growth factor (VEGF), heparin-binding epidermal growth factor (HB-EGF), basic fibroblast growth factor (bFGF), besides others[4,37]. Adipocytes produce furthermore several factors that modulate the development of new blood vessels. Angiopoietin-1 (Ang-1), angiopoietin-2 (Ang-2), hepatocyte growth factor (HGF), stromal derived factor 1 (SDF-1) and tumor-necrosis factor-α (TNF- α), but also already mentioned hormones like VEGF, leptin, IGF and TGF-β play a crucial role in angiogenic functions[38]. As inflammation constitutes one of the most prominent symptoms in obesity, proinflammatory cytokines are also important secreted adipokines. For example, TNF-α, interleukins (IL-2, IL-6 and IL-8), plasminogen activator inhibitor-1 (PAI-1) and angiotensinogen represent an extraordinarily relevant group, which can also affect both glucose and lipid metabolism[4,35,36,39].

As adipose tissue on the one hand regulates energy homeostasis and on the other hand physiological and pathophysiological body functions, the profound understanding of this highly active endocrine organ on the cellular level may help to develop rational approaches to fully restore adipose tissue defects or to treat the metabolic syndrome and other obesity-related diseases.

1.1.3 Adipogenic differentiation

Adipogenic differentiation occurs in mammals not only during embryonic development but is also a lifelong occurring process[40–42]. Development of adipocytes takes place during regular cellular turnover and likewise during hyperplastic growth of the adipose tissue in response to prolonged caloric excess[42,43]. Therefore, multipotent adipose-derived stem cells are recruited from the stromal vascular fraction, arising from a pluripotent stem cell population of mesodermal origin. These cells exhibit a self-renewal as well as multilineage capacity enabling differentiation into various cell types such as adipocytes, chondrocytes, osteoblasts, and myocytes[44]. The arising fibroblast-like, proliferative progenitor cells differentiate along the adipogenic lineage in a defined two-step process involving determination and differentiation to finally form growth-arrested, spherical, lipid-laden functional adipocytes[23,44–46] (Figure 1.1).

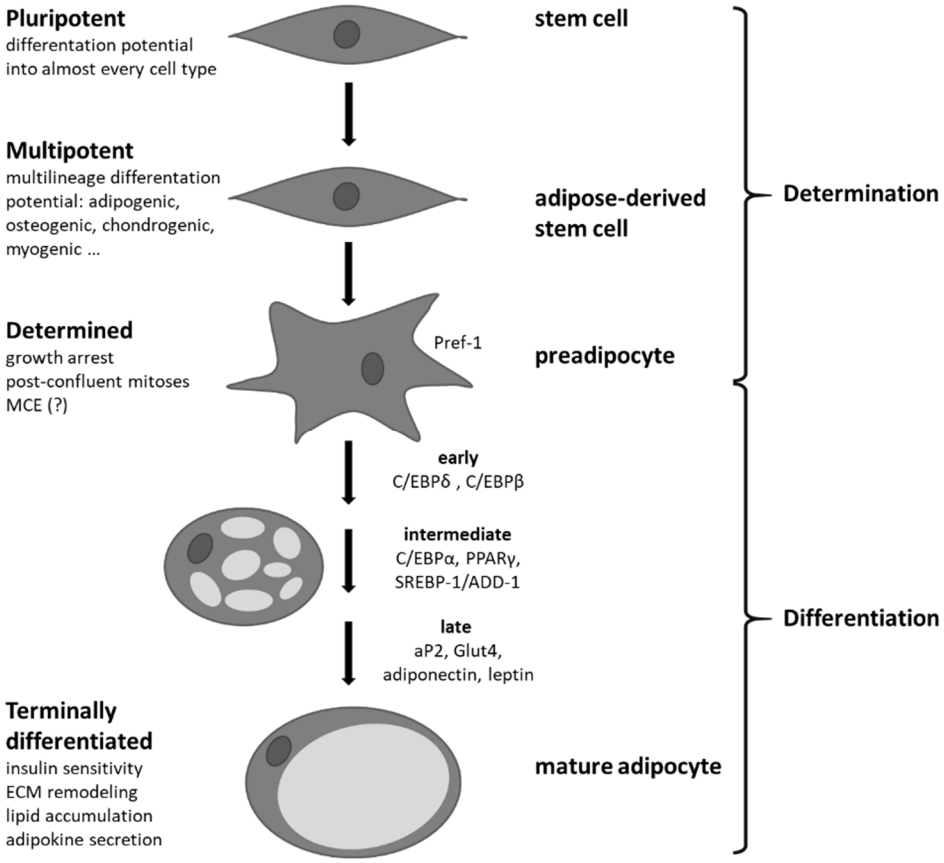

Figure 1.1: Adipogenic differentiation.

Adipocyte development is a two-step process. During determination stem cells are committed to the adipogenic lineage and lose their multilineage differentiation potential. In a second step specified as differentiation, a cascade of transcription factors is spatially and temporally activated during early, intermediate and late differentiation. Thus, an initially pluripotent stem cell becomes a multipotent ASC followed by determination to the adipogenic lineage (preadipocyte) and finally becomes terminally differentiated (mature adipocyte). Pref-1: preadipocyte factor-1; C/EBPα/β/δ: CCAAT/enhancer binding proteins alpha/beta/delta; PPARγ: peroxisome proliferator-activated receptor gamma; SREBP-1/ADD-1: sterol regulatory element-binding protein-1 and differentiation-dependent factor-1; aP2: adipocyte protein 2 or fatty acid binding protein 4 (FABP4); Glut4: glucose transporter 4. Adapted in part from Gregoire et al. 1998, Fève et al. 2005, and Flynn et al. 2008[23,44,46].

The first step implies the determination of pluripotent stem cells to the adipogenic lineage. During the so-called "commitment phase" stem cells become preadipocytes. These cells are growth arrested and have lost their multilineage differentiation potential but are morphologically not properly distinguishable from their precursors. In a second step named differentiation, committed precursor cells acquire the characteristic phenotype of mature adipocytes[23,44,46]. Because adipogenesis is a well-orchestrated multistep process, it requires the sequential activation of numerous genes and transcription factors, which have been extensively studied using model preadipocytes derived from 3T3-L1, 3T3-F442A, C3H10T1/2, and NIH 3T3 mouse cell lines[2,41,44,45]. However, molecular mechanisms underlying the determination phase are still not extensively investigated and are therefore poorly enlightened. Upstream signal transduction mechanisms involving members of the Wnt, TGF-β, BMP as

well as hedgehog signaling pathway are suggested to regulate this process[45,47,48]. Nevertheless, adipocyte differentiation by a coordinated transcriptional program, resulting in lipid-laden and insulin-responsive adipocytes, is extensively studied on the molecular level by means of the above mentioned preadipocyte cell lines. A complex network consisting of transcription factors, cell-cycle regulators as well as specific transcriptional coactivators and corepressors responds to extracellular stimuli eventually activating or repressing adipocyte differentiation[49].

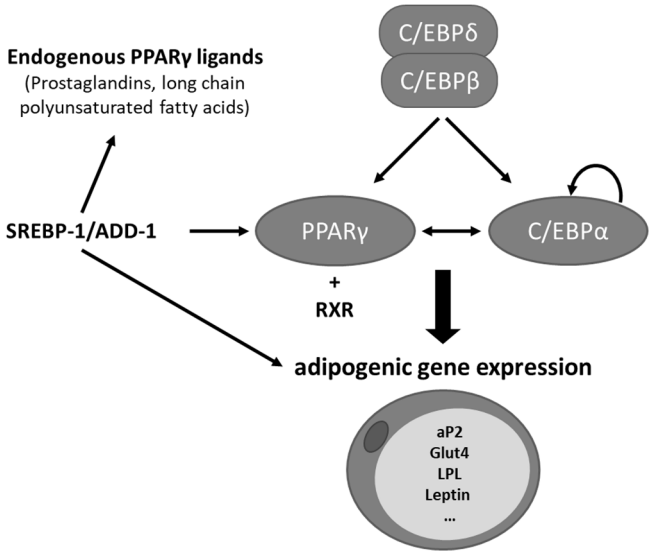

Figure 1.2: Core components of the adipogenic transcriptional cascade leading to the adipogenic phenotype.
The transcriptional cascade comprises C/EBPβ and C/EBPδ in a first step, and PPARγ in C/EBPα in a second step. SREBP-1/ADD-1 promotes the adipogenic program by increasing the production of PPARγ and its ligands. Furthermore, it activates the expression of adipocyte genes directly. After binding of PPARγ to its endogenous ligands, it forms a heterodimer with retinoid X receptor (RXR) and attaches to the transcriptional regulatory regions of the target genes. RXR: retinoid X receptor; C/EBPα/β/δ: CCAAT/enhancer binding protein alpha/beta/delta, PPAR: peroxisome proliferator-activated receptor, SREBP-1/ADD-1: sterol regulatory element binding protein 1/adipocyte differentiation and determination factor-1; aP2: adipocyte protein 2 or fatty acid binding protein 4 (FABP4); Glut4: glucose transporter 4; LPL: lipoprotein lipase. Adapted in part from Flynn et al. 2008, Ali et al. 2013, and MacDougald and Mandrup 2002[23,45,50].

Using preadipocyte cell lines it was demonstrated that after determination cells undergo an additional round of mitosis, referred to as mitotic clonal expansion (MCE), before entering a growth arrest state[45]. Still it is controversially discussed whether this process of mitotic cell reproduction is a required step in differentiation of human preadipocytes. However, it is clear that some of the checkpoint proteins important for mitosis also regulate mechanisms involved in adipogenesis[2,51]. During differentiation committed preadipocytes express numerous genes in a temporally and spatially arranged manner, which are considered as markers of the developmental state. Preadipocyte factor-1 (Pref-1) for example, a transmembrane protein that is believed to play a role in regulating differentiation, is a marker of undifferentiated, yet committed cells[45]. Early during development two members of the CCAAT/enhancer binding protein family, namely C/EBPβ and δ, are expressed and

responsible for the growth arrest of the cells, representing early transient adipogenic markers (Figure 1.2)[23,44,45]. Before their expression decreases, these two core transcription factors trigger the subsequent expression of peroxisome proliferator-activated receptor gamma (PPARγ) and C/EBPα, displaying intermediate differentiation markers. Once activated, PPARγ and C/EBPα promote the expression of adipocyte specific genes like adipocyte protein 2 (aP2), glucose transporter 4 (Glut4), leptin, adiponectin, and lipoprotein lipase (LPL)[23,45–47,50]. Many of these genes contain C/EBP-response elements in their upstream promoter regions together with PPARγ binding sites. The binding of C/EBP family proteins and PPARγ (dimerized with retinoid X receptor (RXR)) to their corresponding proximal binding sites enhances adipogenic gene expression (Figure 1.3)[52]. Additionally, via such a C/EBP-response element, C/EBPα causes self-activation to maintain high levels throughout the differentiation process.

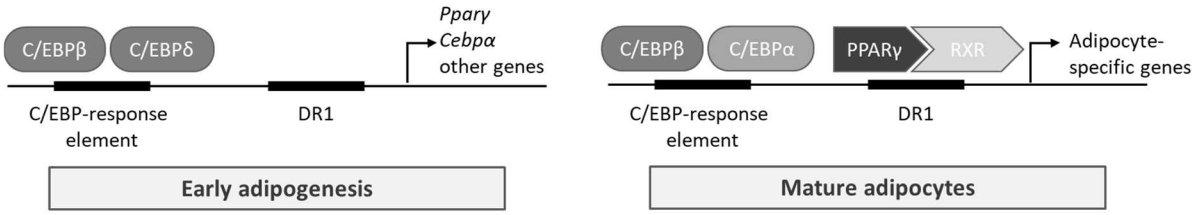

Figure 1.3: Model of PPARγ and C/EBP transcriptional action during adipogenic differentiation.

In early stages of differentiation, C/EBPβ and δ activate the expression of PPARγ, C/EBPα and other adipogenic genes. For terminal differentiation of adipocytes PPARγ binds as a heterodimer with retinoid X receptor (RXR) to its response element in the transcriptional regulatory region of the target genes, with C/EBPα and β frequently occupying C/EBP-response elements nearby. Adapted from Lefterova et al. 2009[52].

To develop terminally differentiated adipocytes, PPARγ and C/EBPα maintain their mutual expression while expression of C/EBPβ and δ decreases. Within this process PPARγ plays a key regulator role being essential for the process as well as maintenance of differentiation[23,53]. Besides PPARγ and the C/EBP family members another key transcription factor is involved in gene expression of adipocytes, the sterol regulatory element binding protein-1/ adipocyte determination and differentiation factor-1 (SREBP-1/ADD-1), a helix-loop-helix-leucin zipper protein[23,44,47]. SREBP-1/ADD-1 promotes the adipogenic program by increasing the production of PPARγ and its ligands, in addition to activating the expression of adipocyte genes directly[50]. It is noted that there are more than 100 other transcription factors that are expressed in adipocytes besides the previously mentioned ones. Among the most important pro-angiogenic transcription factors are kruepple-like factors (KLFs, 5 & 15), Krox20, phosphorylated cAMP response element-binding protein (pCREB), liver X receptors alpha and beta (LXRsα,β), while anti-adipogenic transcription factors are represented by GATA binding proteins 2/3 and transcription factor homologous to CCAAT-enhancer binding proteins (CHOP)[2,45].

It should be emphasized that precursor cells *in vivo* receive repressing and stimulating cytokine signals for differentiation from their cellular environment, but this is not possible for cells *in vitro*. Instead specific, soluble induction factors are required to induce ASCs towards the adipogenic lineage[53]. For the induction of adipogenic differentiation *in vitro* cell culture medium is basically supplemented with three induction factors. Typically, the administered hormonal cocktail consists of a glucocorticoid (dexamethasone), a phosphodiesterase inhibitor (isobutylmethylxanthine (IBMX)), and insulin or IGF-1. While dexamethasone, a synthetic glucocorticoid, increases intracellular cyclic adenosine monophosphate (cAMP) levels, insulin induces differentiation through numerous mechanisms like stimulation of insulin-like growth factor-I receptors. Often the non-steroidal, anti-inflammatory drug indomethacin is further added to induce adipogenic differentiation by acting as direct PPARγ agonist[18,53,54].

Furthermore, adipogenesis can be positively influenced by diverse culture conditions. Several reports have suggested that growth factors (GF) such as epidermal growth factor (EGF), platelet-derived growth factor (PDGF) or basic fibroblast growth factor (bFGF) can promote proliferation of hMSCs and maintain the multilineage capacity without inhibiting their differentiation potential[55,56]. In contrast, several studies prove the impact of growth factor application on differentiation capacity. For example, it is shown that preculture of 3T3-L1 preadipocytes or primary adipose-derived stem cells with bFGF positively impacts on differentiation capacity[57,58]. In the literature, there are also hints that cell density is crucial for adipogenic differentiation. The predominantly accepted practice is to grow the cell layer until confluency prior to hormonal induction of adipogenesis, as seen for mouse preadipocyte cell lines as well as for human stem cells[42,44,46,48,54]. So far, in previous studies exclusively for BMSCs, high cell densities have been shown to positively influence adipogenic differentiation of mesenchymal stem cells[55,59,60]. The underlying process of this density triggered influence still remains to be revealed and gaining insights into the mechanisms would help to integrate this knowledge into *in vitro* adipose tissue applications to improve differentiation results.

1.1.4 Cell-cell communication in adipose tissue

Mammalian tissue is a highly complex structure with many types of interactions. Cells within a tissue interact not only with their extracellular matrix but also with each other. Besides the attachment to ECM structures and to one another, they also communicate via direct or indirect mechanisms. Communication between cells occur in response to changes in their microenvironment, to guarantee proper coordination of the different cell types within the tissue[61]. Specifically, in a smaller group of cells, communication takes place via direct cell contact like adhesion molecule-mediated interaction

or tunneling nanotubules that establish conduits between cells for signal exchange[61]. Over longer distances, also soluble factors can be utilized for communication, acting in auto-, para-, or endocrine manner[39,62]. In this context, especially direct cell-cell communication has been shown to be an essential mechanism, which is involved in a number of tissue and cellular functions, including growth, differentiation, and cell death[63]. Therefore, to understand proper tissue development and differentiation, direct cell-cell communication mechanisms are highly important and need to be investigated in more detail. In this regard, cell junctions accomplish communication links between adjacent cells in different ways. Anchoring junctions, like adherens junctions or desmosomes directly mechanically connect cells including their cytoskeleton to adjacent cells or even the extracellular matrix, transferring mainly mechanical signals for intercellular communication[64,65]. Demonstrably, mechanical (cytoskeletal tension) and morphological signals (cell shape) act as cues, which are involved in driving hMSC commitment between adipocyte and osteoblast differentiation[59]. Furthermore, gap junctions and chemical synapses mediate a direct passage of chemicals or electrical signals between connected cells[66,67]. Gap junctional intercellular communication (GJIC) displays a ubiquitously occurring mechanism for direct cellular crosstalk in vertebrates, which appears at regions of tight cell contact[68,69]. Furthermore, this mechanism is widely acknowledged to play an essential role in tissue development and coordinated cellular activity, and serves as modulators of cellular differentiation[69–71]. Gap junctions (GJ) are formed of clusters of two paired hexametric hemichannels, called connexons, located in the cell membrane of neighboring cells. The basic elements of functional channels are connexin (Cx) proteins. The family of channel forming connexins in humans is comprised of 21 members, being mostly named after their molecular weight[63,67]. Within the collective of channel-forming connexins, connexin 43 represents the most abundant isoform in human tissue[72]. Hemichannels are composed of one or several different isoforms, being homo- or heteromeric, and thus, homotypically or heterotypically paired, regulating permeability and regulatory functions[68,73]. Conformational change of functional GJ to an open condition for bidirectional exchange of molecules as well as GJ turnover is regulated by change of Cx phosphorylation[74–76]. These low-resistance channels are permeable for molecules for the intercellular passage smaller than 1 kDa (~1 nm in size), including second messengers (e.g., cAMP, cGMP, IP_3), ions (e.g., Ca^{2+}, Na^+, H^+, Cl^-, K^+), metabolites (e.g., glucose, glutathione, adenosine, AMP, ADP, ATP) micro RNAs, and small peptides[63,67]. Until now, little attention has been paid to the investigation of gap junctional intercellular communication in adipose tissue and in the context of adipose tissue engineering. In literature a few hints are present, showing the presence of Cx43-containing gap junctions in ASCs in the context of regulated calcium oscillation via NOS and internalization of quantum dots[77,78]. However, no studies exist investigating the impact of gap junctions on tissue development and differentiation processes in these cells. Gaining insights in this

field of cell-cell communication within ASCs would help to foster new tissue engineering approaches for suitable tissue substitutes.

1.1.5 Adipose tissue vascularization

During fetal development a tight temporo-spatial coordination of angiogenesis with formation of fat cell clusters occurs[4]. More precisely, differentiation of arterioles and the blood vessel extracellular matrix (ECM) precedes the development of both, adipocytes and adipogenic ECM[26,79]. During later development of adipose tissue and throughout the whole lifetime, vascular development and maintenance continuously occurs, since adipose tissue displays a great plasticity, being constantly remodeled along with weight gain and loss[80]. Mature adipose tissue needs to be densely supplied with an extensive vascular network, which provides the tissue with oxygen, nutrients, growth factors, hormones, and cytokines. Every adipocyte is connected with at least one capillary and thus vascularization is a key aspect of adipose tissue plasticity[19,80]. As a consequence, the formation of new vasculature is closely linked to the adipogenic tissue expansion in response to weight gain[26,80]. Essential is a process called angiogenesis, which is describing the vascular sprouting out of existing vessels. For angiogenesis to occur, resting endothelial cells (ECs) have to be triggered to interrupt their relative state of quiescence and to activate proliferation and the production of angiogenesis-promoting proteins[81]. Carmeliet and coworkers[82–84] as well as Herbert and Stainier[85] have shown in further detail the formation of new vessels during angiogenesis on a mechanistic and molecular level. A process often treated synonymous with angiogenesis is called vasculogenesis. It is characterized by *de novo* formation of blood vessels and occurs mainly during embryonic development, even though there exist hints that this process also happens in adults[83,86]. In contrast to weight gain associated with vascular growth, weight loss is associated with the regression of blood vessels. However, the underlying mechanisms of vessel regression are less well studied[80].

Angiogenesis is controlled by the subtle balance between pro- and anti-angiogenic molecules referred to as “angiogenic switch”, being turned on whenever the fine balance is in favor of pro-angiogenic regulators[87]. Adipocytes seem to regulate angiogenesis and to communicate with capillary endothelial cells both by cell-cell contact and by adipokine secretion via paracrine signaling[26,88]. In addition to adipocytes, other cell types contribute to angiogenic modulation, including resident macrophages and other inflammatory and stromal cells[89].

Adipocytes mediate vascular development mainly by secretion of the vascular endothelial growth factor A (VEGF-A) and hepatocyte growth factor (HGF), two key angiogenic factors[26,90]. Also other pro-angiogenic factors are known to be produced by growing adipocytes, for instance bFGF, IGF-1, leptin,

adiponectin, Ang-1 and -2, and TGF-β, to name just a few[80,88,91]. Since several years it is known that these paracrine factors are not only secreted by developing and mature adipocytes but also by multipotent adipose tissue-residing ASCs[92,93]. Along with ASCs and developing adipocytes also adipose-infiltrating inflammatory cells produce high levels of cytokines such as TNF-α and interleukins IL-1β, IL-6, and IL-8. Especially TNF-α can be highlighted here as it promotes endothelial cell tube formation *in vitro* by inhibiting endothelial cell proliferation[80,94]. Additionally, TNF-α is a potent inflammatory cytokine that links between inflammation, angiogenesis, and adipogenesis[80]. Hypoxia is another important factor for vascular growth and remodeling, as it arises during triglyceride accumulation due to prolonged excessive caloric intake in rapidly expanding adipose tissue[88]. In response to hypoxia adipose tissue produces hypoxia-inducible factor 1 α (HIF-1α) induced angiogenic factors such as VEGF, leptin, TNF-α, and PAI-1, which similarly regulate angiogenesis[80,88]. In aggregate, the predominantly pro-angiogenic signals result in vessel branching whereby the ECM needs to be remodeled as well. The ECM itself is a highly important and demonstrable modulator of angiogenesis during oncogenesis, wound healing and development[81,95]. Primary mediator of angiogenesis is the composition of the ECM surrounding the endothelial sprouts, with type IV collagen as a major basement membrane protein, shown to both promote the lengthening of neovessels and to prevent their regression[95]. In particular, the degradation and remodeling of the ECM and its basement membrane is an essential requirement for the formation of new vessels. ECM modifying proteins like matrix metalloproteinases (MMPs) and A disintegrin and metalloproteinases (ADAMs) are secreted by adipocytes, inflammatory cells and macrophages[96,97]. Among the produced MMPs, MMP-2 and -9 potentially affect preadipocyte differentiation and microvessel maturation by modulating the ECM, whereas MMP-9 is furthermore capable to release the matrix-bound VEGF and thus to indirectly induce angiogenesis[88]. Therefore, the ECM itself plays also a crucial role during vascular development and tissue plasticity.

Adipocytes and multipotent ASCs are known to secrete pro-angiogenic factors and to induce angiogenesis of quiescent endothelial cells, however, the reverse influence of angiogenesis on adipogenesis was demonstrated, too. Hints in literature exist that show a close spatial and temporal connection between blood vessel formation and adipogenesis in adults. It seems that the sprouting of new blood vessels from preexisting vasculature is coupled to adipocyte differentiation. When angiogenesis was blocked even differentiation was disrupted, which demonstrates that angiogenesis and adipogenesis are mutually dependent[19]. But the underlying mechanism is not yet elucidated.

In summary the knowledge in the field of adipose tissue angiogenesis is still restricted to the temporal and spatial interplay of angiogenesis and adipogenesis on a cellular level, with both processes influencing each other. The favorable influence of ECM on angiogenesis could be capitalized on and integrated in *in vitro* approaches to support both adipogenesis and angiogenesis. Further

investigations utilizing model systems more closely resembling the *in vivo* situation are necessary to shed light on this aspect of adipose tissue development.

1.1.6 Adipose tissue extracellular matrix (ECM)

As the extracellular matrix is not only a scaffolding structure but furthermore constitutes an important functional component of WAT, it will be contemplated in more detail in the following paragraph. The ECM in general displays a multicomponent structure, which forms a dynamic protein network that provides cells with positional and environmental information, while serving as a tissue-specific structural framework that controls cell function[25]. Therefore, besides the physical support, the ECM represents a reservoir of growth factors, enzymes as well as plasma proteins and interacts with its residing cells. This microenvironment triggers both basal cellular functions like cell adhesion, migration, polarization and proliferation, as well as complex biological processes including differentiation (i.e. adipogenesis and angiogenesis), tissue development, maintenance, repair, survival, and regeneration[98,99]. The extracellular matrix is produced in adipose tissue by its residing cells, mainly mature adipocytes but also SVF and endothelial cells[20]. Adipocytes also remodel the ECM in response to tissue plasticity due to caloric excess or deprivation, involving previously mentioned angiogenic processes or adipogenic differentiation[100]. Thus, in response to incoming stimuli, the ECM is continuously remodeled by various destructive and constructive enzymes together with enhancing and inhibiting factors, representing a more dynamic than static structure[20,25]. Even though extracellular matrix components are similar in different tissues, its composition varies according to tissue function and requirements of residing cells[99].

Focusing on adipose tissue extracellular matrix, 20 subunits of 12 different types of collagens (type I-VI, XI, XII, XIV, XV, XVIII, and XXIII) have been identified in rodent adipose tissue, whereas subunits of collagen type II, XI, and XXIII were not found in human visceral fat depots[20]. Type I, IV and VI collagen represent the main collagenous components of mature adipocytes, while collagens type II and III exhibit considerably lower expression levels[101,102]. Nakajima et al. showed for differentiated bovine intramuscular preadipocytes (BIP) that type I-VI collagens exist but collagen type II displayed only a low abundance in immunohistochemical staining[20,102].

Another very important and abundant component of the extracellular matrix are non-collagenous glycoproteins, which include several protein families with diverse origin[99]. Essential representatives of this group in adipose tissue are laminins and fibronectins composed of multiple protein chains[99]. Cross- or T-shaped laminins represent heterotrimeric glycoproteins, which occur in many isoforms according to the composition of three different polypeptide chains, referred to as α, β and γ chains[20,103,104].

Specific for cells of mesenchymal origin are laminin isoforms 8 (α4β1γ1), 9 (α4β2γ1), and 14 (α4β2γ3), all containing the α4 chain, while laminin 1 and 8 are the most prominent isoforms in the adipose ECM[105,106]. Fibronectin, a high molecular weight non-collagenous glycoprotein constitutes another component of the fat tissue ECM[20]. In differentiated bovine intramuscular preadipocytes (BIPs), both laminin and fibronectin were shown to be present, while other reports depicted a decrease in fibronectin around mature subcutaneous adipocytes[102,107].

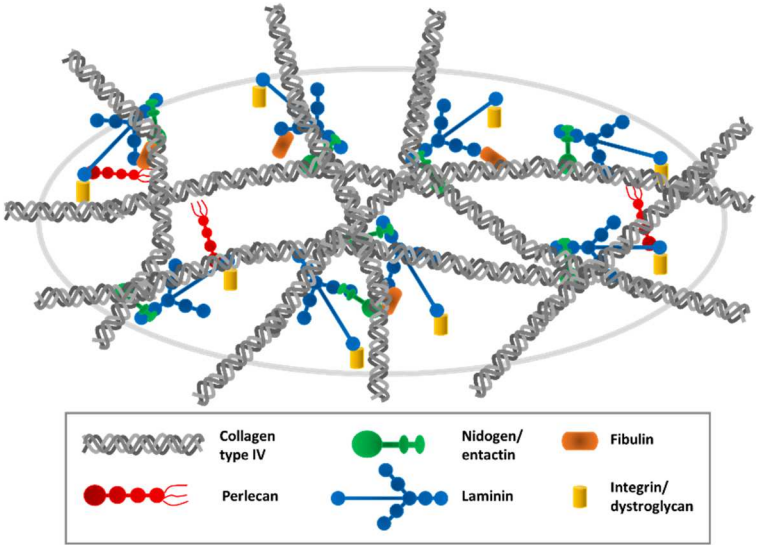

Figure 1.4: Schematic illustration of the basement membrane (BM) of the adipocyte ECM.
Laminin polymerization initiates the formation of the BM at the basolateral surface of cells and is anchored to the cell by integrin and dystroglycans receptors. Nidogen/entactin bridges the laminin polymer and the type IV collagen network. The other components (i.e. fibulin, perlecan) of the BM interact with the laminin polymer and the type IV collagen network to organize a functional BM. Adapted in part from Kalluri et al. 2003[108].

In summary, the main constituents of the adipose extracellular matrix in WAT are collagen (types I, IV, and VI), laminin (LN-1, 8), fibronectin (FN), hyaluronan, and proteoglycans[101,105,109]. Adipogenesis involves extensive ECM remodeling with changes in cell-matrix adhesion and cytoskeletal rearrangement. It leads to the cell-associated ECM alteration by switching from a fibronectin-enriched matrix into an adipocyte specific basement membrane (BM)[105]. Therefore, each mature adipocyte is surrounded by a thick layer of ECM with adhesive and barrier functions, referred to as BM or basal lamina, with collagen type IV as a major component[20,25,107] (Figure 1.4). Other components of the BM are represented by laminin, nidogen/entactin and smaller amounts of other components like heparan sulfate proteoglycan (perlecan)[20,107]. Entactin/nidogen serves as a non-covalent crosslinker, forming stable bridges between laminin and type IV collagen and also binds to perlecan and fibulins[110]. Integrins are heterodimeric transmembrane receptors that link the ECM or BM to the internal cytoskeleton by binding directly to laminins (as well as fibronectin), and additionally indirectly to actin via cytoplasmic binding proteins[98]. Further, together with integrins, dystroglycan receptors are present on the cell

surface and regulate not only the interaction and information transmission, but also ensure correct BM anchoring[25].

As mentioned before, during adipose tissue development profound rearrangement processes take place within the ECM. The main and most important development processes regarding the ECM reorganization during adipocyte differentiation are outlined in the following section. Involved factors are the previously mentioned ECM degrading enzymes, including serine proteases and matrix metalloproteinases (MMPs), and also the respective counterpart namely tissue inhibitors of MMPs (TIMPs)[38,98]. The most essential MMPs in adipose tissue are MMP-2 and -9, as depicted in murine preadipocyte cell lines[111]. As stated earlier, during development and the adipogenic differentiation process, ECM remodeling results demonstrably in a strongly decreased expression of fibronectin[21]. While in general laminin gene expression does not change, it becomes nevertheless enriched in the extracellular space within the basement membrane, accompanied with an increase in entactin deposition[112]. Fibrillar collagen type I and III are demonstrated to decrease during 3T3-L1 preadipocyte differentiation, whereas the gene expression and incorporation of collagen type IV into the BM is significantly increased along with the formation of a fibrous network during progression of terminal differentiation[112,113]. Additionally, a biphasic expression pattern of collagen type VI is described, showing an increased expression level upon induction, which declines later on, but remains at a higher level compared to the starting point, leading to an altered network structure (fine and spiny fibrils)[20,113].

It should be noted that the assembly of the BM is not solely restricted to adipocytes, but also occurs in other tissues, for instance at interfaces between epithelial and mesenchymal tissue[25,98]. Nevertheless, for adipose tissue and its correct function and survival a basement membrane seems to be a basic prerequisite. In recent years, biological scaffold materials derived from the ECM of intact mammalian tissues have been successfully used in a variety of tissue engineering approaches, both in preclinical studies and in clinical applications[114]. Even if the mechanisms by which functional tissue restoration is achieved are not well understood, it is acknowledged that the materials have constructive remodeling properties[114]. Due to its unique structure and function the ECM represents a crucial structure for adipose development and differentiation and therefore worth to be further investigated in this regard.

1.2 Adipose tissue engineering

1.2.1 Background – clinical need for adipose tissue augmentation

Plastic surgery is indispensable to repair soft tissue defects of the subcutaneous fat layer that result from traumatic injury (i.e., significant burns), tumor resections (i.e., mastectomy and carcinoma removal), and congenital defects[1,18]. According to the statistical survey of the American Society of Plastic Surgeons 5.8 million reconstructive procedures were performed in the USA in 2016, whereby 4.5 million of these surgeries were due to tumor resection, thus representing the major cause[115]**.** One of the primary goals in reconstruction is the restoration of natural tissue function. Additionally, another equally important aspect is the recovery of the soft tissue aesthetic function, which often is associated with anxiety and negative psychological feelings due to disfigurement[1]**.** Current strategies for the repair of soft tissue defects include single cell injection of autologously liposuctioned tissue, autologous tissue grafts i.e. free fat tissue grafts and pedicled tissue flaps, as well as implants and fillers, all of which face many drawbacks and are not yet delivering sufficiently satisfactory clinical outcomes[1,116–121]. Synthetic fillers such as silicone or teflon and allogenic materials like bovine collagen also comprise various disadvantages, for instance foreign body reaction, capsule fibrosis, dislocation of the implants, and allergic reactions[120]. Alternatives to these materials are the already mentioned autologous tissue grafts. Minor wrinkles are currently treated by injections of fat cells from liposuction[120]. Drawbacks of this lipotransfer technique are that the adipocytes, which possess a cytoplasm filled with 80-90% lipids, are easily traumatized by the mechanical forces of liposuction damaging approximately 90% of the aspirated cells. The remaining 10% entail the risk of progressive absorption and tend to form cysts or localized necrosis post injection. More recently manufacturers try to overcome this by a gentler isolation procedure of the cells to prevent rupture and to obtain more viable cells. Hence, repeated injections are required for a reasonable and satisfying aesthetic result[18,120]. An advanced strategy is cell assisted lipotransfer (CAL) where the stromal vascular fraction containing ASCs is isolated from a portion of the aspirated fat and then recombined with the remaining fat prior to injection[122]. This strategy, however, remains controversial, as a comparative clinical study reported no significant difference in fat graft retention between CAL and lipotransfer[123,124]. Larger soft tissue defects are filled with autologous fat grafts, which are regarded to be the ideal implant in terms of biocompatibility, immune response and avoidance of tissue rejection. Nevertheless, these grafts are prone to an inconstant outcome due to variable volume loss primarily caused by poor neovascularization, which results in insufficient nutrient and oxygen supply[1,18,120,125,126]. To overcome the hurdle of lacking vascular supply, pedicled autologous grafts are utilized, consisting of subcutaneous fat tissue, which can by microsurgically anastomosed to the blood supply[120,127,128]. Being

preferable in terms of volume stability and vascular supply for the treatment of larger tissue defects, pedicled grafts come along with a considerable donor site morbidity and are associated with extensive and cost-intensive surgical procedures[18].

An alternative to these technics would be represented by tissue engineering (TE), which is still a comparably new interdisciplinary field of applied research combining engineering, biosciences and clinical applications mainly focusing on surgical specialties. It could help to develop living substitutes for tissue and organ regeneration addressing the clinical need for soft tissue regeneration[129]. Several general challenges will be faced in achieving the ambitious aim to serve this demand. First, the shape and dimensions of the engineered constructs at the reconstructive site must be maintained, since current clinical approaches fail at this point. Second, the engineered construct needs to be rapidly supplied with nutrients and oxygen by means of a sufficient vascularization. Third, a tissue substitute that noticeably resemble natural tissue texture is required. And finally, fourth, the clinical application should be facile and predictable with feasible integration for long-term use[18].

1.2.2 The principle of adipose tissue engineering

Tissue engineering, as a relatively new scientific field in conjunction with regenerative medicine, aims for the repair of tissue defects rather than whole organ replacement. Adipose tissue engineering as a subdiscipline in TE focuses on the development of autologous tissue substitutes to regenerate soft tissue defects caused by trauma, injury, disease, or congenital defects. Thus, it potentially serves as an alternative for the current unsatisfying clinical standard[18]. Moreover, tissue engineered soft tissue substitutes represent an equally ideal implant for plastic and aesthetic surgical interventions[130]. The use of autologous cells in tissue engineering could completely avoid the risk of viral infections as well as immunological responses, such as rejection[131]. The basic concept of TE includes a biomaterial scaffold that provides an architecture and cellular microenvironment that fosters hereinafter desired tissue-specific features prior to implantation (Figure 1.5)[131].

For cell-based approaches, an appropriate stem cell population is usually isolated from a donor site with a preferably minimal invasive procedure and then propagated *in vitro*. For adipose tissue engineering approaches, mainly adipose-derived stem cells, which are isolated from liposuctions most commonly of abdominal regions, are enzymatically isolated and expanded in cell culture[40,132]. Adipose tissue represents therefore an abundant and easily accessible source of adult stem cells with multipotent capacity. After the enrichment of a sufficient quantity of cells, they are seeded onto 3D scaffolds (i.e. polymer meshes, hydrogels, microspheres, decellularized organs) and cultured under

tissue-specific inductive conditions *in vitro*[18,121,133]. Finally, the cell-containing 3D constructs are implanted in the soft tissue defect area of the patient to restore natural tissue function and shape.

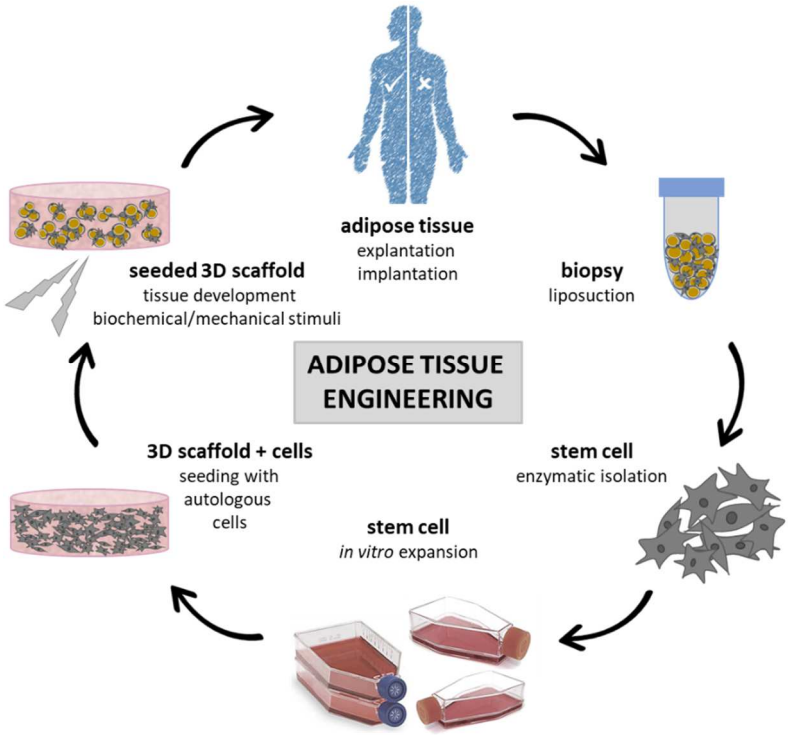

Figure 1.5: Principle of adipose tissue engineering in cell-based approaches.

Cells are isolated from donor/patient tissue biopsies and are propagated *ex vivo* in tissue culture flasks under controlled conditions. Cells of a sufficient quantity are seeded onto 3D scaffolds and cultured under adequate *in vitro* conditions (static or dynamic) with bioinductive stimuli (mechanical or biochemical) prior to implantation at the site of the tissue defect.

1.2.3 Components and strategies for adipose tissue engineering

1.2.3.1 Cell sources for tissue engineering applications

The application of an appropriate cell population is crucial for adipose tissue engineering of transplantable substitutes. Basic requirements are that the applied cells are autologous or even non-immunogenic, and furthermore easily accessible in a sufficient quantity[18,132]. At first sight, mature adipocytes seem to be undoubtedly an ideal cell population for adipose tissue engineering applications. However, these cells are an inapplicable cell source for regenerative medicine, as they are easily traumatized due to their high lipid content and conventional *in vitro* cell culture is very inconvenient due to their buoyancy and fragility[120]. Even though specialized culture methods have

been developed in recent years, isolated mature adipocytes remain unsuitable because of their post-mitotic status and the loss of proliferation capacity[120,126,134].

Since almost 50 years immortalized preadipocyte cell lines (i.e. 3T3-L1, 3T3-F442A, and Ob17) are applied in basic adipose research[42,135–139]. These murine preadipocytes are well characterized and rapidly expanded due to easy cultivation, and they can be efficiently and reproducibly differentiated into adipocytes. Nevertheless, due to the murine origin and their aneuploid status they are unsuitable for clinical applications in human[41]. Yet, these cell lines have been useful for tissue engineering approaches for elucidating basic principles and are still used for TE basic research.

Undoubtedly, human embryonic stem cells (ESCs) represent the ideal cell source for regenerative medicine. ESCs are a type of stem cells, which derive from the inner cell mass of a developing blastocysts and are widely used in tissue engineering and regenerative medicine because of their high differentiating capacity[132]. For regenerative medicine ESCs display a greater potential compared to adult stem cells, owed to their pluripotency and the ability of differentiation into any adult postnatal cell type[132]. However, the application of ESCs for clinical use is limited due to ethical concerns, insufficient sources of these cells, and their potential tumorigenicity[132,140–142]. Induced pluripotent stem cells (iPSCs) have marked a breakthrough in regenerative medicine since their discovery by Takahashi et al. in 2007 and provide the potential to replace ESCs for regenerative medicine applications[143]. No ethical issues are associated with iPSCs and they can be produced from manipulated somatic cells, which display an infinite source. Albeit no ethical concerns exist for these cells, studies show that iPSCs comprise a tumorigenic potential and high risk of chromosomal aberrations due to the extensive but required *in vitro* manipulation[142,144].

Based on studies showing that mature adipocytes, embryonic stem cells and iPSCs are not suitable for tissue engineering and regenerative medicine applications, another cell source has come to the fore. Adult mesenchymal stem cells (MSCs) can be harvested from various adult human tissues and circumvent most of the mentioned restrictions. These cells can be isolated from numerous tissues including bone marrow, adipose tissue, muscle, liver, umbical cord, placenta, and peripheral blood[145]. Adult mesenchymal stem cells, when used in an autologous setting, are immune compatible and have no ethical issues related to their use[125]. In contrast to ESCs or iPSCs, the MSCs have lost their pluripotency, but still exhibit a multilineage differentiation capacity restricted to the cell lineage in which they reside, for instance for adipogenesis, osteogenesis, chondrogenesis, and other lineages[146,147]**.** One major source of MSCs is the human bone marrow, which is a niche of so-called bone marrow-derived stem cells (BMSCs). Besides their multilineage differentiation capacity, the potential of these cells for self-renewal renders them a great source for tissue engineering[132]. Despite these advantages, their practical use has several limitations[125]. BMSCs can only be harvested in small

amounts from bone marrow aspirates, obtained in a difficult and painful surgical procedure[23]. Thus, for clinical applications BMSCs must be further propagated in large quantities limiting their use for clinical applications.

However, another adult stem cell population most often called adipose-derived stem cells (ASCs), have many advantages compared to BMSCs. ASCs are abundantly available in subcutaneous adipose tissue throughout the body and can be easily obtained by minimally invasive liposuction procedure in relatively high quantities[148]. In most individuals adipose tissue is highly abundant and easily accessible. ASCs reside within the stromal vascular fraction (SVF), which can be harvested without notable donor site morbidity[132,149]. A variety of designations have arisen in literature to describe the plastic adherent cell population isolated from collagenase digests of adipose tissue SVF; for instance, these cells are also termed adipose-derived stem/stromal cells (ASCs), adipose-derived adult stem (ADAS) cells, adipose-derived adult stromal cells, adipose-derived stromal cells (ADSCs), adipose stromal cells (ASCs), pericyte, or preadipocyte[40]. According to the International Federation for Adipose Therapeutics and Science (IFATS), these cells are designated as adipose-derived stem cells, which is also used in this work[40]. Although an exact phenotypic definition of ASCs and a clear distinction from fibroblasts is difficult, ASCs display a differentiation potential similar to BMSCs towards bone, cartilage, adipose tissue, muscle, and others. Thus, these cells became one of the most attractive stem cell source for tissue engineering and regenerative medicine[132,150,151]. In recent years also the SVF came to the fore as a promising cell source with regard to vascularization and *in vivo* engraftment of tissue engineered constructs, since the SVF contains many different cell types that contribute to tissue formation[152–154]. In summary, even though both BMSCs and ASCs represent a promising cell source for adipose tissue engineering applications, ASCs are obviously the most suitable cell population for clinical implementation. They can be harvested in a minimal invasive procedure in high quantity and they easily and reproducibly differentiate along the adipogenic lineage as they originate from fat tissue.

1.2.3.2 Three-dimensional scaffolds for tissue engineering applications

Suitable cell carrier systems, referred to as scaffolds, are required to provide mechanical and structural support for seeded cells to develop a transplantable 3D tissue substitute. Therefore, applied biomaterials generally need to be biocompatible, seedable and in many cases even biodegradable with a degradation kinetic of several months. For adipose tissue engineering applications, appropriated materials should provide volume and shape, as well as an adequate pore size, as developing adipocytes drastically increase in size compared to their precursors. This pore size criterion is also important concerning interconnectivity, to deliver sufficient nutrient and oxygen supply as well as the fundament

for vascular ingrowth *in vivo*[18,130]. For this purpose, in regenerative medicine both acellular and cell-based approaches exist. Here, the former approach, which is based on *de novo* adipogenesis *in vivo*, will be included for the sake of completeness. For instance, by the use of a Matrigel-based hydrogel (a tumor product of Engelbreth-Holm-Swarm (EHS) mouse sarcoma) in combination with an angiogenesis inducing growth factor (bFGF) incorporated into the scaffold, it was shown that *de novo* adipose tissue development can be triggered *in vivo*[155–158]. Likewise, hollow structures (i.e. silicone dome) are integrated to protect developing fat tissue for example within the Matrigel matrix and are combined with a vascular pedicle for immediate supply and vascular outgrowth[18,159].

The latter concept of cell-based approaches is of greater importance in this work and is generally separated into approaches with porous scaffolds as well as cell-encapsulating hydrogels and injectable microspheres. Prefabricated porous carriers, comprising synthetic biodegradable polymers, allow the definition and maintenance of shape of the engineered adipose construct. This type of constructs are either implanted directly after cell seeding by surgical intervention or undergo an *in vitro* culture period with or without tissue inductive stimuli prior to implantation[18]. Commonly applied synthetic polymers for adipose tissue engineering attempts are polyglycolic acid (PGA), poly (lactic-co-glycolic) acid (PLGA), and polylactic acid (PLA)[160–164]. These listed materials display ascending degradation kinetics of about a few weeks to a few months, with longer degradation times being favorable for adipose tissue development[18,165]. Over the past years combinations of nanofibrous electrospun PLA scaffolds and hollow PLGA fiber scaffolds encapsulated into hydrogels (i.e. alginate/chitosan) demonstrated the promotion of adipogenic differentiation *in vitro* and *in vivo*[166,167]. Other synthetic biomaterials applied for construct production are represented by polyethylene terephthalate, polycaprolactone, and polycaprolactone-based polyurethane (PU) scaffolds, but these materials are not generally suitable as a single component for adipose tissue formation, since the cells are largely incapable of remodeling the material[89,168]. By contrast, the combination of these shape-providing meshes or foams with other adipogenesis-supportive materials (i.e. fibrin hydrogel) displays a promising attempt for successful fat engineering[169]. Besides the mentioned synthetic materials, also natural materials like silk and extracellular matrix compounds (i.e. hyaluronic acid, collagen) can be applied as meshes, foams, or decellularized scaffolds to generate scaffolding matrices. Silk fibroin-derivates show low immunogenicity, good biocompatibility, and easy processability for tissue engineering applications[18,170]. Displaying a slow degradation rate and a stable structure, this material was shown to support volume-stable adipogenesis of ASCs and BMSCs for *in vitro* cultivation, while satisfactory results were not observed for long term *in vivo* exposure[18,171]. Likewise, a supportive impact on adipogenic differentiation was demonstrated for hyaluronic acid and collagen constructs (i.e. cross-

linked collagen-chitosan), but these constructs showed limited volume-retention and fast degradation kinetics, being unfavorable in the *in vivo* adipogenic context[18,172].

Besides the cross-linked hyaluronan and collagen-chitosan extracellular matrix components, the ECM itself as a scaffolding system has drawn attention for tissue engineering applications. Isolated ECM is applied in tissue engineering attempts both as denatured scaffold (i.e. as foam, mesh, microcarrier, or hydrogels) or as decellularized construct with an intrinsic vasculature. For more detailed information about the latter decellularized matrix scaffolds the reader is referred to Chapter 1.2.3.4. The applied ECM represents a cellular environment that resembles naturally occurring characteristic conditions. Within recent years, denatured scaffolds demonstrated promising results concerning soft tissue engineering, when naturally derived placental decellular matrix (PDM) or decellularized adipose tissue (DAT) was applied as natural matrix meshes, foams, microcarriers and hydrogels [23,173–175]. The latter DAT material, derived from adipose tissue, provided an demonstrable adipo-inductive microenvironment for the adipogenic differentiation of human ASCs even in the absence of exogenous differentiation factors and furthermore facilitated adipose tissue growth *in vivo*[121,175,176]. However, even if the ECM does not derive from adipose tissue, it is expected to direct cellular activities and regenerative events of capital complexity. Therefore, a major prerequisite is the preservation of the complex 3D composition and ultrastructure of the decellularized ECM and the activity of its functional components. Most decellularization protocols preserve the composition of the ECM (comprising collagen, GAGs, laminin etc.), and the ECM remains a physiological depot for various signaling molecules, which retain their functionality. A gentle removal of the cells leaves behind a "footprint" within the ECM, which supports subsequent cell adhesion, proliferation, migration, and differentiation[121]. Autologously applied ECM material is even more favorable, as it displays besides the above mentioned advantages a minimal immunological response[177,178].

An alternative for porous scaffolds are cell-encapsulating hydrogels. A major advantage of hydrogels is the minimal-invasive application by injection, which reduces the risk of infection and scaring, and enables the filling of irregularly shaped defect sites. Alternatively, also in combination with porous scaffolds, cells can be encapsulated in hydrogels by gelling them *in vitro* prior to implantation into the defect site[18]. Alike porous scaffolds, hydrogels can be composed of synthetic materials based on polyethylene glycol (PEG) or its derivates, such as PEG-di(meth)acrylate (PEGDA) or Pluronic F 127[18,179–181]. While PEG represents the most commonly applied synthetic hydrogel material in tissue engineering, a number of studies also applied PEGDA[182,183], both of which are forming stable gels with excellent volume retention[179,180]. Since this material displays a non-adhesive surface, modifications with peptide sequences like RGD (derived from fibronectin), or IKVAV and YIGSR (derived from laminin) improve cell attachment and natural cellular performance[184–186]. In contrast, a naturally

derived material is the previously mentioned Matrigel, which originates from a mouse sarcoma cell line[155]. Therefore, this gel contains many components of the tumor basement membrane like proteoglycans, laminins, collagen type IV and nidogen/entactin. Furthermore, growth factors like transforming growth factor β (TGF-β), basic fibroblast growth factor (bFGF), and platelet-derived growth factor (PDGF) are present within the gel[156,187,188]. Despite the report of a promoting effect on adipogenesis and angiogenesis for *in vivo* application, this gel is unsuitable for human use, due to its potential tumorigenic properties[156,187]. Several years ago, other ECM hydrogels were developed, which are derived from dermal, muscle, or adipose tissue. They also induce adipocyte differentiation *in vitro* and show strong adipogenic potential *in vivo*[189–191]. Furthermore, these hydrogels comprise various ECM components, such as collagen, hyaluronic acid, or fibrin, all of which have been already successfully applied in adipose tissue engineering[192–194]. Among those, fibrin represents the only FDA (American Food and Drug Administration) approved material, which is already clinically applied for wound sealing and during other surgical procedures[18,152]. Additionally, this natural polymer has already been used for many different applications in the field of tissue engineering[195]. Fibrin demonstrates a high degree of biocompatibility and offers the possibility of the generation of autologous scaffolds. However, its fast degradation kinetics due to fibrinolysis and solubility over time, makes fibrin unfavorable for adipose tissue engineering[18]. However, the development of long-term stable fibrin gels can provide a solution, as they demonstrate good results for adipose tissue engineering *in vitro* and *in vivo*[152,169,196].

Another way to administer cells at the defect site is possible through the injection of microspheres to which the cells (ASCs, BMSCs, 3T3-L1) are attached[18]. At present, there exist different materials for the formation of such microspheres, for instance PLGA microspheres[197,198], alginate beads[199], porous collagenous microbeads[200], human ECM powders from adipose tissue[201], and particulate small intestinal submucosa microparticles[18,202].

Taken together there are various scaffolding materials available for adipose tissue engineering, all of which imply many advantages but also some obstacles. Notably, still many scaffolding systems yet display a limitation of size (mostly limited to 1 mL)[18] and largely lack prevascular structures for subsequent *in vivo* vascularization. Currently only a small number of *in vivo* approaches exist exceeding this size limitation for adipose tissue engineering[203–205]. For vascularization strategies in 3D constructs the reader is referred to the next Chapter 1.2.3.3. Due to inherent tissue-promoting properties, the intrinsic prevascular structure and the mostly larger dimension, decellularized matrices represent a pioneering material for future adipogenic engineering approaches to meet this demand. Therefore, the first part of this work aims to generate a construct with prevascular structures in a decellularized jejunal matrix.

1.2.3.3 Vascularization strategies for adipose tissue engineering

A critical point for survival and development of engineered adipose constructs is the supply with nutrients and oxygen, which is hampered by absent, sparse, or delayed vascular supply *in vivo*. Since mature adipose tissue is highly metabolically active and therefore extremely vascularized, with every adipocyte being connected to at least one capillary, it is particularly susceptible to deficient vascularization[19]. An obstacle for larger volume tissue constructs is the diffusion limitation of nutrients and oxygen of about 200 µm[206,207]. Consequently, appropriate vascularization strategies are required for adipose tissue engineering approaches to ensure sufficient vascularization of the construct upon implantation for proper tissue development and prevention of necrosis and volume loss. Different strategies have been developed in order to ensure a vascular supply of the tissue graft.

Scaffold design and fabrication is one possibility to enhance subsequent vascularization *in vivo*. Through integrated microchannels, which provide oxygen and nutrient supply by evading the diffusion limit, vascular migration and alignment are fostered[18,208,209]. In addition, the pore size, the interconnectivity of pores within foams and meshes, and the design of the scaffold architecture (i.e. defined fiber deposition of electrospun meshes) and hydrogels with channels could support vascular ingrowth[18,121,208,210,211]. This kind of approach obviously aims at the development of vasculature upon implantation. Therefore, it may take a while until the scaffold is properly supplied, which contributes to the volume limitation of the implanted construct. In a similar manner, proangiogenic growth factor application, a second kind of potent vascularization strategy, aims at the development of vasculature post implantation. The most prominent applied growth factors are represented by bFGF and VEGF, which are incorporated into the scaffold biomaterial and released into the adjacent host tissue[157,212,213]. This release of growth factors subsequently triggers the ingrowth of host blood vessels[18,129]. It was shown by several studies that controlled and sustained release from microspheres (i.e. PLGA, gelatin, alginate) is more efficient than the application of free growth factors[183,202,214,215]. Furthermore, the incorporation of growth factor-producing cells also triggers vascular ingrowth. In cell-based adipose tissue engineering approaches, cells are integrated within the carrier material, whereby in recent years primarily ASCs have been used for this purpose. Besides their adipogenic differentiation capacity, these cells are strong modulators of adipose tissue angiogenesis, since they release several proangiogenic factors such as VEGF, leptin, HGF and bFGF[26]. To severely increase the secretion of growth factors, ASCs can be transfected to overexpress specific proangiogenic factors, which contribute to vascular cell maturation and development[129,216]. Furthermore, preconditioning under hypoxic condition *in vitro* is capable of triggering enhanced growth factor secretion of ASCs[217]. But even in this kind of approach the limitation of volume and size of the engineered construct remains. Due to delayed vessel ingrowth

in vivo, larger constructs will possibly exhibit lacking tissue development and centrally located necrosis[18].

A third vascularization strategy, which triggers also subsequent *in vivo* vascularization of the implanted construct, is the surgical integration of a vascular pedicle. Employing a complex microsurgical procedure, an arterio-venous (AV) loop or a ligated, flow-through AV bundle are integrated into the developing tissue construct, from which new vessels sprout into the enclosing graft[18,218]. Consequently, within a period of several weeks a vascular network is developed, pervading the scaffold, possibly followed by a subsequent excision of the tissue graft and implantation to the defect site with surgical connection of the main AV bundle to the host circulation[18,218]. An obstacle of this method is donor site morbidity caused by removal of the donor vein graft and scar formation at the site of implantation. However, this technique is not yet transferrable into humans and alike a volume restriction persists due to delayed vascularization[18,218].

Apart from the above-mentioned vascularization strategies, which all rely on subsequent *in vivo* vascular development, prevascularization strategies prior to implantation are a further option. For large, three-dimensional constructs early vascular supply is crucial for homogeneous tissue development, long-term survival, and subsequent successful clinical defect repair[18]. So far, most *in vitro* approaches are based on the application or coculture of endothelial cells. Cocultures of ASCs and endothelial cells, which lead to a prevascularized adipose tissue construct within various scaffold materials (i.e. fibrin microcarrier or a fibrin matrix in combination with a chorioallantoic membrane), have been investigated to a limited extent[18,219,220]. In recent years, the SVF came to the fore by displaying a tremendous vascularization potential for adipose tissue engineering[152,221]. SVF coculture could possibly circumvent some of the endothelial cell-associated obstacles, offering a more physiological cell population for vessel formation, since it contains smooth muscle cells and pericytes together with endothelial and progenitor cells[154,222]. Another approach again concerns scaffold design, which can also achieve prevascularization *in vitro*. Therefore, preformation of microchannels within the construct together with the application of endothelial cells *in vitro* forms prevascular structures, which can supply the tissue upon implantation[18,223].

When implanted, all of these *in vitro* prevascularization strategies rely on the formation of connections between the prevascular scaffold structures and the surrounding vasculature, enabling rapid and sufficient oxygen as well as nutrient supply for further tissue development[18,208,218,224]. In contrast, ECM matrices (e.g., jejunal segments) display a preserved decellularized vasculature, which is reseedable with, for example, endothelial cells (or in future attempts with cells of the stromal vascular fraction, see Chapter 1.2.3.4). Thus, the ECM could possibly circumvent this hurdle, since most of these matrices exhibit an arterio-venous connection, which can be microsurgically connected to the

host circulation[225,226]. This technique is under general investigation with *in vitro* and animal experiments, and it is not only limited to adipose substitutes but also applicable for other tissue grafts.

In conclusion, it must be taken into account that angiogenesis and adipogenesis are in a high physiological dependence and therefore adipose tissue engineering approaches should focus on both processes to generate clinically relevant tissue substitutes[18]. The complexity of adipose tissue physiology is determined by a high coordination of cell interactions, which makes the generation of a vascularized transplantable adipose tissue graft a challenging task. There are various obstacles on this way, such as the choice of cells, a suitable scaffolding as well as the best coculture system and the adjustment of coculture conditions. The challenge is to engineer a solid vascularized construct with mature and functional adipocytes that comes close to the physiological status of mature adipose tissue.

1.2.3.4 Extracellular matrix scaffolds to foster vascularization for adipose tissue engineering

Since tissue engineering evolved from the idea of off-the shelf whole organ replacement to a fusion of tissue engineering and regenerative medicine, which is focusing on tissue and organ restoration and maintenance, the use of whole decellularized organs is out of focus. The ECM itself as scaffolding system draw attention, as biomaterials play a pivotal role in the success of tissue engineering[121,227]. This class of natural biomaterials is termed decellularized tissue-derived biomaterials. It is obtained by the elimination of all cellular components and nuclear material of the native tissue and derives for instance from dermis, heart valves, blood vessels, small intestinal, liver, adipose tissue, or placenta[23,121,176]. As previously mentioned, the extracted ECM is applied in tissue engineering attempts both as denatured scaffold (i.e. as foam, mesh or microcarrier etc.) or as decellularized construct with an intrinsic vasculature. This paragraph is focusing on the latter approach. For more detailed information for denatured ECM scaffolds, the reader is referred to Chapter 1.2.3.2.

Besides decellularized skin/adipose tissue flaps (from rats), placental decellular matrix (from native human placenta), decellularized coronary artery tissue-flap (from native cardiac muscle of the rat), and decellularized porcine jejunal segment (form porcine small bowel) are applied in approaches for tissue engineered grafts[121,173,225,226,228]. The latter represents one of the most established and broadly applied biological matrices termed SIS (small intestinal submucosa), which offers key features of a highly supportive scaffold and presents growth factors and adhesion peptide sequences, which facilitate integration with surrounding tissue upon implantation[114,121,228]. After decellularization and

with preservation of the arterial and venous mesenteric pedicles and all other structures (preserved structures are serosa, muscle layer, submucosa, and mucosa), the decellular jejunum exhibits a perfusable vessel bed creating a biological vascularized scaffold for artificial *in vitro* vascularization[228–230]. After decellularization, terminal sterilization and long-term storage, the matrix still contains a pool of adhesion molecules (e.g., fibronectin and laminin), the proteoglycan decorin, the glycoproteins biglycan and entactin, and intact bioactive molecules like TGF-β, bFGF and VEGF[114,121,228]. Even if the decellularized jejunal segment is from xenogeneic origin, it (frequently applied as SIS material in the clinic, without preserved vasculature) displays excellent biocompatibility in clinical use with low or no immunogenicity[121]. Upon implantation in humans, the material of natural origin demonstrates a slow degradation and is properly replaced or remodeled with a new matrix produced by surrounding or residing cells[121,231]. However, the understanding of the cellular processes involved in the recellularization and revitalization of these biological scaffolds still remains incomplete[121,232]. In recent years, the use of decellularized composite tissue matrix to engineer vascularized composite tissue has developed further[226]. For instance, researchers repopulated these segments of porcine small bowel with its artery and vein structure already with multiple types of cells to generate tissues like human bladder and liver *in vitro* or human vascularized tissue *in vivo*[229,230,233,234]. Reported advantages of this material are based on supporting attachment, proliferation, and differentiation of cells within a luminal matrix. This matrix can be reseeded with a great variety of cells (as for example porcine bladder smooth muscle cells, urothelial cells, or patient's autologous muscle cells with fibroblasts), but also the dense preformed vascular network can be repopulated with vascular cells via its arterial or venous access[121,234,235]. However, disadvantages of the naturally derived biomaterial include generally weak mechanical strength and inconsistency in compositions and properties with batch to batch variability[121]. On the other hand, one of the main advantages of the matrix is that it can be connected to bioreactors enabling the *in vitro* generation of complex tissues, which require sophisticated culture conditions with physiological stimuli[236]. With the bioreactor technology, shown by Schanz et al., 2010 and Schuerlein et al., 2017, the reseeded vasculature can be perfused with culture medium under physiological cell culture conditions (5% CO_2, 37 °C), and an oscillating pulse of 80-120 mmHg, which mimics the physiological blood flow[234,236,237]. Under these conditions, not only the supply of a 50-100 mm long engineered tissue with nutrients and oxygen is ensured, but also a physiological stimulus is applied, that has been reported to support the formation of a functional network of endothelial cells coating the blood vessels, the so-called endothelium[225,234,236]. It has been proven that a more on natural conditions based type of culture leads to improved physiological tissue development[18,238,239].

In summary, the progress in the use of decellularized composite tissue matrices to engineer vascularized composite tissue was progressive in recent years representing a promising approach for adipose tissue engineering[213]. Since most of the recent vascularized adipose tissue engineering attempts have been size restricted due to delayed vascularization or connection of the prevascular structures, such a matrix could provide a remedy in this case. Therefore, the challenging task of this work was to develop functional adipocytes within the lumen and endothelial cell-coated vessels throughout the construct, with a suitable coculture system by using a versatile modular bioreactor platform. A further advantage of the jejunal segment is represented by the possibility of a surgical anastomosis of the prevascularized construct to the host circulation, which could ensure immediate supply *in vivo* and enable clinical transferability.

1.3 Goals of the thesis

In reconstructive and plastic surgery still exists a tremendous need for adequate tissue implants, since available strategies of autologous transplantation are limited by many complications including transplant failure and donor site morbidity. Tissue engineering approaches can potentially meet this need, as they can be used to produce autologous substitutes *in vitro* and *in vivo*. Although it is a promising discipline, several obstacles have to be overcome. One of the major hurdles currently faced by both *in vitro* and *in vivo* adipose tissue engineering approaches is their limitation by inadequate vascularization, which remains a critical factor as only sufficient vascularization enables a certain graft size and survival of the implant in humans. A further obstacle is the still insufficient knowledge of the cells applied. To produce adequate tissue transplants, deeper insights especially into the characteristics and behavior of human adipose-derived stem cells (hASCs) appear desirable. These cells can be easily isolated in large number from liposuction of abdominal fat depots, yielding low donor site morbidity. Physiological properties of ASCs, such as proliferation and intrinsic differentiation capacity, need to be thoroughly investigated. These findings can then be specifically used for new approaches, e.g., through the administration of specific growth factors for improved differentiation. Furthermore, research on their intercellular communication, which has hardly been investigated to date, may also help to produce more suitable tissue substitutes.

Therefore, this thesis aimed at the development of a prevascularized 3D adipose construct *in vitro* and fundamentally investigates strategies for improved adipogenic differentiation of ASCs.

This work included the following objectives:

1. The development of an engineered prevascularized adipose tissue substitute *in vitro* by using a decellularized porcine jejunal segment, seeded with human adipose-derived stem cells (hASCs) and human microvascular endothelial cells (hMVECs) and co-cultured under physiological and dynamic conditions in a custom-made bioreactor system.
2. The evaluation of the effect of basic fibroblast growth factor (bFGF) on ASC proliferation and differentiation capacity by applying different concentrations, at different time points of culture, to foster improved *in vitro* conditions for adipogenic differentiation.
3. The investigation on the presence of gap junctions in ASC and gap junctional intercellular communication (GJIC) in these cells with regard to its impact on adipogenic differentiation.

1.3.1 *In vitro* development of a prevascularized adipose tissue construct using a decellularized porcine jejunal segment

Current clinical approaches to treat severe full-thickness wounds caused by trauma, congenital disease, or tumor resection[240–242] often use either free or pedicled autologous tissue flaps, or artificial replacements[1,116–118]. However, these approaches are often limited by complications including flap failure, donor site morbidity, highly complex and challenging microsurgical procedures with long recovery periods, as well as the rejection and shrinking of autologous and artificial materials[128,183,243]. Thus, an engineered adipose tissue substitute that is capable of reconstructing the function and shape of the subcutaneous soft tissue layer, which upon implantation can be immediately supplied with nutrients, would be highly desirable[18]. Therefore, in this investigation, a recently established decellularized porcine jejunal segment[244,245] was investigated with regard to its usability for engineering adipose tissue *in vitro*. For this purpose, ASCs and MVECs were co-cultured within the matrix (within the lumen and preserved vascular structure, respectively) under physiological conditions by means of a custom-made bioreactor system. Tissue development was examined regarding differentiation and adipose extracellular matrix deposition. Due to its preserved vascular structures as well as connecting vein and artery the engineered construct can potentially be microsurgically anastomosed to the host circulation and may be fully supplied upon implantation (see Chapter 4.1).

1.3.2 Evaluation of the effect of basic fibroblast growth factor (bFGF) on ASC proliferation and differentiation capacity

In tissue engineering and regenerative medicine approaches a huge number of cells are required to entirely seed complex and large 3D matrices or scaffolds. Thus, cells need to be large-scale expanded *in vitro* on the premise of not losing their differentiation capacity, caused by replicative aging[246]. Furthermore, at present an improved differentiation of ASCs in adipose tissue engineering approaches still remains desirable since most engineered constructs exhibit an inhomogeneous differentiation pattern. Regarding these requirements, growth factor application can lead to a significant improvement, since they demonstrably possess a great influence both on proliferation and differentiation capacity of mesenchymal stem cells[247,248]. It has been reported in various culture systems that bFGF represents a potent mitogen for human MSCs, while maintaining or even promoting their osteogenic, chondrogenic, and adipogenic differentiation potential[37,56,249–252]. Currently, different contradictory information on the applied bFGF concentration and the explicit effect of bFGF on ASC differentiation is present in literature, nevertheless indicating a high potential for adipose tissue

engineering applications. Therefore, in this work the effect of bFGF in 2D culture on ASC proliferation and differentiation capacity, by applying different concentrations of bFGF at different time points of culture, was addressed (see Chapter 4.2).

1.3.3 Investigation on gap junctional intercellular communication in ASCs with regard to its impact on adipogenic differentiation

Despite the multitude of literature on the differentiation capacity of ASCs, little is reported about the physiological properties contributing to and controlling the process of lineage differentiation[253,254]. Direct intercellular communication between adjacent cells via gap junctions has been shown to modulate differentiation processes in other cell types, with connexin 43 (Cx43) being the most abundant isoform of the gap junction-forming connexins[68,69,72]. Since investigations on gap junctions in ASCs were nearly absent in literature, first the basis for the examination of gap junctional intercellular communication (GJIC) had to be laid with regard to immunohistochemical detection of Cx43 and effective blocking of GJIC (see Chapter 4.3). In a next step, investigations focused on the expression of Cx43 and GJIC in human ASCs were conducted. Functionality of gap junctional intercellular communication was proven by dye transfer analysis and its significance for adipogenic differentiation of these cells was evaluated (see Chapter 4.4).

2 Materials

2.1 Instruments

Table 2.1: Overview of instruments.

Instrument	Supplier	Central office
Accu-jet® pro	Brand	Wertheim, Germany
Centrifuge Rotina 420 R	Hettich	Tuttlingen, Germany
Centrifuge SIGMA 1-14	SIGMA Laborzentrifugen GmbH	Osterode, Germany
CO_2 incubator	IBS Integra Biosciences	Fernwald, Germany
Cryostat CM 3050S	Leica	Wetzlar, Germany
Custom-made bioreactor system incl. custom-made roller pump	Department of Tissue Engineering and Regenerative Medicine	University of Würzburg, Germany
FACSCanto flow cytometer	BD Biosciences	Heidelberg, Germany
FluorChem FC2 Imager	Alpha Innotec	San Leandro, USA
Electrophoresis- and blotting chamber	Bio-Rad	Munich, Germany
Hemacytometer Neubauer	Paul Marienfeld GmbH	Lauda, Germany
Laminar flow box Typ-HS18	Heraeus	Hanau, Germany
Laminator	Severin	Sundern, Germany
Orbital shaker Unimax 1010	Heidolph	Schwabach, Germany
Mastercycler® Gradient	Eppendorf	Hamburg, Germany
Magnetic stirrer	VWR	Darmstadt, Germany
Microscope BX51/DP71 camera	Olympus	Hamburg, Germany
Microscope IX51/XC30 camera	Olympus	Hamburg, Germany
Mini-PROTEAN™ Tetra Cell System	Bio-Rad	Munich, Germany
MRX microplate reader	Dynatech Laboratories	Chantilly, USA
NanoDrop 2000c	Thermo Scientific	Waltham, USA
pH-meter HI2210	Hanna Instruments	Kehl am Rhein, Germany
Pipettes Research® Plus	Eppendorf	Hamburg, Germany
PowerPac® basic power supply	Bio-Rad	Munich, Germany

Instrument	Supplier	Central office
Real-Time PCR Detection System CFX96T™	Bio-Rad	Munich, Germany
Tecan GENios pro spectrofluorometer	Tecan	Crailsheim, Germany
TissueLyser	Qiagen	Hilden, Germany
Thermomixer comfort MTP	Eppendorf	Hamburg, Germany
Thermomixer MHR 23	DITABIS	Pforzheim, Germany
Ultrasonic homogenizer SonoPlus	Bandelin	Berlin, Germany
Vortex, IKAR MS3 basic	IKAR	Staufen, Germany
Water bath	Memmert	Schwabach, Germany

2.2 Consumables

Table 2.2: Overview of used consumables.

Consumable	Supplier	Central office
Bottle top-filter Nalgene®	Thermo Scientific	Waltham, USA
Coverslip 24 x 60 mm	MENZEL	Braunschweig, Germany
Coverslip Ø 15 mm	Hartenstein	Würzburg, Germany
Cryovials CryoPure 2.0 mm	Sarstedt	Nümbrecht, Germany
Disposable forceps ratiomed®	Megro GmbH	Wesel, Germany
Falcon cell strainers 100 µm	BD Biosciences	Heidelberg, Germany
Hardshell PCR plates, 96-well, thin wall	Bio-Rad	Munich, Germany
Microseal® 'C' Film	Bio-Rad	Munich, Germany
Microtome blades	Feather	Osaka, Japan
6 & 12-well plates	Greiner Bio-One	Frickenhausen, Germany
24-well plates	Thermo Scientific	Waltham, USA
96-well plate	TPP	Trasadingen, Switzerland
96-well plate black	Thermo Scientific	Waltham, USA
Parafilm	Pechiney	Chicago, USA
PAP pen liquid blocker	Sigma-Aldrich	Munich, Germany
PCR-strips 8 tubes 0.2 mL	Carl Roth GmbH	Karlsruhe, Germany
Pipette filter tips	Starstedt	Nümbrecht, Germany

Consumable	Supplier	Central office
Pipette tips	Starlab	Hamburg, Germany
Pipettes serological	Greiner Bio-One	Frickenhausen, Germany
Polypropylene Tubes 15 mL/50 mL	Greiner Bio-One	Frickenhausen, Germany
SafeSeal micro tubes 1.5 mL/2.0 mL	Sarstedt	Nümbrecht, Germany
Sample cup PE 2.5 mL	Hartenstein	Würzburg, Germany
Scalpels	Feather	Osaka, Japan
SuperFrost™ plus glass slide	R. Langenbrinck	Emmendingen, Germany
Syringe Filter Minisart® 0.2 µm	Sartorius AG	Göttingen, Germany
Syringes	BD Biosciences	Heidelberg, Germany
Syringes Omnican40	B. Braun	Melsungen, Germany
Tissue culture flasks T25/ T75/ T175	Greiner Bio-One	Frickenhausen, Germany
Whatman® cellulose chromatography paper	Simga-Aldrich	Munich, Germany
Whatman® nitrocellulose membrane	Simga-Aldrich	Munich, Germany

2.3 Chemicals

If not otherwise stated in Table 2.3 or the Methods section (Chapter 3), all chemicals and reagents utilized for the preparation of buffers and solutions were obtained from Sigma-Aldrich (Munich, Germany) and Carl Roth GmbH (Karlsruhe, Germany).

Table 2.3: Overview of used chemicals.

Chemical	Supplier	Central office
AGA (18α-glycyrrhetinic acid)	Santa Cruz	Heidelberg, Germany
Amersham™ ECL Prime Western Blotting Detection Reagent	GE Healthcare	Freiburg, Germany
Ambion RNaseZAP	Life Technologies	Karlsruhe, Germany
Antibody diluent, Dako REAL™	Dako	Hamburg, Germany
Aqua ad iniectabilia	B. Braun	Melsungen, Germany
bFGF (basic fibroblast growth factor)	BioLegend	London, UK
Biological vascularized jejunal segment, porcine	Department of Tissue Engineering and Regenerative Medicine	University of Würzburg, Germany
BODIPY 493/503	Invitrogen	Karlsruhe, Germany

Chemical	Supplier	Central office
Bovine Insulin	Sanofi-Aventis	Frankfurt, Germany
Brilliant III Ultra-Fast SYBRR Green qPCR Master Mix	Agilent	Santa Clara, USA
Calcein-AM Viability Stain	BD Biosciences	Heidelberg, Germany
Collagenase NB4	Serva Electrophoresis	Heidelberg, Germany
DAPI mounting medium ImmunoSelect®	Dako	Hamburg, Germany
DiD Vybrant™ cell-labeling solution	Thermo Scientific	Waltham, USA
DNase I	Roche	Basel, Swiss
Dulbecco's phosphate-buffered saline (DPBS) no calcium, no magnesium	Life Technologies	Karlsruhe, Germany
Distilled water (DNase/RNase free)	Life Technologies	Karlsruhe, Germany
FACS clean solution	BD Biosciences	Franklin Lakes, USA
FACS sheath solution	BD Biosciences	Franklin Lakes, USA
FACS shutdown solution	BD Biosciences	Franklin Lakes, USA
Glycergel® Mounting Medium	Dako	Hamburg, Germany
GZA (glycyrrhizic acid)	Santa Cruz	Heidelberg, Germany
Hematoxylin	Bio Optica	Milan, Italy
Hoechst 33258 dye	Polysciences	Warrington, USA
ImProm-II™ Reverse Transcriptation System Kit	Promega	Madison, USA
IBMX (3-Isobutyl-1-methylxanthine)	Serva Electrophoresis	Heidelberg, Germany
Live/Dead Cell Staining Kit II	PromoKine	Heidelberg, Germany
MESA GREEN qPCR MasterMix Plus for SYBR® Assay	Eurogentec	Seraing, Belgium
Microplate BCA™ Protein Assay Kit	Thermo Scientific	Waltham, USA
MTT (3-(4,5-dimethylthiazol-2-yl)-2,5 diphenyltetrazoliumbro-mid)	Serva Electrophoresis	Heidelberg, Germany
Novex® sharp protein standard	Life Technologies	Karlsruhe, Germany
PBS (Dulbecco A)	Thermo Scientific	Waltham, USA
Pepsin (Digest All™-3)	Invitrogen,	Karlsruhe, Germany
Phalloidin-iFluor 555 Reagent - CytoPainter	Abcam	Cambridge, UK
Phosphate buffered saline (Dulbecco A) tablets	Thermo Scientific	Waltham, USA
Proteinase K (Digest-All 4)	Life Technologies	Karlsruhe, Germany
Serum Triglyceride Determination Kit	Simga-Aldrich	Munich, Germany

Chemical	Supplier	Central office
Terralin Liquid® disinfectant	Schülke	Norderstedt, Germany
Thesit®	Gepepharm	Hennef, Germany
TISSEEL fibrin sealant	Baxter	Unterschleißheim, Germany
Tissue-Tek® O.C.T. compound	Sakura Finetek	Zoeterwonde, Netherlands
TRIzol® reagent	Life Technologies	Karlsruhe, Germany
Tween® 20	Applichem	Darmstadt, Germany
Trypsin-EDTA 0.25%	Life Technologies	Karlsruhe, Germany
ZombieNIR™ Fixable Viability Kit	BioLegend	London, UK

2.4 Antibodies

Table 2.4: Overview of used antibodies.

Antibody	Type/Source	Application/Dilution	Supplier
Alexa Fluor™ 488 anti-rabbit	Polyclonal IgG goat	IHC: 1:400	Jackson Immuno (111-545-003)
Alexa Fluor™ 594 anti-rabbit	Polyclonal IgG goat	IHC: 1:400	Jackson Immuno (111-585-008)
Anti-β-actin	Monoclonal IgG mouse	IHC: 1:500	Sigma-Aldrich (A5441)
Anti-CD31	Monoclonal IgG mouse	IHC: 1:200	Dako Clone JC70A (M0823)
Anti-ColIV	Monoclonal IgG mouse	IHC: 1:25	Dako (M0785)
Anti-Cx43 (GJA1)	Polyclonal IgG rabbit	IHC: 1:500 WB: 1:6,000	Abcam (ab11370)
Anti-laminin	Polyclonal IgG rabbit	IHC: 1:200	Abcam (ab11575)
Anti-Ki-67	Monoclonal IgG mouse	IHC: 1:150	Dako Clone MIB1 (M7240)
Cy™3 anti-mouse	Polyclonal IgG donkey	IHC: 1:400	Dako (22-165-003)
HRP anti-rabbit	Polyclonal IgG goat	WB 1:1,000	Dako (P0448)

Antibody	Type/Source	Application/Dilution	Supplier
HRP anti-mouse	Polyclonal IgG rabbit	WB 1:1,000	Dako (P0161)
IgG1 negative control	Polyclonal IgG mouse	IHC: according to primary antibody concentration	Dako (X0931)
IgG1 isotype control	Polyclonal IgG rabbit	IHC: according to primary antibody concentration	Dianova Clone pAK (DLN-13121)

2.5 Primers

Table 2.5: Overview of used primers.

Gene	Gene Symbol	Unique Assay ID/ Sequence	Supplier
C/EBPα	*CEBPA*	QT01667694	Qiagen
PPARɣ	*PPARG1*	QT00029841	Qiagen
aP2	*FABP4*	QT00203357	Qiagen
Adiponectin	*ADIPOQ*	QT00058716	Qiagen
Cx43	*GJA1*	qHsaCID0012977	BioRad
EF1α	*EEF1A1*	F: CCCCGACACAGTAGCATTTG R: TGACTTTCCATCCCTTGAACC	Biomers

2.6 Cells

Besides purchased cells, which are listed in this section, also enzymatically purified adipose-derived stem cells were used from abdominal adipose tissue from female donors.

Table 2.6: Overview of used cells.

Cell Type	Source	Ref./Lot Number	Supplier
Adipose-derived stem cells (Amp)	Human abdominal adipose tissue (female)	PT5006 Lot 0000407088	Lonza, Walkersville, USA
Microvascular endothelial cells (HMVEC-dBIAd)	Human dermal blood	CC2811 Lot 0000125028	Lonza, Walkersville, USA

2.7 Cell culture media

Table 2.7: ASC medium.

Medium	Composition
ASC basal medium	Dulbecco's Modified Eagle's Medium/Ham's F-12 (DMEM/F12, Invitrogen, Karlsruhe, Germany) supplemented with 1% penicillin/streptomycin (100 U/mL penicillin, 0.1 mg/mL streptomycin) and 10% fetal bovine serum (both from Invitrogen, Karlsruhe, Germany)
ASC growth medium	Preadipocyte basal medium-2 (PBM-2; Lonza, Walkersville, USA) supplemented with 1% penicillin/streptomycin (100 U/mL penicillin, 0.1 mg/mL streptomycin) and 10% fetal bovine serum (both from Invitrogen, Karlsruhe, Germany)
ASC differentiation medium	Growth medium with 1.7 µM insulin (Sanofi-Aventis, Frankfurt, Germany), 1 µM dexamethasone, 200 µM indomethacin (both from Sigma-Aldrich, Steinheim, Germany) and 500 µM 3-isobutyl-1-methylxanthin (IBMX; Serva Electrophoresis, Heidelberg, Germany)
ASC maintenance medium	Growth medium with 1.7 µM insulin (Sanofi-Aventis, Frankfurt, Germany)
ASC cryopreservation medium	Basal medium, supplemented with 5% DMSO

Table 2.8: MVEC medium.

Medium	Composition
MVEC growth medium	VascuLife® growth medium (VascuLife® basal medium (LM0002) with VascuLife®VEGF LifeFactors Kit (LS1020); LifeLine, Troisdorf, Germany) supplemented with 1% penicillin/streptomycin (100 U/mL penicillin, 0.1 mg/mL streptomycin; Invitrogen, Karlsruhe, Germany)
MVEC cryopreservation medium	MVEC growth medium, supplemented with 5% DMSO

Table 2.9: Co-culture medium.

Medium	Composition
1:1 growth medium	1:1 ASC and MVEC growth medium
1:1 differentiation medium	1:1 ASC and MVEC growth medium with 1.7 µM insulin (Sanofi-Aventis, Frankfurt, Germany), 1 µM dexamethasone, 200 µM indomethacin (both from Sigma-Aldrich, Steinheim, Germany)

Medium	Composition
	and 500 µM 3-isobutyl-1-methylxanthin (IBMX; Serva Electrophoresis, Heidelberg, Germany)
1:1 maintenance medium	1:1 ASC and MVEC growth medium with 1.7 µM insulin (Sanofi-Aventis, Frankfurt, Germany)

2.8 Buffers and solutions

Table 2.10: Overview of used buffers and solutions.

Buffer / Solution	Composition
Adipogenic inducer stock solutions	Insulin (1.7 mM): 10 mg/mL dissolved in 30 mM HCl. IBMX (25 mM): 5.55 mg/mL dissolved in ddH_2O, Na_2CO_3. Dexamethasone (10 mM): 3.925 mg/mL dissolved in abs. ethanol. Indomethacin (50 mM): 17.89 mg/mL dissolved in abs. ethanol.
Basic FGF stock solution	10 mg/mL are dissolved in PBS with 1% BSA.
Blocking solution (IHC)	1.5% BSA dissolved in PBS.
Blocking buffer (WMS)	1.5% BSA dissolved in PBS with 0.3% Triton X-100
BODIPY stock solution	1 mg/mL is dissolved in DMSO.
PBS/Triton X-100	0.3% Triton X-100 diluted in PBS.
Buffered formalin	3.7% formalin (37% stock solution) diluted in PBS.
Citric acid buffer	25 g citric acid monohydrate, 6 mL glacial acid, 60 g sodium acetate trihydrate and 17 g NaOH, are dissolved in ddH_2O (ad 500 mL). Add 100 mL ddH_2O, and 150 mL 2-propanol. Adjust carefully to pH 6.0 and store at 4°C under toluene.
Collagenase buffer	0.1 M Hepes, 0.12 M NaCl, 0.05 M KCl, 0.001 M $CaCl_2$, and 0.005 M glucose are dissolved in ddH_2O. Adjust carefully to pH 7.4 and store at 4 °C. For digestion freshly add 1.5% bovine serum albumin and 0.1% collagenase NB4 from *Clostridium histolyticum* and sterilize with a 0.2 µm bottle top-filter.
FACS buffer	1% BSA is dissolved in PBS.
Hoechst 33258 stock solution	2 mg/mL is dissolved in ddH_2O.
Nile red stock solution	1 mg/mL is dissolved in DMSO.
ORO staining solution	0.5 g ORO is dissolved in 100 mL isopropanol and 66.6 mL ddH_2O are added. Filtrate twice before use.

Buffer / Solution	Composition
Papain digestion buffer	17 mg L-cysteine and 2 U/mL papain are dissolved in 20 mL PBE buffer and sterilized with a 0.2 µm syringe-filter.
PBE buffer	6.53 g Na_2HPO_4, 6.48 g NaH_2PO_4, 10 mL 500 mM EDTA are dissolved in 900 mL ddH_2O. Adjust to pH 6.5 and bring volume to 1 L with ddH_2O and sterilize with a 0.2 µm bottle top-filter.
PBS	10 PBS (Dulbecco A) tablets are dissolved in 1 L ddH_2O.
PBST	0.1% Tween® 20 dissolved in PBS.
Phosphate saline buffer	50 mM (Na_2HPO_4*$2H_2O$ (178 g/mol), NaH_2PO_4*H_2O (138 g/mol)), 2 mM Na_2EDTA*$2H_2O$, and 2 M NaCl are dissolved in ddH_2O and pH is adjusted to 7.4 with NaOH or HCl.
Running buffer	25 mM Tris, 192 mM Glycin, 0.1 % SDS are dissolved in ddH_2O. pH 8.3 (don't adjust the pH with HCl or NaOH).
Running gel buffer	1 M Tris is dissolved in ddH_2O and pH is adjusted to 8.8 with NaOH or HCl.
Stacking gel buffer	0.5 M Tris-HCl is dissolved in ddH_2O and pH is adjusted to 6.8 with NaOH or HCl.
TEN buffer	0.1 M NaCl, 1 mM EDTA, 10 mM Tris is dissolved in ddH_2O; adjust to pH 7.4.
Transfer buffer	25 mM Tris, 192 mM, 10% methanol are dissolved in ddH_2O.
Thrombin dilution buffer	40 mM $CaCl_2$, 171 mM NaCl and 40 mM glycine dissolved in ddH_2O. Adjust to pH 7.4.
WB blocking solution	5% non-fat dried milk powder is dissolved in PBST.

2.9 Software

Table 2.11: Overview of used software.

Software/Version	Supplier	Central office
CellSense™ 1.16	Olympus	Hamburg, Germany
FlowJo v.10.0.7	Treestar	San Carlos, USA
GraphPad Prism Version 6.0	GraphPad Sofware	LaJolla, USA
Microsoft Office 2016	Microsoft	Redmond, USA

3 Methods

3.1 Isolation of adipose-derived stem cells

Human adipose-derived stem cells (hASCs) were isolated from subcutaneous abdominal adipose tissue of healthy female patients undergoing plastic surgery. Donors were between 20 and 40 years of age and had a body mass index ranging from 28 to 33. Written informed consent was obtained from all patients. The obtained tissue was minced and digested in fresh collagenase buffer (Hepes 0.1 M, NaCl 0.12 M, KCl 0.05 M, $CaCl_2$ 0.001 M, glucose 0.005 M, 1.5% bovine serum albumin (BSA) and 0.1% Collagenase NB4 from *Clostridium histolyticum*) for 2h at 37 °C under dynamic conditions (50 rpm) on an orbital shaker. The resulting digested adipose suspension was centrifuged at 300 x g for 10 minutes, the floating top fat layer was decanted, and the remaining suspension was filtered through a 100 µm nylon mesh. After another centrifugation step (300 x g for 10 min) the remaining cell pellet was washed with PBS. The obtained stromal vascular fraction (SVF) was resuspended in basal medium, consisting of Dulbecco's Modified Eagle's Medium / Ham's F-12 (DMEM/F12; Thermo Scientific, MA, USA) containing 1% penicillin/streptomycin (100 U/mL penicillin, 0.1 mg/mL streptomycin) and 10% fetal bovine serum (FBS). The obtained cell fraction was either cultured (see Chapter 3.2) or stored in liquid nitrogen by adding 5% DMSO to the basal medium, for cryopreservation.

3.2 Cell culture of ASCs and MVECs

3.2.1 Expansion culture

Both purchased human ASCs (human adipose-derived stem cells (Amp), #PT5006; Lonza, Walkersville, USA) and isolated ASCs (described in Chapter 3.1) were applied in the experiments presented in this work (as indicated). The cells were routinely expanded and cultured in tissue culture-treated plastic flasks in basal medium (DMEM/F12, supplemented with 1% penicillin/streptomycin (100 U/mL penicillin, 0.1 mg/mL streptomycin), 10% fetal bovine serum (FCS)), and 3 ng/mL basic fibroblast growth factor (bFGF, BioLegend, London, United Kingdom), if not otherwise stated. Human microvascular endothelial cells (HMVEC-dBlAd; CC2811; Lonza, Walkersville, USA) were cultured in VascuLife® growth medium (VascuLife® basal medium LM0002 with VascuLife®VEGF LifeFactors Kit LS1020; LifeLine, Troisdorf, Germany) supplemented with 1% penicillin/streptomycin for routine expansion. Cultures were maintained at 37 °C in a humified atmosphere at 5% CO_2 and 21% O_2, with culture medium exchanged every other day. Cells were passaged and harvested for experiments by

using a 0.25% trypsin-EDTA solution. For subsequent experiments, both cell types were used in passage 3 or 4. From the moment of seeding into an experiment, ASCs were cultured in growth medium consisting of preadipocyte basal medium-2 (PBM-2, supplemented with 1% penicillin/streptomycin and 10% FBS) and MVECs further on with VascuLife® growth medium. Cells were either seeded into tissue culture-treated well plates (6-well and 24-well plates), for immunohistochemical staining procedures (Cx43 staining) additionally equipped with coverslips (ø 15 mm, see Chapter 3.11.2), into 3D hydrogel constructs (see Chapter 3.7.1) or onto the decellularized porcine jejunal matrix (see Chapter 3.6).

3.2.2 Investigation of gap junctional intracellular communication (GJIC)

For subsequent experiments, cells in passage 3 or 4 were used and seeded with different densities ranging from 5,000 to 100,000 cells per cm^2 in growth medium consisting of preadipocyte basal medium-2 (PBM-2; Lonza, Walkersville, USA) supplemented with 1% penicillin/streptomycin and 10% FBS. To block gap junctional intercellular communication (GJIC), the reversible inhibitor 18-α-glycyrrhetinic acid (AGA) and the non-inhibitory analog of AGA, glycyrrhizic acid (GZA), were used, both purchased from Santa Cruz Biotechnologies (Santa Cruz, USA)[255]. AGA and GZA were prepared as 20 mM stock solutions dissolved in dimethyl sulfoxide (DMSO) and used in appropriate dilutions. The final concentration of DMSO as a solvent control was kept in all experiments at a maximum concentration of 0.5%.

3.3 Adipogenic induction of ASCs in 2D

Adipogenic differentiation was induced by changing growth medium to differentiation medium (growth medium (preadipocyte basal medium-2 (PBM-2) supplemented with 1% penicillin/streptomycin and 10% FBS) with 1.7 µM insulin, 1 µM dexamethasone, 500 µM 3-isobutyl-1-methylxanthine (IBMX), and 200 µM indomethacin). According to the experimental setup, cells were cultured up to 14 days, while media exchange was performed every other day. As a control, cells were cultured in growth medium without adipogenic induction for the entire period of culture (permanent induction). For short-term induction, medium was exchanged to maintenance medium (growth medium with 1.7 µM insulin) after two days and continued for the final culture period.

3.4 Isolation and decellularization of a porcine jejunal segment

All experiments employing porcine jejunal segments in a flow-through bioreactor system were performed in the Department of Tissue Engineering and Regenerative Medicine, University of Würzburg, Head: Prof. Dr. Heike Walles.

Biological vascularized scaffolds (decellularized porcine jejunal segment) were obtained from German Landrace pigs (weighing 15 to 25 kg). The animals received humane care in compliance with the Directive 2010/63/EU of the European Parliament and of the Council of 22 September 2010 on the protection of animals used for scientific purposes and the German Animal Welfare Act (last amended by Art. 3 G v. 28.7.2014 I 1308) after approval from the institutional animal protection board. Using a standardized previously described decellularization protocol[230,244], the vascular structure of the native tissue stays intact and can be then reseeded with human endothelial cells generating a functional vasculature (see Chapter 3.6). Briefly, an approximately 120 mm long porcine jejunum segment that was supplied by a single artery-vein-pair was explanted carefully without harming the outer vascular system. The native tissue was decellularized by perfusing the vasculature with sodium-desoxycholate (Sigma-Aldrich, Steinheim, Germany) under constant pressure conditions at 100 mmHg and by DNase I (Roche, Basel, Swiss) digestion. After sterilization by gamma irradiation, the matrix was stored at 4 °C.

3.5 Custom-made bioreactor system for dynamic culture

To ensure robust culture conditions, a specific bioreactor system was previously developed[236]. A schematic of the bioreactor system and an outline of the experimental set-up are depicted in Figure 3.1. The decellularized matrix segments were put into medium-filled glass reactors and connected with their artery to the circulation (Figure 3.1 A). Perfusion was performed under simulated physiological conditions. The dynamic culture was designed to provide medium flow by a roller pump (500 mL/min) in the same way as the heart pumps blood through the human circulatory system in pulses. In the bioreactor the pulse is adjusted in a range from 80 to 200 ± 30 mmHg, with a variable stroke volume of 0-10 mL/stroke, and a pulse rates from 60-180 beats/minute. The perfusion system provides intra luminal pulsatile flow ensuring the necessary shear stress for endothelial cells. A computer regulates the arterial oxygen and nutrient supply via parameters such as blood pressure, temperature, and flow rate[235,256]. In Figure 3.1 B a photograph of the bioreactor system within the drawer of the incubator is depicted. Important components are medium reservoirs with fresh medium, and silicone tubes through which the pump drives the medium, passing by the pressure sensor positioned directly in front of the influx of the jejunal segment, located in the glass reactor.

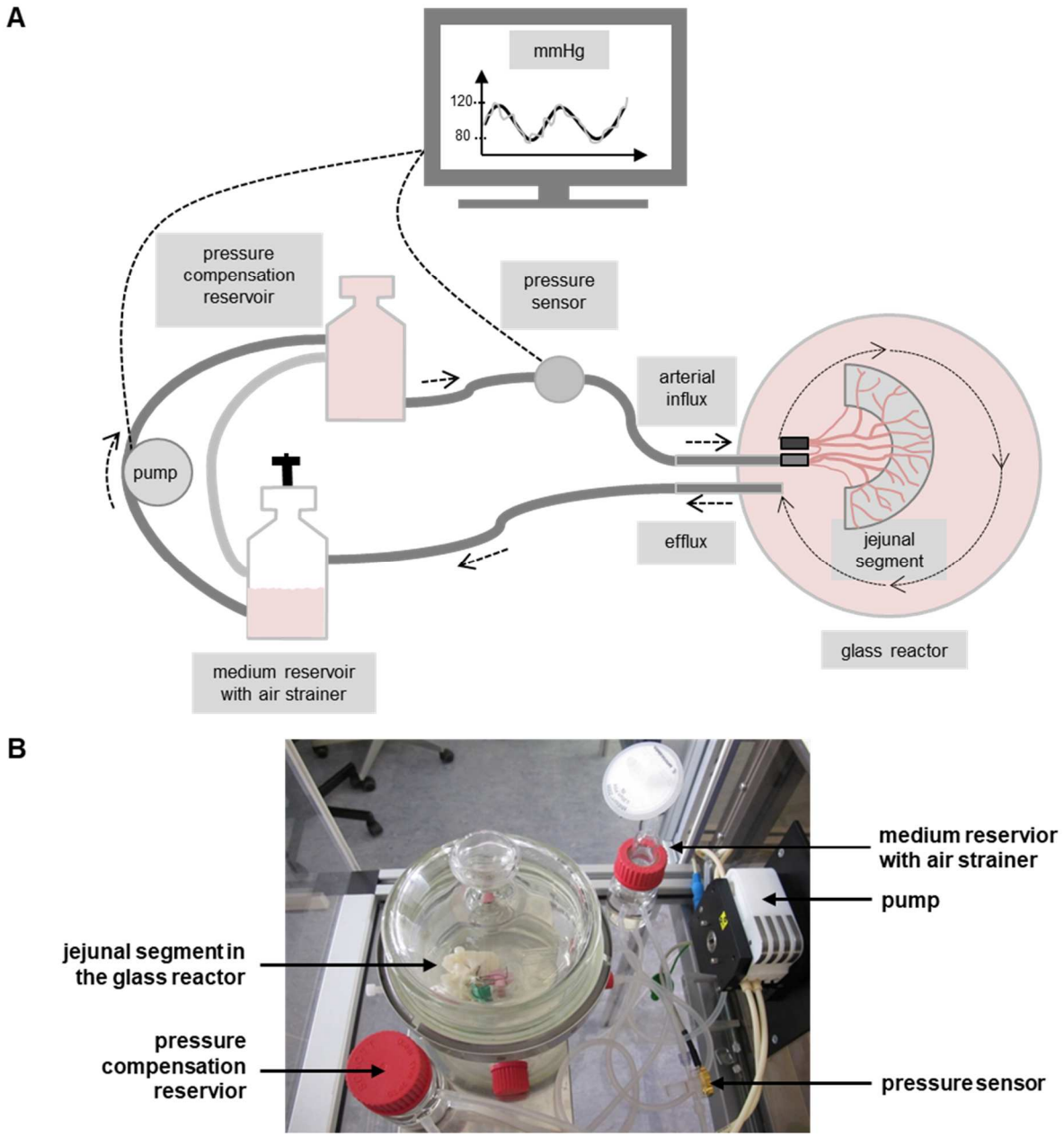

Figure 3.1: Custom-made bioreactor system.

A) Scheme of the custom-made bioreactor system. Arterial connection of the jejunal segment to the circulation in a medium-filled glass reactor. Arrows indicate the direction of the medium flow. Medium was pumped through the system with a pressure oscillating between 80 and 120 mm Hg, monitored by a pressure sensor (modified from Schanz et al. 2010 and K. Werner doctoral thesis, 2014[234,257]). **B**) Image of the bioreactor incubator with the glass reactor and its components.

3.6 Seeding of decellularized jejunal segments with MVECs & ASCs, and co-culture in the bioreactor system

Initially the autoclaved bioreactor system was filled with VascuLife® growth medium supplemented with 1% penicillin/streptomycin. The biological vascularized scaffold (decellularized porcine jejunal segment) was plugged into the perfusion via its artery and was perfused with constant flow rate (10 rpm). The seeding of the preexisting vascular structures was performed according to Schanz et al. 2010[234]. Briefly, a total of $1x10^6$ MVECs per 10 mm were seeded in two phases using the arterial and venous access of the jejunal matrix with an intermediate settling time of 3h without flow. After seeding, the scaffold was cultured statically for 12h before a pulsatile medium flow of 80-120 mmHg was applied. MVECs were subsequently cultured at 37 °C and 5% CO_2 and humid conditions in the reactor wall for 2 weeks. At day 14, ASCs ($1.5x10^6$ per 1 cm in total) were seeded into the lumen of the matrix. The lumen was closed with clamps for 24h to allow for ASC adhesion. The bioreactor medium was changed to co-culture medium (1:1 growth medium (PBM-2 with 1% pen/strep and 10% FBS) and VascuLife® growth medium (VascuLife® basal medium with VascuLife®VEGF LifeFactors Kit, 1% pen/strep but without the EGF growth factor). After one week of co-culture, in order to induce adipogenic induction, the co-culture medium was exchanged with differentiation medium (1:1 co-culture medium supplemented with 1.7 µM insulin, 1 µM dexamethasone, 500 µM 3-isobutyl-1-methylxanthine (IBMX) and 200 µM indomethacin). After 10 days (day 31 of culture), medium was changed to maintenance medium (1:1 co-culture medium supplemented with 1.7 µM insulin) for the remaining culture period (see Figure 4.1). A 50% media exchange was performed every second day throughout the 42 days of culture. For non-induced control conditions, cell-seeded constructs were cultured in the corresponding growth medium without adipogenic induction for the entire period of culture.

3.7 Preparation of hydrogels and 3D culture

3.7.1 Preparation of fibrin hydrogels

TISSEEL fibrin sealant was obtained from Baxter (Unterschleißheim, Germany). $8.0x10^5$ cells were mixed into 20 µL of the ready-to-use thrombin L solution. An equal volume of the ready-to-use TISSEEL fibrinogen component (20 µL) was further added. The total solution was gently mixed and quickly transferred into sterile glass rings (5 mm) that had been placed in 12-well culture dishes. The hydrogels were subjected to 45 minutes of polymerization under 37 °C and 5% CO_2.

3.7.2 3D cell culture

After gelation 2 mL of growth medium, consisting of preadipocyte basal medium-2 (PBM-2, supplemented with 1% penicillin/streptomycin and 10% FBS) was added to the constructs, glass rings were removed, and samples were cultured under constant agitation of 50 rpm on an orbital shaker. Adipogenic differentiation was induced by changing growth medium to differentiation medium (growth medium with 1.7 µM insulin, 1 µM dexamethasone, 500 µM 3-isobutyl-1-methylxanthine (IBMX), and 200 µM indomethacin) with 3 ng/mL bFGF. Samples were cultured for 21 days and media exchange was performed every other day. For control conditions cell-seeded hydrogels were cultured in growth medium for the entire culture period without adipogenic induction.

3.8 Biochemical assays

For each assay a total number of 3 biological replicates per sample were harvested and applied for the analysis. In 2D 1=n consisted always of 2 wells of a 24-well plate, and in 3D 1n was represented by one hydrogel. For the different analyses and culture technics, different harvesting solutions were needed specified in the next paragraph.

3.8.1 Quantitative analysis of DNA content

The DNA content of samples was measured with the intercalating dye Hoechst 33258 from Polysciences (Warrington, USA). For this purpose, cells grown in 2D were harvested in 250 µL phosphate-saline buffer per n and were further sonified for breaking the cell membranes. In 3D, hydrogels (TISSEEL and stable fibrin gels) were harvested each in 500 µL PBE buffer (supplemented with 0.85 mg/mL L-cysteine). Hydrogels were disintegrated using the TissueLyser (5 min, 25 Hz). Samples were then digested in a total volume of 1 mL of papainase digestion buffer (100 mmol Na_2HPO_4, 10 mmol Na_2EDTA, pH 6.5, with 0.85 mg/mL L-cysteine and 3 U/mL papainase) for 16 h at 60 °C. After addition of the dye solution, quantification of DNA content was carried out with a spectrofluorometer at 340 nm and 465 nm.

3.8.2 Quantitative analysis of triglyceride content

The Serum Triglyceride Determination Kit of Sigma-Aldrich (Steinheim, Germany) was used for the determination of lipid content. Cells and constructs were harvested in Thesit® solution (0.5% Thesit® in H_2O; Gepepharm, Hennef, Germany). 3D constructs were further disintegrated by the use of the

TissueLyser (5 min, 25 Hz). After sonification of the samples (2D & 3D) triglyceride quantification was performed in accordance with manufacturer specifications and measured with a Microplate ELISA-Reader (Dynatech Laboratories, EL Passo, USA) at 570 nm. Triglyceride content was normalized to the total DNA content of the respective samples.

3.9 RNA isolation and real time qRT-PCR analysis

For real-time quantitative reverse transcription-polymerase chain reaction (qRT-PCR), 2D cultured cells of two wells (6-well plate) were pooled for 1n in TRIzol® reagent (Invitrogen, Karlsruhe, Germany). For jejunal matrix constructs, samples of 0.5 cm were harvested for 1n in TRIzol® reagent and before RNA isolation, disintegration of the cells was performed by the use of the TissueLyser (5 min, 25 Hz). cDNA was synthesized from total RNA via ImProm-II Reverse Transcription System (Promega, Mannheim, Germany). The MESA GREEN qPCR MasterMix Plus with MeteorTaq polymerase (Eurogentec, Seraing, Belgium) was used for real time qRT-PCR (real-time quantitative reverse transcription PCR) analysis, performed with an MJ Research Opticon2 Cycler (BioRad, Hercules, CA, USA). Expression analysis of adipogenic transcription factors PPARγ and C/EBPα, and the adipogenic marker gene aP2 and adiponectin were carried out with the corresponding QuantiTect® Primer Assays from Qiagen (Hilden, Germany). Expression analysis of Cx43 was performed with the PrimePCR™ SYBR® Green Assays from BioRad. The following cycling protocol was applied for all primers: 95 °C for 15 minutes initial denaturation followed by 40 cycles at 95 °C for 15 seconds, 60 °C for 30 seconds, and 72 °C for 30 seconds. A melting curve analysis for PCR product integrity was performed. The resulting mRNA expression levels were normalized to eukaryotic translation elongation factor 1 alpha (eEF1α; Biomers, Ulm, Germany)[258] for each group and time point. The fold increase in expression levels for each gene was determined using the $2^{-\Delta\Delta CT}$ method[259]. For easier comparison, the obtained values were further normalized to the respective d0 or initial sample value.

3.10 Investigation on cell viability

3.10.1 Live/dead staining

Cell viability was evaluated using the live/dead cell staining kit from PromoKine (Heidelberg, Germany). 2D cultured cells and 3D scaffolds were washed three times with PBS and stained by applying 0.5 mL of staining solution containing 4 µM ethidium bromide homodimer III (EthD-III) and 2 µM calcein acetoxymethyl ester (Calcein-AM) in PBS per well and scaffold. After 1 hour, the dye was

removed, and the constructs were washed with PBS. 3D scaffolds were cut in half and the middle section was subsequently analyzed. Images were taken using an Olympus BX51 fluorescence microscope and analyzed with the Olympus CellSens™ Software.

3.10.2 MTT staining

Cell viability within the engineered jejunal matrix constructs was checked at different time points via MTT (3-[4,5-dimethylthiazol-2-yl]-2,5-diphenyl tetrazolium bromide) staining. The MTT solution (stock 3 mg/mL in ddH_20; Serva, Heidelberg, Germany) was added to the samples in a 1:2 dilution in preheated growth medium and incubated for 90 minutes at 37 °C. After rinsing with PBS whole constructs were macroscopically imaged.

3.11 Histology and immunohistochemistry

For histological and immunohistochemical evaluation, cells and constructs were fixed in 3.7% buffered formalin and stored until histological investigation in PBS. Dehydration of 3D constructs (hydrogel, jejunal matrix construct) was performed according to Ruan et al.[260] prior to embedding in TissuTek® O.C.T. Compound (Sakura Finetek, Zoeterwonde, Netherlands). Constructs were cut into 8-10 µm-thick sections. For immunohistochemical evaluation all samples were mounted with IS DAPI Mounting Medium (Dako, Hamburg, Germany) to visualize the cell nuclei. Sample imaging was performed, using an Olympus BX51 fluorescence microscope in combination with Olympus CellSens™ Dimension Microscope Imaging Software.

3.11.1 Histological investigation of adipogenesis in 2D & 3D

Adipogenic differentiation of the cells in 2D and 3D was investigated by staining with Oil Red O. Fixed samples were washed with ddH_2O and stained with Oil Red O solution (3 mg/mL Oil Red O in 60% isopropanol; Sigma-Aldrich, Steinheim, Germany). Cell nuclei were visualized with hematoxylin (Bio Optica, Milan, Italy). Sliced 3D samples were mounted using Glycergel® Mounting Medium (Dako, Hamburg, Germany). Samples were imaged using an Olympus BX51 or IX51 microscope (Olympus, Hamburg, Germany). The Olympus CellSens™ Dimension Microscope Imaging Software was utilized to analyze images.

3.11.2 Immunohistochemical staining

3.11.2.1 Laminin, collagen type IV, and CD31 staining on jejunal construct sections

Extracellular matrix development and the presence of endothelial cells were examined by immunofluorescence staining. Cryosections were incubated in blocking solution (1.5% BSA, PBS) for 20 minutes before overnight incubation with the primary antibodies diluted in antibody diluent from Dako (Hamburg, Germany). For the extracellular matrix components laminin and collagen type IV the following antibodies were utilized: polyclonal rabbit anti-laminin (ab11575, 1:200; Abcam, Cambridge, USA) and monoclonal mouse anti-human collagen IV (M0785, 1:25; Dako, Hamburg, Germany); and for visualization of endothelial cells: monoclonal mouse anti-human CD31 antibody (Clone JC70A, IR610 (1:200); Dako, Hamburg, Deutschland). To remove unbound antibody, samples were washed with PBS three times for 10 minutes and further incubated in the dark for 1h with the corresponding secondary antibody: Alexa Fluor™ 594-conjugated AffiniPure goat anti-rabbit (1:400; Jackson Immuno Research, West Grove, USA) or Cy™3-conjugated AffiniPure donkey anti-mouse (1:400; Dako, Hamburg, Germany). For additional staining of lipid droplets, samples were incubated with BODIPY 493/503 (stock 1 mg/mL, 1:100 in PBS; Invitrogen, Karlsruhe, Germany) for 20 minutes.

3.11.2.2 Cx43 staining in 2D culture

The presence of Cx43 on ASCs was examined by immunohistochemical staining. Therefore, staining had to be established by testing different antigen retrieval (Triton X-100 (1h at RT), pepsin (10 min at 37 °C), Proteinase K (2-10 min at RT) and citrate buffer (20 min at 100 °C, o/n at 65° and o/n at 55 °C)) and unspecific antigen blocking methods (1% BSA, 5% FBS both 15 min, RT), besides different Cx43 antibody dilutions (1:200, 1:500) and cytoskeletal counter staining techniques (fluorescence-labelled phalloidin, β-actin antibody). Finally, antigen retrieval on cell-seeded coverslip (ø 15 mm) samples was performed by heat mediation in citrate puffer (10 mM trisodium citrate dehydrate, 0.05% Tween® 20, pH 6.0) for 20 minutes. Unspecific binding sites were blocked for 20 minutes with 5% FBS containing PBS, before overnight incubation with primary antibodies, Cx43 and β-actin (ab11370, polyclonal rabbit anti-Cx43/GJA1 (1:500); Abcam, Cambridge, United Kingdom; and A5441, monoclonal mouse anti-β-actin (1:500); Sigma-Aldrich, Steinheim, Germany) diluted in antibody diluent from Dako (Hamburg, Germany). To remove unbound antibody, samples were washed with PBS and further incubated for 1h with the corresponding secondary antibody: Alexa Fluor™ 488-

conjugated AffiniPure goat anti-rabbit (1:400; Jackson Immuno Research, West Grove, USA) or Cy™3-conjugated AffiniPure donkey anti-mouse (1:400; Dako, Hamburg, Germany).

3.11.2.3 Ki-67 on 3D samples

The presence of proliferative cells (Ki-67) was examined by immunofluorescence staining. Cryosections were incubated in blocking solution (1.5% BSA, PBS) for 20 minutes before overnight incubation with the primary antibodies diluted in antibody diluent from Dako (Hamburg, Germany). As primary antibodies anti-Ki-67 (Clone MIB1, M7240, monoclonal mouse anti-Ki-67 (1:150); Dako, Hamburg, Germany) was used. To remove unbound antibody, samples were washed with PBS three times for 10 minutes and further incubated in the dark for 1h with the corresponding secondary antibody, Cy™3-conjugated AffiniPure donkey anti-mouse (1:400; Dako, Hamburg, Germany).

3.12 Whole mount staining

For the visualization of tissue formation and architecture 3D samples were whole mount-stained according to Wittmann et al.[152]. Engineered jejunal matrix constructs (4 x 10 mm), engineered hydrogel constructs and for comparison native human adipose tissue (4 x 4 mm) were fixed in 3.7% buffered formalin for 20h and washed three times with PBS for 1h, followed by an incubation overnight in blocking buffer (1.5% BSA in PBST [PBS with 0.3% Triton X]). After removal of the blocking buffer the samples were washed with PBST for 2h. The primary antibody anti-human CD31 (Clone JC70A, IR610, monoclonal mouse anti-human CD31 (1:200); Dako, Hamburg, Deutschland), for endothelial cells) or anti-human Vimentin (Clone SP20, 522-3201, monoclonal rabbit anti-vimentin (1:2); Zytomed Systems; Berlin, Germany 1:2, for cell shape in hydrogels) was diluted in antibody diluent (Dako, Hamburg, Germany) and added overnight to the samples. To remove unbound antibody, samples were washed with PBST for 2h and incubated for further 2h in blocking buffer. Next, whole mounts were incubated with the respective secondary antibody (Cy™3-conjugated AffiniPure donkey anti-mouse (1:400; Dako, Hamburg, Germany) or Alexa Fluor™ 594-conjugated AffiniPure goat anti-rabbit (1:400; Jackson Immuno Research, West Grove, USA) for another 2h and washed with PBS overnight. For staining of differentiating ASCs and mature adipocytes whole mounts were incubated with a 1:100 dilution of BODIPY in PBS (stock 1 mg/mL) for 1h. After removal of the BODIPY solution, whole mounts were rinsed with PBS for 2h and counterstained with DAPI (IS DAPI Mounting Medium). The whole staining procedure was performed at room temperature on an orbital shaker (50 rpm). For imaging of whole mount-stained constructs and native tissue, samples were mounted on object slides with coverslips

with PBS and examined using the Olympus BX51 fluorescent microscope. Images were overlaid using the Olympus CellSens™ Dimension Microscope Imaging software.

3.13 Quantification of protein content

Cell lysates were obtained by harvesting the cells in Laemmli's buffer. After physical disruption of the cells, total protein content was quantified using the Microplate BCA® Protein Assay Kit (Thermo Scientific, Waltham, USA). The assay was performed in accordance with manufacturer specifications. Spectroscopic quantification was performed at 562 nm using a MRX microplate reader (Dynatech Laboratories, Chantilly, Virginia). Albumin served as standard for total protein calculation. After protein content determination samples were supplemented with 5% β-mercaptoethanol, heated for 10 minutes at 95 °C and stored at -20 °C for further analysis.

3.13.1 Sodium dodecyl sulfate polyacrylamid gel electrophoresis

For the immunological detection of connexin 43 equal amounts of protein (20 µg) were subjected to SDS-PAGE by means of an 8% polyacrylamide gel. The composition of the gel is listed below:

Table 3.1: Running gel recipe for an 8% polyacrylamide gel.

Solutions	Volume for two gels
30% acrylamide	4.08 mL
running gel buffer	5.70 mL
ddH_2O	4.92 mL
10% SDS	150 µL
10% APS	150 µL
TEMED	7.5 µL

The running gel solution was cast into the gel tray quickly after mixing all components. Isopropanol was put on top, for flattening the surface. After polymerization the isopropanol was removed, and the stacking gel was cast on top and a gel comb was inserted to form wells.

Table 3.2: Stacking gel recipe.

Solutions	Volume for two gels
30% acrylamide	0.9 mL
stacking gel buffer	1.5 mL
ddH_2O	3.24 mL
10% SDS	60 µL
10% APS	60 µL
TEMED	6 µL

The polyacrylamide gel was inserted into the tank according to the instruction manual and the tank was filled with running buffer (25 mM Tris, 192 mM glycine, 0.1% SDS). Samples were loaded into the wells of the stacking gel with 20 µg protein of respective volumes (determined by Microplate BCA® Protein Assay Kit) and 10 µL of a protein ladder (Novex™ sharp protein standard, Life Technologies). For the separation of proteins with the SDS-PAGE the Bio-Rad Mini-PROTEAN™ Tetra Cell System (Bio-Rad, Munich, Germany) was utilized. The gel was run at 30 mA.

3.14 Western blot analysis

After separation of the proteins with SDS-PAGE, the proteins were transferred to a nitrocellulose membrane by wet blotting, using the Bio-Rad Mini-PROTEAN™ Tetra Cell System (BioRad). The gel holder cassette was inserted into the tank, according to manufacturer instructions, and was filled with transfer buffer (25 mM tris base, 192 mM glycine, 10% methanol). The proteins were transferred by applying 300 mA for 2 h. The protein containing nitrocellulose membrane was further blocked with 5% (m/V) non-fat dried milk powder in PBST (0.1% Tween® 20) for 1h at RT on an orbital shaker. The membrane was incubated with the primary antibody Cx43 (ab11370, polyclonal rabbit anti-Cx43/GJA1 (1:6,000); Abcam, Cambridge, United Kingdom) diluted in WB blocking solution (PBST containing 5% nonfat dried milk powder) at 4 °C overnight under constant shaking. The membrane was washed three times for 10 minutes with PBST and the HRP conjugated secondary antibody, goat anti-rabbit IgG (P0448, 1:1,000, Dako) was added to the membrane for 1h at RT. The membrane was washed again three times with PBS for 10 minutes to remove unbound antibody. Finally, the antibody-labelled proteins were detected by chemiluminescence using the Amersham ECL Prime Western Blotting Detection Reagent (GE Healthcare, Buckinghamshire, UK). For control of protein loading uniformity, the bound antibodies were removed by incubating the membrane with 0.2 M NaOH for 15 minutes. Blocking, antibody incubation and detection was redone as described. For loading control GAPDH

(Clone 6C5, monoclonal mouse anti-GAPDH (1:500), Merck Millipore, Darmstadt, Germany) and the respective secondary antibody rabbit anti-mouse IgG (P0161, 1:1,000, Dako) were applied.

3.15 Flow cytometry

3.15.1 Nile red

To determine the percentage of differentiated ASCs with regard to different seeding densities, cells were stained with nile red and analyzed by flow cytometry according to Neubauer et al.[261]. Briefly, after a culture period of 10 to 12 days under adipogenic conditions, cells were carefully harvested by treatment with 0.25% trypsin/EDTA (200 x g at 4 °C for 7 min) and stained with the lipophilic fluorescent dye nile red (1:100 in PBS, stock solution of 1 mg/mL in DMSO; Sigma Aldrich, Steinheim, Germany) for 30 minutes on ice. With a Zombie NIR Fixable Viability Kit staining (BioLegend, London, United Kingdom), dead cells could be excluded from the total cell population. Cells were evaluated using a FACSCanto flow cytometer (BD Biosciences, Palo Alto, USA), and the resulting data were analyzed using the FlowJo v.10.0.7 software (Treestar, San Carlos, USA). To determine the number of differentiated ASCs, a selection marker (M1-Gate) was set-up by overlaying the corresponding undifferentiated control-sample with the differentiated sample. The number of differentiated cells was defined by determining the percentage of cells within the (1%-gating) set M1-Gate.

3.15.2 Dye transfer

To analyze functional coupling of ASCs by gap junctional communication a flow cytometry analysis of dye transfer between cells was performed according to Fonseca et al. 2004 and 2006[262,263]. Briefly, a half portion of ASCs were stained with BD Pharmingen Calcein-AM Viability Stain (2.5 µM, BD Biosciences, Palo Alto, USA) and the other half were incubated with DiD Vybrant Cell-Labeling Solution (5 µM, Thermo Scientific, Waltham, USA). Staining was performed in accordance with manufacturer specifications. To allow diffusion of non-metabolized Calcein-AM, cells were kept for an additional 30 minutes in fully supplemented DMEM/F12 basal medium. Calcein-AM- and DiD-labeled cells were finally seeded in a 1:1 proportion at different densities (5,000, 25,000 and 100,000 cells per cm^2) on tissue culture-treated plastic 6-well plates. Cells were cultured in growth medium (without bFGF). GJIC inhibition was carried out by addition of 70 µM AGA. For control conditions, cells were incubated with 70 µM GZA and 0.35% DMSO. After a co-culture period of 4 hours, cells were harvested and the presence of double positive cells (+/+ DiD/Calcein cells) was evaluated using a FACSCanto flow

cytometer (BD Biosciences, Palo Alto, USA), and the resulting data were analyzed using the FlowJo v.10.0.7 software (Treestar, San Carlos, USA).

3.16 Statistical analysis

Quantitative results are expressed as mean values ± standard deviation. Statistically significant differences between experimental groups were assessed using a two-way analysis of variance (ANOVA) in conjunction with a Tukey or Bonferroni post hoc analysis at the level of $p<0.05$. Statistical significance for nile red experiments between groups were assessed using an unpaired Student's t-test and a one-way ANOVA. Statistical analysis was performed using GraphPad Prism, Version 5.0 (GraphPad Software, La Jolla, USA). Analyses were performed in triplicate, if not stated otherwise.

4 Results and Discussion

4.1 Engineering of prevascularized adipose tissue *in vitro* using decellularized porcine jejunal segments

In plastic and reconstructive surgery, there exists a growing demand for adequate tissue transplants for the reconstruction of soft tissue defects resulting from trauma, congenital disease, or tumor resection[240–242]. Especially after complex traumatic injuries, in the resulting deep wounds, adhesion of mobile structures such as nerves, tendons and blood vessels is likely to occur due to the severe damage to the subcutaneous fat layer, causing restricted motion and disabling pain[177]. Current clinical approaches to treat these severe full-thickness wounds often use either free or pedicled autologous tissue flaps, or artificial replacements[1,116–118]. However, these approaches are limited by complications including flap failure, donor site morbidity, highly complex and challenging microsurgical procedures with long recovery periods, as well as the rejection and shrinking of autologous and artificial materials[128,183,243]. Thus, an engineered adipose tissue substitute that is capable of reconstructing the function and shape of the subcutaneous soft tissue layer would be highly desirable[18].

As native adipose tissue is a highly vascularized and metabolically active organ, and mature adipocytes exhibit low tolerance to ischemia, a sufficient degree of vascularization represents a key prerequisite for the engineering of large-scale adipose tissue constructs[19,26,264]. Previous approaches in adipose tissue engineering have attempted to combine adipogenesis and angiogenesis, known to be spatially and temporally linked within the process of tissue maturation[26]. Coculturing of preadipocytes or ASCs together with endothelial cells in hydrogels, as well as the additional incorporation of proangiogenic cytokines, have been investigated *in vitro*[219,265–267]. These studies have demonstrated principles towards the formation of capillary networks[18], however, up until now, there is still a lack of adequately vascularized adipose constructs *in vitro*. The most promising approaches *in vivo* so far used the integration of a vascular pedicle into the construct upon implantation, relying on sprouting into the developing tissue[169,205,268], or the implantation of an empty scaffold, with a subsequent vascularization period by host cells followed by fat injection[204]. Although these *in vivo* strategies may achieve a considerable degree of soft tissue formation, they require several weeks or months for tissue development and maturation, and strongly rely on the host response for timely and adequate vascularization. Consequently, a directly applicable, already vascularized adipose tissue construct appears highly desirable.

Therefore, in this study, a recently established biological vascularized scaffold[244,245] was investigated with regard to its use in engineering adipose tissue *in vitro*. The scaffold consists of a decellularized porcine jejunal segment, i.e., a cell-free native extracellular 3D matrix structure taken from porcine small bowel[229,230,233]. The preexisting capillary structures can be repopulated with human microvascular endothelial cells (hMVEC)[234], and the jejunal lumen enables the seeding of any other cell type, which here in this study were represented by human adipose-derived stromal cells (hASC). In previous studies of our group ASCs have been successfully employed with regard to adipogenic differentiation in other scaffolding systems[169,269]. In addition, the decellularized jejunum can be connected to a flow-through system via an arterial and a venous port, which may also facilitate direct applicability in a clinical setting[234,236]. Furthermore, in a pilot study in our laboratory and in collaboration with the group of Professor Walles (Department of Tissue Engineering and Regenerative Medicine), the groundwork was already done for the engineering of a vascularized adipose tissue construct *in vitro* within the doctoral thesis of Katharina Werner[257]. In her thesis she conducted preliminary testing on jejunal sections and performed one pilot experiment with a decellularized jejunal construct cultured in the custom-made bioreactor system, where capillary structures were reseeded with hMVECs and the jejunal lumen was seeded with hASCs[257]. General suitability and feasibility of the experimental setting were shown; the obtained preliminary insights were integrated in this work to further optimize and establish the method.

Thus, in this work, employing the decellularized porcine jejunal segment, furthermore in-depth investigations were performed with regard to ASC differentiation and tissue development. The adipose-specific extracellular matrix was analyzed, especially its development during the adipogenic differentiation process in comparison to non-induced constructs. Furthermore, *in vitro* cell survival under long-term conditions as well as adipogenic differentiation capacity of ASCs in coculture with MVECs were proven on the cellular and molecular level compared to non-adipogenically induced samples. The development of mature-like adipose structures along with reendothelialized vasculature was demonstrated, underscoring the promising approach to the engineering of prevascularized adipose tissue substitutes.

4.1.1 Engineered prevascularized adipose tissue *in vitro* - Experimental design

For *in vitro* engineering of vascularized adipose tissue whole decellularized jejunal segments (80-100 mm) were used in 6-week co-culture experiments, dynamically cultivated in a custom-made bioreactor system. At day 0 MVECs were seeded into the preexisting vasculature of the scaffold and cultured for 14 days (Figure 4.1). Subsequently, ASCs were seeded into the lumen of the jejunal matrix onto the mucosa. Adipogenic induction was started at day 21 under co-culture conditions and continued for a further 10 days period. Maintenance medium was applied until constructs were finally harvested at day 42. As control samples, non-induced matrices were cultivated in the same manner in corresponding growth medium for the entire period of culture. For detailed schematic of the custom-made bioreactor system please refer to Methods section (see Chapter 3.5, Figure 3.1; Figure 4.1).

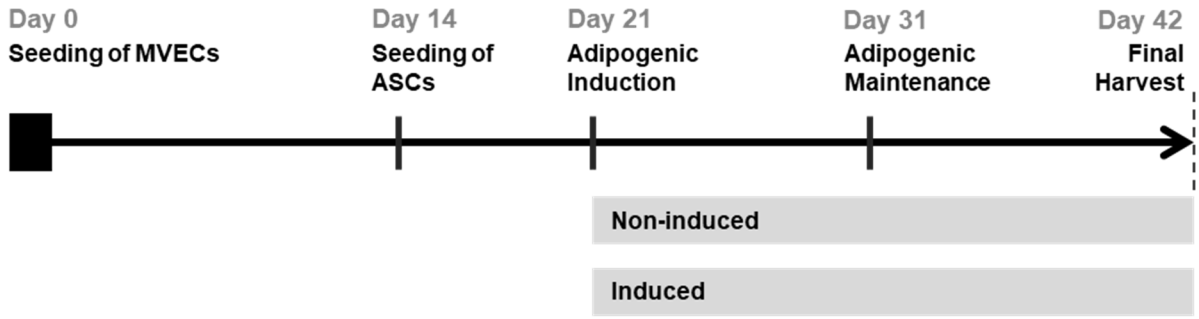

Figure 4.1: Experimental setup – timeline of seeding and cultivation of the jejunal segment.

At day 0, MVECs were seeded into the preexisting vascular structures. At day 14, ASCs were seeded into the jejunal lumen and adipogenic induction was started at day 21. Adipogenic maintenance was performed from day 31 until day 42. The constructs were finally harvested after 6 weeks of culture. Non-induced samples were cultured as a control.

4.1.2 Cell viability

Cell viability within the dynamically cultured constructs was determined by MTT staining after 14 days of monoculture of MVECs in the vasculature of the jejunal matrix and after the co-culture with ASCs at day 42 (Figure 4.2). After 14 days viable endothelial cells were stained purple in the preexisting vasculature displaying an extensive branching network of vessels (Figure 4.2 A). After the whole culture period of 42 days, the constructs were cut open and were almost completely colored purple at the inside, indicating living cells (Figure 4.2 B). Unopened samples at day 42 displayed the location of cells within the scaffold (Figure 4.2 C). The arrows indicate ASCs within the lumen of the jejunal matrix and living MVECs located in the vascular structures visible from the outside of the scaffold. The schematic (Figure 4.2 D) demonstrates the positions the samples were taken from within the whole matrix framework.

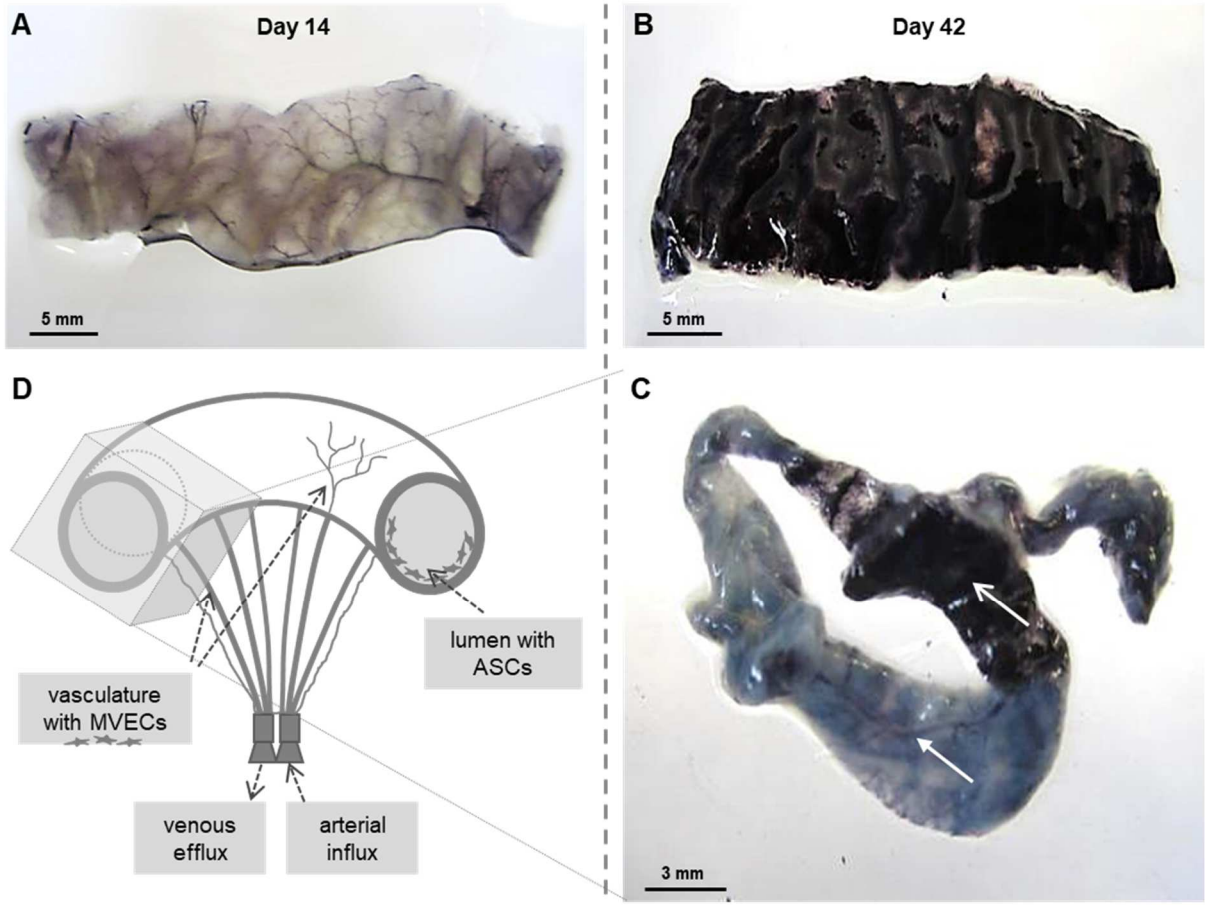

Figure 4.2: MTT staining for living cells on jejunal segments cultured in a custom-made bioreactor.

Viable cells were labeled dark purple by MTT staining. Cut open jejunal construct pieces are shown in the first row, taken from the whole scaffold. On day 14, viable cells are visible in the preexisting vascular structures (MVECs) of the scaffold (**A**, top view, outside) and on day 42 the total investigated piece is stained purple (**B**, inside view, lumen) by living cells (ASCs and MVECs). **C**) Unopened construct piece, taken from the whole scaffold, the inner lumen containing the ASCs being distinguishable from the exterior with the vascular structures and living MVECs (indicated by arrows, → & ➔ respectively); scale bars represent 5 and 3 mm. **D**) Depiction of the jejunal segment and the seeding locations of MVECs and ASCs as well as the position of the samples taken in the entire construction frame.

4.1.3 Adipogenesis in engineered jejunal matrix constructs

Adipogenic differentiation of ASCs within the jejunal matrix was analyzed by histological staining and gene expression analysis of adipogenic marker genes. Oil Red O staining of lipid droplets revealed the occurrence of lipid-laden cells in induced matrices at day 31 (corresponding to day 10 after induction) distributed within the submucosal structure of the decellularized jejunum (Figure 4.3 A). In the course of the culture a further accumulation of differentiated cells was observed, with some cells even showing monovacuolar lipid droplets that indicate fully mature adipocytes. In contrast, no

differentiation took place in the non-induced samples, as shown by the absence of Oil Red O staining (Figure 4.3 A).

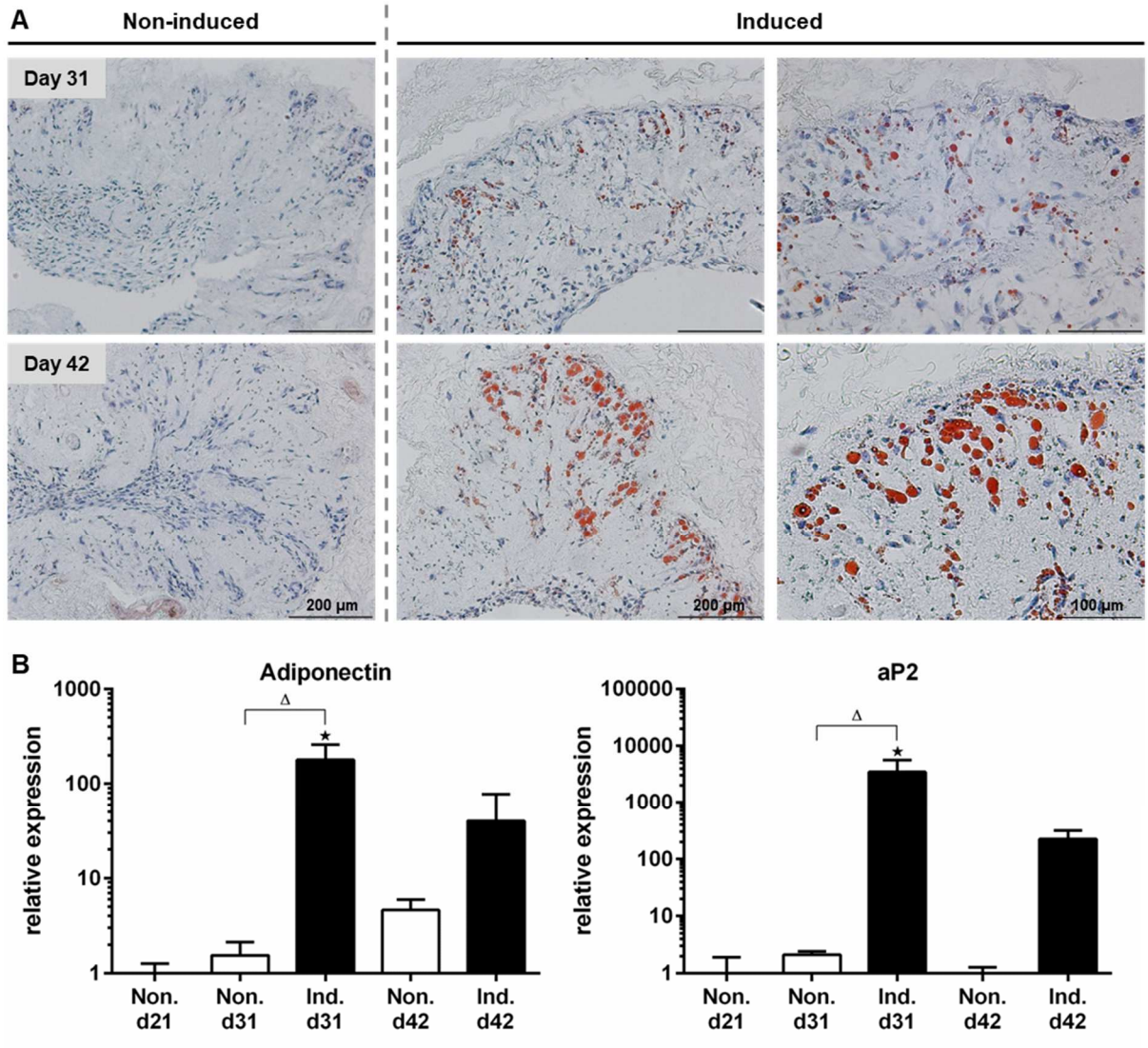

Figure 4.3: Investigation of adipogenesis in the jejunal construct.

A) Analysis of adipogenic differentiation on cross-sections (non-induced, induced; day 31 and day 42) by staining with Oil Red O (ORO, red) and hematoxylin (blue). The formation of lipid-laden ASCs over time (day 31; day 42) in comparison to non-induced samples is shown. Images were taken at a 10-fold and 20-fold magnification; scale bars represent 200 and 100 µm. **B**) Adipogenic marker gene expression of differentiated ASCs was determined by qRT-PCR. Gene expression was normalized to EF1α; the obtained values were normalized to day 21 non-induced. Values are expressed as mean with standard deviation (n=3). Statistically significant differences ($p<0.05$) between adipogenic induction (induced) and day 21 non-induced are indicated by *; significant differences between non-induced and induced samples of the same day are indicated by $^{\triangle}$ ($p<0.05$). Three independent experiments were conducted; representative results of one experiment are shown here.

To further characterize adipogenesis within the constructs, two marker genes of late adipogenesis, namely aP2 and adiponectin, were chosen for quantitative gene expression analysis (Figure 4.3 B). qRT-PCR analysis was performed at day 21, 31 and 42 (corresponding to day 0, 10 and 21 of adipogenic induction). Both marker genes showed significantly elevated expression levels upon adipogenic induction compared to day 21. Expression levels were low at all time points in the non-induced constructs.

4.1.4 Extracellular matrix development in engineered jejunal matrix constructs

To assess the adipose-like tissue structure within the jejunal matrix constructs, the formation of adipose-specific matrix components in the developing tissue was investigated (Figure 4.4 A and B). Immunohistochemical staining of laminin and collagen type IV as integral components of the basal lamina of adipocytes revealed the presence of both ECM components on day 31 (day 10 after induction). As differentiation progresses, a markedly detectable accumulation of laminin and collagen type IV fibrils emerged (day 42), while both structures were nearly absent in non-induced samples. In the latter samples, some distinct laminin and collagen type IV spots were detected, due to the human MVECs residing within the vasculature, producing these components as part of their basement membrane. The staining pattern in differentiated samples was closely linked to the differentiation process as indicated by the distinct co-localization of adipose-specific ECM and lipid vacuoles (Figure 4.4 A and B, higher magnification inserts).

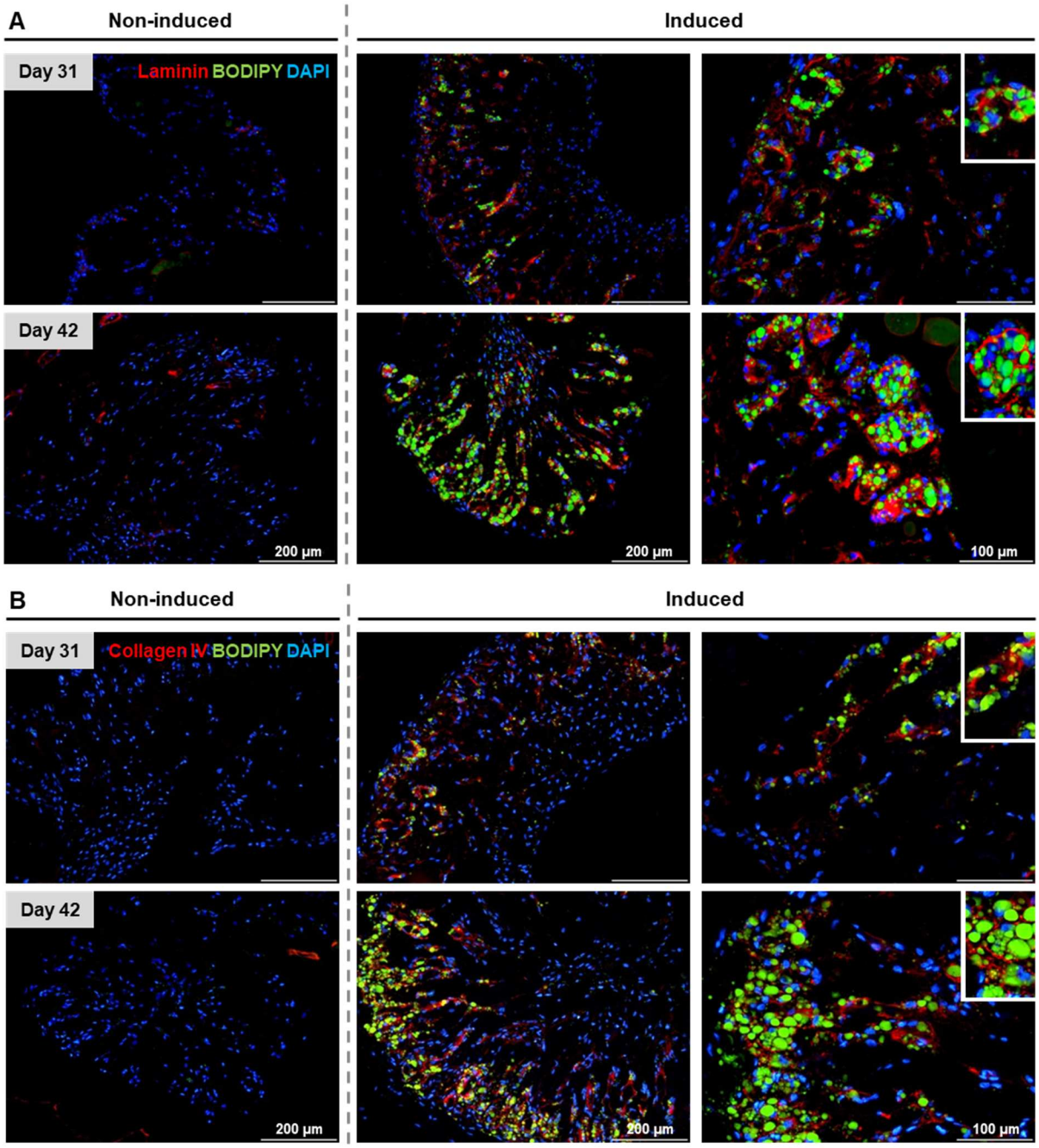

Figure 4.4: Development of adipose-specific extracellular matrix in the jejunal construct.

Immunohistochemical staining of extracellular matrix (ECM) components laminin (**A**) and collagen type IV (**B**) was conducted. The staining revealed the formation of laminin and collagen type IV structures surrounding adipocytes on day 31 and day 42 in adipogenically induced constructs in a time dependent manner. In non-induced constructs, specific staining for these integral parts of the basal lamina was only associated with blood vessel structures. Laminin and collagen type IV were stained red, lipid droplets were stained with BODIPY (green), and nuclei with DAPI (blue). Images were taken at 10-fold and 20-fold magnifications; scale bars represent 200 and 100 µm, respectively.

4.1.5 Visualization of tissue architecture of engineered adipose tissue

The presence of MVECs was demonstrated by CD31 staining on histological cross-sections at four different time points, starting from the day of ASC seeding (day 14) until the final harvest (day 42) of the induced constructs (Figure 4.5 A). CD31-positive vascular structures could be detected at all times distributed over the entire construct. Since the three-dimensional tissue structure of the constructs can hardly be represented by histological staining on sections, the samples were analyzed by whole mount staining to better illustrate the spatial development of adipocytes and prevascular structures within the engineered adipose tissue. (Figure 4.5 B).

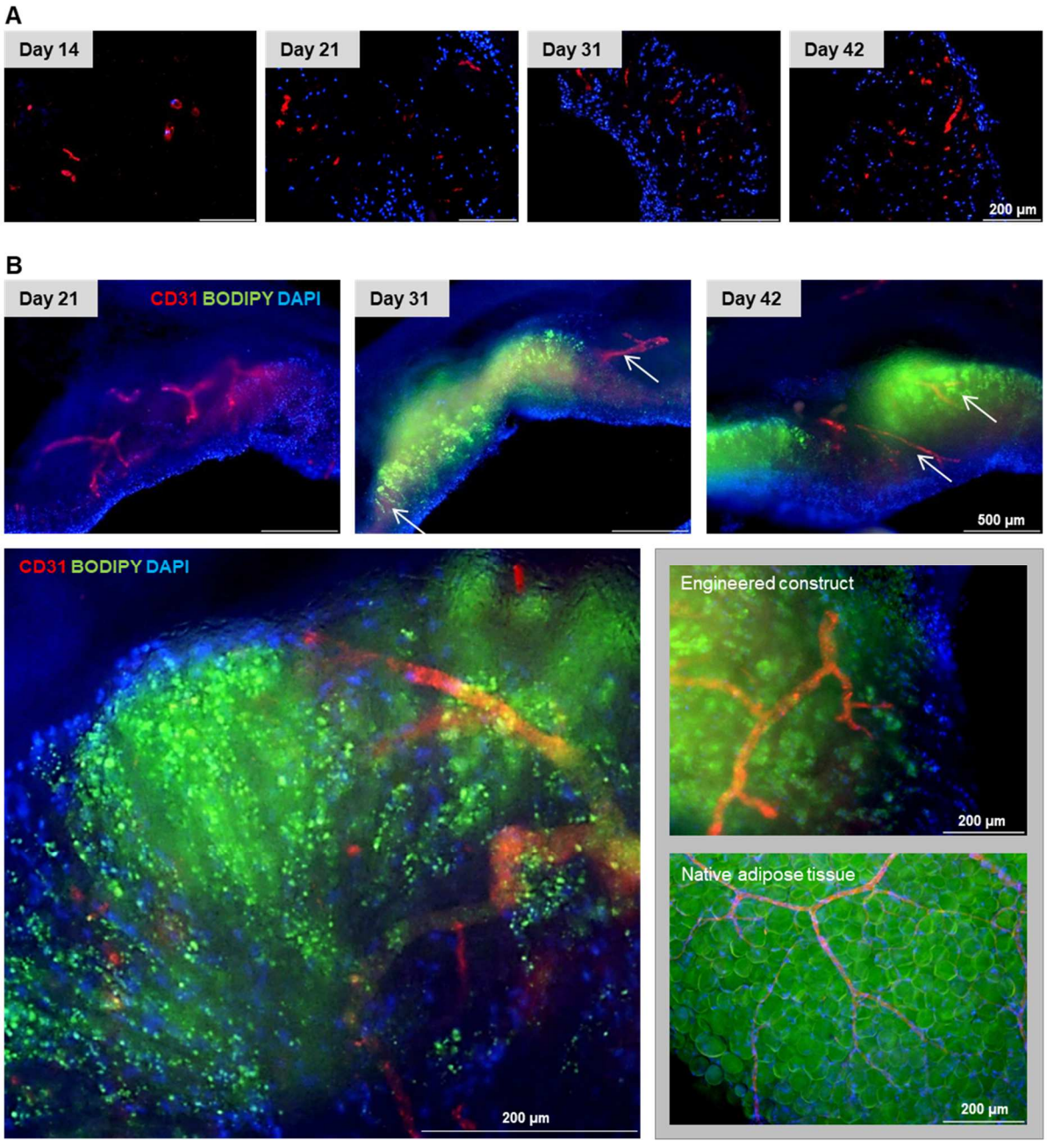

(legend on next page)

Figure 4.5: Illustration of tissue development within the porcine jejunal segment.

A) Presence of endothelial cells was demonstrated by CD31 (red) and DAPI (blue) staining on cryosections over time at day 14 (only MVECs), day 21 (MVECs and ASCs), day 31, and day 42 (final harvest); scale bars represent 200 µm. **B**) Visualization of *in vitro* tissue maturation by whole mount staining. Interaction of endothelial laden vascular structures and adipocytes in engineered constructs was demonstrated by CD31/BODIPY/DAPI (red/green/blue) staining. The three top row images show a time course of tissue formation (day 21; start of adipogenic induction until day 42; final harvest). Arrows indicate vascular structures. Images were taken at a 4-fold magnification; scale bars represent 500 µm. The lower left image illustrates a higher magnification of a differentiated construct (10-fold magnification); scale bar represents 200 µm. An engineered construct was compared with native adipose tissue in the lower right images. Images were taken at a 10-fold magnification; scale bars represent 200 µm.

Concurrent CD31 and BODIPY staining of blood vessels and lipid-laden cells, respectively, demonstrated the occurrence of adipogenic development, and revealed the close co-localization of differentiated adipocytes and prevascular structures within the jejunal matrix (Figure 4.5 B). In comparison to equivalently stained native human adipose tissue, the *in vitro* generated adipose tissue construct reflected the native tissue structure, representing a prevascularized transplantable tissue substitute.

4.1.6 Discussion

To date, restoration of large soft tissue defects remains challenging in plastic and reconstructive surgery. Common approaches for autologous tissue transfer still face many limitations and drawbacks, namely necrosis, volume loss of the implant and donor site morbidity[177]. The field of tissue engineering and regenerative medicine offers promising concepts for engineering soft tissue to serve this demand[1,18,120]. However, most of the *in vivo* tissue engineering approaches are associated with long timeframes for the formation of coherent tissue, strongly relying on the host response, with uncertain outcome. Many of the already existing *in vivo* vascularization strategies for soft tissue regeneration, like the application of a vascular pedicle or growth factors[155–158,169,205,268], may achieve considerable degrees of tissue formation, however comprising a time-consuming development process, with a period of undersupply with oxygen and nutrients. Current *in vitro* concepts suffer from insufficient vascularization with subsequent necrosis or apoptosis. Therefore, a principal challenge is to develop engineered substitutes, which are sufficiently prevascularized and directly connectable to the host vasculature[18,270]. Nevertheless, i*n vitro* approaches also exist and have demonstrated principles towards the formation of capillary networks, but also still facing limitations, as they are still suffering from a lack of adequate vascularization of the soft tissue construct, and consequently size limitations[18]. To address this challenge, in this study we utilized a decellularized jejunal segment (with a size of 80-100 mm) with preexisting blood vessel structures displaying an arterial and venous connection,

which was seeded with MVECs and ASCs to foster both angiogenesis and adipogenesis. In recent years, researchers repopulated different kinds of extracellular matrix scaffolds with cells, demonstrating the usability of these matrices in tissue regeneration approaches, intending to prospectively restore natural tissue function[121]. Especially the naturally derived extracellular matrix segment of porcine small bowel with its preserved artery and vein structure employed in these experiments has already been combined with multiple types of cells to generate tissues like human bladder and liver *in vitro* or human vascularized tissue *in vivo*[121,230,233,234].

A prerequisite for the engineering of functional vascular surrogates is the creation of a natural-like environment and biomechanical conditions similar to the human body[271–273], such as a pulsatile blood flow encountered by endothelial cells[274,275]. Bioreactor systems can realize these requirements *in vitro* for the formation of native-like tissue constructs[236,238]. By means of a construct with dense preformed vasculature, such as the decellularized jejunal matrix, and a bioreactor system, the supply with nutrients as well as oxygen can be provided. Thus, not only the outer areas but also the center of the tissue can be sufficiently supplied, overcoming the limitation of naturally occurring diffusion distances of about 150-200 µm[208,224] and ensuring the viability of cells over a long-term culture period[270]. In this study, in a long-term culture set-up, MVECs and ASCs were co-cultured on decellularized jejunal segments in a custom-made bioreactor system, which has previously been introduced[234].

According to this approach, repopulation of the preexisting vascular structure of the decellularized jejunal segments with endothelial cells was performed and tested positive for viability. After seeding of ASCs and an additional 4-week co-culture period, for both endothelial cells and ASCs sustained viability could be demonstrated.

As already observed in the small-scale static culture using cell crowns[257], upon adipogenic induction ASCs developed cytoplasmic lipid inclusions within the luminal matrix accompanied by a rounded morphology, also in the bioreactor system. At day 42, i.e., day 21 of induction, many ASCs even exhibited monovacuolar lipid depositions indicating an advanced adipogenic state. Well in agreement with histological findings, gene expression analyses revealed elevated levels of late markers of adipogenesis, adiponectin and aP2, within the induced constructs. In both cases, on morphological and gene expression level, a clear difference compared to non-induced constructs could be demonstrated. Even though the here engineered substitute is not yet as mature as native adipose tissue, the *in vitro* adipogenic pretreatment of adipose precursor cells prior to implantation has previously been proven to be beneficial in various studies to enhance the development potential *in vivo*[18,276].

In the dense framework of native adipose tissue, each adipocyte is surrounded by a compact sheet-like ECM structure, namely the basement membrane. The functions of the ECM include regulation of cellular behavior by influencing cell proliferation, survival, migration, and differentiation, besides the important task of shaping and protecting the fragile mature lipid-filled adipocyte[20,98]. Key components of the basement membrane are laminin and collagen type IV, thus, indicators of an advanced state and a sign for physiological and functional adipose tissue[107]. In our study, within the engineered constructs it was demonstrated that both components, laminin and collagen type IV, were secreted into the extracellular space by the differentiating ASCs upon induction, accumulating over time. Higher magnifications displayed a dense sheet-like enclosing ECM deposition for laminin as well as for collagen type IV around lipid-laden ASCs at day 42 indicating adipose-specific tissue development. To date, adipose-specific ECM composition and development has profoundly been investigated in 2D conditions, in most cases by means of the mouse 3T3-L1 cell line[20]. In contrast, ECM development of tissue-engineered adipogenic specimens has, to the best of our knowledge, not been investigated so far. In this study, we demonstrate the development of a human adipose tissue-specific matrix within an engineered fat construct *in vitro*.

Subsequent to the pilot experiment by Katharina Werner[257], we could demonstrate in this work the reproducible long-term survival of both cell types within the construct, and the differentiation of ACSs in the presence of MVECs in an established co-culture medium on morphological and molecular level. In contrast to the pilot experiment the adipogenic differentiation conditions were changed, to short-term induction (10 days of adipogenic induction, followed by 10 days of adipogenic maintenance, see Figure 4.1), as in preliminary experiments a negative influence of permanent induction on endothelial viability was observed (data not shown).

With regard to vascular development, the preexisting vascular structures of the decellularized jejunal segments were reseeded with endothelial cells at the start of the culture and tested positive for viability over the full culture period. Time-dependent immunohistochemical staining revealed the anchoring of MVECs in the dense, already existing vessel network during the whole culture period, advancing to the smallest capillaries in the mucosal layer. As a side note, vascular structures also showed distinct immunohistochemical staining for the ECM proteins laminin and collagen IV that was well distinguishable from ECM deposition around differentiating ASCs and particularly noticeable in non-induced samples, apparently caused by residing endothelial cells secreting these ECM components as part of their endothelial basement membrane[277,278]. In principle, researchers have shown the feasibility of reseeding capillary structures of different extracellular matrix constructs, albeit for shorter *in vitro* culture time periods[225,226]. Furthermore, endothelial cells are necessary to provide a non-thrombotic barrier for the decellularized tissue matrix and to ensure that medium and blood

flow is confined to the vascular spaces *in vitro* and later on *in vivo*, respectively[270,279]. By combining a prevascularized scaffold matrix with a tissue specific bioreactor, appropriate nutrient supply throughout the complex 3D-bioartificial tissue models can be ensured *in vitro*[234].

Aubin and coworkers for instance generated a native-derived coronary artery tissue-flap model *in vitro*, manufactured from decellularized rat hearts, in a 5 day culture period by ensuring medium supply by manual perfusion[225]. 3T3 cell attachment was traced for 5 days, showing cell attachment to the vasculature of the ECM scaffold, while tissue development within this proof of principle construct under coculture of endothelial cells (HUVECs) with primary cardiac cells was investigated for 24h after seeding[225]. In contrast, Zhang and coworkers reseeded a decellularized skin/adipose tissue flap matrix and demonstrated reendothelialization with HUVECs for 7 days under static culture conditions[226]. The generalistic approach from Schanz and colleagues demonstrated the feasibility of reendothelialization in the decellularized jejunal segment in combination with dynamic *in vitro* culture condition (pulsatile medium flow) by means of a custom made-bioreactor system[234]. In accordance with this study, we could demonstrate here a long-term survival and viability of MVECs attached to the dense vascular network of our construct under dynamic culture conditions, demonstrated by immunohistochemical staining for CD31 over the course of time.

Applying a whole mount staining technique the architecture of the developed tissue could be investigated for an in-depth examination of the construct[169]. This method permits the illustration of the native-like architecture of the engineered construct and the analysis of incorporated structures in relation to each other. Close proximity of blood vessels and adipocytes could be demonstrated at each time point. Reseeded and branched vasculature co-localized with developing adipocytes, in agreement with the mutual interaction between angiogenesis and adipogenesis[26,280]. Vascular development promoting conditions are probably further supported by the secretion of proangiogenic factors of differentiating ASCs, which may be investigated more closely in future studies[57,280,281]. Higher resolution images revealed the striking resemblance between the engineered constructs exhibiting angiogenic and adipogenic development and native adipose tissue.

Recently, Zhang and coworkers have used in their approach a naturally derived decellularized skin/adipose tissue flap matrix with preserved vasculature, reseeded with ASCs and human umbilical vein endothelial cells (HUVECs), investigating the *in vivo* development of a soft-tissue flap[226]. Seven days after reseeding, the construct was anastomosed in rats and soft tissue formation was followed up for 3 months *in vivo*. The results indicated the feasibility of *in vitro* reseeding and *in vivo* development of bioengineered vascularized human tissue substitutes.

In the current approach, by means of a naturally derived decellularized ECM scaffold and a custom-made bioreactor system, a viable and prevascularized adipose tissue substitute could be developed *in vitro* in a long-term culture. The inherent vascular network and the advanced adipogenic status of the engineered constructs make them promising candidates for preclinical testing and potential clinical application as free flap transplant in plastic and reconstructive surgery.

4.2 Investigations on the effects of bFGF on ASC proliferation and differentiation capacity

Tissue engineering and regenerative medicine approaches require a huge number of cells, as previously demonstrated in Chapter 4.1, to entirely seed complex and large 3D matrices or scaffolds. Due to the very high demand in tissue engineering applications cells need to be large-scale expanded *in vitro* without losing differentiation capacity, caused by replicative aging[246]. Furthermore, at present an improved differentiation of ASCs in adipose tissue engineering approaches remains still desirable. Regarding these demands, growth factor application can have a great influence both on the proliferation and differentiation capacity of mesenchymal stem cells[247,248]. It has been reported in various culture systems that basic fibroblast growth factor (bFGF) is a potent mitogen for human MSCs, while maintaining or even promoting their osteogenic, chondrogenic and adipogenic differentiation potential[37,56,249–252]. Furthermore, bFGF has been shown to promote proliferation as well as osteogenic and adipogenic differentiation of rat bone marrow derived stem cells (rBMSCs), when incorporated into 3D collagen hydrogel constructs or applied in 2D culture *in vitro*[282,283]. Moreover, basic FGF has been repeatedly demonstrated to be effective to induce *de novo* adipogenesis in *in vivo* tissue engineering approaches in combination with biomaterials, such as Matrigel or microspheres[156,158,283,284]. Interestingly, the promoting effect of bFGF on adipogenic differentiation is nevertheless controversially discussed in literature for adipose tissue engineering applications. In addition, in *in vitro* applications diverse amounts of bFGF are applied, showing mostly concentration dependent effects, while application time points during experimental set-up differ also greatly, causing presumably alike different experimental outcomes. While inhibitory effects are described in the context of bFGF administration on mesenchymal stem cells during differentiation and transdifferentiation[285–288], Neubauer et al. and Kakudo et al. demonstrated a highly improved adipogenesis for rat BMSCs and human ASCs respectively, being precultured with different concentrations of bFGF[58,261]. Additionally, bFGF administration promotes verifiable proliferation of MSCs by preserving the multipotent capacity[249,289].

Basic fibroblast growth factor or FGF2 as it is also termed, belongs to the FGF family consisting of 22 identified members, numbered consecutively from 1 to 22, which induce mitogenic, chemotactic, and angiogenic activity in cells of mesodermal origin[248,290,291]. bFGF has a molecular weight of 18 kDa, while the *fgf2* gene contains 3 other isotypes, and is a heparin-binding polypeptide being stored in the extracellular matrix[290,291]. The growth factor acts extracellularly via FGF-receptors (FGFRs), which dimerize after binding, resulting in auto- or reciprocal phosphorylation of contained kinase domains (specific tyrosine residues) and activation of various intracellular signaling pathways[290,292]. Cytosolic signaling can be activated either on the cell surface and therefore by membrane-bound FGFRs or via

internalized FGFRs. Intracellular phosphorylation results in activation of FGFRs, which mediate interaction with cytosolic adaptor proteins and signaling via the RAS-MAPK, PI3K-AKT, PLCγ, and STAT intracellular pathways. Furthermore, synthesis and degradation of FGFRs can modulate and regulate the strength of the FGFR signal[293].

So far, contradictory information concerning the applied bFGF concentration and its explicit effect on ASC differentiation is present in literature, nevertheless indicating a high potential for adipose tissue engineering applications. Therefore, we addressed in the present chapter the effect of bFGF on ASC proliferation and differentiation capacity by applying different concentrations of the growth factor, at different time points of culture.

4.2.1 Influence of bFGF on ASC cell growth and morphology

The impact of the application of bFGF on the proliferation of ASCs was investigated by analyzing the DNA content per well during culture time (Figure 4.6). A clear and continuous increase in DNA content attributed to the application of different bFGF concentrations (3 and 10 ng/mL) was observed in comparison to control conditions (0 ng/mL) (Figure 4.6 A). While cells cultured without bFGF grew very slowly and only reached an amount of approximately 2 µg DNA per well after 14 days, the bFGF-treated cells grew very fast to much higher level (about 10-11 µg on day 14). However, both bFGF concentrations (3 and 10 ng/mL) showed a similar effect on the proliferation capacity of ASCs, as the higher concentration caused no further increase. These differences in DNA content reflecting great differences in cellular proliferation between control and bFGF-treated cells were further corroborated by microscopic analysis. All three culture conditions displayed a confluent cell layer, however with a distinct difference in cell morphology (Figure 4.6 B). Cells cultured without bFGF displayed a flattened and spread shape, while bFGF-treated ASCs appeared much smaller and spindle-shaped. Besides the effect of acceleration of the proliferation, bFGF provoked thus a change in cell shape, being responsible for the ability of the cells to form a much denser cell layer than the cells cultured without.

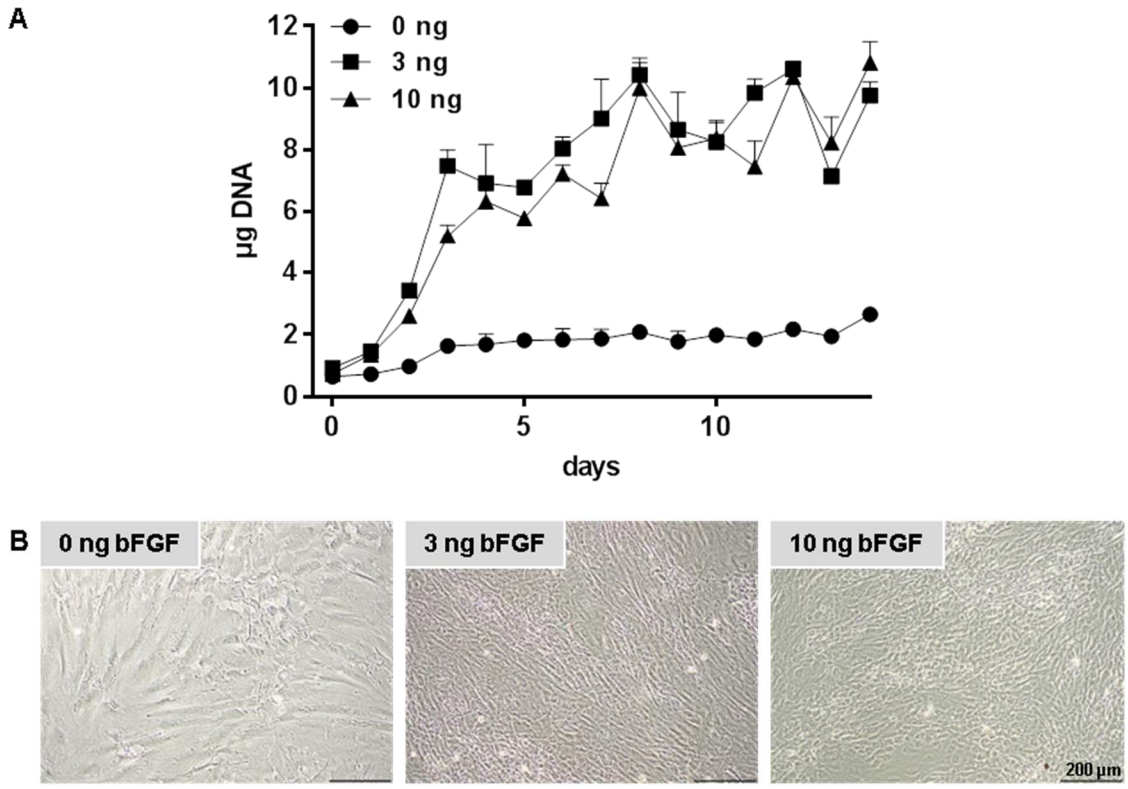

Figure 4.6: Effect of different bFGF concentrations on cell growth of ASCs.

Cells were seeded with an initial seeding density of 5,000/cm^2, and were cultured in the presence of 0, 3, and 10 ng bFGF per mL culture medium. **A**) Growth curve determination by DNA content. Samples were taken every other day for a 14 days culture period. Values are expressed as mean with standard deviation (n=3) in µg DNA per sample. **B**) Histological documentation of cell density and morphology after 14 days of cell growth in the presence of 0, 3, and 10 ng bFGF. Representative images were taken at a 10-fold magnification by phase contrast microscopy; scale bars represent 200 µm.

4.2.2 Effect of bFGF preculture vs. continuous application on adipogenic differentiation capacity of ASCs

In order to investigate the effect of bFGF on adipogenic differentiation of ASCs, cells were precultured (PC, i.e. bFGF application only during proliferation phase), continuously treated (during PC and adipogenic differentiation) or only supplemented during adipogenic induction phase with different concentrations of bFGF (0, 3 and 10 ng/mL). The detailed experimental setup was visualized in Figure 4.7. For this experiment, cells were seeded with 25,000 per cm^2 and were hormonally induced (differentiation medium) to undergo adipogenesis 2 days after seeding. Induction was either performed permanently (Figure 4.8 A) for 14 days or under short-term conditions (2 days: differentiation medium & 12 days: maintenance medium; Figure 4.8 B). Histological examination by Oil Red O staining clearly revealed an influence of bFGF preculture on the ASC differentiation potential

(Figure 4.8). Under permanent induction, it was evident that more cells precultured with 3 and 10 ng bFGF were able to differentiate, compared to the expansion without bFGF (Figure 4.8 A). In contrast, permanent application of bFGF (Figure 4.8 A, second and third row, last images) or solely during induction phase (Figure 4.8 A, first row, last two images) of either 3 or 10 ng/mL bFGF had no specific, additional effect on adipogenesis, in comparison to its respective preculture only group. For short-term induced samples, the same promoting effect of bFGF application was shown (Figure 4.8 B). Here, cells were only treated with the hormonal cocktail for 2 days (differentiation medium), followed by continuous application of maintenance medium for the final differentiation period of 12 days. The findings of the histological investigation of short-term induced ASCs, corroborated the results of the permanent-induced cells, demonstrating clearly an adipogenesis-promoting effect of the bFGF preculture on the cells, but no further promoting influence was evident when bFGF was administered permanently or only during differentiation.

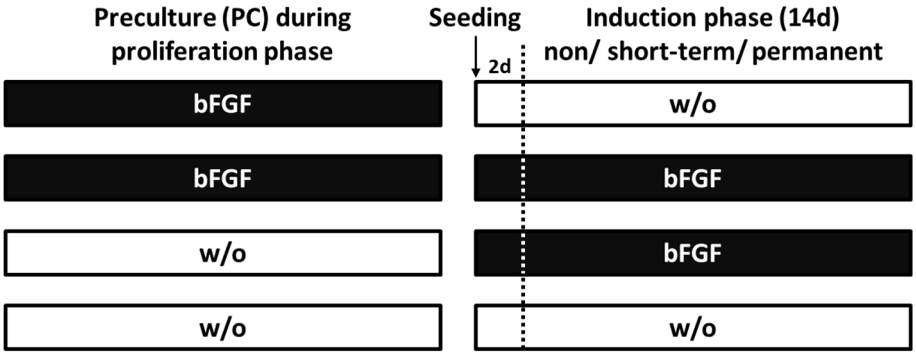

Figure 4.7: Schematic illustration of the experimental setup of bFGF supplementation during different periods of ASC culture.

ASCs were exposed to bFGF only during proliferation phase (preculture; PC), during the whole time in both proliferation phase and during induction, or only during induction (since seeding). Cells cultured in the absence of bFGF served as control. Cell proliferation was performed in basal medium. For induction, cells were initially cultured in growth medium for 2 days. After that, growth medium was supplemented at day 2 after seeding with a hormonal cocktail (differentiation medium), for either the whole period of 14 days (permanent) or for 2 days followed by maintenance medium for 12 days (short-term). Non-induced samples (non) served as control. The respective culture medium was further supplemented with bFGF according to experimental setup. White bars represent cell cultivation w/o bFGF, black bars represent supplementation with 3 or 10 ng/mL bFGF. Results are displayed in Figure 4.8 and Figure 4.9.

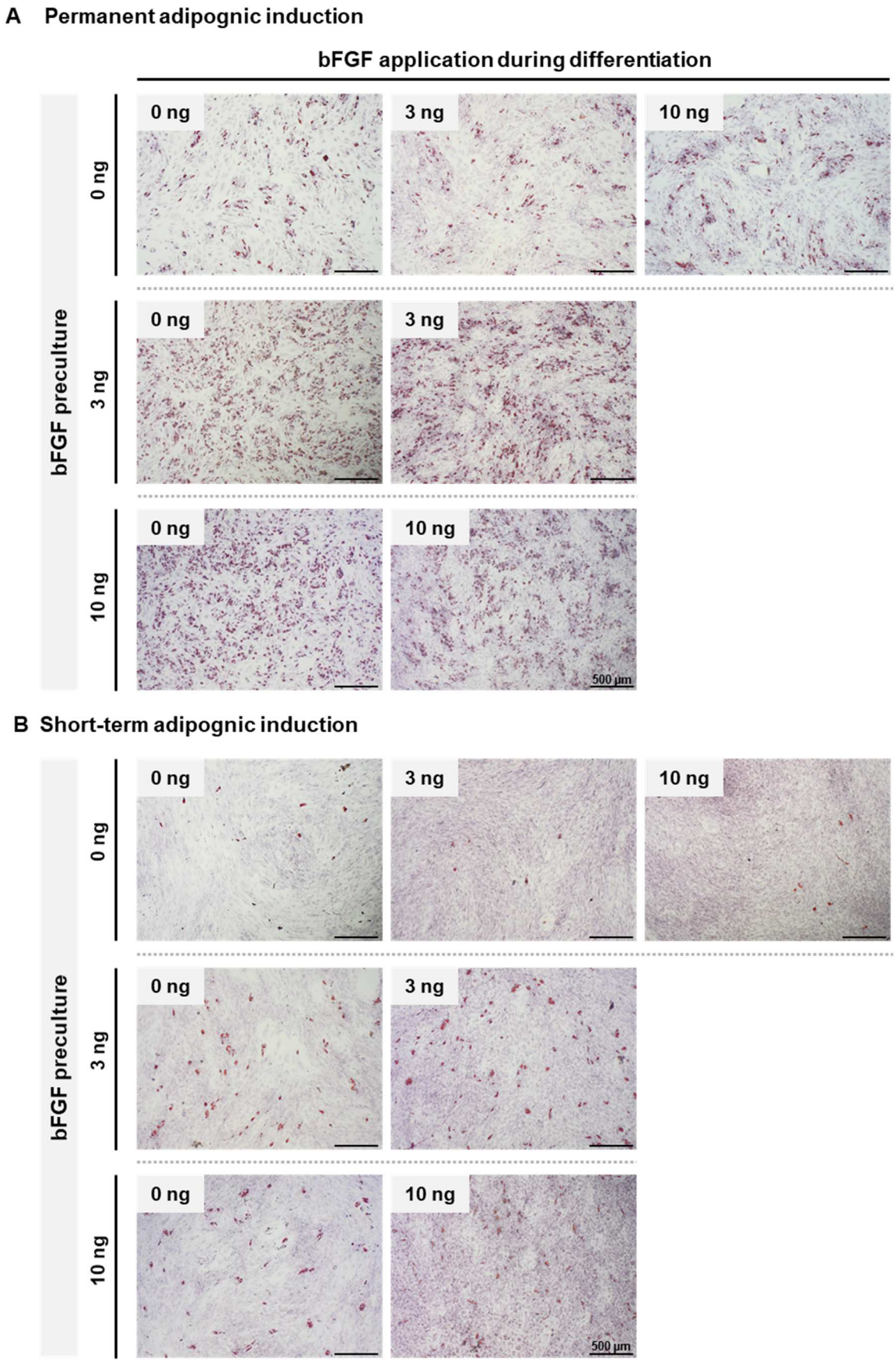

(legend on next page)

Figure 4.8: Histological investigation of the influence of bFGF application at different time points of culture on adipogenic differentiation of ASCs.

Histological examination of the influence of bFGF preculture, continuous application or administration only during induction (of 0, 3 and 10 ng/mL bFGF) on adipogenic differentiation of ASCs. Cells were initially seeded with 25,000/cm^2 and cultured for 2 days in 24-well plates before adipogenic induction (permanent and short-term). Histological analysis of adipogenesis of **A**) permanently and **B**) short-term induced samples was performed by staining with Oil Red O (ORO, red) and hematoxylin (blue) on day 14 of adipogenic induction. Representative images are shown. Images were taken at a 4-fold magnification; scale bars represent 500 µm.

Quantification of DNA content revealed a highly significant difference in cell proliferation capacity between PC groups, provoked by the bFGF preculture and enhanced by the two-day culture period before adipogenic induction (Figure 4.9 A). Short-term induced samples showed generally the highest proliferative activity. Most strikingly, cell density on the day of induction was significantly elevated in the 3 and 10 ng preculture groups in comparison to cells cultured without bFGF. This disparity in proliferative capacity between preculture groups, resulted in significant different initial cell densities at day 0, the point of induction (2 days after seeding). Quantification of the triglyceride amount corroborated the histological findings, with an apparent significant increase in triglyceride content per DNA for permanently induced cells, being again even more pronounced for bFGF precultured cells (3 and 10 ng; Figure 4.9 B). However, the preculture with 3 ng bFGF displayed a strikingly significant promoting effect on adipogenic differentiation compared to the 10 ng precultured cells. Both, continuous application and addition only during adipogenic differentiation, showed likewise no additional effect on triglyceride accumulation in comparison to the preculture only group. The triglyceride accumulation, which was seen for short-term induced samples in the histological investigation, was not reflected in the quantitative triglyceride content, caused by the high proliferation activity of these cells. Summarizing, it could be clearly demonstrated that the precultivation of ASCs with 3 ng bFGF before adipogenic induction significantly promoted the adipogenic differentiation capacity of the cells in comparison to all other groups.

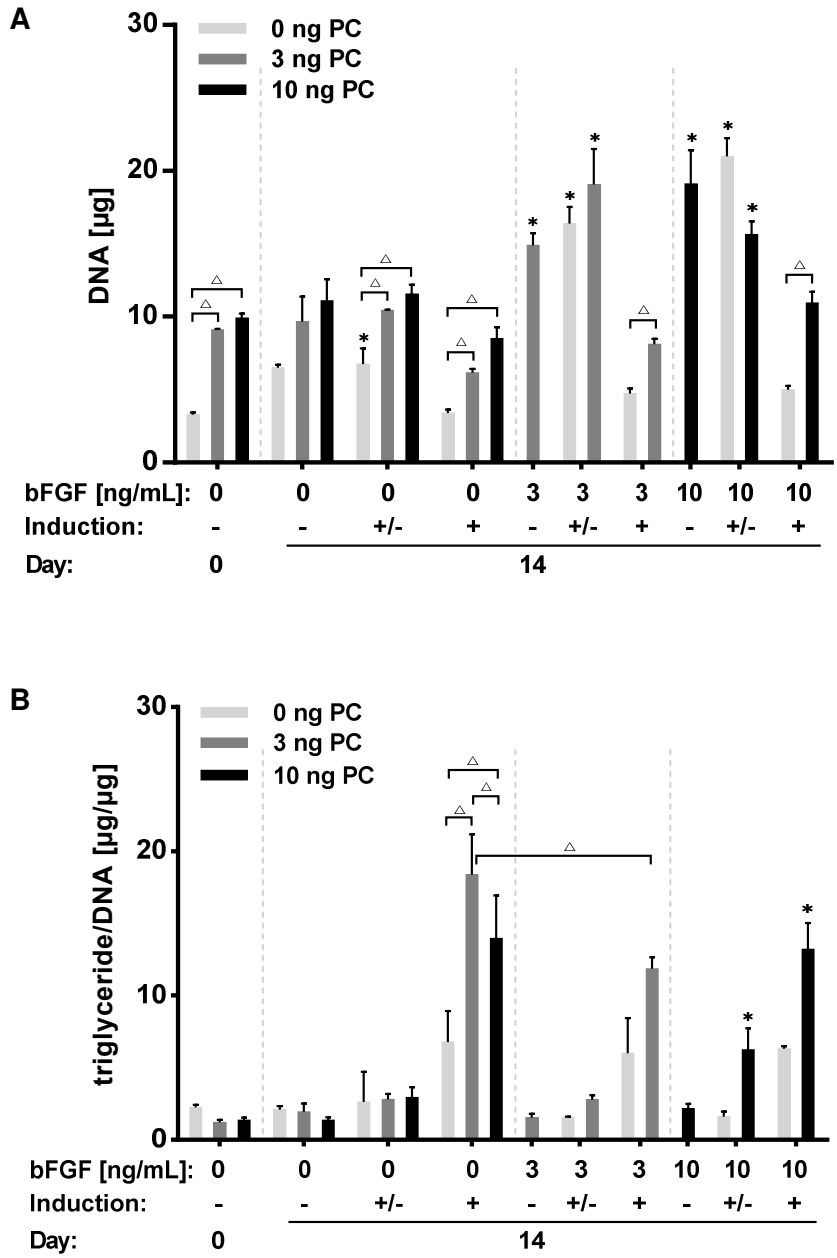

Figure 4.9: Influence of bFGF application at different points of culture on adipogenic triglyceride accumulation on ASCs. Influence of the bFGF preculture (PC), continuous application or administration only during induction (of 0, 3 and 10 ng/mL) on the triglyceride accumulation of adipogenically induced ASCs. Cells, precultured with 0, 3 and 10 ng bFGF, were initially seeded with 25,000/cm² and cultured for 2 days in 24-well plates before adipogenic induction. After that, cells were cultured under non-induced (-), short-term (+/-) and permanent (+) induction conditions. During subsequent culture period bFGF was again administered in different concentrations (0, 3 and 10 ng/mL). **A**) Determination of the DNA content was performed on day 0 and 14 within the three experimental groups (0, 3 and 10 ng/mL PC). Values are expressed as mean with standard deviation (n=3). Statistically significant differences ($p<0.05$) to d0 value of the respective group (d0 of 0, 3 or 10 ng/mL PC) are indicated by * and to the respective value in the 0 ng PC group by △. **B**) Quantification of triglyceride content was performed for day 0 and day 14 samples. Triglyceride values were normalized to the DNA content of the respective sample (µg TG per µg DNA). Values are expressed as mean with standard deviation (n=3). Statistically significant differences ($p<0.05$) to reference value (d0) of the respective group (0, 3 or 10 ng PC) are indicated by *, to other values by △.

4.2.3 Impact of bFGF preculture in conjunction with a 2-day proliferation phase

The previous findings raised the question if the bFGF-attributed and observed significant cell density difference at the time point of induction (POI) is responsible for the promoting effect of bFGF preculture on ASC differentiation capacity. Consequently, the following experiment was designed to eliminate the effect of varying cell density at POI, by eliminating the standard 2-day culture before induction. The detailed experimental setup is depicted in Figure 4.10. Hence, cells were cultured in two groups, with adipogenic induction 4 hours (Group A: POI 4h) or 2 days after seeding (Group B: POI 2d; standard experimental setup), under non, short-term, and permanent induction conditions, both groups being precultured w/o or with 3 ng bFGF, respectively. The induction after 4 hours prevented cellular proliferation and ensured comparable cell densities at time point of induction (POI).

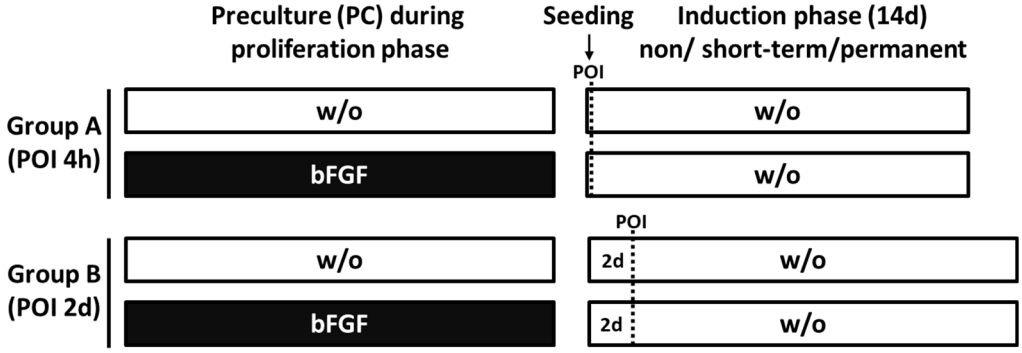

Figure 4.10: Schematic illustration of the experimental setup of bFGF preculture in conjunction with a 2-day proliferation phase on ASC differentiation capacity.

Investigation on the impact of the standard 2-day culture period before adipogenic induction in conjunction with bFGF preculture (results displayed in Figure 4.11). ASCs were precultured w/o or with 3 ng/mL bFGF only during proliferation phase (preculture; PC); no bFGF was applied during induction phase (since seeding). Generally, cell proliferation was performed in basal medium, while cells were cultured in growth medium for induction (after seeding). Induction was performed either 4 hours (Group A; Point of induction = POI 4h) or 2 days (Group B; POI 2d) after seeding. For differentiation, growth medium was supplemented at POI with the hormonal cocktail (differentiation medium), for either the whole period of 14 days (permanent) or for 2 days followed by maintenance medium for 12 days (short-term). Non-induced samples (non) served as control. White bars represent cell cultivation w/o bFGF, black bars represent supplementation with 3 ng/mL bFGF.

Histological evaluation of cells cultured under permanent induction in group B (POI 2d) showed an apparent improvement of adipogenic differentiation in comparison to group A (POI 4h), alike displayed for both PC settings (0 and 3 ng/mL bFGF; Figure 4.11 A). Likewise, short-term induced samples in group B showed likewise a more pronounced ability to differentiate, than the cells in group A. This was observed for the 3 ng PC short-term induced samples, while the 0 ng PC short-term induced samples failed to differentiate in both groups. However, a slightly more pronounced

differentiation capacity of cells precultured with 3 ng bFGF was detectable demonstrated by the short-term and permanent induced samples within both groups.

Quantitative DNA content analysis revealed a statistically significant cell density difference at time point of induction (POI) between both experimental groups A and B, being obviously more elevated with continued culture (2 days, Group B) before adipogenic differentiation (Figure 4.11 B). This difference between groups did not exist anymore at day 14 for permanently induced samples. Triglyceride quantification per µg DNA confirmed the histological observations, demonstrating a significant impact of the 2-day culture period prior to induction, on the ASC differentiation capacity (Figure 4.11 C). Additionally, the bFGF preculture still significantly improved the adipogenic potential of ASCs within both groups. Taken together, it could be shown that the difference in differentiation capacity between both groups can be explained by the differences in cell proliferation prior to induction, resulting in different cell densities at the point of induction. However, bFGF preculture still positively influenced the differentiation capacity of ASCs, independent of the attributed proliferative influence.

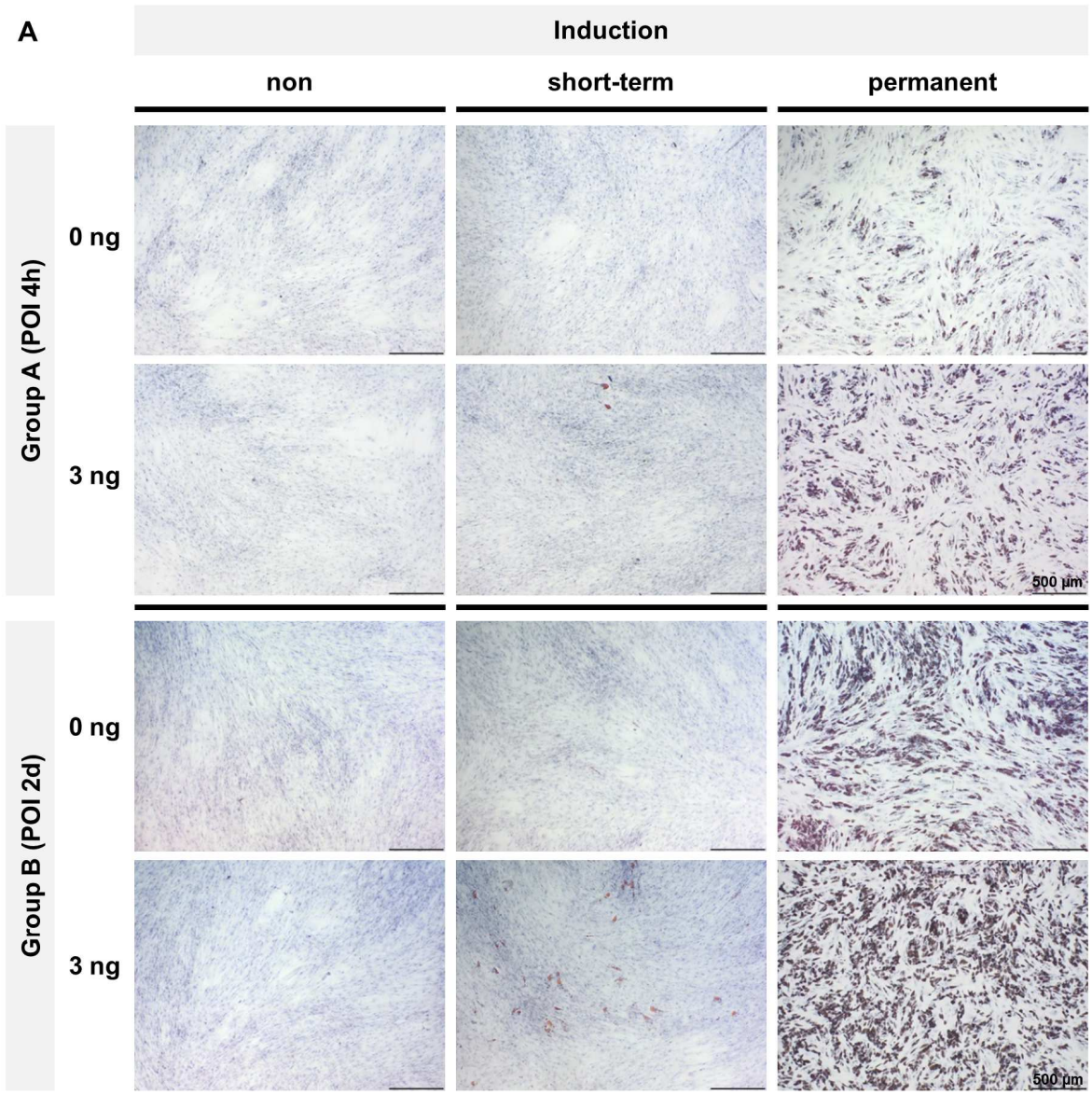

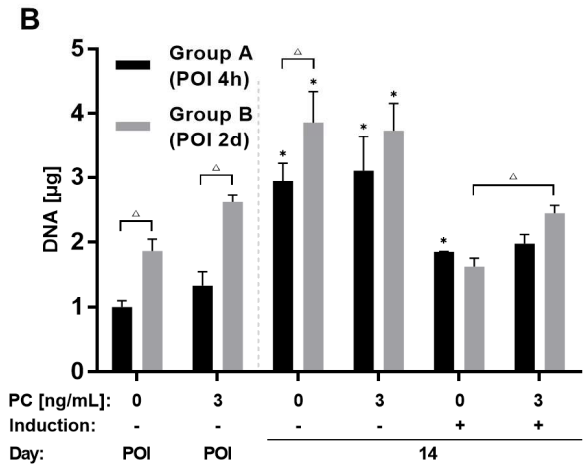

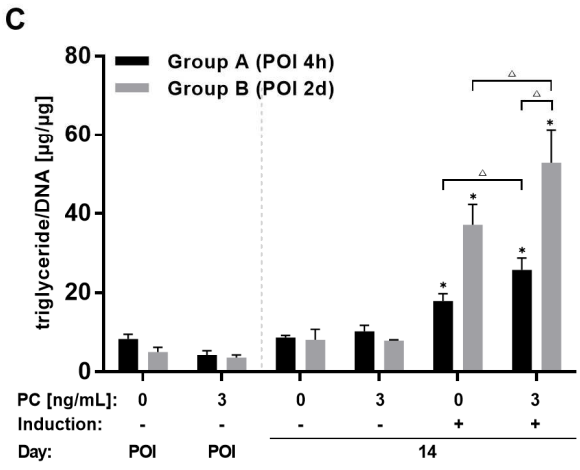

(legend on next page)

Figure 4.11: Impact of the standard 2-day preculture period before adipogenic induction in conjunction with a 0 and 3 ng/mL bFGF preculture (PC).

Impact of the standard 2-day preculture period before adipogenic induction in conjunction with a 0 and 3 ng/mL bFGF preculture (PC). Cells were precultured with 0 or 3 ng/mL bFGF for cellular expansion (proliferation phase). Initial seeding density was 25,000/cm^2 and induction was performed either 4 hours (Group A; Point of induction = POI 4h) or 2 days (Group B; POI 2d) after seeding into 24-well plates. No bFGF was administered after seeding. Cells were cultured under non-induced (-), short-term (+/-; only depicted for histology) and permanent (+) induction conditions **A**) Histological analysis of adipogenesis of permanently and short-term induced samples by staining with Oil Red O (red) and hematoxylin (blue) on day 14 of adipogenic induction. Representative images are shown. Images were taken at a 4-fold magnification; scale bars represent 500 µm. **B**) Determination of DNA content was performed on day 0 and 14 in µg DNA in the two experimental groups (A: POI 4h and B: POI 2d). Values are expressed as mean with standard deviation (n=3). Statistically significant differences ($p<0.05$) to reference value of the respective group (POI, 0 or 3 ng of group A and group B) are indicated by * and to other values by $^{\triangle}$. **C**) Quantification of triglyceride content was performed for day 0 and day 14 samples. Triglyceride values were normalized to the DNA content of the respective sample (µg triglyceride per µg DNA). Values are expressed as mean with standard deviation (n=3). Statistically significant differences ($p<0.05$) to reference value of the respective group (POI, 0 or 3 ng of group A and group B) are indicated by * and to other values by $^{\triangle}$.

4.2.4 Investigation of bFGF preculture in a 3D hydrogel system

Hereinafter, we transferred our previous investigations into a 3D hydrogel system and initially tested cellular proliferation and survival of ASCs within these scaffolds under bFGF application. Therefore, cells were seeded in TISSEEL hydrogels with 8×10^5 cells per 40 µL construct and were cultured for 14 days with 3 ng/mL bFGF. To test proliferation capacity and survival of the cells, Ki-67 and live/dead staining was performed (Figure 4.12). Histological analysis of cell development in the hydrogel clearly demonstrated the survival of the cells (green staining with calcein for living cells, and red staining with ethidium bromide for dead cells) and hardly any proliferative cells in comparison to d0 samples. Thus, a proliferative effect causing density differences at the POI could be excluded in this system. In general, cells displayed a roundish cell shape having only little contact to neighboring cells.

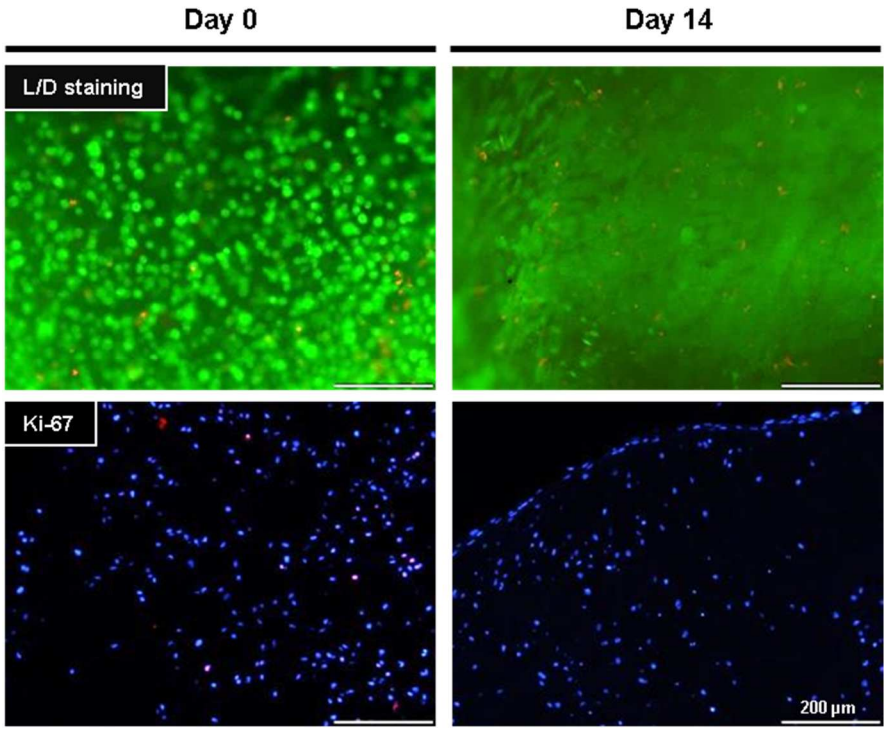

Figure 4.12: Survival and proliferation of ASCs in the 3D fibrin hydrogel constructs.

Live/dead staining on whole constructs seeded with ASCs (8 x 10^5 cells per 40 µL gel) cultured with 3 ng/mL bFGF was performed on day 0 and day 14. Living cells are stained green (calcein) and dead cells are stained red (ethidium bromide). Immunohistochemical staining for Ki-67 was conducted on cryosections (8 µm) of the 3D hydrogels (day 0 and 14). Ki-67 was stained red and nuclei blue with DAPI. For each staining representative images are depicted. Images were taken at a 10-fold magnification; scale bars represent 200 µm.

Within this culture system preventing undesired cell density differences at any time, the promoting influence of bFGF preculture on adipogenesis in 3D culture was examined. ASCs precultured with 0 and 3 ng/mL bFGF were seeded into the TISSEEL hydrogel constructs and were hormonally induced (differentiation medium) for 21 days. Histological evaluation of cryosections by Oil Red O staining demonstrated a profound differentiation of the ASCs in comparison to the non-induced controls (Figure 4.13 A). No difference between preculture groups became apparent. DNA examination confirmed the before described absence of proliferation (Figure 4.13 B), and histologically demonstrated ASC differentiation was corroborated by triglyceride assay, with a slight but not statistically significant tendency for improvement of adipogenic differentiation with 3 ng/mL bFGF preculture (Figure 4.13 C). Even if this 3D hydrogel cell culture system is not comparable to the previous 2D culture conditions, it still implies some slight cues. As enhanced cell density and thus increased cell-cell contact was absent and furthermore the previously seen bFGF effect was not detected in this 3D hydrogel system, it seems that both factors, cell density and cell-cell contact, might play a critical role for ASC adipogenic differentiation capacity.

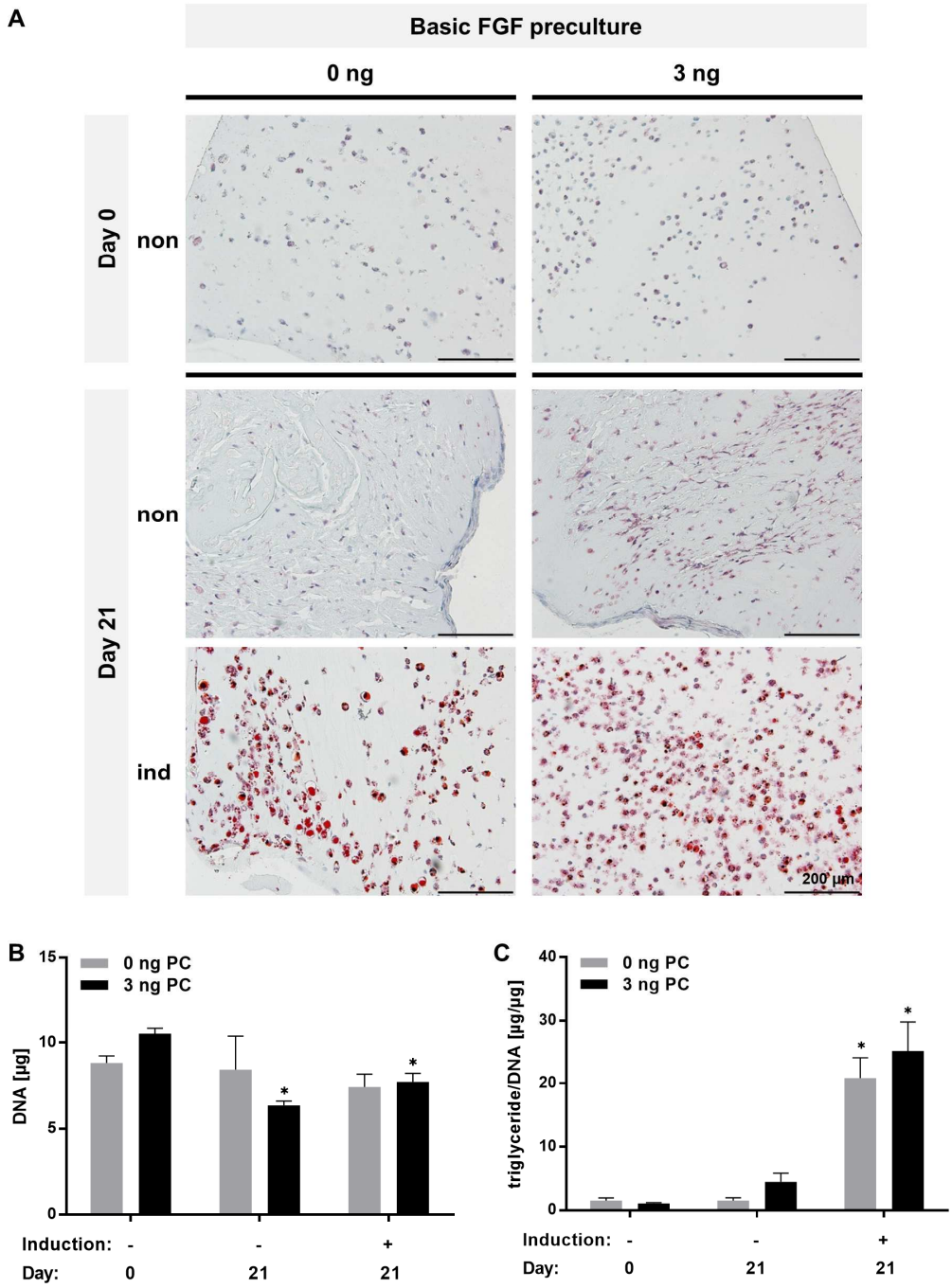

Figure 4.13: Impact of bFGF (3 ng/mL) preculture on the differentiation capacity of ASCs in 3D culture.

Cells were precultured with 0 or 3 ng/mL bFGF and seeded (8 x 10^5 cells per scaffold) into TISSEEL gel constructs of 40 µL. Cells were cultured two days after seeding under non-induced and permanent-induced conditions (w/o bFGF) for 21 days. **A**) Histological investigation with Oil Red O (ORO, red) and hematoxylin (blue) on cryosections (8 µm) of the 3D hydrogel constructs (d0 and d21). Representative images are depicted. Images were taken at a 10-fold magnification; scale bars represent 200 µm. **B**) DNA content determination was conducted on day 0 and 21 for both preculture groups (0 and 3 ng/mL). Values are expressed as mean with standard deviation (n=3). Statistically significant differences ($p<0.05$) to reference value of the respective group (d0 of 0 or 3 ng/mL PC) are indicated by *. **C**) Determination of the triglyceride content was performed and normalized to the respective DNA value (µg triglyceride per µg DNA). Values are expressed as mean with standard deviation (n=3). Statistically significant differences ($p<0.05$) to reference value of the respective group (d0 of 0 or 3 ng/mL PC) are indicated by *.

4.2.5 bFGF preculture, cell density, and adipogenesis

As the so far conducted experiments on the impact of bFGF on adipogenesis of ASCs indicated a crucial role of cell density at the point of induction (POI), influenced by bFGF preculture, the influence of cell density on adipogenesis in conjunction with bFGF PC was examined in more detail. Therefore, cells were seeded at four different initial cell seeding densities, ranging from 12,500 to 100,000 cells/cm^2, each being precultured both with 0 and 3 ng/mL bFGF. With increasing initial cell seeding density an apparent higher amount of triglyceride containing cells was demonstrated by histological evaluation via Oil Red O staining after 14 days of induction, as depicted in Figure 4.14 A. Comparison of bFGF preculture groups again displayed a distinct increase in differentiated cells in the 3 ng/mL PC group, compared to the respective cell seeding densities in the 0 ng/mL PC group. This effect was also observed regarding the short-term induced ASCs. Here, 3 ng precultured cells displayed some differentiated ASCs already at a density of 50,000/cm^2, while 0 ng precultured cells only marginally differentiated at a density of 100,000/cm^2. Quantitative DNA analysis confirmed the seeding ratio comparable in both groups at the point of induction (day 0), the maintenance of the density gradient over the whole culture period and the equality of proliferation level between PC groups (Figure 4.14 B). Quantitative triglyceride measurement, which displayed a statistically significant increase in triglyceride content per DNA with increasing cell seeding density in both preculture groups, corroborated the observation of the Oil Red O histology (Figure 4.14 C). Furthermore, a slight but statistically not significant tendency between preculture groups remained.

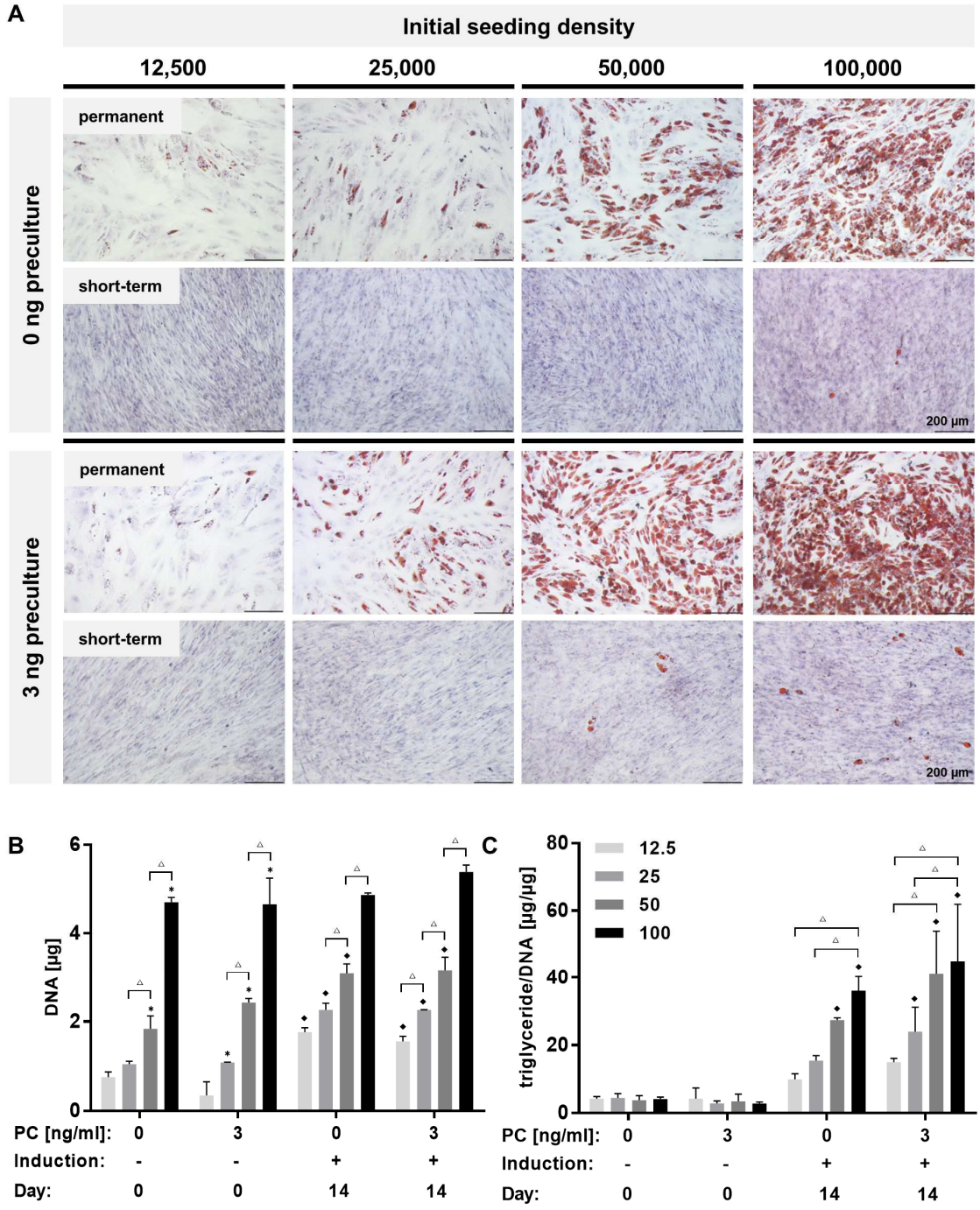

Figure 4.14: Influence of the initial seeding density and the bFGF PC on adipogenesis of ASCs.

A) Histological analysis of adipogenesis by staining with Oil Red O (ORO, red) and hematoxylin (blue). Differences in adipogenic differentiation for permanently and short-term induced samples on day 14 were examined for both experimental groups (0 and 3 ng/mL bFGF PC) regarding different seeding densities (12,500, 25,000, 50,000 and 100,000/cm²). Representative images are shown. Images were taken at a 10-fold magnification; scale bars represent 200 µm. **B**) DNA and **C**) triglyceride quantification was performed for permanently induced samples (d0, d14). For each preculture group the four different seeding densities are displayed. DNA content is depicted in µg per sample and triglyceride content in µg triglyceride per µg DNA of the respective DNA sample. Statistically significant differences ($p<0.05$) to the respective reference value (d0 precultured with 0 or 3 ng/mL bFGF) are indicated by * and between densities within one group by △. Statistically significant differences between day 0 and day 14 among respective densities are depicted by ◆.

Taken together, we could demonstrate an effect of bFGF preculture on ASC differentiation capacity. Our observations indicate as underlying mechanism an impact of this preculture on cell proliferation capacity resulting in an increased cellular density at the time point of adipogenic induction and furthermore that this cell density difference at POI is pivotal for increased adipogenic capacity of the cells. However, the latter experiment still hints at another additional underlying mechanism, as the cells still show a slight but not significant influence of the bFGF preculture on adipogenic differentiation when proliferation is prevented. The depicted results therefore suggest that a cell-cell contact-mediated mechanism positively influences adipogenic differentiation.

4.2.6 Discussion

Adipose-derived stem cells, which are frequently used in regenerative medicine and are typically obtained by liposuction mainly from adult abdominal fat depots, carry as well as bone marrow stem cells (BMSCs) a multi-lineage capacity for differentiation into different tissue cell types. Those stem cells are commonly applied for autologous cell transplantation in order to regenerate defect sites of bone, cartilage, tendon and adipose tissue[18,56,294]. For this purpose, ASCs need to be expanded on a large scale *in vitro* while retaining their differentiation capacity, without replicative aging[246,247,295,296]. In order not to limit their clinical application capacity by a short lifespan or a reduction of their differentiation potential, suitable cell culture methods need to be evaluated. Thus, it could be shown that growth factor application can be helpful in meeting these challenges[247,248]. bFGF was reported to promote proliferation of MSCs by simultaneously positively impacting maintenance of multipotency and thus differentiation capacity as well as self-renewal of the cells[56,249,297]. However, concerning the effect of bFGF *in vitro*, inconsistent and divergent information is present in literature. Therefore, the purpose of this study was to investigate the application of different amounts of bFGF at different time points during cultivation, studying the effect on the proliferation and differentiation potential of ASCs.

By cell growth analysis it could be demonstrated that ASC proliferation can be significantly increased by applying bFGF (3 and 10 ng/mL bFGF) in comparison to culture conditions without bFGF, reaching 5 times the number of cells of the control condition within 14 days. Previously this proliferation fostering effect was similarly shown for ASCs and BMSCs, in some publications yet in a dose-dependent manner[248,289]. In comparison, this increase of cell number with higher concentrations of bFGF was absent in our experiments, displaying the same proliferation properties for 3 and 10 ng/mL. Previously also comparable effects were demonstrated, showing likewise no significant further increase of proliferation of ASCs with higher bFGF (1 vs. 10 vs. 100 ng/mL bFGF) concentrations[249,283]. Increased proliferation activity with bFGF was corroborated by histological

investigations, demonstrating for all settings a confluent cell layer, however greatly differing in cell morphology and therefore density. ASCs cultured with bFGF displayed a fibroblastic, spindle-shaped phenotype, whereas control cells cultured without bFGF progressively acquired a larger, more flattened phenotype, both similarly demonstrated in literature[37,249,289,298]. The difference in cell morphology is furthermore responsible for the ability of the bFGF cultured cells to form a much denser cell layer than cells under control conditions.

Investigations on the impact of bFGF on the differentiation capacity of ASCs have demonstrated varying effects depending on the growth factor concentration (ranging from 0.4 to 1,000 ng/mL)[58,248,283,285,289]. Kakudo et al.[58] and Neubauer et al.[261] demonstrated that preculture with 10 and 3 ng/mL bFGF, respectively, only during proliferation phase, promoted the most prominent increase of subsequent adipogenic differentiation capacity. Furthermore, an inhibitory effect of bFGF on differentiation was shown, every time FGF was applied during induction or trans-differentiation processes[285–288]. Hence, a key aspect in this case obviously seemed to be the time point of bFGF application. Concerning the bFGF concentration, Inoue and coworkers could only see a promoting impact of bFGF on adipogenesis of ASCs with a high concentration of 100 ng/mL, possibly owed to the short preculture period of 5 days[283]. In contrast, our cells were cultured under growth factor conditions over the whole proliferation period for 3 passages. Another work of Kim et al. nevertheless demonstrated a promoting effect of bFGF on adipogenesis of ASCs by low concentrations between 0.4 and 2 ng/mL, even though showing an inhibitory effect of 10 ng/mL or higher bFGF concentrations[299]. In our analysis, regarding application time point (preculture, preculture and induction phase, or only during induction phase) and concentration (0, 3 and 10 ng/mL bFGF), we have demonstrated a great impact on adipogenic differentiation capacity of ASCs both on a histological level and by quantitative triglyceride determination. In accordance with the results published by Kakudo et al.[58] we demonstrated that only preculture with bFGF during proliferation phase, promoted adipogenic differentiation. However, application during proliferation and differentiation or just during induction led to no further increase in differentiation capacity, similarly depicted for short-term induction. Additionally, 3 ng/mL bFGF preculture turned out to foster the most prominent improvement of adipogenesis in our investigations.

In this experiment, it became obvious that bFGF preculture triggered, even without continued growth factor application, subsequent proliferation of the cells. This resulted in greatly varying cell density at POI (point of induction, 2 days after seeding), for cultures precultured with bFGF compared to the respective control group without growth factor application. To investigate the impact of the observed cell density differences provoked by bFGF preculture, two experimental settings were compared, either immediately induced 4 hours (POI 4h) or as previously performed 2 days (POI 2d)

after seeding, with the most beneficial preculture condition of 3 ng/mL bFGF. The obtained data clearly demonstrated again a promoting effect of the bFGF precultivation on the differentiation capacity for both, permanent and short-term induced ASCs. However, adipogenesis was in general more pronounced for cells being induced 2 days after seeding, indicating an additional involvement of proliferation and thus cell density.

In order to investigate the differentiation-promoting effect of the bFGF preculture in a three-dimensional set-up, cells were additionally cultivated in a fibrin hydrogel system. The applied hydrogel system (TISSEEL) represents a commonly used FDA-approved allogeneic fibrin sealant for adipose tissue engineering approaches[300]. Nevertheless, we primarily analyzed cell survival and proliferation capacity in these 3D hydrogels. It turned out that ASCs were not able to replicate in these TISSEEL hydrogel constructs, proven by DNA quantification and histological investigation on proliferation. On histological and quantitative level, a slight but by far not significant increased adipogenesis caused by bFGF preculture could be demonstrated. In general, a substantial adipogenesis could be shown for both groups. However, the applied 3D hydrogel system represented a completely different cell culture system, which is not comparable to our previous 2D conditions, but still can provide hints for our bFGF investigation. Since proliferation was impaired in the 3D hydrogels, the effect of bFGF preculture can obviously be more pronounced and powerful in 2D conditions, allowing more direct cell-cell contact. Taken as a whole, due to previous bFGF-attributed findings in 2D and the results gathered in 3D hydrogels, it seems that cell density besides the not negligible morphological change, impacts adipogenic differentiation capacity of ASCs.

In previous studies a variety of bFGF-induced mode of actions on the differentiation of MSCs were discussed. Besides the acknowledged proliferative action, it was concluded that cells are maintained in an immature, precommitted state with support of their self-renewal capacity[56,249,286,287,299]. Another investigation discovered a preferential proliferation of a subpopulation or even selection of early progenitor hBMSCs, depicted by an early increase in telomere size with bFGF incubation[246,251]. The mode of action of bFGF was associated in 3T3-L1 preadipocytes with an involvement of the MEK/ERK signaling pathway, to enhance the peroxisome proliferator-activated receptor γ (PPARγ) expression, which has a key role in the adipogenic conversion[301]. Furthermore, it was illustrated that continued bFGF application during differentiation of 3T3-L1 cells caused a prolonged MEK activation, or likewise, higher bFGF concentrations (>10 ng/mL bFGF) during hASC preculture caused sustained phosphorylation of ERK, inhibiting subsequent adipogenesis in both cases[299,301]. Neubauer et al. demonstrated an enhancement of PPARγ by FGF2 application in rat BMSCs, displaying an adipogenesis promoting mechanism[261]. Additionally, a FGF2 action through a JNK signaling pathway for ASC proliferation and adipose tissue regeneration and suppression of fibrogenesis after injury was

previously demonstrated[289]. In these investigations, proliferation and therefore increased cell density is an often mentioned, even though neglected effect of bFGF application. Our experiments suggest that increased cell density has a considerable impact on differentiation of ASCs.

Hence, we assumed cell density and thus altered cell-cell contact, also due to morphological changes, to be a further explanation for the bFGF impact on differentiation capacity. To check this presumption, cells were seeded in four different initial seeding densities (12,500-100,000/cm^2), and in order to prevent proliferation, cells were directly induced as previously tested 4 hours after seeding. Additionally, different bFGF preculture conditions (0 and 3 ng/mL bFGF) were applied. Clearly, this experiment illustrated a significant increase in adipogenic capacity, demonstrated both by histological and quantitative analysis, being associated with increased cell density. Despite the histological observations and the elevated triglyceride amount per DNA, it remained unclear if more cells were able to differentiate at higher densities, or if just more triglycerides could be accumulated per cell with the ratio of differentiated vs. undifferentiated cells being unchanged. This aspect could not be clarified at this moment and had to be examined in more detail hereafter (see Chapter 4.4.2). Furthermore, among preculture groups, the impact of the 3 ng/mL bFGF preculture was statistically not significant, yet marginally present. The here demonstrated apparent enhanced differentiation capacity of ASCs was previously, similarly shown to be dependent on an increased proliferation rate, administering FGF2 not exogenously, but through an autocrine and paracrine release by the cells, indicating as well a cell density related effect of bFGF[37].

In summary, the strong impact of bFGF application on ASC proliferation and adipogenic differentiation capacity was demonstrated. It became obvious that a precultivation of ASCs with bFGF is beneficial for subsequent adipogenic induction, while growth factor application during induction had no promoting influence. Furthermore, an influence on cell proliferation in conjunction with an altered cell morphology was depicted, hence, subsequently fostering a modified cell-cell framework and a higher cell density. In general, the latter appears to be a crucial requirement for ASC differentiation. Gaining insight into the mode of action of bFGF on the adipogenic differentiation process yields interesting conclusions to further understand the process of adipogenesis *in vitro*, to henceforth integrate this knowledge in tissue engineering and regenerative medicine approaches.

4.3 Establishment of analytical tools for investigations on gap junctional intercellular communication (GJIC)

The results presented in the previous chapter demonstrated, in agreement with literature that a precultivation with bFGF resulted in enhanced ASC proliferation and differentiation capacity. Presumed mechanisms and explanations for the bFGF mode of action concerning differentiation included PPARγ enhancement or selection of a preferential subpopulation with increased telomere size [246,251,261,301]. Apart from that, it became apparent that besides the so far supposed effects, also the alteration in cell density and thus, cell-cell contact is likely to influence adipogenic differentiation. Hence, this finding suggests that there is an apparently underlying cell-cell communication mechanism that directly impacts lineage commitment of ASCs, which would be very revealing to gain insights in.

Cell junctions accomplish communication links between adjacent cells in different ways. Anchoring junctions, like adherens junctions or desmosomes directly mechanically attach cells including their cytoskeleton to neighboring cells or the extracellular matrix, transferring mainly mechanical signals for intercellular communication[64,65]. Mechanical and morphological signals are demonstrably involved in differentiation of hMSCs into adipocytes[59]. Furthermore, gap junctions and chemical synapses mediate a direct passage of chemicals or electrical signals between connected cells[66,67]. Direct cell-cell communication processes like gap junctional intercellular communication are demonstrably involved in the contribution to cellular functions, including growth, differentiation, and cell death in stem cells[63]. Furthermore, it was previously demonstrated that FGF-2 prestimulation increased functional coupling of mesenchymal stem cells and cardiac cells via enhanced expression of the gap junctional component Cx43[302,303]. This led to the assumption that the involvement of gap junctions and thus cell-cell communication influences differentiation.

Gap junctions are formed of clusters of two paired hexametric hemichannels, called connexons, located in the cell membrane of adjacent cells. The basic building blocks of these functional channels are connexin (Cx) proteins. The family of channel forming connexins in humans is comprised of 21 members, being mostly named after their molecular weight, for instance Cx43 weighs 43 kDa[63,67]. Hemichannels are composed of one or several different isoforms, being homo- or heteromeric, and thus, homotypically or heterotypically paired, regulating permeability and regulatory functions[68,73]. Conformational change of functional GJ to an open condition for bidirectional exchange of molecules, as well as GJ turnover is regulated by change of Cx phosphorylation[74–76]. Through opened channels the intercellular passage of molecules smaller than 1 kDa (~1 nm in size) is feasible, including second messengers (e.g., cAMP, cGMP, IP_3), ions (e.g., Ca^{2+}, Na^+, H^+, Cl^-, K^+), metabolites (e.g., glucose, glutathione, adenosine, AMP, ADP, ATP), micro RNAs, and small peptides[63,67]. For functional investigation of gap junctional intercellular communication several acknowledged inhibitors are

described in literature, for instance carbenoxolone, 1-heptanol and 18α-glycyrrhetinic acid (AGA) besides others[78,255,262,304–307]. Yet, little is known about gap junctional communication in the context of ASCs and no research was done on its impact on adipogenic differentiation of these cells. So far, at least only the presence of Cx43-containing gap junctions in ASCs was depicted in literature[77,78].

Hence, in this chapter the basis was laid for the examination of gap junctional intercellular communication (GJIC) in ASCs. Therefore, dose responses for the acknowledged gap junctional inhibitor AGA were investigated with regards to effects on cell growth, and its principle impact on adipogenic differentiation, in comparison to the non-inhibitory analog of AGA, glycyrrhizic acid (GZA)[308]. Furthermore, an immunohistochemical staining protocol on undifferentiated ASCs was established, and verified the presence of the ubiquitously occurring gap junction channel-forming connexin Cx43.

4.3.1 Effect of different AGA concentrations on the proliferation of ASCs

For specific blocking of gap junctional intercellular communication (GJIC), 18α-glycyrrhetinic acid (AGA) was utilized. Gap junction blocking via AGA, besides other inhibitors, is a widely used tool in literature for the examination of GJIC in different cell types. In order to determine an appropriate concentration not affecting cell viability, the effect of different AGA concentrations on the proliferation of ASCs was evaluated. The non-inhibitory structural analog of AGA, GZA, was utilized as control. As both agents were dissolved in DMSO, it served as one of the controls (final maximum concentration was 0.5%), besides a control sample (w/o), which contained no further additives. Cells were seeded with 75,000 per cm^2 and were cultured in the presence of 35, 70 and 100 µM AGA as well as GZA in growth medium for 14 days. Quantitative DNA analysis demonstrated a statistically significant proliferation for all groups compared to d0, except for 100 µM AGA. 100 µM AGA significantly affected the DNA amount and therefore the cell proliferation of ASCs in comparison to control conditions (w/o, DMSO). GZA showed no influence concerning the DNA content, for none of the tested concentrations. Clearly, it could be demonstrated that a concentration of 100 µM AGA impaired the proliferation capacity of ASCs (Figure 4.15).

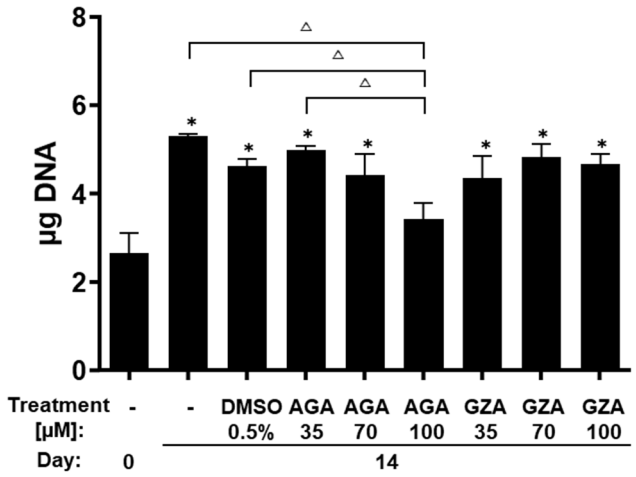

Figure 4.15: Examination of the influence of different concentrations of AGA and GZA on ASC proliferation.
Cells were precultured with 3 ng/mL bFGF and seeded with 75,000 cells per cm^2. Concentrations of 35, 70 and 100 µM of 18-α-glycyrrhetinic acid (AGA), and as non-inhibitory AGA analog glycyrrhizic acid (GZA) were tested during a 14 days period. In addition, ASCs were cultured under control conditions, without any other substance (w/o) and in the presence of the DMSO solvent (0.5%). Determination of the DNA content was performed on day 0 and 14 in µg DNA. Values are expressed as mean with standard deviation (n=3). Statistically significant differences ($p<0.05$) to reference value (d0 w/o) are indicated by * and to other values by △.

4.3.2 Effect of different AGA concentrations on the adipogenic differentiation

Successful inhibition of gap junctional intercellular communication in ASCs had to be furthermore evaluated for different AGA and GZA concentrations regarding adipogenic differentiation. For ensuring a robust degree of differentiation, again an initial cell seeding density of 75,000 cells/cm^2 was chosen (POI 4h) for the establishment of AGA and GZA concentration within the adipogenic context, since 25,000 cells/cm^2 previously showed a weak differentiation capacity when induced 4 hours after seeding (see Chapter 4.2; Figure 4.14). Histological analysis by Oil red O staining of samples revealed a considerable decline in triglyceride containing cells for 70 and 100 µM AGA (Figure 4.16 A). All other groups did not display any impairment of adipogenic differentiation, as emphasized also by images of the whole well, depicted in Figure 4.16 B. Accordingly, quantification of triglyceride amount showed a statistically significant increase in triglyceride content per DNA with adipogenic induction for all groups, with exception of 100 µM AGA (Figure 4.17 A). In comparison to control conditions (d14 ind: w/o and DMSO) 70 µM and 100 µM AGA demonstrated a statistically significant adipogenic decline, which corroborated the histological findings. In contrast to AGA, GZA did not display such an inhibitory effect, with none of the concentrations. Generally, it could be demonstrated for 35 µM AGA and all

GZA concentrations that adipogenic differentiation was not affected, while the solvent DMSO seemed to additionally influence adipogenesis, in comparison to the w/o ind control. The impact of concentration-dependent AGA inhibition on the differentiation capacity of ASCs was also analyzed at the gene expression level by measuring relative mRNA levels of the adipogenic marker genes PPARγ, C/EBPα, and the fatty acid binding protein aP2 (Figure 4.17 B). An inhibition of gene expression was shown for PPARγ with 100 µM AGA and C/EBPα with both 70 and 100 µM AGA, while all other samples for the three investigated marker genes displayed a significantly increased expression upon adipogenic induction in comparison to day 0. Whereas PPARγ displayed the least pronounced inhibition by AGA, C/EBPα and aP2 demonstrated a decrease in gene expression level for 70 and 100 µM AGA, in comparison to the DMSO d14 ind group, in a comparable manner for both concentrations. Again, DMSO supplemented samples were generally slightly affected in comparison to d14 w/o ind, significantly demonstrated for C/EBPα. GZA showed no concentration-dependent effect on mRNA expression level for all three adipogenic marker genes, which was in line with the quantitative triglyceride measurement. Histological analysis via live/dead staining demonstrated, furthermore, the viability of the adipogenically induced ASCs after 14 days of induction for all eight groups (Figure 4.18). Here, a slight impairment of viability could be seen for the 100 µM AGA group, since a few more dead (red) cells were visible. Taken together, 70 and 100 µM are effective concentrations of AGA for the inhibition of adipogenesis, while 100 µM showed in addition a slight impairment of cell viability. In general, GZA was demonstrated to be a good control agent in this context. Summing all these results up, 70 µM AGA was chosen as experimental concentration for all upcoming GJIC inhibition approaches.

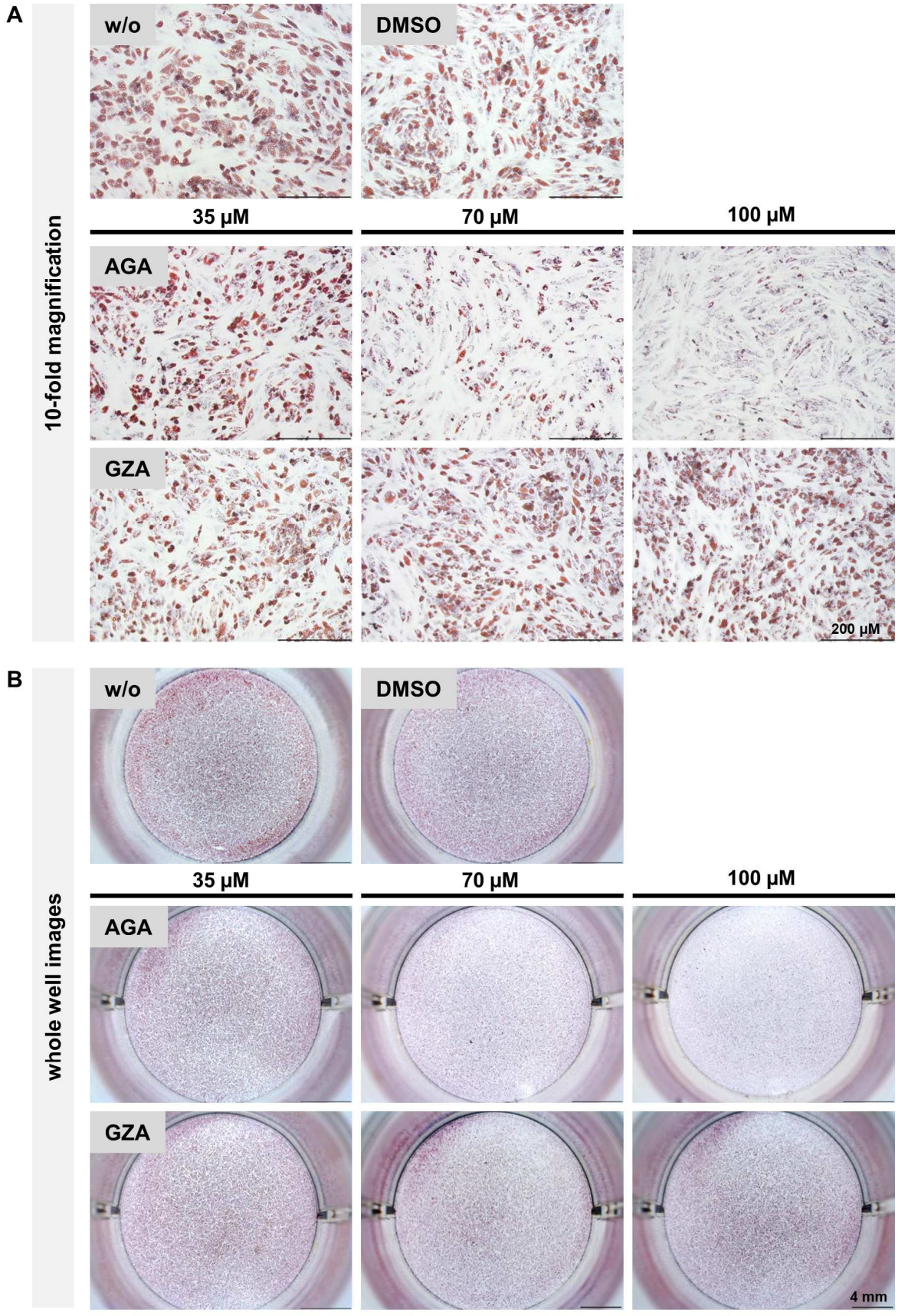

(legend on next page)

Figure 4.16: Analysis of adipogenesis under AGA and GZA influence.

Histological examination of the influence of 35, 70 and 100 µM AGA on adipogenic differentiation capacity of ASCs on day 14. Cells were precultured with 3 ng/mL bFGF, initially seeded with 75,000 cells per cm^2 and adipogenically induced after 4 hours. During induction, ASCs were cultured under control conditions (without any other substance (w/o) and in the presence of the DMSO solvent (0.5%)) and 35, 70, 100 µM AGA or GZA. Histological analysis of adipogenesis of induced samples by staining with Oil Red O (ORO, red) and hematoxylin (blue) was performed. Images were taken at **A**) a 4-fold magnification and **B**) by whole well imaging; scale bars represent 200 µm and 4 mm, respectively.

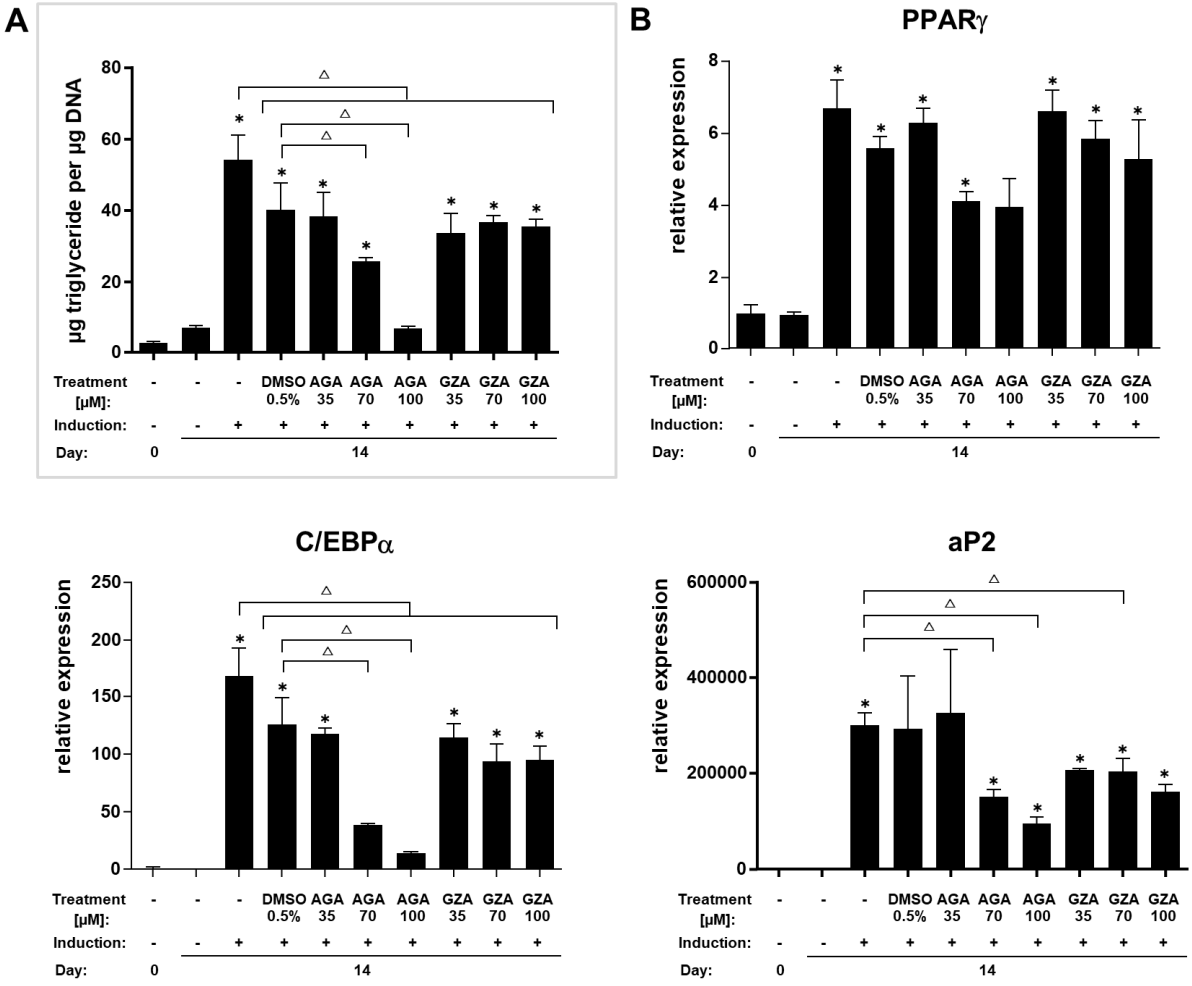

Figure 4.17: Analysis of the inhibition of GJIC by different AGA concentrations during differentiation.

Cells were precultured with 3 ng/mL bFGF, initially seeded with 75,000 cells per cm^2 and adipogenically induced 4 hours after seeding (induction for 14 days). During adipogenic induction, 35, 70 and 100 µM of 18-α-glycyrrhetinic acid (AGA), and as non-inhibitory AGA-analog, glycyrrhizic acid (GZA) were applied. In addition, ASCs were cultured under control conditions, either without additives (w/o), or in the presence of the solvent DMSO (0.5%). **A**) Triglyceride determination was performed for day 0 and day 14 samples (non, ind). Values are depicted in µg triglyceride per µg DNA of the respective sample. Statistically significant differences ($p<0.05$) to the reference value (d0 w/o) are indicated by * and to other values by $^{\triangle}$. **B**) Adipogenic marker gene expression (PPARɣ, C/EBPα, aP2) of ASCs was determined by qRT-PCR. Gene expression was normalized to EF1α; the obtained values were further normalized to day 0 w/o. Values are expressed as mean with standard deviation (n=3). Statistically significant differences ($p<0.05$) to the respective reference value (d0 w/o) are indicated by * and to other values by $^{\triangle}$.

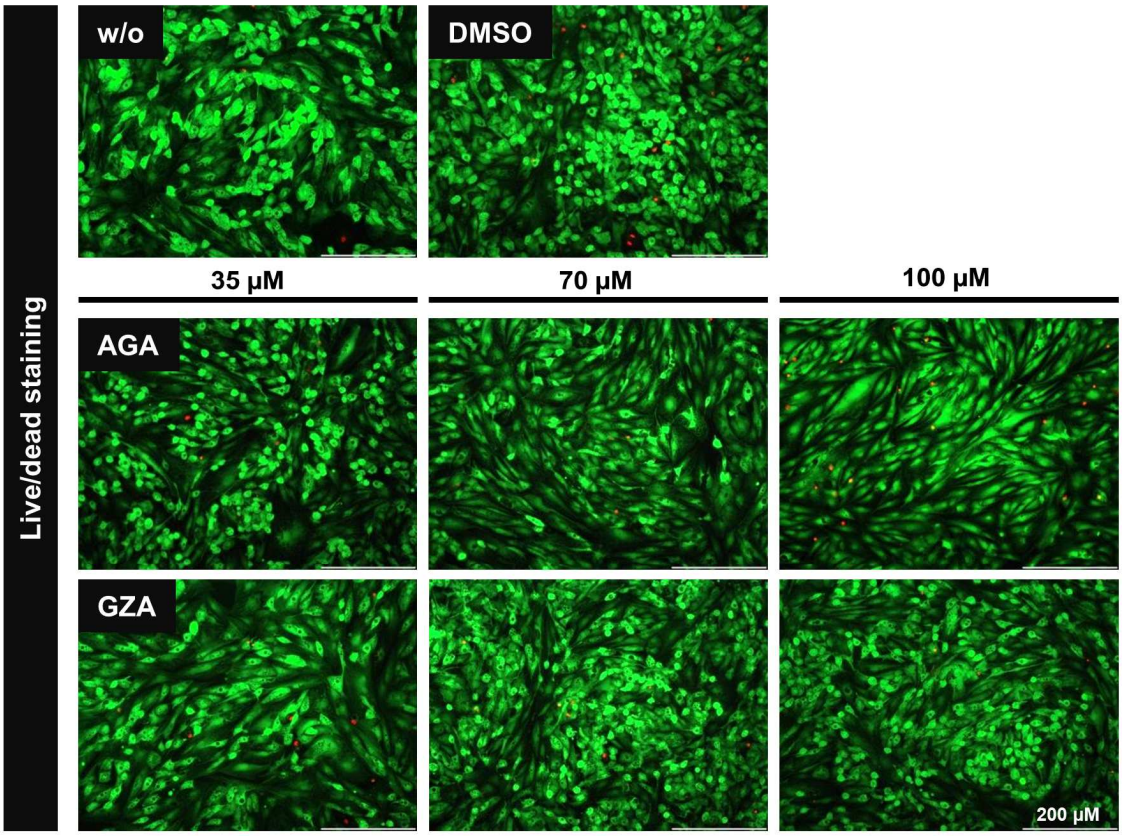

Figure 4.18: Analysis of cell viability under different AGA, GZA, and DMSO concentrations during adipogenesis.
Examination of the influence of 35, 70 and 100 µM AGA, GZA and the DMSO solvent alone on cell viability during adipogenic differentiation. Cells were precultured with 3 ng/mL bFGF, initially seeded with 75,000 cells per cm^2 and adipogenically induced after 4 hours. During induction, ASCs were cultured under control conditions (w/o) and in the presence of the solvent DMSO (0.5%) and 35, 70, 100 µM AGA or GZA. Histological analysis of living cells, stained green (calcein) and dead cells, stained red (ethidium bromide) was performed on day 14. Images were taken at a 10-fold magnification; scale bars represent 200 µm.

4.3.3 Establishment of the Cx43 immunohistochemical staining on ASCs

Another analytic tool, which had to be established for the examination of GJIC in ASCs was the immunohistochemical staining of basic building blocks of gap junctions, namely connexins. Therefore, a specific immunohistochemical staining for connexin 43, being the most abundant isoform of the gap junction-forming connexins, needed to be established. For this purpose, procedures for specific antigen retrieval and unspecific antigen blocking had to be evaluated, since no specific immunohistochemical staining for Cx43 on cultured ASCs could be achieved without these techniques (data not shown). Cells were initially treated with Triton X-100 and citric buffer, two frequently used retrieval methods on frozen and paraffin embedded cells. As heat-mediated antigen retrieval at 100 °C

cannot be done with cells grown on culture treated plastic plates, ASCs were cultured on coverslips (ø 15 mm) for all Cx43 immunohistochemical staining testing procedures. Firstly, unspecific binding was blocked for 15 minutes with either 1% BSA or 5% FCS, and cells were incubated with two different primary antibody dilutions of 1:200 and 1:500 (Figure 4.19). It could be demonstrated that both unspecific antigen-blocking methods worked the same way, hence, only the 5% FCS blocking is depicted in (Figure 4.19). The antibody dilution of 1:500 evoked a clearer and less blurry signal and both antigen retrievals seemed to work equally, albeit no counterstaining was performed to see cellular borders. Hence, it can be recorded, therefore, that antigen retrieval is needed and effective, and blocking with 5% FCS as well as a 1:500 dilution of the antibody can be retained.

In a next step a straightforward counterstaining of the cytoskeleton by a fluorescent labelled phalloidin was utilized, to visualize cell-cell boarders for the localization of the Cx43 signal, and was tested in combination with Triton X, citric buffer and additional demasking methods (Figure 4.20). Cells were treated again with the mild non-denaturating surfactant Triton X-100 (at RT), with the proteinases pepsin (at RT) and proteinase K (at 37 °C), and afresh with the acidic agent citrate buffer, by applying high temperatures (at 55 C, 63 °C and 100 °C) (Figure 4.20 A). The phalloidin counterstaining for the visualization of the actin filaments of adjacent cells worked very well for lower temperature methods, while the treatment with citrate buffer at temperatures of 55-100 °C impaired significantly the effective actin labeling (Figure 4.20 B). This can be explained by the heat-mediated destruction of the quaternary protein structure of F-actin, to which phalloidin normally binds with high affinity. The pepsin digestion at 37 °C for 10 min showed no effect, as literally no specific Cx43 staining was finally detected (data not shown). As counterstaining with phalloidin worked out for Triton X-100 treatment and proteinase K digestion, the localization of the Cx43 immunohistochemical staining could be assessed. Both methods sparsely displayed specific staining at cell-cell borders but showing only little background staining. Since in the first attempt citrate buffer produced the most convincing Cx43 signal, and cytoskeletal staining by phalloidin did not work out under high temperature procedures in the second attempt, localization and therefore evaluation of the Cx43 staining under the three different citrate buffer demasking methods remained elusive. Therefore, in these cases cytoskeletal visualization was conducted by means of a β-actin antibody (Figure 4.20 B, last row). In doing so, and visualizing likewise the cytoskeleton and cell boundaries, citrate buffer antigen retrieval could be identified to evoke the most convincing, specific Cx43 immunohistochemical staining. In direct comparison with all other methods, heat-mediated demasking with citrate buffer at 100 °C for 20 minutes turned out to be the most appropriate method, depicting a specific spotted Cx43 signal located at cell-cell interfaces and, furthermore, a specific signal in perinuclear intracellular regions (Figure 4.21).

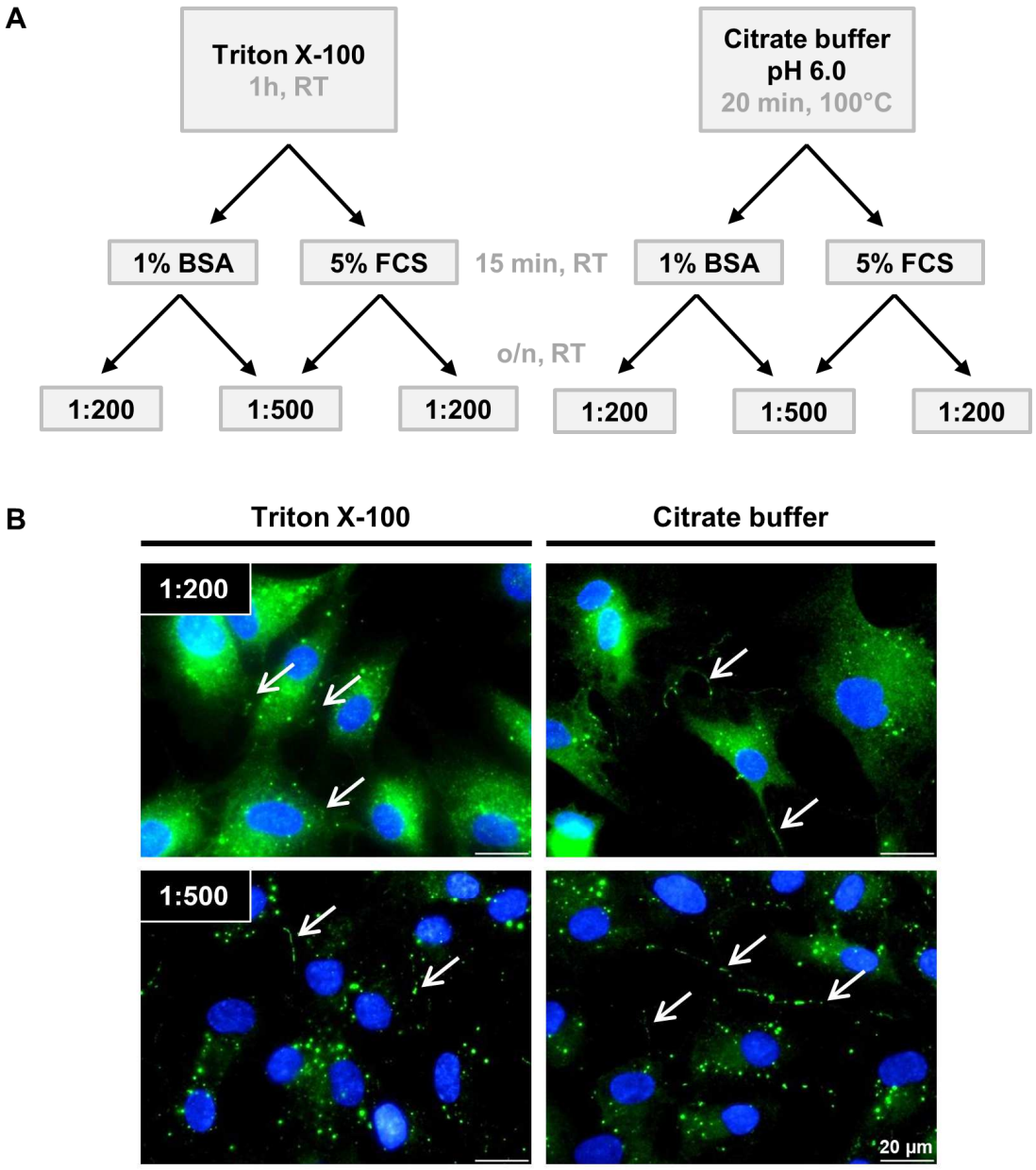

Figure 4.19: I. Establishment of the immunohistochemical staining for Cx43.

A) Schematic representation of the staining procedure steps and test variables. Antigen retrieval was performed for formalin fixated cells via 1% Triton X-100 treatment or by heat-mediation with ctitrate buffer. Cells were further whether blocked with 5% FCS in PBS, and the primary antibody was tested in different diltuions (1:200 and 1:500). **B**) Immunohistochemical staining for Cx43 on cultured ASCs was conducted. Cx43 was stained green and nuclei blue with DAPI. Antigen retrieval was performed with Triton X-100 treatment or heat-mediated with ctitrate buffer, cells were blocked with 5% FCS in PBS for 15 min and further incubated with a 1:200 or 1:500 antibody dilution. Arrows (→) indicate a localization of Cx43 at cell-cell borders. Images were taken at a 60-fold magnification; scale bars represent 20 µm.

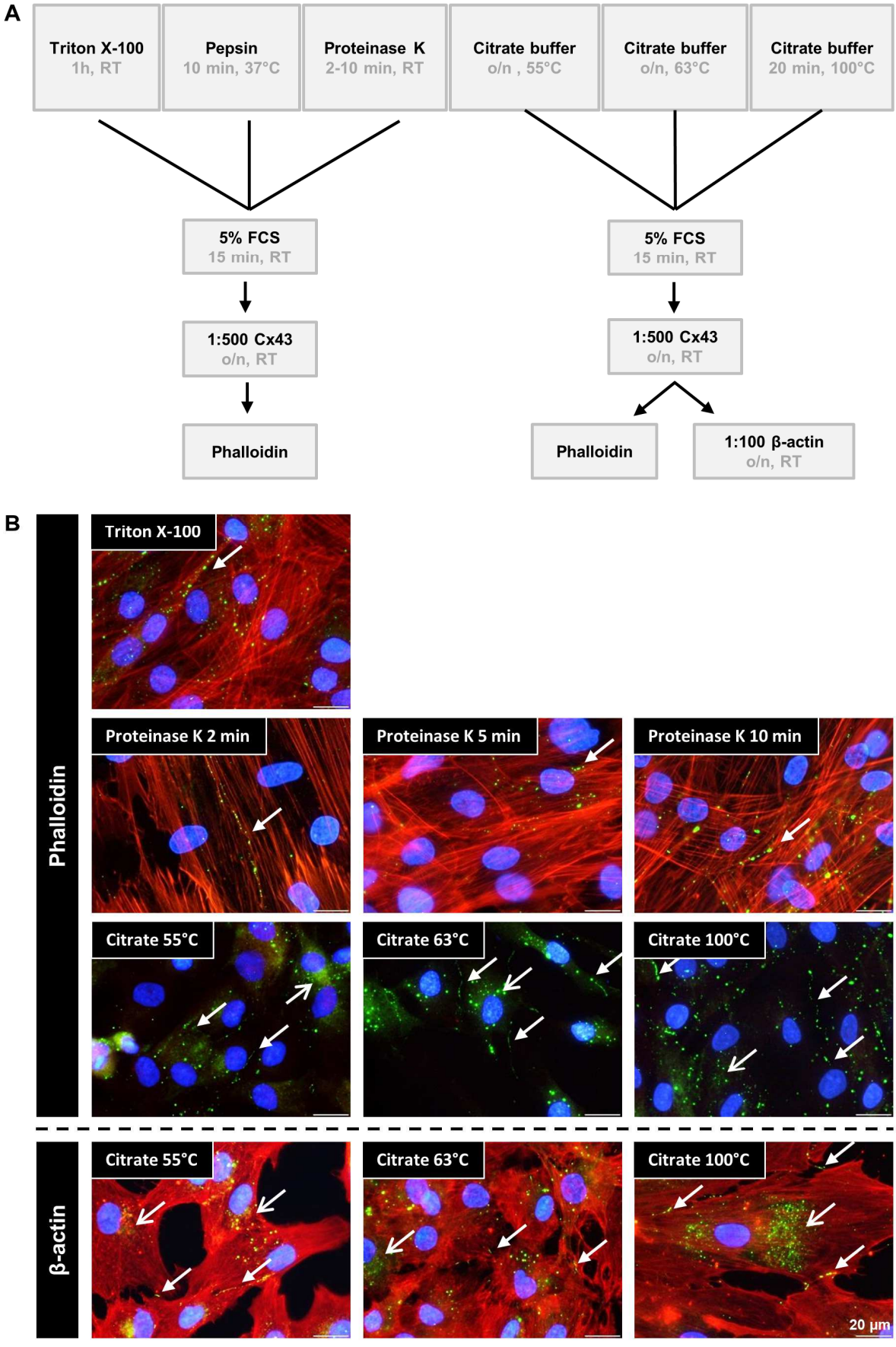

(legend on next page)

Figure 4.20: II. Establishment of the immunohistochemical staining for Cx43.

Testing of different antigen retrieval methods and counterstaining for the visualization of cellular borders and the cytoskeleton. **A**) Schematic representation of the staining procedure steps and testing variables. Antigen retrieval was performed for formalin fixed cells using Triton X-100 (1h at RT), pepsin (10 min at 37 °C), proteinase K (2-10 min at RT) and citrate buffer (20 min at 100 °C, o/n at 65 °C and o/n at 55 °C). Counterstaining was performed either with phalloidin or β-actin antibody. **B**) Immunohistochemical staining for Cx43 on cultured ASCs was conducted. Antigen retrieval was performed with methods listed above and cells were counterstained with phalloidin. In addition, heat-mediated antigen retrieval with citrate buffer (all three settings) was counterstained with β-actin antibody. Cx43 was stained green, phalloidin or β-actin for the visualization of the cytoskeleton red and nuclei blue with DAPI. Arrows indicate cytoplasmic (→) and membranous (➔) localization of Cx43. Images were taken at a 60-fold magnification; scale bars represent 20 µm.

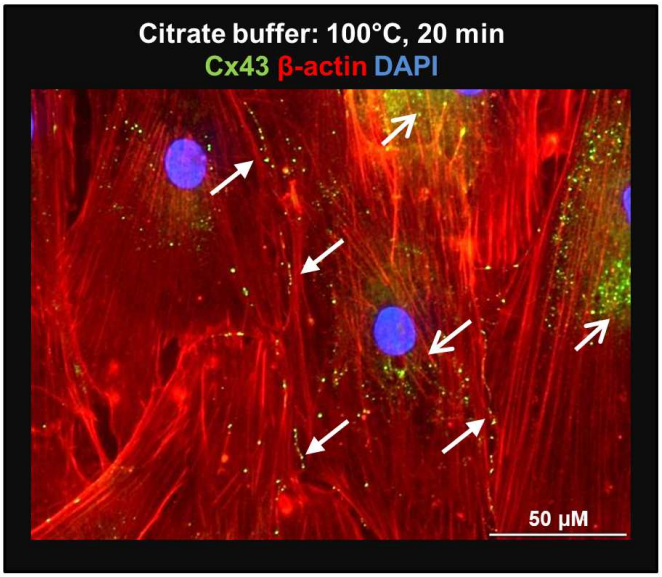

Figure 4.21: III. Establishment of the immunohistochemical staining for Cx43.

Heat-mediated antigen retrieval was performed with citrate buffer for 20 minutes at 100 °C for Cx43 (green) staining. The cytoskeleton was stained red for β-actin and nuclei in blue with DAPI. Arrows indicate cytoplasmic (→) and membranous (➔) localization of Cx43. Images were taken at a 40-fold magnification; scale bars represent 50 µm.

4.3.4 Discussion

Hereinafter, it was the aim to investigate gap junctional intercellular communication (GJIC) in ASCs. Due to the scarcity of literature about gap junctions and GJIC in these cells, analytical methods had to be established and adapted. Therefore, testing and confirmation of the adequate concentration of the gap junctional inhibitor 18α-glycyrrhetinic acid (AGA) and the immunohistochemical staining conditions for gap junction localization had to be carried out. 18α-glycyrrhetinic acid originates from licorice root, is an aglycone of glycyrrhizic acid, and is a frequently utilized specific gap junction inhibitor for functional cellular investigations[309–311]. Even though AGA is an acknowledged inhibitor, the exact mode of action on gap junctional intercellular communication is not yet fully understood. In

the past, an incorporation into the cellular membrane along with a binding to the gap junctional connexon and a conformational change of the GJ channel, causing opening and closing, was proposed[312]. Furthermore, the aglycone was expected to modulate gap junctional intercellular communication by altering the basal phosphorylation pattern of connexins in a dose-dependent and reversible manner and therefore, influencing the disassembly of gap junction plaques[310,313–315]. AGA was reported to cause isoform-specific dephosphorylation of Cx43 in a rat hepatocyte-like cell line, associated with the disassembly of gap junctions[309].

In literature, a range of 2 to 150 µM AGA has been used for gap junctional blocking for different cell types[310,311]. Therefore, we tested in a first approach its cytocompatibility for ASCs under growth conditions and adipogenic induction, referring to concentrations used in the adipogenic context [306,316]. We tested AGA and its non-inhibitory analog glycyrrhizic acid (GZA[308]) with concentrations of 35, 70 and 100 µM (referred to Yanagiya et al. 2007 and Tang et al. 2010[306,316]). The highest concentration of 100 µM AGA showed a slight but significant impact on cell growth. Applied during differentiation, 100 µM AGA displayed a mild effect on cell viability shown by life/dead staining, whereas, 35 and 70 µM AGA and the analog GZA had no effect in this regard. A dose-dependent increasing cytotoxic effect has been reported for inhibition of Cx43-mediated GJIC of cultured alveolar epithelial cells, already for concentrations > 20 µM AGA[313]. A likely reason for this finding was that cells were cultured during GJ inhibition under serum-free conditions. This is in accordance with early findings of Davidson in 1986, who demonstrated that GJIC inhibition of human fibroblasts under serum-free conditions was reversible by the addition of 10% serum, and consequently higher doses of AGA were required to elicit again communication inhibition[310]. Furthermore, an inhibitory effect on cellular proliferation was depicted for 3T3-L1 mitotic clonal expansion (MCE) and for hepatic stellate cells (HSCs), with an additional increased apoptosis rate, both illustrating a dose-dependent action[306,317].

Regarding GJIC inhibition, we investigated the effect of AGA on adipogenic differentiation of ASCs versus its non-inhibitory analog. Here, we demonstrated successfully likewise an increasing impact of AGA in a dose-dependent manner on adipogenesis by histological and biochemical analysis, demonstrating the most prominent and significant impact on differentiation with 70 and 100 µM, while GZA again had no impact at all. In a previous study, a similar dose-dependent decrease of adipogenesis could be seen with the same AGA and GZA concentrations for 3T3-L1 cells. In addition to our experimental set-up, in this publication the cells were treated with the inhibitor at different time points during induction, demonstrating furthermore an influence of application timing[306]. Equally, Tang and coworkers showed for MSCs derived from rats a comparable dose-dependent increase in adipogenic inhibition with AGA, which was demonstrably also dependent on the number of cell-cell contacts per cell[316]. In summary, in the subsequent experiments on gap junctional intercellular

communication in ASCs (see Chapter 4.4), a concentration of 70 µM AGA was chosen, which is demonstrably effective for GJ blocking, while having a good cytocompatibility.

Since Cx43 is a widely and ubiquitously occurring channel-forming connexin isoform and literature demonstrated its presence in adipose tissue of mice and human and its involvement during mesenchymal cell coupling[77,303,318], we decided to investigate this isoform in the context of ASCs. Therefore, an immunohistochemical staining protocol for Cx43 was established. As no specific immunohistochemical staining was detected for Cx43 on cultured ASCs without antigen retrieval, several known antigen retrieval methods were examined[319]. As counterstaining, for the visualization of cellular boundaries and cellular attachment zones, a fluorescence-labeled phalloidin (the toxic components of *Amanita phalloides*) conjugate was applied. Since phalloidin binds to filamentous actin (F-actin) with much higher affinity than to actin monomers[320,321] and since heat-mediated antigen retrieval with citric acid even at mild temperatures (> 55 °C) destroyed the physiological F-actin structure, an antibody based counterstaining for β-actin was established for these staining protocols. Finally, an antigen retrieval with citric acid in combination with a β-actin cytoskeletal counterstaining turned out to generate the best result for Cx43 staining, comparable to Cx43 patterns described in literature for human mesenchymal stem cells and vascular smooth muscle cells (VSMC) from rabbit[72,304]. Furthermore, both, a spotted staining pattern at cell borders, representing clusters of paired hemichannels, and a distinct signal near the nucleus (located at the endoplasmic reticulum or Golgi) could be depicted, comparable to described cellular appearance of Cx43 in literature[75,322].

Altogether, with the establishment of these methods the groundwork was done for further experimental investigations on cell density-dependent cell-cell communication via gap junctions in ASCs under growth and adipogenic conditions.

4.4 Gap junctional intercellular communication in adipose-derived stromal/stem cells is cell density-dependent and positively impacts adipogenic differentiation

Miriam Wiesner*, Oliver Berberich*, Christiane Hoefner*, Torsten Blunk*, Petra Bauer-Kreisel*

**Department of Trauma, Hand, Plastic and Reconstructive Surgery, University of Würzburg, Würzburg, Germany*

Journal of Cellular Physiology 2018; 233:3315-3329.

As an easily accessible cell source with a broad differentiation capacity, adipose-derived stem cells (ASCs) are widely used for regenerative medicine and tissue engineering approaches [18,40,297,323]. However, despite their acknowledged multi-lineage potential and widespread use in these fields, the fundamental biology and physiological features that regulate ASC differentiation capacities are still not fully understood[253,254]. Direct cell-cell communication is an essential mechanism shown to be involved in a number of cellular functions, including growth, differentiation, and cell death[63]. Investigating the impact of direct cell-cell communication in ASCs would further the understanding of these cells and, in turn, may help to advance strategies for proper tissue development and maintenance in tissue engineering applications. A ubiquitous mechanism for direct cellular crosstalk in vertebrates appearing at regions of cell contact is gap junctional intercellular communication (GJIC) [68,69]. Gap junctions are clusters of paired hemichannels composed of six connexins (Cx) representing the basic structural unit. These low-resistance channels are permeable for small molecules (<1 kDa) such as ions, second messengers, and small metabolites[68,69,71]. Within the collective of channel-forming connexins, connexin 43 represents the most abundant isoform in human tissue[72]. It is widely acknowledged that gap junctions play an essential role in tissue development and coordinated cellular activity, and serve as modulators of cellular differentiation[69–71]. Previous studies revealed a role of GJIC in bone regeneration for the differentiation of osteoprogenitor cells and maturation of osteoblasts[307,314]. Furthermore, the relevance of GJIC for neuronal, odontoblastic, and mammary epithelial cell differentiation has also been demonstrated[70,322,324]. For mesenchymal stem cells, the impact of gap junctions on cellular differentiation was mainly investigated in the case of bone marrow-derived mesenchymal stem cells (BMSCs)[325,326]. In this context, high cell density and cell-cell contact were reported to positively influence adipogenic differentiation of rat BMSCs[316].

So far, little attention has been given to the impact of gap junctional coupling in human ASCs. The presence of Cx43-containing gap junctions in ASCs was depicted in the context of regulated calcium oscillation via NOS and internalization of quantum dots[77,78]. However, no studies exist investigating the impact of gap junctions on differentiation processes in these cells.

Therefore, in the present study, we addressed the expression and functionality of Cx43-containing gap junctions in ASCs, and the impact of GJIC on their adipogenic differentiation capacity. A strong correlation was found between the expression and function of gap junctions and cell seeding density, the latter also clearly influencing adipogenic differentiation behavior. Blockage of GJIC significantly impaired the adipogenic capacity, demonstrating the importance of direct cell-cell communication for differentiation processes of ASCs.

4.4.1 Expression and functionality of gap junctions in ASCs

The expression of connexin 43 (Cx43) in ASCs was demonstrated by immunohistochemical staining of cells at different time points of culture (Figure 4.22 A). The staining revealed the presence of Cx43 at day 0 (4h after seeding), mostly located intracellularly at the periphery of the nucleus. However, several gap junctions were also detectable at cell-cell boundaries at this early time point. During culture in growth medium, a time-dependent shift toward membrane-located Cx43 expression and formation of gap junctions was evident. This development was shown to be highly influenced by cell density, with cells seeded at lower densities (5,000 and 25,000 cells/cm^2) exhibiting less membranous Cx43 signal in comparison to cells seeded at high density (100,000 cells/cm^2). Accordingly, gene expression analysis revealed an increase of signal over time, which was significantly elevated in the high density culture (100,000 cells/cm^2) compared to lower density (25,000 cells/cm^2) at days 5 and 10 (Figure 4.22 B). In general, western blot analysis confirmed these findings at the protein expression level. For Cx43 protein, higher expression was already detected at day 0 for the cells seeded at higher density, and the amounts of Cx43 were markedly increased during the cultivation period in a density-dependent manner (Figure 4.22 C). Additionally, using an antibody that detects phosphorylated (P1, P2) isoforms, representing membrane-located Cx43, as well as unphosphorylated (P0) Cx43, the expression of the phosphorylated isoform P2 (> 43 kDa) became detectable at day 2 for both cell densities, whereas only slight traces appeared at day 0 (Figure 4.22 C). This is in accordance with the histological findings.

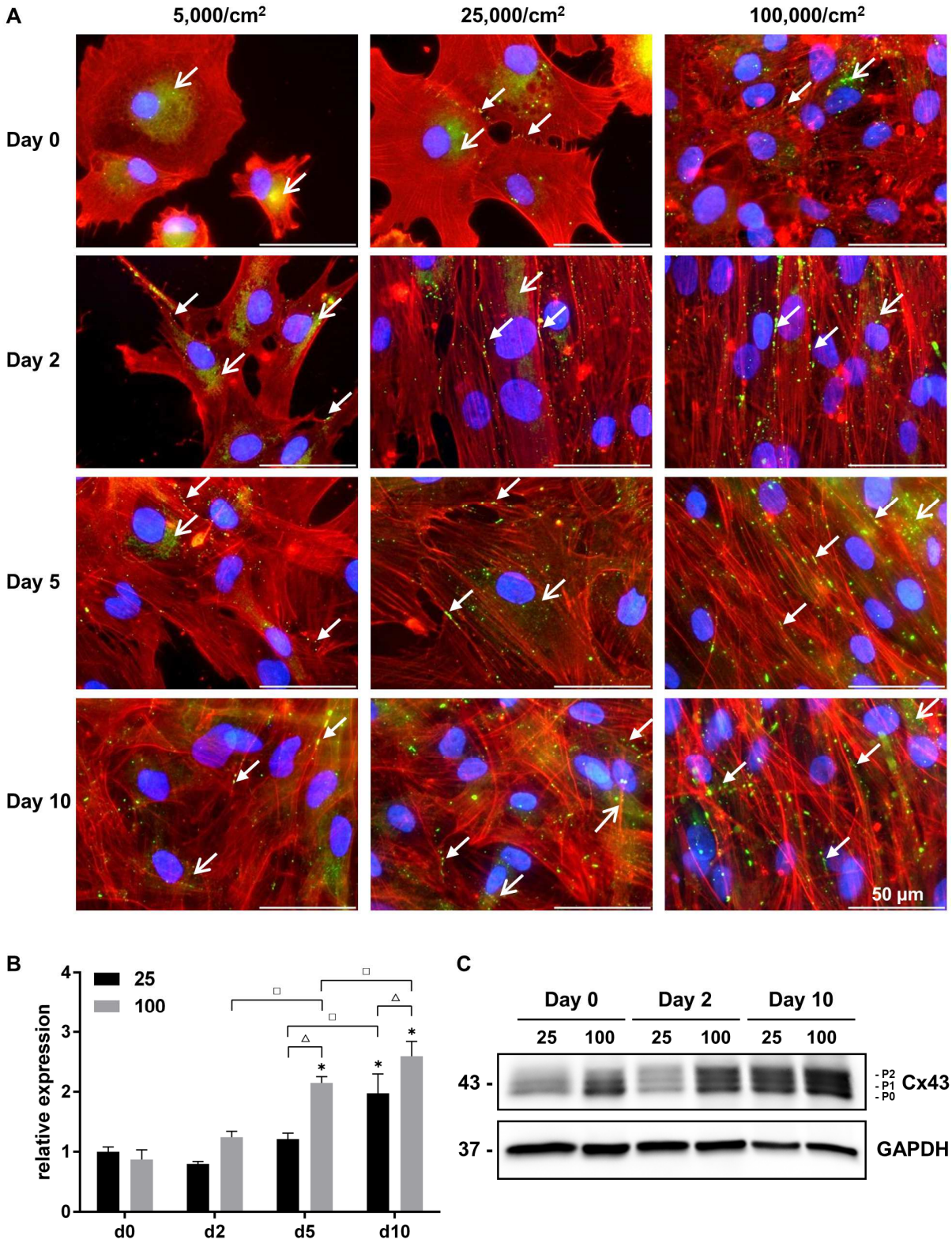

Figure 4.22: Cx43 expression in ASCs cultured at different seeding densities in growth medium.

A) Immunohistochemical staining for Cx43 was conducted. Cx43 was stained green, β-actin for the visualization of the cytoskeleton red, and nuclei blue with DAPI. Three different cell seeding densities were examined (5,000, 25,000, and 100,000/cm²) at different time points (d0, d2, d5, d10) of culture. Arrows indicate cytoplasmic (→) and membranous (➔) localization of Cx43. Representative images are shown. Images were taken at a 60-fold magnification; scale bars represent 50 µm.

Figure 4.22: Cx43 expression in ASCs cultured at different seeding densities in growth medium (continued).
B) Cx43 gene expression of cultured ASCs was determined by qRT-PCR for cell seeding densities of 25,000 and 100,000/cm^2. Gene expression was normalized to EF1α; the obtained values were further normalized to day 0, 25,000/cm^2. Values are expressed as mean with standard deviation (n=3). Statistically significant differences ($p<0.05$) to values at day 0 (d0, 25,000/cm^2 and 100,000/cm^2, respectively) are indicated by *; differences between densities at the same day by △, and significant differences over time within a density group are indicated by □. **C**) For the investigation of Cx43 protein expression western blot analysis was performed (cell seeding densities of 25,000 and 100,000/cm^2). Cx43 (43 kDa) detection revealed three bands, the lower band represents unphosphorylated protein (P0), whereas the upper two bands represent phosphorylation levels (P1, P2) of the protein. GAPDH (37 kDa) served as the loading control.

For functional examination of gap junctional intercellular communication (GJIC) in ASCs, a flow cytometry analysis of dye transfer was performed at an early time point, that is, 4h after seeding (representing day 0 in all depicted experiments). Therefore, donor cells stained with green calcein-AM were seeded in a 1:1 ratio with red DiD-labeled recipient cells. The intercellular exchange of calcein via gap junctions results in an increase of double-stained green/red fluorescent recipient cells, thus, the fraction of double positive cells (+/+ calcein/DiD) represents a measure for the GJIC potential (Figure 4.23 A, upper right quadrant in the dot plots). The population of double-stained cells increased significantly in a density-dependent manner (Figure 4.23 A and B), confirming the impact of culture density on the GJIC potential of ASCs. The significant reduction in dye transfer by adding the established specific gap junction blocker AGA (18α-glycyrrhetinic acid), ascertaining the dependence of the dye transmission on GJIC, demonstrated the functionality of gap junctions in these cells. A concentration of 70 µM AGA was administered, which was shown to potently inhibit GJIC in the dye transfer analysis but did not affect cell viability and cell number as demonstrated by live/dead staining and analysis of DNA content (as demonstrated in the previous Chapter 4.3). The non-inhibitory structural analog of AGA (glycyrrhizic acid; GZA) had no effect on the amount of transferred dye.

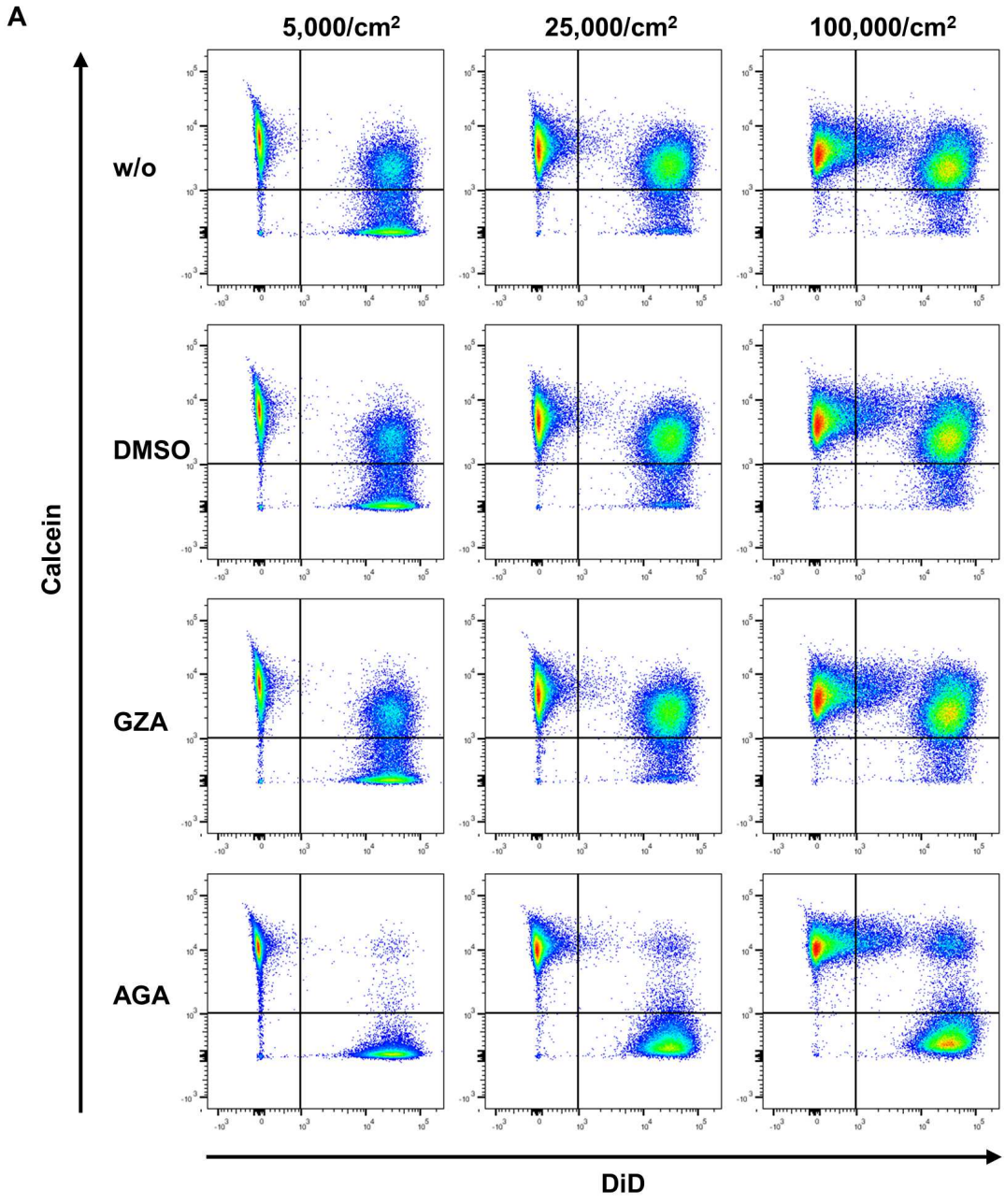

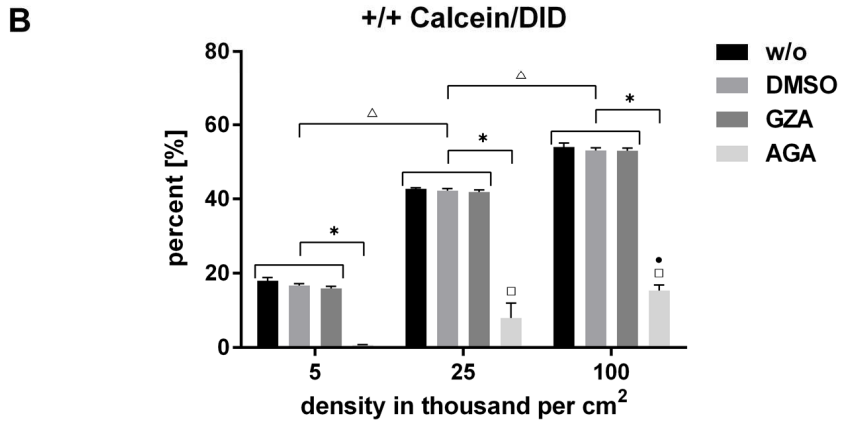

(legend on next page)

Figure 4.23: Functional examination of gap junctional intercellular communication (GJIC) in ASCs at different seeding densities.

A) Donor cells labeled with calcein-AM and recipient cells labeled with DiD were cocultured in a 1:1 ratio for 4h. Three different cell seeding densities were examined (5,000, 25,000, and 100,000/cm^2). 70 µM 18α-glycyrrhetinic acid (AGA) was applied for inhibition of GJIC. Stained ASCs were co-cultured under control conditions, that is, either in growth medium only (w/o) or in the presence of the solvent DMSO (0.35%), or cultures were supplemented with the GJIC inhibitor AGA (70 µM) or with the non-inhibitory AGA-analog glycyrrhizic acid (GZA, 70 µM). The increase of double positive-stained cells due to dye transfer as a measure of GJIC was evaluated by flow cytometry analysis (upper right quadrant of the dot plots). Unitary quartile gates were set manually by the examination of single-stained populations. **B**) Percentage values represent the detected double-stained cells (calcein/DiD) of each group and density (fraction of cells in upper right quadrant in a). Values are expressed as mean with standard deviation (n=3). Statistically significant differences ($p<0.05$) of GJIC inhibition by AGA at the respective densities are indicated by *, and of AGA effects between densities are indicated by □ (to AGA, 5,000/cm^2) and by • (to AGA, 25,000/cm^2). Other statistically significant differences between densities are indicated by △.

4.4.2 Cell density and adipogenesis

In order to investigate the effect of cell density and GJIC on the adipogenic differentiation of ASCs, at first, cells were seeded with different densities (5,000, 25,000, and 100,000/cm^2) and were adipogenically induced with a commonly used hormonal cocktail. Induction was performed immediately after attachment to cell culture plastic (4h after seeding) in order to prevent cell growth and to ensure accurately defined initial cell densities. The impact of cell density on the differentiation capacity was analyzed at the gene expression level by measuring relative mRNA levels of adipogenic marker genes (PPARγ, C/EBPα, and fatty acid binding protein aP2) (Figure 4.24 A). All three marker genes investigated showed significantly increased expression upon adipogenic induction from day 0 to 10. PPARγ and C/EBPα, the two most prominent transcription factors of adipogenesis, displayed a significant increase in gene expression level in cells seeded at 100,000 cells/cm^2 compared to 25,000 cells/cm^2 at day 5. For aP2, also at the later time points, a density-dependent tendency was obvious. After 5 and 10 days, histological observations in Oil Red O stained cultures revealed an apparent higher amount of triglyceride-containing cells in the 100,000 cells/cm^2 group than for those seeded at 25,000 cells/cm^2. At the 5,000 cells/cm^2 density, ASCs were barely able to differentiate and only a few triglyceride-containing cells were visible (Figure 4.24 B). Quantification of triglyceride amount, which displayed a statistically significant increase in triglyceride content per DNA with increasing cell seeding density (25,000 vs. 100,000 cells/cm^2), corroborated this observation (Figure 4.24 C). DNA analysis confirmed the seeding ratio at the time point of induction and the maintenance of the density difference over the whole culture period (Figure 4.24 C).

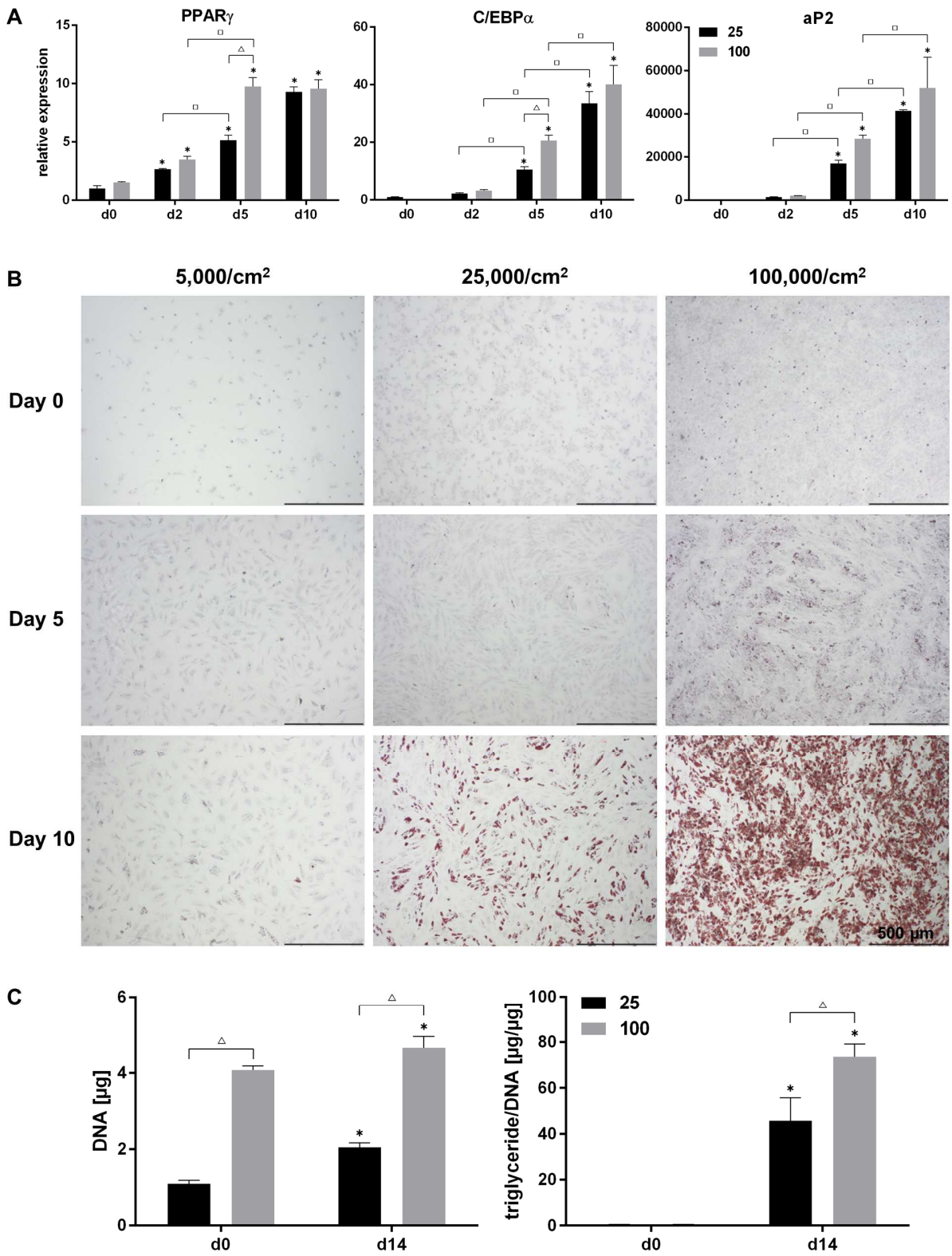

Figure 4.24: Impact of seeding density on adipogenesis of ASCs.

A) Adipogenic marker gene expression (PPARγ, C/EBPα, aP2) of ASCs was determined by qRT-PCR. Gene expression was normalized to EF1α; the obtained values were further normalized to day 0, 25,000/cm^2. Values are expressed as mean with standard deviation (n=3). Statistically significant differences ($p<0.05$) to day 0 (d0, 25,000/cm2 and 100,000/cm^2, respectively) are indicated by *, between densities at the same day by △, and significant differences over time within a density group are indicated by □.

Figure 4.24: Impact of seeding density on adipogenesis of ASCs (continued).

B) Histological analysis of adipogenesis by staining with Oil Red O (ORO, red) and hematoxylin (blue). Differences in adipogenic differentiation at different seeding densities (5,000, 25,000 and 100,000/cm^2) were examined over time (d0, d5, d10). Representative images are shown. Scale bars represent 500 µm. **C**) Determination of DNA and triglyceride content was performed for adipogenically induced samples (d0, d14) at seeding densities of 25,000 and 100,000 cells per cm^2. Values are expressed as mean with standard deviation (n=3). Statistically significant differences ($p<0.05$) to day 0 (d0, 25,000/cm^2 and 100,000/cm^2, respectively) are indicated by * and between densities at the same day by $^{\triangle}$.

To determine if more cells were able to differentiate at high density, or if just more triglyceride was accumulated per cell with the ratio of differentiated vs. undifferentiated cells being unchanged, a flow cytometry analysis utilizing the lipophilic fluorescent dye nile red was performed. This method allows the determination of the percentage of differentiated cells and the relative amount of incorporated triglyceride per differentiated cell. As displayed in Figure 4.25 and Table 4.1, the fraction of adipogenically differentiated cells was strongly elevated in the high density-seeded group compared to the lower density-seeded group (27.2% ± 0.7 for 25,000 cells/cm^2, 58.7% ± 2.2 for 100,000 cells/cm^2). Furthermore, the median fluorescence intensity (MFI) representing accumulated triglyceride per differentiated cell, and the median cell size (MCS) of the differentiated fraction of ASCs were analyzed (Table 4.1). It became apparent that at high cell density, more cells were committed to differentiation upon adipogenic induction, but less triglyceride was accumulated, which also had an impact on cell size.

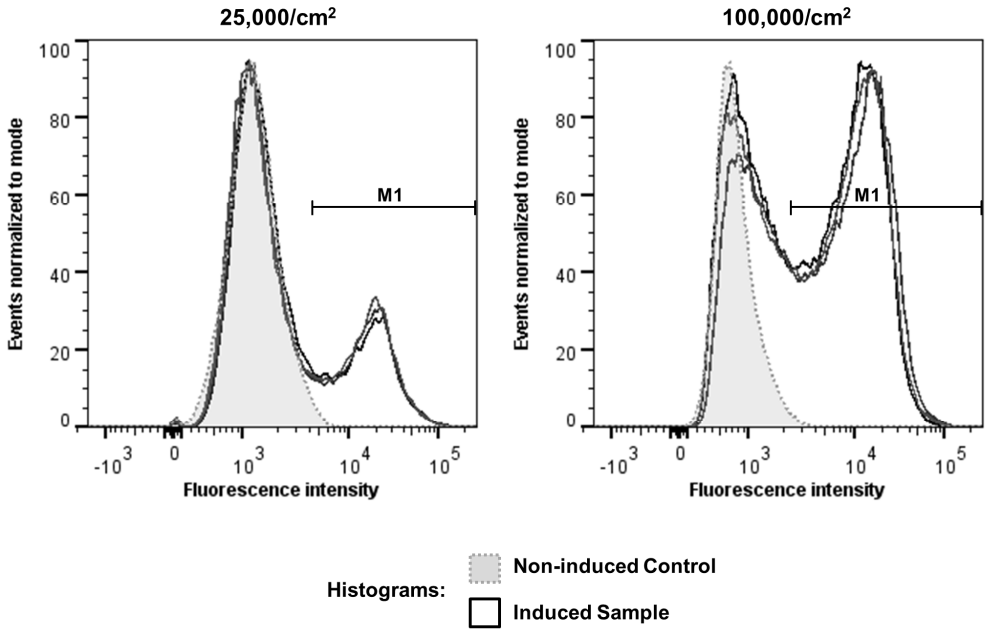

Figure 4.25: Impact of seeding density on adipogenesis of ASCs – Flow cytometry analysis.

Adipogenically differentiated ASCs seeded at different densities (25,000 and 100,000/cm^2) were stained with nile red at day 12 after induction. Nile red fluorescence intensity histograms are displayed. The gray-shaded histograms with dotted line represent the respective non-induced controls and the bold-lined histograms the induced samples (n=3).

Table 4.1: Nile red flow cytometry analysis of adipogenically differentiated ASCs at different seeding densities.

Differentiated cells:	**25,000/cm²**	**100,000/cm²**
M1-Gate [%]	27.2 ± 0.7	58.7 ± 2.2 *
Median fluorescence intensity	17711.3 ± 45.0	11513.0 ± 715.5 *
Median cell size	156369.0 ± 7802.4	112063.3 ± 5997.1 *

The M1-gate percentage represents the fraction of differentiated ASCs at different seeding densities (25,000 and 100,000/cm²). Within this differentiated population, the median fluorescence intensity (MFI) and the median cell size (MCS) were determined. Values are expressed as median with standard deviation (n=3). Statistically significant differences ($p<0.05$) between different seeding densities are indicated by *.

4.4.3 Influence of GJIC inhibition on adipogenesis

The results obtained so far showed an increased GJIC potential as well as increased adipogenesis at higher cell seeding densities, suggesting a possible impact of GJIC on adipogenesis. To further investigate the influence of GJIC on adipogenesis of ASCs, adipogenic differentiation was examined in the presence of the gap junction-specific inhibitor AGA in cultures seeded at high density (Figure 4.26). Histological evaluation of cells seeded with 100,000/cm² demonstrated a distinct impairment of adipogenic differentiation with 70 µM AGA in comparison to the solvent control, whereas addition of the non-inhibitory AGA-analog GZA showed no impact on lipid accumulation (Figure 4.26 A). Quantification of accumulated triglycerides confirmed the significant impact of GJIC on adipogenesis, with the triglyceride amount in AGA-treated cells markedly reduced compared to solvent control and GZA conditions (Figure 4.26 B). The inhibitory effect of AGA on adipogenic differentiation was also confirmed at the gene expression level for two main transcription factors of adipogenesis (PPARγ and C/EBPα), which were reduced upon addition of AGA. Expression of aP2 as a late marker for adipogenic differentiation was slightly, although not significantly decreased in the presence of AGA (Figure 4.26 C). The expression of all three marker genes in general increased upon adipogenic induction.

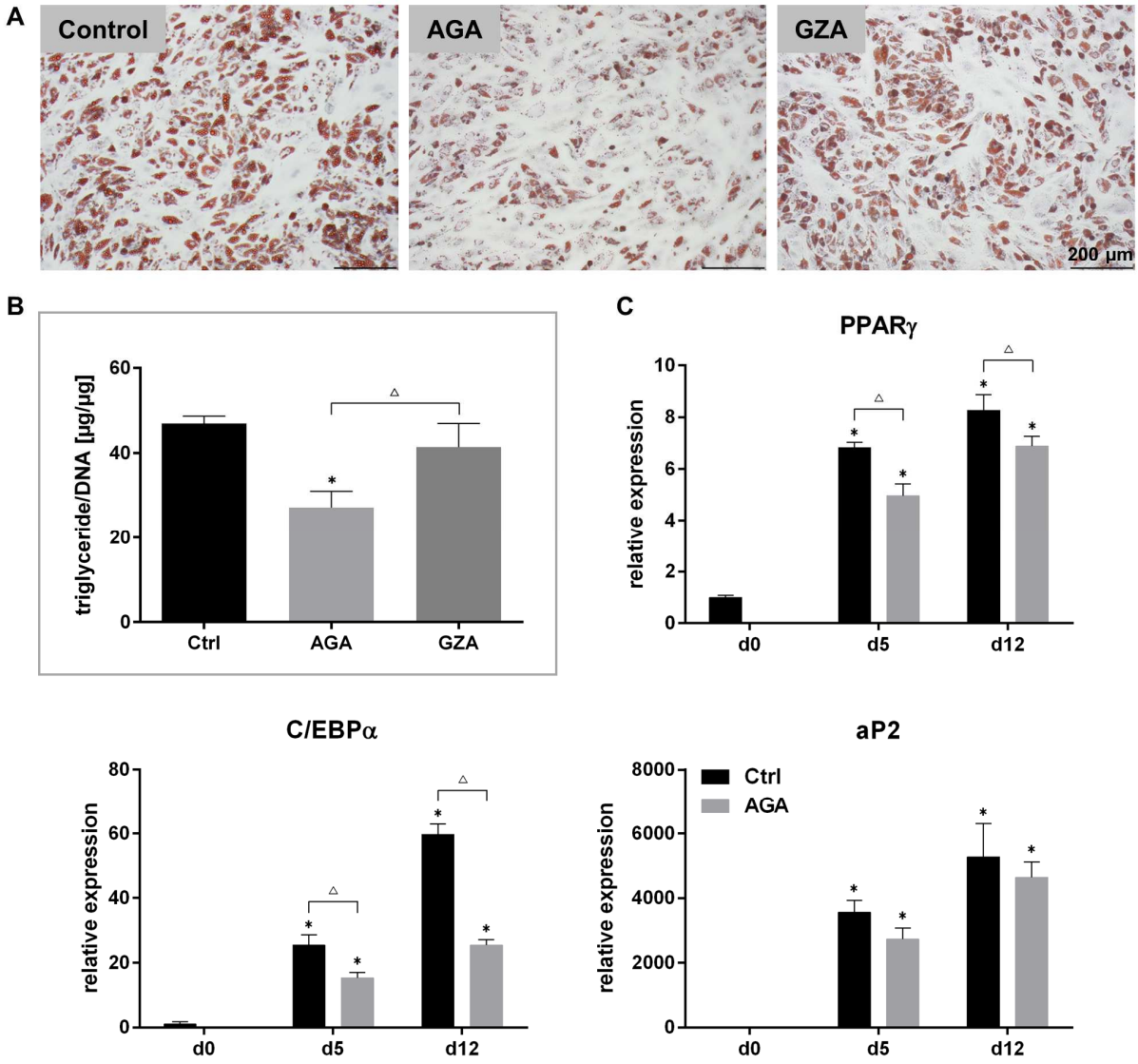

Figure 4.26: Impact of GJIC inhibition on adipogenesis of ASCs.

A) Histological analysis of adipogenically induced samples (100,000/cm², day 12) by staining with Oil Red O (ORO, red) and hematoxylin (blue). GJIC was inhibited by addition of 70 µM AGA (Control: 0.35% DMSO, GZA: 70 µM non-inhibitory analog of AGA). Representative images are shown. Scale bars represent 200 µm. **B**) Determination of triglyceride content was performed for adipogenically induced samples (100,000/cm², day 12). Values are expressed as mean with standard deviation (n=3). Statistically significant differences ($p<0.05$) to reference value (control) are indicated by * and significant differences between other groups by △. **C**) Adipogenic marker gene expression (PPARɣ, C/EBPα, aP2) of ASCs was determined by qRT-PCR (100,000/cm²; d0, d5, d12). Gene expression was normalized to EF1α; the obtained values were further normalized to day 0. (Note: Day 0 values are the same for both groups.) Values are expressed as mean with standard deviation (n=3). Statistically significant differences ($p<0.05$) to day 0 are indicated by * and between control and AGA at the same day by △.

To further investigate if GJIC inhibition by AGA reduced the fraction of cells able to differentiate, flow cytometry analysis of ASCs (100,000 cells/cm², day 10 of induction) was performed in the presence of AGA (Figure 4.27). A decrease in the fraction of differentiated cells was evident in the AGA (70 µM) treated group in comparison to control conditions, which was reflected by the significantly diminished percentage of differentiated cells (Figure 4.27 and Table 4.2; control: 51.4% ± 2.3 vs. AGA:

36.8% ± 1.0). Furthermore, a reduction in MFI and MCS of the differentiated cells was detected for cells treated with AGA, indicating the formation of smaller cells with less triglyceride incorporation. This data indicated that through GJIC, more cells were recruited to undergo adipogenic differentiation, possibly through synchronization of the commitment process. Clearly, it could be demonstrated that the suppression of GJIC via AGA significantly inhibited adipogenic differentiation of ASCs.

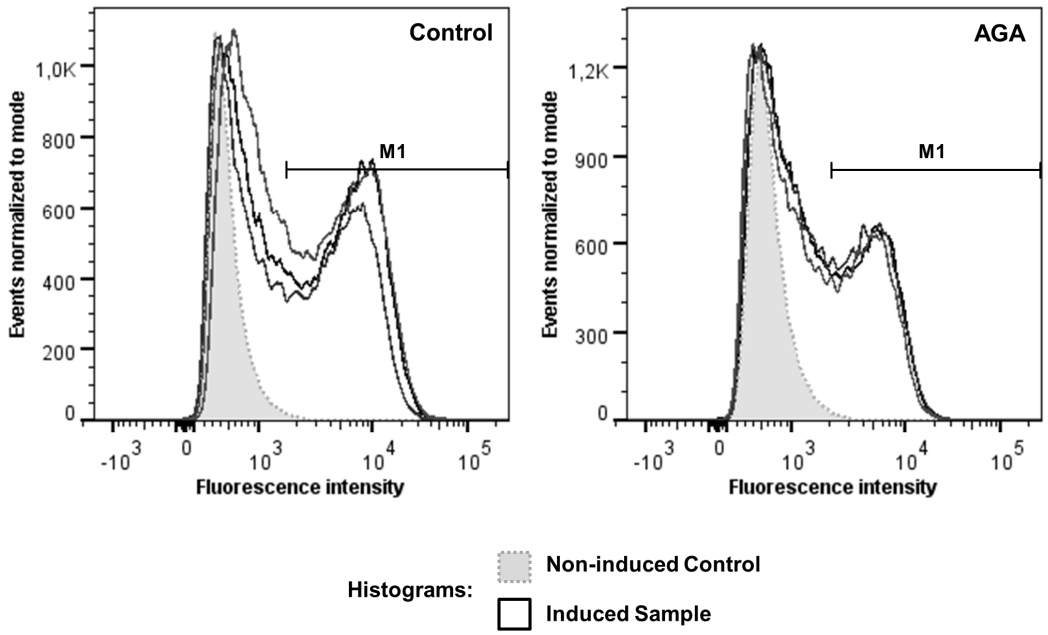

Figure 4.27: Impact of GJIC inhibition on adipogenesis of ASCs, flow cytometry analysis.

Adipogenically differentiated ASCs (100,000/cm²) cultured either in the presence of the GJIC inhibitor AGA (70 µM) or with DMSO (0.35%) solvent control were stained with nile red at day 10 after induction. Nile red fluorescence intensity histograms are displayed. The gray-shaded histograms with dotted line represent the respective non-induced control and the bold-lined histograms the induced samples (n=3).

Table 4.2: Nile red flow cytometry analysis of adipogenically differentiated ASCs treated with AGA.

Differentiated cells:	**Control**	**AGA**
M1-Gate [%]	51.4 ± 2.3	36.8 ± 1.0 *
Median fluorescence intensity	6298.7 ± 399.9	5082.7 ± 136.8 *
Median cell size	104359.7 ± 6850.0	85008.0 ± 3830.2 *

The M1-gate percentage represents the fraction of differentiated ASCs after culture (100,000/cm²) in the presence of AGA or solvent control. Within this differentiated cell population, the median fluorescence intensity (MFI) and the median cell size (MCS) were determined. Values are expressed as median with standard deviation (n=3). Statistically significant differences ($p<0.05$) between groups are indicated by *.

4.4.4 Cx43 expression during adipogenic differentiation

As the conducted experiments on the inhibition of GJIC clearly demonstrated a crucial role of gap junctions for ASC adipogenesis, the presence and evolution of Cx43 expression throughout the adipogenic differentiation process was examined in cultures seeded at high density (100,000 cells/cm^2). At the time point of adipogenic induction (d0), gap junctions were already present in the culture (Figure 4.28 A, see also Figure 4.22 A). Histological examination of differentiating ASCs revealed a decline in membranous Cx43 expression at later stages of adipogenesis (Figure 4.28 A). Until day 5, cells appeared to couple via membrane bound Cx43. At day 10 and 14, a clear decline of specific Cx43 signal could be observed. The blurry green signal at day 10 and 14 was only observed in experiments with adipogenically differentiated cells and was also observed in isotype controls not specific for Cx43 (data not shown), suggesting that it was caused by incorporated triglycerides. A slight cytoplasmic Cx43 signal could be seen almost throughout the culture. The decline in Cx43 expression over time was also confirmed by gene expression analysis using qRT-PCR (Figure 4.28 B). Western blot results further confirmed the decline in Cx43 expression at the protein level in these adipogenically induced cells (Figure 4.28 C), which was in contrast to the observed increase in Cx43 protein level in non-induced cells in growth medium (Figure 4.22 C). Comparable results regarding decreased expression of Cx43 during adipogenesis were obtained with a seeding density of 25,000 cells/cm^2, although not as distinct as with the high cell density due to the generally lower Cx43 expression at lower seeding density (data not shown). Taken together, the presented results suggest an essential role of gap junctional communication particularly in the onset or early phase of the adipogenic differentiation process in ASCs.

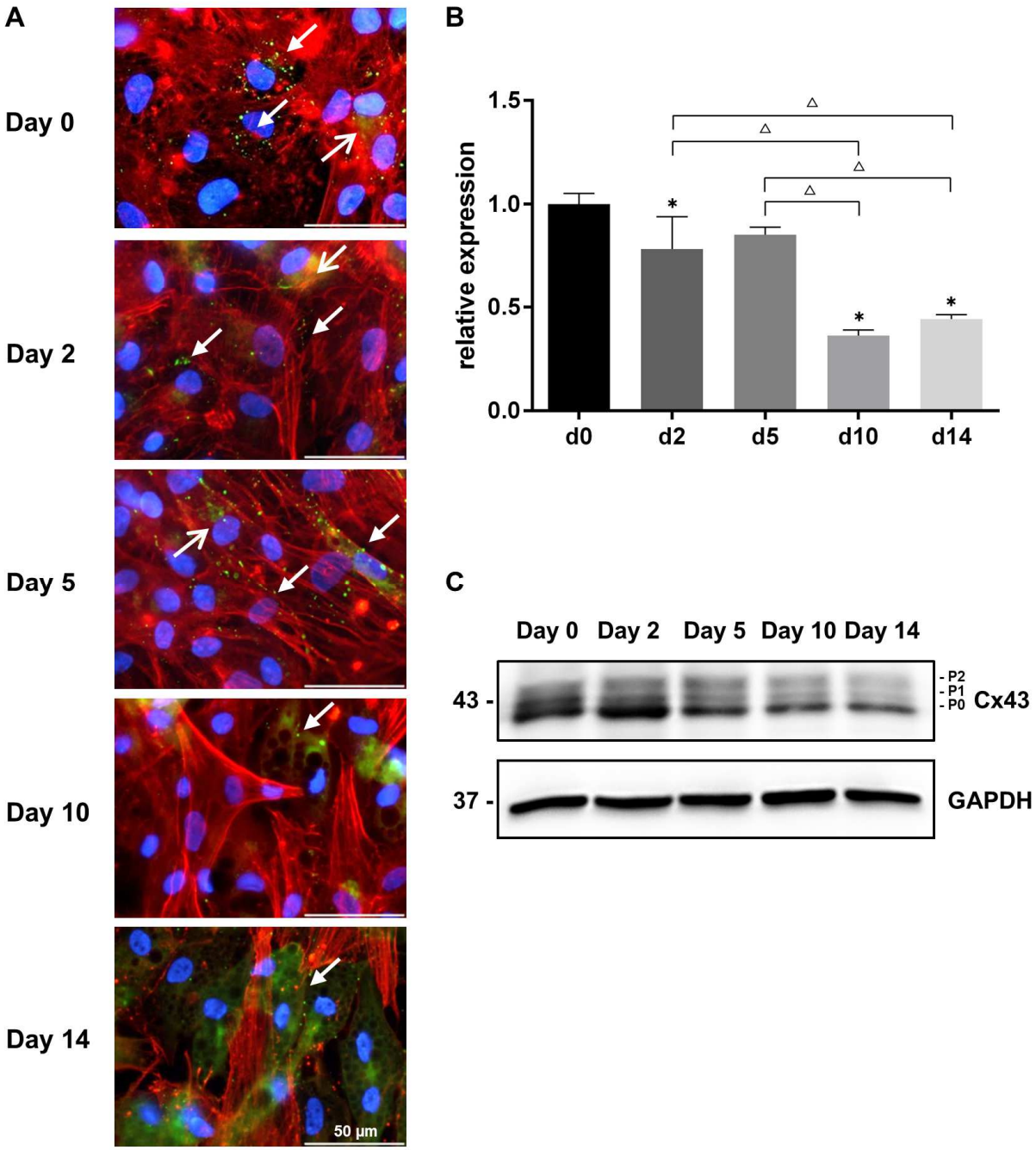

Figure 4.28: Analysis of Cx43 expression during adipogenic differentiation.

A) Immunohistochemical staining for Cx43 on differentiated ASCs was conducted. Cx43 was stained green, β-actin for visualization of the cytoskeleton red, and nuclei blue with DAPI. Cells seeded at high density (100,000/cm^2) were examined at different time points after induction (d0, d2, d5, d10, d14). Arrows indicate cytoplasmic (→) and membranous (➔) localization of Cx43. Representative images are shown. Images were taken at a 60-fold magnification; scale bars represent 50 µm. **B**) Cx43 gene expression of cultured ASCs was determined by qRT-PCR (100,000/cm^2). Gene expression was normalized to EF1α; the obtained values were further normalized to day 0. Values are expressed as mean with standard deviation (n=3). Statistically significant differences ($p<0.05$) to day 0 are indicated by * and between other groups by △. **C**) For investigation of Cx43 protein expression, western blot analysis was performed (100,000/cm^2). Cx43 (43 kDa) detection revealed three bands, the lower band represents unphosphorylated protein (P0), while the upper two bands represent phosphorylation levels (P1, P2) of Cx43. GAPDH (37 kDa) served as the loading control.

4.4.5 Discussion

ASCs represent an attractive and extensively used cell source for tissue engineering applications due to their stemness[18,132,327]. Multi-lineage capacity, for example, for osteogenesis, myogenesis, chondrogenesis, and adipogenesis, has been abundantly demonstrated[41,58,328–330]. Despite the multitude of literature on their differentiation capacity, little is known about the physiological properties that contribute to the process of lineage commitment and differentiation of ASCs. Cell density is a very common yet not fully understood factor reported to affect lineage commitment of stem cells[59]. As a certain degree of cell density is a prerequisite for direct cellular communication by allowing contact between adjacent cells, processes implicated in direct exchange between cells are likely involved in the control of lineage commitment and differentiation[60,316]. In the present study, we investigated the expression of Cx43-containing gap junctions and gap junctional intercellular communication (GJIC) in ASCs, as the most direct form of intercellular communication, and showed, for the first time, its correlation with the adipogenic differentiation potential of these cells.

By histological staining and examination of Cx43 gene and protein expression, we successfully demonstrated the presence of Cx43-containing gap junctions at contact regions of adjacent ASCs. Focusing on different initial cell seeding densities (low: 5,000 cells/cm^2, medium: 25,000 cells/cm^2, and high: 100,000 cells/cm^2), a density-dependent Cx43 expression pattern was evident. Immediately after seeding and adhesion of the cells in the high density culture, gap junctions were present in the cell-cell contact regions and generally accumulated during growth in accordance with increased cell density. Additional cytoplasmic Cx43 staining appeared notably at early time points but also throughout the entire culture period. Western blot analysis revealed the emergence of the phosphorylated isoform P2 of Cx43 with ongoing growth. Different phosphorylation patterns of Cx43 were previously shown to be responsible for the incorporation into the plasma membrane, opening and closing of the channel, and internalization and degradation events[74,75]. Whereas unphosphorylated Cx43 is primarily found in the cytoplasm and associated with the endoplasmic reticulum (ER)/Golgi network, locations of protein translation and assembly, the phosphorylated protein mainly localizes to the plasma membrane and is associated with an increase in GJIC[75,76,322].

Thus far, the existence of Cx43-containing gap junctions in ASCs has been shown in the context of Ca^{2+} oscillation on histological and functional level[78]; furthermore, an influence of quantum dot internalization on GJIC was reported[77]. The correlation between upregulation of Cx43 expression and cell density in our study is in accordance with earlier results on gene expression analysis in ASCs, which revealed an upregulation of genes linked to cell communication and signal transduction in high density cultures[331]. An increase of Cx43 expression with increasing cell density during ongoing cell culture also has been demonstrated for mouse BMSCs[303].

In order to examine the functionality of the observed GJ clusters, we conducted a flow cytometric analysis using dye transfer. The obtained data clearly demonstrated the functionality of the Cx43-containing gap junctions, allowing the exchange of the dye between donor and recipient cells. This finding was further confirmed by effective inhibition of the dye transfer by the acknowledged specific gap junction blocker 18α-glycyrrhetinic acid (AGA). Furthermore, no inhibitory effect was shown with the non-inhibitory pharmacological analog, glycyrrhizic acid (GZA). In accordance with the observed density-dependent expression pattern of Cx43, the dye transfer rate was also significantly influenced by cell density.

In previous studies, high cell densities have been shown to positively influence adipogenic differentiation of mesenchymal stem cells, as demonstrated so far exclusively for BMSCs[55,59,60]. Here, we examined the impact of cell density on adipogenesis in hormonally induced ASCs by means of adipogenic marker gene expression analysis, histological investigation, and quantification of the triglyceride content. A clear dependence of the adipogenic differentiation capability of ASCs on cell density was found. At a low seeding density of 5,000 cells/cm^2, which enables few cell-cell contacts and hence minimal direct communication between cells, adipogenesis was almost abolished. Conversely, adipogenic differentiation was promoted with increasing cell density. Flow cytometry analysis of differentiated cells clearly demonstrated that at a high seeding density, a larger proportion of cells were able to differentiate in comparison to a lower seeding density, suggesting that via increased cell-cell communication, more cells were triggered to undergo adipogenic differentiation. Additionally, the incorporated lipid droplets became smaller in the higher cell density group, an effect, which was similarly reported for BMSCs[55] and may be explained by the limiting amount of available nutrients in these high density cultures.

In order to reveal the impact of GJIC on adipogenesis of ASCs in a high density culture, AGA was used to suppress GJIC during adipogenic induction and differentiation. A distinct reduction of adipogenesis was obvious under these conditions, as shown by histology and triglyceride content analysis. Gene expression of two early adipogenic marker genes, PPARγ and C/EBPα were also significantly downregulated under GJIC inhibition, whereas the late adipogenic marker gene aP2 was less affected. This observation coincided with the downregulation of Cx43 expression at later stages of adipogenesis (see also next paragraph) and may indicate a role of GJIC especially in the early differentiation process. As expected, the non-inhibitory analog GZA had no effect on adipogenesis. Moreover, flow cytometry analysis revealed a significant reduction in the number of differentiated cells, caused by GJIC blockage. The inhibitory effect of AGA on adipogenic differentiation has also been demonstrated in rat BMSCs and in the mouse preadipocyte cell line 3T3-L1, indicating the significance of GJIC for adipogenic differentiation in different cell systems[306,316].

Further studies in 3T3-L1 cells investigating kinetics of GJIC inhibition by AGA during the differentiation process suggested a role of GJIC particularly in early adipogenesis, through synchronization of mitotic clonal expansion and C/EBPβ expression[306], while a downregulation occurred during the differentiation process of these cells, which was critical for adipogenic maturation[76]. In our study, a comparable downregulation of GJ was evident through the differentiation process of ASCs, as shown by histology, gene expression, and protein expression of Cx43. This distinctly affected all isoforms including the phosphorylated, that is, membrane-located forms of the protein. In conclusion, GJIC was demonstrated to strongly impact adipogenic differentiation in ASCs, and it may be especially important for the synchronization of cells during the onset of adipogenesis or early adipogenic processes in ASCs. Studies performing kinetics of GJIC inhibition by administration of the inhibitor at different time points of induction and differentiation may further clarify the role of GJIC in the differentiation process of these primary cells. While AGA is a well acknowledged inhibitor of gap junction functionality (as was also shown in this study), additional genetic gain or loss of function studies by knockdown or overexpression of Cx43 in ASCs would help to further confirm the relevance of GJIC for the adipogenic differentiation behavior of these cells.

Studies using Cx43 knockout or mutant mouse models investigating adipogenesis or fat formation are missing so far except for a recent study from Zappitelli et al. 2015[332]. In this study using a genetic mouse model, which carries a G60S Cx43 mutation, resulting in reduced gap junction formation and function, increased bone marrow adipogenesis was observed and postulated to be arising from upregulation of BMP2/4 signaling in the marrow microenvironment. No effect on other fat depots or the differentiation capability of isolated stromal cells was observed, which, at least in part, was attributed to residual levels of gap junction communication in this model. Thus, in order to further elucidate the role of GJIC on adipogenesis and fat formation in the organism, explicit studies on this topic in Cx43 knockout or mutant murine models are necessary and moreover may provide indications if Cx43 may be a potential pharmacological target for the treatment of adipose tissue disorders such as obesity and metabolic syndrome

As gap junctions are permeable for small molecules less than 1 kDa, cyclic adenosine monophosphate (cAMP) may be a candidate exchanged among Cx43-coupled ASCs[68,333]. A role of cAMP signaling in controlling C/EBPβ expression, an early adipogenic transcription factor, has previously been shown, and is responsible for the need of cAMP inducers like isobutylmethylxanthine (IBMX) in the hormonal cocktails for inducing adipogenesis[49]. A pivotal role for cAMP signaling in the initiation of adipogenesis of ASCs was demonstrated by Jia et al. 2012[334]. cAMP-dependent production of an endogenous PPARγ ligand, which was shown to be critical for the process of adipogenic differentiation, was further shown in 3T3-L1 cells only in the first 2 days of differentiation, after which

its activity rapidly declined[335]. Thus, the GJ-mediated exchange of cAMP between adipocyte precursor cells may be facilitated in high density cultures of ASCs, leading to synchronized behavior of adjacent cells in the early phase of the differentiation process. Another small molecule effector, which has been demonstrated to be efficiently exchanged via gap junctions is microRNA[336,337]. MicroRNAs are short (19-25 nucleotides) RNAs, forming a linear molecule with a diameter of ~1.0 nm, which is in the same order of magnitude as the gap junctional channel pore size[338]. They mainly act as gene regulators in a posttranscriptional manner to modulate differentiation processes and determine cell fate decisions. As miR-143, -24, -31, -30c, and -642a-3p have been shown to regulate adipogenesis[339], the gap junctional transfer of these microRNAs might represent a further mechanism of intercellular signaling involved in modulating adipogenic differentiation of ASCs. Investigations focusing on specific phases of the differentiation process, as well as the actual nature of the exchanged molecule(s) and mediated downstream effects, may help to further elucidate the underlying mechanism.

Altogether, in this study, the expression and functionality of Cx43-containing gap junctions in ASCs was demonstrated, which were strongly dependent on cell density. Through the use of the specific gap junction blocker AGA, the impact of cell-cell contact mediated GJIC on adipogenic differentiation of these cells was proven. Gaining insight into the impact of direct cell-cell communication on lineage commitment and differentiation of ASCs may help to further integrate direct intercellular crosstalk in rationales for tissue engineering and regenerative medicine approaches.

5 Conclusion and Outlook

To serve the growing demand of adequate tissue transplants for plastic and reconstructive surgery by means of tissue engineered autologous constructs, several obstacles still need to be overcome for a successful application. A significant limitation of large-scale tissue replacements still remains the sufficient *in vitro* vascularization for adequate tissue supply upon transplantation. To address this challenge, in the presented approach a recently established decellularized porcine jejunal segment was applied with regard to its usability for the engineering of adipose tissue *in vitro*. The decellularized jejunal segments represented a suitable scaffolding system with preexisting capillary structures, which were repopulated with human microvascular endothelial cells (hMVECs), and a luminal matrix, which was seeded with human adipose-derived stem cells (hASCs) followed by adipogenic induction. The co-culture of these cells within the jejunal segment was performed by means of a custom-made bioreactor system under physiological conditions and the construct was finally characterized in terms of vascularization and adipose tissue development. Substantial adipogenesis of hASCs could be demonstrated within the jejunal lumen in contrast to non-induced controls, and increased expression of key adipogenic markers was shown over time upon induction. The development of major extracellular matrix components of mature adipose tissue, such as laminin and collagen IV, was also demonstrated for the induced samples. Furthermore, the vascular network was successfully reseeded with hMVECs, demonstrated in long-term culture, and co-localization of vascular structures and adipogenically differentiated hASCs could also be observed. Thus, in the current approach, a viable and prevascularized adipose tissue substitute (large-scale of 80-100 mm) has been developed *in vitro* in a long-term culture. The inherent vascular network and the advanced adipogenic status of the engineered constructs make them promising candidates for preclinical testing and potential clinical application as free flap transplant in plastic and reconstructive surgery. In the future, this type of construct might be able to replace autologous pedicled grafts, which are associated with a considerable donor site morbidity and extensive and cost-intensive surgical procedures. However, before clinical application may be approached, vascular supply, tissue development, and volume stability upon implantation still remains to be proven in an animal model within preclinical studies.

Another limitation in the field of adipose tissue engineering is the yet insufficient knowledge about the applied cells, for instance the understanding of how cells can be optimally expanded and differentiated for successful engineering of adipose tissue transplants. Even though ASCs can be easily isolated from abdominal fat depots by liposuction, large numbers of cells are required to entirely seed complex and large 3D matrices or scaffolds, as shown for the study described above employing the decellularized jejunal segments. Hence, cells need to be large-scale expanded *in vitro* on the premise

of not losing their differentiation capacity caused by replicative aging. Likewise, an improved differentiation of hASCs in adipose tissue engineering approaches still remains desirable since most engineered constructs exhibit an inhomogeneous differentiation pattern. With regard to these requirements, the application of growth factors can be utilized, as they demonstrably have a great influence on both proliferation and differentiation capacity of mesenchymal stem cells. In various culture systems it has been reported that specifically bFGF represents a potent mitogen for human MSCs, while maintaining or even promoting their osteogenic, chondrogenic and adipogenic differentiation potential. Although a high potential for adipose tissue engineering applications has been suggested, contradictory information on the effective bFGF concentration and the explicit effect of bFGF on ASC differentiation is present in literature. Thus, in this work the effect of bFGF on hASC proliferation and differentiation capacity was investigated by the application of different concentrations at different time points of culture. While preculture of hASCs with bFGF prior to adipogenic induction could be demonstrated to remarkably affect adipogenic differentiation, application during culture did not improve differentiation capacity. The results of the experiments indicated an influence of this preculture on the cell proliferation ability, which led to an increased cell density at the time of adipogenic induction. It appeared that the difference in cell density at this time is pivotal for increased adipogenic capacity of the cells, which was furthermore confirmed employing different seeding densities. Taken together, the results suggested that a cell-cell contact-mediated mechanism positively influences adipogenic differentiation, which was further investigated in subsequent studies.

Even though a large body of literature exists on the differentiation capacity of ASCs, only little is reported concerning physiological properties contributing to and controlling the process of lineage differentiation of ASCs. Intercellular communication of these cells has hardly been investigated to date. Therefore, as the obtained results indicated, research on this topic could potentially help to optimize suitable tissue substitutes. Connexin 43 (Cx43) is the most abundant isoform of the gap junction-forming connexins, being involved in direct intercellular communication between adjacent cells via gap junctions, which has been shown to modulate differentiation processes in other cell types. Thus, in the present work investigations on the expression of Cx43 and gap junctional intercellular communication (GJIC) in human ASCs, and its significance for adipogenic differentiation of these cells were carried out. Cx43 expression in hASCs was successfully analyzed on histological, gene, and protein level. Furthermore, its expression was shown to be greatly positively influenced by cell seeding density, and functionality of gap junctions was proven by dye transfer analysis. It was also shown that adipogenic differentiation of hASCs was distinctly elevated at higher cell seeding densities. By the application of 18α-glycyrrhetinic acid (AGA), a potent inhibitor of GJIC, adipogenic differentiation was significantly

compromised, demonstrated by histology, triglyceride quantification, and adipogenic marker gene expression. It was shown by flow cytometry analysis that a lower proportion of cells could undergo adipogenesis when GJIC was inhibited, further indicating the importance of GJIC in the differentiation process. Altogether, these results demonstrate the impact of direct cell-cell communication via gap junctions on the adipogenic differentiation process of hASCs. Despite the multitude of literature on the differentiation capacity of ASCs and their widespread use in tissue engineering, many aspects are still in their infancy and further research has to be carried out. The present work indicates that it is worthwhile to include further studies on gap junctions and GJIC in future adipose tissue engineering approaches. Investigations focusing on specific phases of the differentiation process, as well as the actual nature of the exchanged molecule(s) and mediated downstream effects, may help to further elucidate the underlying mechanisms.

Taken together, this work shows a promising approach to engineering vascularized adipose tissue *in vitro* and provides new insights into the adipogenic differentiation capacity of ASCs, specifically with regard to direct cell-cell communication. The obtained results contribute to the body of knowledge in the area of adipose tissue engineering and may aid in a faster translation into the clinic.

References

1. Gomillion, C.T., and Burg, K.J.L. (2006). Stem cells and adipose tissue engineering. Biomaterials *27*, 6052–63.
2. Rosen, E.D., and MacDougald, O. a (2006). Adipocyte differentiation from the inside out. Nature reviews. Molecular cell biology *7*, 885–96.
3. Shen, W., Wang, Z., Punyanita, M., Lei, J., Sinav, A., Kral, J.G., Imielinska, C., Ross, R., and Heymsfield, S.B. (2003). Adipose tissue quantification by imaging methods: a proposed classification. Obesity research *11*, 5–16.
4. Frühbeck, G. (2008). Overview of adipose tissue and its role in obesity and metabolic disorders. Methods in molecular biology *456*, 1–22.
5. Prunet-Marcassus, B., Cousin, B., Caton, D., André, M., Pénicaud, L., and Casteilla, L. (2006). From heterogeneity to plasticity in adipose tissues: site-specific differences. Experimental cell research *312*, 727–36.
6. Sun, K., Kusminski, C.M., and Scherer, P.E. (2011). Adipose tissue remodeling and obesity. The Journal of clinical investigation *121*, 2094–101.
7. Bjørndal, B., Burri, L., Staalesen, V., Skorve, J., and Berge, R.K. (2011). Different adipose depots: their role in the development of metabolic syndrome and mitochondrial response to hypolipidemic agents. Journal of obesity *2011*, 490650.
8. Kopelman, P.G. (2000). Obesity as a medical problem. Nature *404*, 635–43.
9. WHO (2017). Data and statistics. World Health Organization - Regional Office for Europeat <http://www.euro.who.int/en/health-topics/noncommunicable-diseases/obesity/data-and-statistics>.
10. Waki, H., and Tontonoz, P. (2007). Endocrine functions of adipose tissue. Annual review of pathology *2*, 31–56.
11. Hausman, D.B., DiGirolamo, M., Bartness, T.J., Hausman, G.J., and Martin, R.J. (2001). The biology of white adipocyte proliferation. Obesity reviews : an official journal of the International Association for the Study of Obesity *2*, 239–54.
12. Trayhurn, P. (2007). Adipocyte biology. Obesity reviews : an official journal of the International Association for the Study of Obesity *8*, 41–4.
13. Cannon, B., and Nedergaard, J. (2004). Brown adipose tissue: function and physiological significance. Physiological reviews *84*, 277–359.
14. Farmer, S.R. (2008). Molecular determinants of brown adipocyte formation and function. Genes & development *22*, 1269–75.
15. Nedergaard, J., Bengtsson, T., and Cannon, B. (2007). Unexpected evidence for active brown adipose tissue in adult humans. American journal of physiology. Endocrinology and metabolism *293*, E444-52.
16. Frühbeck, G., Becerril, S., Sáinz, N., Garrastachu, P., and García-Velloso, M.J. (2009). BAT: a new target for human obesity? Trends in pharmacological sciences *30*, 387–96.
17. Virtanen, K.A., Lidell, M.E., Orava, J., Heglind, M., Westergren, R., Niemi, T., Taittonen, M., Laine, J., Savisto, N., Enerbäck, S., and Nuutila, P. (2009). Functional brown adipose tissue in healthy adults. The New England journal of medicine *360*, 1518–25.
18. Bauer-Kreisel, P., Goepferich, A., and Blunk, T. (2010). Cell-delivery therapeutics for adipose tissue regeneration. Advanced drug delivery reviews *62*, 798–813.

19. Nishimura, S., Manabe, I., Nagasaki, M., Hosoya, Y., Yamashita, H., Fujita, H., Ohsugi, M., Tobe, K., Kadowaki, T., Nagai, R., and Sugiura, S. (2007). Adipogenesis in obesity requires close interplay between differentiating adipocytes, stromal cells, and blood vessels. Diabetes *56*, 1517–26.

20. Mariman, E.C.M., and Wang, P. (2010). Adipocyte extracellular matrix composition, dynamics and role in obesity. Cellular and molecular life sciences *67*, 1277–92.

21. Kubo, Y., Kaidzu, S., Nakajima, I., Takenouchi, K., and Nakamura, F. (2000). Organization of extracellular matrix components during differentiation of adipocytes in long-term culture. In vitro cellular & developmental biology. Animal *36*, 38–44.

22. Sethi, J.K., and Vidal-Puig, A.J. (2007). Thematic review series: adipocyte biology. Adipose tissue function and plasticity orchestrate nutritional adaptation. Journal of lipid research *48*, 1253–62.

23. Flynn, L., and Woodhouse, K. a (2008). Adipose tissue engineering with cells in engineered matrices. Organogenesis *4*, 228–35.

24. Otto, T.C., and Lane, M.D. (2005). Adipose development: from stem cell to adipocyte. Critical reviews in biochemistry and molecular biology *40*, 229–42.

25. Schwarzbauer, J. (1999). Basement membranes: Putting up the barriers. Current biology : CB *9*, R242-4.

26. Christiaens, V., and Lijnen, H.R. (2010). Angiogenesis and development of adipose tissue. Molecular and cellular endocrinology *318*, 2–9.

27. Friedman, J.M., and Halaas, J.L. (1998). Leptin and the regulation of body weight in mammals. Nature *395*, 763–770.

28. Friedman, J.M. (2011). Leptin and the regulation of body weight. Harvey lectures *95*, 107–36.

29. Theodore Kelesidis, Iosif Kelesidis, Sharon Chou, C.S.M. (2010). Review Narrative Review : The Role of Leptin in Human Physiology : Emerging. Annals of Internal Medicine *152*, 93–101.

30. Margetic, S., Gazzola, C., Pegg, G.G., and Hill, R.A. (2002). Leptin: a review of its peripheral actions and interactions. International journal of obesity and related metabolic disorders : journal of the International Association for the Study of Obesity *26*, 1407–33.

31. Flier, J.S. (2001). Diabetes. The missing link with obesity? Nature *409*, 292–3.

32. Kadowaki, T., and Yamauchi, T. (2011). Adiponectin receptor signaling: a new layer to the current model. Cell metabolism *13*, 123–4.

33. Berg, A.H., Combs, T.P., Du, X., Brownlee, M., and Scherer, P.E. (2001). The adipocyte-secreted protein Acrp30 enhances hepatic insulin action. Nature medicine *7*, 947–53.

34. Fischer-Posovszky, P., Wabitsch, M., and Hochberg, Z. (2007). Endocrinology of adipose tissue - an update. Hormone and metabolic research *39*, 314–21.

35. Lago, F., Gómez, R., Gómez-Reino, J.J., Dieguez, C., and Gualillo, O. (2009). Adipokines as novel modulators of lipid metabolism. Trends in biochemical sciences *34*, 500–10.

36. Kershaw, E.E., and Flier, J.S. (2004). Adipose tissue as an endocrine organ. The Journal of clinical endocrinology and metabolism *89*, 2548–56.

37. Rider, D. a, Dombrowski, C., Sawyer, A. a, Ng, G.H.B., Leong, D., Hutmacher, D.W., Nurcombe, V., and Cool, S.M. (2008). Autocrine fibroblast growth factor 2 increases the multipotentiality of human adipose-derived mesenchymal stem cells. Stem cells *26*, 1598–608.

38. Halberg, N., Wernstedt-Asterholm, I., and Scherer, P.E. (2008). The adipocyte as an endocrine cell. Endocrinology and metabolism clinics of North America *37*, 753–68.

39. Ahima, R.S., and Flier, J.S. (2000). Adipose tissue as an endocrine organ. Trends in endocrinology and metabolism *11*, 327–32.

40. Gimble, J.M., Katz, A.J., and Bunnell, B. a (2007). Adipose-derived stem cells for regenerative medicine. Circulation research *100*, 1249–60.

41. Rosen, E.D., and Spiegelman, B.M. (2000). Molecular regulation of adipogenesis. Annual review of cell and developmental biology *16*, 145–71.

42. Avram, M.M., Avram, A.S., and James, W.D. (2007). Subcutaneous fat in normal and diseased states 3. Adipogenesis: from stem cell to fat cell. Journal of the American Academy of Dermatology *56*, 472–92.

43. Rosen, E.D., and Spiegelman, B.M. (2000). Molecular regulation of adipogenesis. Annual review of cell and developmental biology *16*, 145–71.

44. Gregoire, F.M., Smas, C.M., and Sul, H.S. (1998). Understanding adipocyte differentiation. Physiological reviews *78*, 783–809.

45. Ali, A.T., Hochfeld, W.E., Myburgh, R., and Pepper, M.S. (2013). Adipocyte and adipogenesis. European journal of cell biology *92*, 229–36.

46. Fève, B. (2005). Adipogenesis: cellular and molecular aspects. Best practice & research. Clinical endocrinology & metabolism *19*, 483–99.

47. Moseti, D., Regassa, A., and Kim, W.-K. (2016). Molecular Regulation of Adipogenesis and Potential Anti-Adipogenic Bioactive Molecules. International journal of molecular sciences *17*, 124.

48. Tang, Q.Q., and Lane, M.D. (2012). Adipogenesis: from stem cell to adipocyte. Annual review of biochemistry *81*, 715–36.

49. Farmer, S.R. (2006). Transcriptional control of adipocyte formation. Cell metabolism *4*, 263–73.

50. MacDougald, O.A., and Mandrup, S. (2002). Adipogenesis: forces that tip the scales. Trends in endocrinology and metabolism *13*, 5–11.

51. Entenmann, G., and Hauner, H. (1996). Relationship between replication and differentiation in cultured human adipocyte precursor cells. The American journal of physiology *270*, C1011-6.

52. Lefterova, M.I., and Lazar, M.A. (2009). New developments in adipogenesis. Trends in Endocrinology & Metabolism *20*, 107–114.

53. Zhang, Y., Khan, D., Delling, J., and Tobiasch, E. (2012). Mechanisms underlying the osteo- and adipo-differentiation of human mesenchymal stem cells. The scientific world journal *2012*, 793823.

54. Bunnell, B.A., Flaat, M., Gagliardi, C., Patel, B., and Ripoll, C. (2008). Adipose-derived stem cells: isolation, expansion and differentiation. Methods *45*, 115–20.

55. Cárcamo-Orive, I., Tejados, N., Delgado, J., Gaztelumendi, A., Otaegui, D., Lang, V., and Trigueros, C. (2008). ERK2 protein regulates the proliferation of human mesenchymal stem cells without affecting their mobilization and differentiation potential. Experimental cell research *314*, 1777–88.

56. Tsutsumi, S., Shimazu, A., Miyazaki, K., Pan, H., Koike, C., Yoshida, E., Takagishi, K., and Kato, Y. (2001). Retention of multilineage differentiation potential of mesenchymal cells during proliferation in response to FGF. Biochemical and biophysical research communications *288*, 413–9.

57. Fischbach, C., Seufert, J., Staiger, H., Hacker, M., Neubauer, M., Göpferich, A., and Blunk, T. (2004). Three-dimensional in vitro model of adipogenesis: comparison of culture conditions. Tissue engineering *10*, 215–29.

58. Kakudo, N., Shimotsuma, A., and Kusumoto, K. (2007). Fibroblast growth factor-2 stimulates adipogenic differentiation of human adipose-derived stem cells. Biochemical and biophysical research communications *359*, 239–44.

59. McBeath, R., Pirone, D.M., Nelson, C.M., Bhadriraju, K., and Chen, C.S. (2004). Cell shape, cytoskeletal tension, and RhoA regulate stem cell lineage commitment. Developmental cell *6*, 483–95.

60. Peng, R., Yao, X., Cao, B., Tang, J., and Ding, J. (2012). The effect of culture conditions on the adipogenic and osteogenic inductions of mesenchymal stem cells on micropatterned surfaces. Biomaterials *33*, 6008–19.

61. Camussi, G., Deregibus, M.C., Bruno, S., Cantaluppi, V., and Biancone, L. (2010). Exosomes/microvesicles as a mechanism of cell-to-cell communication. Kidney international *78*, 838–48.

62. Majka, M., Janowska-Wieczorek, A., Ratajczak, J., Ehrenman, K., Pietrzkowski, Z., Kowalska, M.A., Gewirtz, A.M., Emerson, S.G., and Ratajczak, M.Z. (2001). Numerous growth factors, cytokines, and chemokines are secreted by human CD34(+) cells, myeloblasts, erythroblasts, and megakaryoblasts and regulate normal hematopoiesis in an autocrine/paracrine manner. Blood *97*, 3075–85.

63. Wong, R.C.B., Pera, M.F., and Pébay, A. (2008). Role of gap junctions in embryonic and somatic stem cells. Stem cell reviews *4*, 283–92.

64. Rübsam, M., Broussard, J.A., Wickström, S.A., Nekrasova, O., Green, K.J., and Niessen, C.M. (2018). Adherens Junctions and Desmosomes Coordinate Mechanics and Signaling to Orchestrate Tissue Morphogenesis and Function: An Evolutionary Perspective. Cold Spring Harbor perspectives in biology *10*, a029207.

65. Mège, R.-M., Gavard, J., and Lambert, M. (2006). Regulation of cell-cell junctions by the cytoskeleton. Current opinion in cell biology *18*, 541–8.

66. Alberts, B., Johnson, A., Lewis, J., Raff, M., Roberts, K., and Walter, P. (2002). *Molecular biology of the cell*, Garland Science.

67. Gleisner, M.A., Navarrete, M., Hofmann, F., Salazar-Onfray, F., and Tittarelli, A. (2017). Mind the Gaps in Tumor Immunity: Impact of Connexin-Mediated Intercellular Connections. Frontiers in immunology *8*, 1067.

68. Evans, W.H., and Martin, P.E.M. (2002). Gap junctions: structure and function (Review). Molecular membrane biology *19*, 121–36.

69. Rosselló, R.A., Wang, Z., Kizana, E., Krebsbach, P.H., and Kohn, D.H. (2009). Connexin 43 as a signaling platform for increasing the volume and spatial distribution of regenerated tissue. Proceedings of the National Academy of Sciences of the United States of America *106*, 13219–24.

70. El-Sabban, M.E., Sfeir, A.J., Daher, M.H., Kalaany, N.Y., Bassam, R. a, and Talhouk, R.S. (2003). ECM-induced gap junctional communication enhances mammary epithelial cell differentiation. Journal of cell science *116*, 3531–41.

71. Goodenough, D. a, Goliger, J. a, and Paul, D.L. (1996). Connexins, connexons, and intercellular communication. Annual review of biochemistry *65*, 475–502.

72. Valiunas, V., Doronin, S., Valiuniene, L., Potapova, I., Zuckerman, J., Walcott, B., Robinson, R.B., Rosen, M.R., Brink, P.R., and Cohen, I.S. (2004). Human mesenchymal stem cells make cardiac connexins and form functional gap junctions. The Journal of physiology *555*, 617–26.

73. Nielsen, M.S., Axelsen, L.N., Sorgen, P.L., Verma, V., Delmar, M., and Holstein-Rathlou, N.-H. (2012). Gap junctions. Comprehensive Physiology *2*, 1981–2035.

74. Solan, J.L., and Lampe, P.D. (2005). Connexin phosphorylation as a regulatory event linked to gap junction channel assembly. Biochimica et biophysica acta *1711*, 154–63.

75. Solan, J.L., and Lampe, P.D. (2014). Specific Cx43 phosphorylation events regulate gap junction turnover in vivo. FEBS letters *588*, 1423–9.

76. Yeganeh, A., Stelmack, G.L., Fandrich, R.R., Halayko, A.J., Kardami, E., and Zahradka, P. (2012). Connexin 43 phosphorylation and degradation are required for adipogenesis. Biochimica et biophysica acta *1823*, 1731–44.

77. Chang, J.-C., Hsu, S.-H., and Su, H.-L. (2009). The regulation of the gap junction of human mesenchymal stem cells through the internalization of quantum dots. Biomaterials *30*, 1937–46.

78. Sauer, H., Sharifpanah, F., Hatry, M., Steffen, P., Bartsch, C., Heller, R., Padmasekar, M., Howaldt, H.-P., Bein, G., and Wartenberg, M. (2011). NOS inhibition synchronizes calcium oscillations in human adipose tissue-derived mesenchymal stem cells by increasing gap-junctional coupling. Journal of cellular physiology *226*, 1642–50.

79. Hausman, G.J., and Richardson, R.L. (2004). Adipose tissue angiogenesis. Journal of animal science *82*, 925–34.

80. Lemoine, A.Y., Ledoux, S., and Larger, E. (2013). Adipose tissue angiogenesis in obesity. Thrombosis and haemostasis *110*, 661–8.

81. Stupack, D.G., and Cheresh, D. a (2002). ECM remodeling regulates angiogenesis: endothelial integrins look for new ligands. Science's signal transduction knowledge environment *2002*, pe7.

82. Carmeliet, P. (2003). Angiogenesis in health and disease. Nature medicine *9*, 653–60.

83. Carmeliet, P., and Jain, R.K. (2011). Molecular mechanisms and clinical applications of angiogenesis. Nature *473*, 298–307.

84. Potente, M., and Carmeliet, P. (2017). The Link Between Angiogenesis and Endothelial Metabolism. Annual review of physiology *79*, 43–66.

85. Herbert, S.P., and Stainier, D.Y.R. (2011). Molecular control of endothelial cell behaviour during blood vessel morphogenesis. Nature reviews. Molecular cell biology *12*, 551–64.

86. Miranville, A., Heeschen, C., Sengenès, C., Curat, C.A., Busse, R., and Bouloumié, A. (2004). Improvement of postnatal neovascularization by human adipose tissue-derived stem cells. Circulation *110*, 349–55.

87. Ribatti, D., Conconi, M.T., and Nussdorfer, G.G. (2007). Nonclassic endogenous novel [corrected] regulators of angiogenesis. Pharmacological reviews *59*, 185–205.

88. Cao, Y. (2007). Angiogenesis modulates adipogenesis and obesity. The Journal of clinical investigation *117*, 2362–8.

89. Cho, C.-H., Koh, Y.J., Han, J., Sung, H.-K., Jong Lee, H., Morisada, T., Schwendener, R.A., Brekken, R.A., Kang, G., Oike, Y., Choi, T.-S., Suda, T., Yoo, O.-J., and Koh, G.Y. (2007). Angiogenic role of LYVE-1-positive macrophages in adipose tissue. Circulation research *100*, e47-57.

90. Saiki, A., Watanabe, F., Murano, T., Miyashita, Y., and Shirai, K. (2006). Hepatocyte growth factor secreted by cultured adipocytes promotes tube formation of vascular endothelial cells in vitro. International journal of obesity *30*, 1676–84.

91. Lijnen, H.R. (2008). Angiogenesis and obesity. Cardiovascular research *78*, 286–93.

92. Rehman, J., Traktuev, D., Li, J., Merfeld-Clauss, S., Temm-Grove, C.J., Bovenkerk, J.E., Pell, C.L., Johnstone, B.H., Considine, R. V., and March, K.L. (2004). Secretion of angiogenic and antiapoptotic factors by human adipose stromal cells. Circulation *109*, 1292–8.

93. Kilroy, G.E., Foster, S.J., Wu, X., Ruiz, J., Sherwood, S., Heifetz, A., Ludlow, J.W., Stricker, D.M., Potiny, S., Green, P., Halvorsen, Y.-D.C., Cheatham, B., Storms, R.W., and Gimble, J.M. (2007). Cytokine profile of human adipose-derived stem cells: expression of angiogenic, hematopoietic, and pro-inflammatory factors. Journal of cellular physiology *212*, 702–9.

94. Papetti, M., and Herman, I.M. (2002). Mechanisms of normal and tumor-derived angiogenesis. American journal of physiology. Cell physiology *282*, C947-70.

95. Ucuzian, A.A., Gassman, A.A., East, A.T., and Greisler, H.P. (2010). Molecular mediators of angiogenesis. Journal of burn care & research : official publication of the American Burn Association *31*, 158–75.

96. Otrock, Z.K., Mahfouz, R.A.R., Makarem, J.A., and Shamseddine, A.I. (2007). Understanding the biology of angiogenesis: review of the most important molecular mechanisms. Blood cells, molecules & diseases *39*, 212–20.

97. Cao, Y. (2010). Adipose tissue angiogenesis as a therapeutic target for obesity and metabolic diseases. Nature reviews. Drug discovery *9*, 107–15.

98. Daley, W.P., Peters, S.B., and Larsen, M. (2008). Extracellular matrix dynamics in development and regenerative medicine. Journal of Cell Science *121*.

99. Rozario, T., and DeSimone, D.W. (2010). The extracellular matrix in development and morphogenesis: a dynamic view. Developmental biology *341*, 126–40.

100. Pope, B.D., Warren, C.R., Parker, K.K., and Cowan, C.A. (2016). Microenvironmental Control of Adipocyte Fate and Function. Trends in cell biology *26*, 745–755.

101. Khan, T., Muise, E.S., Iyengar, P., Wang, Z. V, Chandalia, M., Abate, N., Zhang, B.B., Bonaldo, P., Chua, S., and Scherer, P.E. (2009). Metabolic dysregulation and adipose tissue fibrosis: role of collagen VI. Molecular and cellular biology *29*, 1575–91.

102. Nakajima, I., Yamaguchi, T., Ozutsumi, K., and Aso, H. (1998). x. Differentiation *63*, 193–200.

103. Timpl, R. (1996). Macromolecular organization of basement membranes. Current opinion in cell biology *8*, 618–24.

104. Aumailley, M. (2013). The laminin family. Cell adhesion & migration *7*, 48–55.

105. Nie, J., and Sage, E.H. (2009). SPARC functions as an inhibitor of adipogenesis. Journal of cell communication and signaling *3*, 247–54.

106. Wondimu, Z., Geberhiwot, T., Ingerpuu, S., Juronen, E., Xie, X., Lindbom, L., Doi, M., Kortesmaa, J., Thyboll, J., Tryggvason, K., Fadeel, B., and Patarroyo, M. (2004). An endothelial laminin isoform, laminin 8 (alpha4beta1gamma1), is secreted by blood neutrophils, promotes neutrophil migration and extravasation, and protects neutrophils from apoptosis. Blood *104*, 1859–66.

107. Pierleoni, C., Verdenelli, F., Castellucci, M., and Cinti, S. (1998). Fibronectins and basal lamina molecules expression in human subcutaneous white adipose tissue. European journal of histochemistry : EJH *42*, 183–8.

108. Kalluri, R. (2003). Basement membranes: structure, assembly and role in tumour angiogenesis. Nature reviews. Cancer *3*, 422–33.

109. Wilsie, L.C., Chanchani, S., Navaratna, D., and Orlando, R.A. (2005). Cell surface heparan sulfate proteoglycans contribute to intracellular lipid accumulation in adipocytes. Lipids in health and disease *4*, 2.

110. Cheng, Y.S., Champliaud, M.F., Burgeson, R.E., Marinkovich, M.P., and Yurchenco, P.D. (1997). Self-assembly of laminin isoforms. The Journal of biological chemistry *272*, 31525–32.

111. Bouloumié, A., Sengenès, C., Portolan, G., Galitzky, J., and Lafontan, M. (2001). Adipocyte produces matrix metalloproteinases 2 and 9: involvement in adipose differentiation. Diabetes *50*, 2080–6.

112. Aratani, Y., and Kitagawa, Y. (1988). Enhanced synthesis and secretion of type IV collagen and entactin during adipose conversion of 3T3-L1 cells and production of unorthodox laminin complex. The Journal of biological chemistry *263*, 16163–9.

113. Nakajima, I., Muroya, S., Tanabe, R., and Chikuni, K. (2002). Extracellular matrix development during differentiation into adipocytes with a unique increase in type V and VI collagen. Biology of the cell *94*, 197–203.

114. Badylak, S.F., Freytes, D.O., and Gilbert, T.W. (2015). Reprint of: Extracellular matrix as a biological scaffold material: Structure and function. Acta biomaterialia *23 Suppl*, S17-26.

115. Statistics of the American Society of Plastic Surgeons (ASPS). Plastic Surgery Statistics 2016. www.plasticsurgery.org.

116. Billings, E., and May, J.W. (1989). Historical review and present status of free fat graft autotransplantation in plastic and reconstructive surgery. Plastic and reconstructive surgery *83*, 368–81.

117. von Heimburg, D., Kuberka, M., Rendchen, R., Hemmrich, K., Rau, G., and Pallua, N. (2003). Preadipocyte-loaded collagen scaffolds with enlarged pore size for improved soft tissue engineering. The International journal of artificial organs *26*, 1064–76.

118. Ashinoff, R. (2000). Overview: soft tissue augmentation. Clinics in plastic surgery *27*, 479–87.

119. Klein, A.W., and Elson, M.L. (2000). The history of substances for soft tissue augmentation. Dermatologic surgery *26*, 1096–105.

120. Patrick, C.W. (2001). Tissue engineering strategies for adipose tissue repair. The Anatomical record *263*, 361–6.

121. Chen, F.-M., and Liu, X. (2016). Advancing biomaterials of human origin for tissue engineering. Progress in polymer science *53*, 86–168.

122. Yoshimura, K., Sato, K., Aoi, N., Kurita, M., Hirohi, T., and Harii, K. (2008). Cell-assisted lipotransfer for cosmetic breast augmentation: supportive use of adipose-derived stem/stromal cells. Aesthetic plastic surgery *32*, 48–57.

123. McArdle, A., Senarath-Yapa, K., Walmsley, G.G., Hu, M., Atashroo, D.A., Tevlin, R., Zielins, E., Gurtner, G.C., Wan, D.C., and Longaker, M.T. (2014). The role of stem cells in aesthetic surgery: fact or fiction? Plastic and reconstructive surgery *134*, 193–200.

124. Peltoniemi, H.H., Salmi, A., Miettinen, S., Mannerström, B., Saariniemi, K., Mikkonen, R., Kuokkanen, H., and Herold, C. (2013). Stem cell enrichment does not warrant a higher graft survival in lipofilling of the breast: a prospective comparative study. Journal of plastic, reconstructive & aesthetic surgery *66*, 1494–503.

125. Tanzi, M.C., and Farè, S. (2009). Adipose tissue engineering: state of the art, recent advances and innovative approaches. Expert review of medical devices *6*, 533–51.

126. Patrick, C.W. (2000). Adipose tissue engineering: the future of breast and soft tissue reconstruction following tumor resection. Seminars in surgical oncology *19*, 302–11.

127. Garvey, P.B., Buchel, E.W., Pockaj, B.A., Casey, W.J., Gray, R.J., Hernández, J.L., and Samson, T.D. (2006). DIEP and pedicled TRAM flaps: a comparison of outcomes. Plastic and reconstructive surgery *117*, 1711–21.

128. Tachi, M., and Yamada, A. (2005). Choice of flaps for breast reconstruction. International journal of clinical oncology *10*, 289–97.

129. Walgenbach, K.J., Voigt, M., Riabikhin, a W., Andree, C., Schaefer, D.J., Galla, T.J., and Björn, G. (2001). Tissue engineering in plastic reconstructive surgery. The Anatomical record *263*, 372–8.

130. Weiser, B., Neubauer, M., Göpferich, A., and Blunk, T. (2008). Tissue Engineering, fat. Encyclopedia of Biomaterials and Biomedical Engineering, Second Edition, pp 2725–2736.

131. Stock, U.A., and Vacanti, J.P. (2001). Tissue engineering: current state and prospects. Annual review of medicine *52*, 443–51.

132. Dai, R., Wang, Z., Samanipour, R., Koo, K.-I., and Kim, K. (2016). Adipose-Derived Stem Cells for Tissue Engineering and Regenerative Medicine Applications. Stem cells international *2016*, 6737345.

133. Khademhosseini, A., and Langer, R. (2016). A decade of progress in tissue engineering. Nature protocols *11*, 1775–81.

134. Asada, S., Kuroda, M., Aoyagi, Y., Fukaya, Y., Tanaka, S., Konno, S., Tanio, M., Aso, M., Satoh, K., Okamoto, Y., Nakayama, T., Saito, Y., and Bujo, H. (2011). Ceiling culture-derived proliferative adipocytes retain high adipogenic potential suitable for use as a vehicle for gene transduction therapy. American journal of cell physiology *301*, C181-5.

135. Green, H., and Kehinde, O. (1976). Spontaneous heritable changes leading to increased adipose conversion in 3T3 cells. Cell *7*, 105–13.

136. Green, H., and Kehinde, O. (1975). An established preadipose cell line and its differentiation in culture. II. Factors affecting the adipose conversion. Cell *5*, 19–27.

137. Green, H., and Kehinde, O. (1974). Sublines of mouse 3T3 cells that accumulate lipid. Cell *1*, 113–116.

138. Rizzatti, V., Boschi, F., Pedrotti, M., Zoico, E., Sbarbati, A., and Zamboni, M. (2013). Lipid droplets characterization in adipocyte differentiated 3T3-L1 cells: size and optical density distribution. European journal of histochemistry : *57*, e24.

139. Sarjeant, K., and Stephens, J.M. (2012). Adipogenesis. Cold Spring Harbor perspectives in biology *4*, a008417.

140. Thomson, J.A., Itskovitz-Eldor, J., Shapiro, S.S., Waknitz, M.A., Swiergiel, J.J., Marshall, V.S., and Jones, J.M. (1998). Embryonic stem cell lines derived from human blastocysts. Science (New York, N.Y.) *282*, 1145–7.

141. Lerou, P. (2011). Embryonic stem cell derivation from human embryos. Methods in molecular biology (Clifton, N.J.) *767*, 31–5.

142. Ben-David, U., and Benvenisty, N. (2011). The tumorigenicity of human embryonic and induced pluripotent stem cells. Nature reviews. Cancer *11*, 268–77.

143. Takahashi, K., Tanabe, K., Ohnuki, M., Narita, M., Ichisaka, T., Tomoda, K., and Yamanaka, S. (2007). Induction of pluripotent stem cells from adult human fibroblasts by defined factors. Cell *131*, 861–72.

144. Steinemann, D., Göhring, G., and Schlegelberger, B. (2013). Genetic instability of modified stem cells - a first step towards malignant transformation? American journal of stem cells *2*, 39–51.

145. Spencer, N.D., Gimble, J.M., and Lopez, M.J. (2011). Mesenchymal stromal cells: past, present, and future. Veterinary surgery : VS *40*, 129–39.

146. Lindroos, B., Suuronen, R., and Miettinen, S. (2011). The potential of adipose stem cells in regenerative medicine. Stem cell reviews *7*, 269–91.

147. Salibian, A.A., Widgerow, A.D., Abrouk, M., and Evans, G.R. (2013). Stem cells in plastic surgery: a review of current clinical and translational applications. Archives of plastic surgery *40*, 666–75.

148. Illouz, Y.G. (1983). Body contouring by lipolysis: a 5-year experience with over 3000 cases. Plastic and reconstructive surgery *72*, 591–7.

149. Tremp, M., Alemi, S., Gobet, R., Sulser, T., and Eberli, D. (2011). Adipose-Derived Stem Cells (ASCs) for Tissue Engineering. Regernerative Medicine and Tissue Engineering - Cells and Biomaterials, p 450doi:10.5772/51895.

150. Semon, J.A., Maness, C., Zhang, X., Sharkey, S.A., Beuttler, M.M., Shah, F.S., Pandey, A.C., Gimble, J.M., Zhang, S., Scruggs, B.A., Strong, A.L., Strong, T.A., and Bunnell, B.A. (2014). Comparison of human adult stem cells from adipose tissue and bone marrow in the treatment of experimental autoimmune encephalomyelitis. Stem cell research & therapy *5*, 2.

151. Schäffler, A., and Büchler, C. (2007). Concise review: adipose tissue-derived stromal cells--basic and clinical implications for novel cell-based therapies. Stem cells *25*, 818–27.

152. Wittmann, K., Dietl, S., Ludwig, N., Berberich, O., Hoefner, C., Storck, K., Blunk, T., and Bauer-Kreisel, P. (2015). Engineering vascularized adipose tissue using the stromal-vascular fraction and fibrin hydrogels. Tissue engineering. Part A *21*, 1343–53.

153. Müller, A.M., Mehrkens, A., Schäfer, D.J., Jaquiery, C., Güven, S., Lehmicke, M., Martinetti, R., Farhadi, I., Jakob, M., Scherberich, A., and Martin, I. (2010). Towards an intraoperative engineering of osteogenic and vasculogenic grafts from the stromal vascular fraction of human adipose tissue. European cells & materials *19*, 127–35.

154. Lin, S.-D., Huang, S.-H., Lin, Y.-N., Wu, S.-H., Chang, H.-W., Lin, T.-M., Chai, C.-Y., and Lai, C.-S. (2011). Engineering adipose tissue from uncultured human adipose stromal vascular fraction on collagen matrix and gelatin sponge scaffolds. Tissue engineering. Part A *17*, 1489–98.

155. Orkin, R.W., Gehron, P., McGoodwin, E.B., Martin, G.R., Valentine, T., and Swarm, R. (1977). A murine tumor producing a matrix of basement membrane. The Journal of experimental medicine *145*, 204–20.

156. Kimura, Y., Ozeki, M., Inamoto, T., and Tabata, Y. (2002). Time course of de novo adipogenesis in matrigel by gelatin microspheres incorporating basic fibroblast growth factor. Tissue engineering *8*, 603–13.

157. Tabata, Y., Miyao, M., Inamoto, T., Ishii, T., Hirano, Y., Yamaoki, Y., and Ikada, Y. (2000). De novo formation of adipose tissue by controlled release of basic fibroblast growth factor. Tissue engineering *6*, 279–89.

158. Kawaguchi, N., Toriyama, K., Nicodemou-Lena, E., Inou, K., Torii, S., and Kitagawa, Y. (1998). De novo adipogenesis in mice at the site of injection of basement membrane and basic fibroblast growth factor. Proceedings of the National Academy of Sciences of the United States of America *95*, 1062–6.

159. Walton, R.L., Beahm, E.K., and Wu, L. (2004). De novo adipose formation in a vascularized engineered construct. Microsurgery *24*, 378–84.

160. Göpferich, A. (1996). Mechanisms of polymer degradation and erosion. Biomaterials *17*, 103–14.

161. Patrick, C.W., Zheng, B., Johnston, C., and Reece, G.P. (2002). Long-term implantation of preadipocyte-seeded PLGA scaffolds. Tissue engineering *8*, 283–93.

162. Neubauer, M., Hacker, M., Bauer-Kreisel, P., Weiser, B., Fischbach, C., Schulz, M.B., Goepferich, A., and Blunk, T. (2005). Adipose tissue engineering based on mesenchymal stem cells and basic fibroblast growth factor in vitro. Tissue engineering *11*, 1840–51.

163. Fischbach, C., Spruß, T., Weiser, B., Neubauer, M., Becker, C., Hacker, M., Göpferich, A., and Blunk, T. (2004). Generation of mature fat pads in vitro and in vivo utilizing 3-D long-term culture of 3T3-L1 preadipocytes. Experimental Cell Research *300*, 54–64.

164. Patrick, C.W., Chauvin, P.B., Hobley, J., and Reece, G.P. (1999). Preadipocyte seeded PLGA scaffolds for adipose tissue engineering. Tissue engineering *5*, 139–51.

165. Weiser, B., Prantl, L., Schubert, T.E.O.O., Zellner, J., Fischbach-Teschl, C., Spruss, T., Seitz, A.K., Tessmar, J., Goepferich, A., and Blunk, T. (2008). In vivo development and long-term survival of engineered adipose tissue depend on in vitro precultivation strategy. Tissue engineering. Part A *14*, 275–84.

166. Morgan, S.M., Ainsworth, B.J., Kanczler, J.M., Babister, J.C., Chaudhuri, J.B., and Oreffo, R.O.C. (2009). Formation of a human-derived fat tissue layer in P(DL)LGA hollow fibre scaffolds for adipocyte tissue engineering. Biomaterials *30*, 1910–7.

167. Shanti, R.M., Janjanin, S., Li, W.-J., Nesti, L.J., Mueller, M.B., Tzeng, M.B., and Tuan, R.S. (2008). In vitro adipose tissue engineering using an electrospun nanofibrous scaffold. Annals of plastic surgery *61*, 566–71.

168. Kang, X., Xie, Y., and Kniss, D.A. (2005). Adipose tissue model using three-dimensional cultivation of preadipocytes seeded onto fibrous polymer scaffolds. Tissue engineering *11*, 458–68.

169. Wittmann, K., Storck, K., Muhr, C., Mayer, H., Regn, S., Staudenmaier, R., Wiese, H., Maier, G., Bauer-Kreisel, P., and Blunk, T. (2016). Development of volume-stable adipose tissue constructs using polycaprolactone-based polyurethane scaffolds and fibrin hydrogels. Journal of tissue engineering and regenerative medicine *10*, E409–E418.

170. Altman, G.H., Diaz, F., Jakuba, C., Calabro, T., Horan, R.L., Chen, J., Lu, H., Richmond, J., and Kaplan, D.L. (2003). Silk-based biomaterials. Biomaterials *24*, 401–16.

171. Mauney, J.R., Nguyen, T., Gillen, K., Kirker-Head, C., Gimble, J.M., and Kaplan, D.L. (2007). Engineering adipose-like tissue in vitro and in vivo utilizing human bone marrow and adipose-derived mesenchymal stem cells with silk fibroin 3D scaffolds. Biomaterials *28*, 5280–90.

172. Itoi, Y., Takatori, M., Hyakusoku, H., and Mizuno, H. (2010). Comparison of readily available scaffolds for adipose tissue engineering using adipose-derived stem cells. Journal of plastic, reconstructive & aesthetic surgery *63*, 858–64.

173. Flynn, L., Semple, J.L., and Woodhouse, K.A. (2006). Decellularized placental matrices for adipose tissue engineering. Journal of biomedical materials research. Part A *79*, 359–69.

174. Yu, C., Bianco, J., Brown, C., Fuetterer, L., Watkins, J.F., Samani, A., and Flynn, L.E. (2013). Porous decellularized adipose tissue foams for soft tissue regeneration. Biomaterials *34*, 3290–302.

175. Turner, A.E.B., Yu, C., Bianco, J., Watkins, J.F., and Flynn, L.E. (2012). The performance of decellularized adipose tissue microcarriers as an inductive substrate for human adipose-derived stem cells. Biomaterials *33*, 4490–4499.

176. Flynn, L.E. (2010). The use of decellularized adipose tissue to provide an inductive microenvironment for the adipogenic differentiation of human adipose-derived stem cells. Biomaterials *31*, 4715–24.

177. Choi, J.H., Gimble, J.M., Lee, K., Marra, K.G., Rubin, J.P., Yoo, J.J., Vunjak-Novakovic, G., and Kaplan, D.L. (2010). Adipose tissue engineering for soft tissue regeneration. Tissue engineering. Part B, Reviews *16*, 413–26.

178. Flynn, L., Prestwich, G.D., Semple, J.L., and Woodhouse, K.A. (2009). Adipose tissue engineering in vivo with adipose-derived stem cells on naturally derived scaffolds. Journal of biomedical materials research. Part A *89*, 929–41.

179. Stosich, M.S., Bastian, B., Marion, N.W., Clark, P.A., Reilly, G., and Mao, J.J. (2007). Vascularized adipose tissue grafts from human mesenchymal stem cells with bioactive cues and microchannel conduits. Tissue engineering *13*, 2881–90.

180. Alhadlaq, A., Tang, M., and Mao, J.J. (2005). Engineered adipose tissue from human mesenchymal stem cells maintains predefined shape and dimension: implications in soft tissue augmentation and reconstruction. Tissue engineering *11*, 556–66.

181. Vashi, A. V., Keramidaris, E., Abberton, K.M., Morrison, W.A., Wilson, J.L., O'Connor, A.J., Cooper-White, J.J., and Thompson, E.W. (2008). Adipose differentiation of bone marrow-derived mesenchymal stem cells using Pluronic F-127 hydrogel in vitro. Biomaterials *29*, 573–9.

182. Nicodemus, G.D., and Bryant, S.J. (2008). Cell encapsulation in biodegradable hydrogels for tissue engineering applications. Tissue engineering. Part B, Reviews *14*, 149–65.

183. Drury, J.L., and Mooney, D.J. (2003). Hydrogels for tissue engineering: scaffold design variables and applications. Biomaterials *24*, 4337–51.

184. Wang, P.-Y., Wu, T.-H., Tsai, W.-B., Kuo, W.-H., and Wang, M.-J. (2013). Grooved PLGA films incorporated with RGD/YIGSR peptides for potential application on skeletal muscle tissue engineering. Colloids and surfaces B: Biointerfaces *110*, 88–95.

185. Wu, B., Zheng, Q., Wu, Y., Guo, X., and Zou, Z. (2010). Effect of IKVAV peptide nanofiber on proliferation, adhesion and differentiation into neurocytes of bone marrow stromal cells. Journal of Huazhong University of Science and Technology. Medical sciences = Hua zhong ke ji da xue xue bao. Yi xue Ying De wen ban = Huazhong keji daxue xuebao. Yixue Yingdewen ban *30*, 178–82.

186. Patel, P.N., Gobin, A.S., West, J.L., and Patrick, C.W. (2005). Poly(ethylene glycol) hydrogel system supports preadipocyte viability, adhesion, and proliferation. Tissue engineering *11*, 1498–505.

187. Kawaguchi, N., Toriyama, K., Nicodemou-Lena, E., Inou, K., Torii, S., and Kitagawa, Y. (1999). Reconstituted basement membrane potentiates in vivo adipogenesis of 3T3-F442A cells. Cytotechnology *31*, 215–20.

188. Kleinman, H.K., McGarvey, M.L., Liotta, L.A., Robey, P.G., Tryggvason, K., and Martin, G.R. (1982). Isolation and characterization of type IV procollagen, laminin, and heparan sulfate proteoglycan from the EHS sarcoma. Biochemistry *21*, 6188–93.

189. Cheng, M.-H., Uriel, S., Moya, M.L., Francis-Sedlak, M., Wang, R., Huang, J.-J., Chang, S.-Y., and Brey, E.M. (2010). Dermis-derived hydrogels support adipogenesis in vivo. Journal of biomedical materials research. Part A *92*, 852–8.

190. Abberton, K.M., Bortolotto, S.K., Woods, A.A., Findlay, M., Morrison, W.A., Thompson, E.W., and Messina, A. (2008). Myogel, a novel, basement membrane-rich, extracellular matrix derived from skeletal muscle, is highly adipogenic in vivo and in vitro. Cells, tissues, organs *188*, 347–58.

191. Uriel, S., Huang, J.-J., Moya, M.L., Francis, M.E., Wang, R., Chang, S., Cheng, M.-H., and Brey, E.M. (2008). The role of adipose protein derived hydrogels in adipogenesis. Biomaterials *29*, 3712–9.

192. Torio-Padron, N., Baerlecken, N., Momeni, A., Stark, G.B., and Borges, J. (2007). Engineering of adipose tissue by injection of human preadipocytes in fibrin. Aesthetic plastic surgery *31*, 285–93.

193. Gentleman, E., Nauman, E.A., Livesay, G.A., and Dee, K.C. (2006). Collagen composite biomaterials resist contraction while allowing development of adipocytic soft tissue in vitro. Tissue engineering *12*, 1639–49.

194. Zhu, Y., Crewe, C., and Scherer, P.E. (2016). Hyaluronan in adipose tissue: Beyond dermal filler and therapeutic carrier. Science translational medicine *8*, 323ps4.

195. Eyrich, D., Göpferich, A., and Blunk, T. (2006). Fibrin in tissue engineering. Advances in experimental medicine and biology *585*, 379–92.

196. Eyrich, D., Brandl, F., Appel, B., Wiese, H., Maier, G., Wenzel, M., Staudenmaier, R., Goepferich, A., and Blunk, T. (2007). Long-term stable fibrin gels for cartilage engineering. Biomaterials *28*, 55–65.

197. Choi, Y.S., Park, S.-N., and Suh, H. (2008). The effect of PLGA sphere diameter on rabbit mesenchymal stem cells in adipose tissue engineering. Journal of materials science. Materials in medicine *19*, 2165–71.

198. Chung, H.J., and Park, T.G. (2009). Injectable cellular aggregates prepared from biodegradable porous microspheres for adipose tissue engineering. Tissue engineering. Part A *15*, 1391–400.

199. Halberstadt, C., Austin, C., Rowley, J., Culberson, C., Loebsack, A., Wyatt, S., Coleman, S., Blacksten, L., Burg, K., Mooney, D., and Holder, W. (2002). A hydrogel material for plastic and reconstructive applications injected into the subcutaneous space of a sheep. Tissue engineering *8*, 309–19.

200. Rubin, J.P., Bennett, J.M., Doctor, J.S., Tebbets, B.M., and Marra, K.G. (2007). Collagenous microbeads as a scaffold for tissue engineering with adipose-derived stem cells. Plastic and reconstructive surgery *120*, 414–24.

201. Choi, J.S., Yang, H.-J., Kim, B.S., Kim, J.D., Kim, J.Y., Yoo, B., Park, K., Lee, H.Y., and Cho, Y.W. (2009). Human extracellular matrix (ECM) powders for injectable cell delivery and adipose tissue engineering. Journal of controlled release : official journal of the Controlled Release Society *139*, 2–7.

202. Marra, K.G., Defail, A.J., Clavijo-Alvarez, J.A., Badylak, S.F., Taieb, A., Schipper, B., Bennett, J., and Rubin, J.P. (2008). FGF-2 enhances vascularization for adipose tissue engineering. Plastic and reconstructive surgery *121*, 1153–64.

203. Chhaya, M.P., Melchels, F.P.W., Holzapfel, B.M., Baldwin, J.G., and Hutmacher, D.W. (2015). Sustained regeneration of high-volume adipose tissue for breast reconstruction using computer aided design and biomanufacturing. Biomaterials *52*, 551–60.

204. Chhaya, M.P., Balmayor, E.R., Hutmacher, D.W., and Schantz, J.-T. (2016). Transformation of Breast Reconstruction via Additive Biomanufacturing. Scientific reports *6*, 28030.

205. Dolderer, J.H., Dolderer, J.H., Doldere, J.H., Thompson, E.W., Slavin, J., Trost, N., Cooper-White, J.J., Cao, Y., O'connor, A.J., Penington, A., Morrison, W.A., and Abberton, K.M. (2011). Long-term stability of adipose tissue generated from a vascularized pedicled fat flap inside a chamber. Plastic and reconstructive surgery *127*, 2283–92.

206. Folkman, J., and Hochberg, M. (1973). Self-regulation of growth in three dimensions. The Journal of experimental medicine *138*, 745–53.

207. Jain, R.K., Au, P., Tam, J., Duda, D.G., and Fukumura, D. (2005). Engineering vascularized tissue. Nature biotechnology *23*, 821–3.

208. Kaully, T., Kaufman-Francis, K., Lesman, A., and Levenberg, S. (2009). Vascularization--the conduit to viable engineered tissues. Tissue engineering. Part B, Reviews *15*, 159–69.

209. Lovett, M., Lee, K., Edwards, A., and Kaplan, D.L. (2009). Vascularization strategies for tissue engineering. Tissue engineering. Part B, Reviews *15*, 353–70.

210. Sill, T.J., and von Recum, H.A. (2008). Electrospinning: applications in drug delivery and tissue engineering. Biomaterials *29*, 1989–2006.

211. Stosich, M.S., Moioli, E.K., Wu, J.K., Lee, C.H., Rohde, C., Yoursef, A.M., Ascherman, J., Diraddo, R., Marion, N.W., and Mao, J.J. (2009). Bioengineering strategies to generate vascularized soft tissue grafts with sustained shape. Methods *47*, 116–21.

212. Rustad, K.C., Sorkin, M., Levi, B., Longaker, M.T., and Gurtner, G.C. (2010). Strategies for organ level tissue engineering. Organogenesis *6*, 151–7.

213. Zhang, Q., Hubenak, J., Iyyanki, T., Alred, E., Turza, K.C., Davis, G., Chang, E.I., Branch-Brooks, C.D., Beahm, E.K., and Butler, C.E. (2015). Engineering vascularized soft tissue flaps in an animal model using human adipose-derived stem cells and VEGF+PLGA/PEG microspheres on a collagen-chitosan scaffold with a flow-through vascular pedicle. Biomaterials *73*, 198–213.

214. Kimura, Y., Tsuji, W., Yamashiro, H., Toi, M., Inamoto, T., and Tabata, Y. (2010). In situ adipogenesis in fat tissue augmented by collagen scaffold with gelatin microspheres containing basic fibroblast growth factor. Journal of tissue engineering and regenerative medicine *4*, 55–61.

215. Hiraoka, Y., Yamashiro, H., Yasuda, K., Kimura, Y., Inamoto, T., and Tabata, Y. (2006). In situ regeneration of adipose tissue in rat fat pad by combining a collagen scaffold with gelatin microspheres containing basic fibroblast growth factor. Tissue engineering *12*, 1475–87.

216. Nauta, A., Seidel, C., Deveza, L., Montoro, D., Grova, M., Ko, S.H., Hyun, J., Gurtner, G.C., Longaker, M.T., and Yang, F. (2013). Adipose-derived stromal cells overexpressing vascular endothelial growth factor accelerate mouse excisional wound healing. Molecular therapy : the journal of the American Society of Gene Therapy *21*, 445–55.

217. Wittmann, K. (2014). Adipose Tissue Engineering. Development of Volume-Stable 3-Dimensional Constructs and Approaches Towards Effective Vascularization. Doktoral Thesis.

218. Lokmic, Z., and Mitchell, G.M. (2008). Engineering the microcirculation. Tissue engineering. Part B, Reviews *14*, 87–103.

219. Frerich, B., Lindemann, N., Kurtz-Hoffmann, J., and Oertel, K. (2001). In vitro model of a vascular stroma for the engineering of vascularized tissues. International Journal of Oral and Maxillofacial Surgery *30*, 414–420.

220. Borges, J., Mueller, M.C., Padron, N.T., Tegtmeier, F., Lang, E.M., and Stark, G.B. (2003). Engineered adipose tissue supplied by functional microvessels. Tissue engineering *9*, 1263–70.

221. Scherberich, A., Müller, A.M., Schäfer, D.J., Banfi, A., and Martin, I. (2010). Adipose tissue-derived progenitors for engineering osteogenic and vasculogenic grafts. Journal of cellular physiology *225*, 348–53.

222. Klar, A.S., Güven, S., Biedermann, T., Luginbühl, J., Böttcher-Haberzeth, S., Meuli-Simmen, C., Meuli, M., Martin, I., Scherberich, A., and Reichmann, E. (2014). Tissue-engineered dermo-epidermal skin grafts prevascularized with adipose-derived cells. Biomaterials *35*, 5065–78.

223. Morgan, J.P., Delnero, P.F., Zheng, Y., Verbridge, S.S., Chen, J., Craven, M., Choi, N.W., Diaz-Santana, A., Kermani, P., Hempstead, B., López, J. a, Corso, T.N., Fischbach, C., and Stroock, A.D. (2013). Formation of microvascular networks in vitro. Nature protocols *8*, 1820–36.

224. Laschke, M.W., Harder, Y., Amon, M., Martin, I., Farhadi, J., Ring, A., Torio-Padron, N., Schramm, R., Rücker, M., Junker, D., Häufel, J.M., Carvalho, C., Heberer, M., Germann, G., Vollmar, B., and Menger, M.D. (2006). Angiogenesis in tissue engineering: breathing life into constructed tissue substitutes. Tissue engineering *12*, 2093–104.

225. Aubin, H., Kranz, A., Hülsmann, J., Pinto, A., Barth, M., Fomin, A., Lichtenberg, A., and Akhyari, P. (2013). A novel native derived coronary artery tissue-flap model. Tissue engineering. Part C, Methods *19*, 970–80.

226. Zhang, Q., Johnson, J.A., Dunne, L.W., Chen, Y., Iyyanki, T., Wu, Y., Chang, E.I., Branch-Brooks, C.D., Robb, G.L., and Butler, C.E. (2016). Decellularized skin/adipose tissue flap matrix for engineering vascularized composite soft tissue flaps. Acta biomaterialia *35*, 166–84.

227. Hanker, J.S., and Giammara, B.L. (1988). Biomaterials and biomedical devices. Science *242*, 885–92.

228. Andrée, B., Bär, A., Haverich, A., and Hilfiker, A. (2013). Small intestinal submucosa segments as matrix for tissue engineering: review. Tissue engineering. Part B, Reviews *19*, 279–91.

229. Mertsching, H., Walles, T., Hofmann, M., Schanz, J., and Knapp, W.H. (2005). Engineering of a vascularized scaffold for artificial tissue and organ generation. Biomaterials *26*, 6610–7.

230. Mertsching, H., Schanz, J., Steger, V., Schandar, M., Schenk, M., Hansmann, J., Dally, I., Friedel, G., and Walles, T. (2009). Generation and transplantation of an autologous vascularized bioartificial human tissue. Transplantation *88*, 203–10.

231. Atala, A., Kasper, F.K., and Mikos, A.G. (2012). Engineering complex tissues. Science translational medicine *4*, 160rv12.

232. Hoshiba, T., Kawazoe, N., Tateishi, T., and Chen, G. (2009). Development of stepwise osteogenesis-mimicking matrices for the regulation of mesenchymal stem cell functions. The Journal of biological chemistry *284*, 31164–73.

233. Schultheiss, D., Gabouev, A.I.., Cebotari, S., Tudorache, I., Walles, T., Schlote, N., Wefer, J., Kaufmann, P.M., Haverich, A., Jonas, U., Stief, C.G.., and Mertsching, H. (2005). Biological vascularized matrix for bladder tissue engineering: matrix preparation, reseeding technique and short-term implantation in a porcine model. The Journal of urology *173*, 276–80.

234. Schanz, J., Pusch, J., Hansmann, J., and Walles, H. (2010). Vascularised human tissue models: a new approach for the refinement of biomedical research. Journal of biotechnology *148*, 56–63.

235. Linke, K., Schanz, J., Hansmann, J., Walles, T., Brunner, H., and Mertsching, H. (2007). Engineered Liver-Like Tissue on a Capillarized Matrix for Applied Research. Tissue Engineering *13*, 2699–2707.

236. Schuerlein, S., Schwarz, T., Krziminski, S., Gätzner, S., Hoppensack, A., Schwedhelm, I., Schweinlin, M., Walles, H., and Hansmann, J. (2017). A versatile modular bioreactor platform for Tissue Engineering. Biotechnology journal *12*.

237. Hansmann, J., Groeber, F., Kahlig, A., Kleinhans, C., and Walles, H. (2013). Bioreactors in tissue engineering - principles, applications and commercial constraints. Biotechnology journal *8*, 298–307.

238. Moll, C., Reboredo, J., Schwarz, T., Appelt, A., Schürlein, S., Walles, H., and Nietzer, S. (2013). Tissue engineering of a human 3D in vitro tumor test system. Journal of visualized experiments *78*, e50460.

239. Pusch, J., Votteler, M., Göhler, S., Engl, J., Hampel, M., Walles, H., and Schenke-Layland, K. (2011). The physiological performance of a three-dimensional model that mimics the microenvironment of the small intestine. Biomaterials *32*, 7469–78.

240. Brouwer, K.M., Lundvig, D.M.S., Middelkoop, E., Wagener, F.A.D.T.G., and Von den Hoff, J.W. (2015). Mechanical cues in orofacial tissue engineering and regenerative medicine. Wound repair and regeneration *23*, 302–11.

241. Radtke, C., Panzica, M., Dastagir, K., Krettek, C., and Vogt, P.M. (2015). Soft Tissue Coverage of the Lower Limb following Oncological Surgery. Frontiers in oncology *5*, 303.

242. Langstein, H.N., and Robb, G.L. (1999). Reconstructive approaches in soft tissue sarcoma. Seminars in surgical oncology *17*, 52–65.

243. Kakagia, D., and Pallua, N. (2014). Autologous fat grafting: in search of the optimal technique. Surgical innovation *21*, 327–36.

244. Scheller, K., Dally, I., Hartmann, N., Münst, B., Braspenning, J., and Walles, H. (2013). Upcyte® microvascular endothelial cells repopulate decellularized scaffold. Tissue engineering. Part C, Methods *19*, 57–67.

245. Groeber, F., Engelhardt, L., Lange, J., Kurdyn, S., Schmid, F.F., Rücker, C., Mielke, S., Walles, H., and Hansmann, J. (2016). A first vascularized skin equivalent as an alternative to animal experimentation. ALTEX *33*, 415–422.

246. Bianchi, G., Banfi, A., Mastrogiacomo, M., Notaro, R., Luzzatto, L., Cancedda, R., and Quarto, R. (2003). Ex vivo enrichment of mesenchymal cell progenitors by fibroblast growth factor 2. Experimental cell research *287*, 98–105.

247. Suga, H., Shigeura, T., Matsumoto, D., Inoue, K., Kato, H., Aoi, N., Murase, S., Sato, K., Gonda, K., Koshima, I., and Yoshimura, K. (2007). Rapid expansion of human adipose-derived stromal cells preserving multipotency. Cytotherapy *9*, 738–45.

248. Hebert, T.L., Wu, X., Yu, G., Goh, B.C., Halvorsen, Y.C., Wang, Z., Moro, C., and Gimble, J.M. (2009). Culture effects of epidermal growth factor (EGF) and basic fibroblast growth factor (bFGF) on cryopreserved human adipose-derived stromal/stem cell proliferation and adipogenesis. Journal of tissue engineering and regenerative medicine *3*, 553–61.

249. Martin, I., Muraglia, A., Campanile, G., Cancedda, R., and Quarto, R. (1997). Fibroblast growth factor-2 supports ex vivo expansion and maintenance of osteogenic precursors from human bone marrow. Endocrinology *138*, 4456–62.

250. van den Bos, C., Mosca, J.D., Winkles, J., Kerrigan, L., Burgess, W.H., and Marshak, D.R. (1997). Human mesenchymal stem cells respond to fibroblast growth factors. Human cell *10*, 45–50.

251. Solchaga, L.A., Penick, K., Porter, J.D., Goldberg, V.M., Caplan, A.I., and Welter, J.F. (2005). FGF-2 enhances the mitotic and chondrogenic potentials of human adult bone marrow-derived mesenchymal stem cells. Journal of cellular physiology *203*, 398–409.

252. Hankemeier, S., Keus, M., Zeichen, J., Jagodzinski, M., Barkhausen, T., Bosch, U., Krettek, C., and Van Griensven, M. (2005). Modulation of proliferation and differentiation of human bone marrow stromal cells by fibroblast growth factor 2: potential implications for tissue engineering of tendons and ligaments. Tissue engineering *11*, 41–9.

253. Uzbas, F., May, I.D., Parisi, A.M., Thompson, S.K., Kaya, A., Perkins, A.D., and Memili, E. (2015). Molecular physiognomies and applications of adipose-derived stem cells. Stem cell reviews *11*, 298–308.

254. Mizuno, H., Tobita, M., and Uysal, A.C. (2012). Concise review: Adipose-derived stem cells as a novel tool for future regenerative medicine. Stem cells (Dayton, Ohio) *30*, 804–10.

255. Schiller, P.C., D'Ippolito, G., Balkan, W., Roos, B.A., and Howard, G.A. (2001). Gap-junctional communication mediates parathyroid hormone stimulation of mineralization in osteoblastic cultures. Bone *28*, 38–44.

256. Walles, T., Weimer, M., Linke, K., Michaelis, J., and Mertsching, H. (2007). The potential of bioartificial tissues in oncology research and treatment. Onkologie *30*, 388–94.

257. Werner, K. (2014). Adipose Tissue Engineering - In vitro Development of a Subcutaneous Fat Layer and a Vascularized Adipose Tissue Construct utilizing Extracellular Matrix Structures. Doktoral Thesis.

258. Studer, D., Lischer, S., Jochum, W., Ehrbar, M., Zenobi-Wong, M., and Maniura-Weber, K. (2012). Ribosomal protein l13a as a reference gene for human bone marrow-derived mesenchymal stromal cells during expansion, adipo-, chondro-, and osteogenesis. Tissue engineering. Part C, Methods *18*, 761–71.

259. Livak, K.J., and Schmittgen, T.D. (2001). Analysis of relative gene expression data using real-time quantitative PCR and the 2(-Delta Delta C(T)) Method. Methods *25*, 402–8.

260. Ruan, J.-L., Tulloch, N.L., Muskheli, V., Genova, E.E., Mariner, P.D., Anseth, K.S., and Murry, C.E. (2013). An improved cryosection method for polyethylene glycol hydrogels used in tissue engineering. Tissue engineering. Part C, Methods *19*, 794–801.

261. Neubauer, M., Fischbach, C., Bauer-Kreisel, P., Lieb, E., Hacker, M., Tessmar, J., Schulz, M.B., Goepferich, A., and Blunk, T. (2004). Basic fibroblast growth factor enhances PPARgamma ligand-induced adipogenesis of mesenchymal stem cells. FEBS letters *577*, 277–83.

262. Fonseca, P.C., Nihei, O.K., Urban-Maldonado, M., Abreu, S., de Carvalho, A.C.C., Spray, D.C., Savino, W., and Alves, L.A. (2004). Characterization of connexin 30.3 and 43 in thymocytes. Immunology letters *94*, 65–75.

263. Fonseca, P.C., Nihei, O.K., Savino, W., Spray, D.C., and Alves, L.A. (2006). Flow cytometry analysis of gap junction-mediated cell-cell communication: advantages and pitfalls. Cytometry. Part A *69*, 487–93.

264. Planat-Benard, V., Silvestre, J.-S., Cousin, B., André, M., Nibbelink, M., Tamarat, R., Clergue, M., Manneville, C., Saillan-Barreau, C., Duriez, M., Tedgui, A., Levy, B., Pénicaud, L., and Casteilla, L. (2004). Plasticity of human adipose lineage cells toward endothelial cells: physiological and therapeutic perspectives. Circulation *109*, 656–63.

265. Borges, J., Müller, M.C., Momeni, A., Stark, G.B., and Torio-Padron, N. (2007). In vitro analysis of the interactions between preadipocytes and endothelial cells in a 3D fibrin matrix. Minimally invasive therapy & allied technologies : MITAT : official journal of the Society for Minimally Invasive Therapy *16*, 141–8.

266. Lai, N., Jayaraman, A., and Lee, K. (2009). Enhanced proliferation of human umbilical vein endothelial cells and differentiation of 3T3-L1 adipocytes in coculture. Tissue engineering. Part A *15*, 1053–61.

267. Verseijden, F., Posthumus-van Sluijs, S.J., van Neck, J.W., Hofer, S.O.P., Hovius, S.E.R., and van Osch, G.J.V.M. (2012). Vascularization of prevascularized and non-prevascularized fibrin-based human adipose tissue constructs after implantation in nude mice. Journal of tissue engineering and regenerative medicine *6*, 169–78.

268. Findlay, M.W., Dolderer, J.H., Trost, N., Craft, R.O., Cao, Y., Cooper-White, J., Stevens, G., and Morrison, W.A. (2011). Tissue-engineered breast reconstruction: bridging the gap toward large-volume tissue engineering in humans. Plastic and reconstructive surgery *128*, 1206–15.

269. Werner, K., Jakubietz, M.G., Jakubietz, R.G., Schmidt, K., Muhr, C., Bauer-Kreisel, P., and Blunk, T. (2014). Toward reconstruction of the subcutaneous fat layer with the use of adipose-derived stromal cell-seeded collagen matrices. Cytotherapy *16*, 1700–8.

270. Badylak, S.F., Taylor, D., and Uygun, K. (2011). Whole-organ tissue engineering: decellularization and recellularization of three-dimensional matrix scaffolds. Annual review of biomedical engineering *13*, 27–53.

271. Uygun, B.E., Soto-Gutierrez, A., Yagi, H., Izamis, M.-L., Guzzardi, M.A., Shulman, C., Milwid, J., Kobayashi, N., Tilles, A., Berthiaume, F., Hertl, M., Nahmias, Y., Yarmush, M.L., and Uygun, K. (2010). Organ reengineering through development of a transplantable recellularized liver graft using decellularized liver matrix. Nature medicine *16*, 814–20.

272. Petersen, T.H., Calle, E.A., Zhao, L., Lee, E.J., Gui, L., Raredon, M.B., Gavrilov, K., Yi, T., Zhuang, Z.W., Breuer, C., Herzog, E., and Niklason, L.E. (2010). Tissue-engineered lungs for in vivo implantation. Science *329*, 538–41.

273. Price, A.P., England, K.A., Matson, A.M., Blazar, B.R., and Panoskaltsis-Mortari, A. (2010). Development of a decellularized lung bioreactor system for bioengineering the lung: the matrix reloaded. Tissue engineering. Part A *16*, 2581–91.

274. Chien, S. (2007). Mechanotransduction and endothelial cell homeostasis: the wisdom of the cell. American journal of physiology. Heart and circulatory physiology *292*, H1209-24.

275. Davis, C.A., Zambrano, S., Anumolu, P., Allen, A.C.B., Sonoqui, L., and Moreno, M.R. (2015). Device-based in vitro techniques for mechanical stimulation of vascular cells: a review. Journal of biomechanical engineering *137*, 040801.

276. Verseijden, F., Posthumus-van Sluijs, S.J., Farrell, E., van Neck, J.W., Hovius, S.E.R., Hofer, S.O.P., and van Osch, G.J.V.M. (2010). Prevascular structures promote vascularization in engineered human adipose tissue constructs upon implantation. Cell transplantation *19*, 1007–20.

277. Bahramsoltani, M., Slosarek, I., De Spiegelaere, W., and Plendl, J. (2014). Angiogenesis and collagen type IV expression in different endothelial cell culture systems. Anatomia, histologia, embryologia *43*, 103–15.

278. Yousif, L.F., Di Russo, J., and Sorokin, L. (2013). Laminin isoforms in endothelial and perivascular basement membranes. Cell adhesion & migration *7*, 101–10.

279. Vunjak-Novakovic, G., Tandon, N., Godier, A., Maidhof, R., Marsano, A., Martens, T.P., and Radisic, M. (2010). Challenges in cardiac tissue engineering. Tissue engineering. Part B, Reviews *16*, 169–87.

280. Han, J., Lee, J.-E., Jin, J., Lim, J.S., Oh, N., Kim, K., Chang, S.-I., Shibuya, M., Kim, H., and Koh, G.Y. (2011). The spatiotemporal development of adipose tissue. Development *138*, 5027–37.

281. Gonzalez-Perez, R.R., Lanier, V., and Newman, G. (2013). Leptin's Pro-Angiogenic Signature in Breast Cancer. Cancers *5*, 1140–62.

282. Oh, S.-A., Lee, H.-Y., Lee, J.H., Kim, T.-H., Jang, J.-H., Kim, H.-W., and Wall, I. (2012). Collagen three-dimensional hydrogel matrix carrying basic fibroblast growth factor for the cultivation of mesenchymal stem cells and osteogenic differentiation. Tissue engineering. Part A *18*, 1087–100.

283. Inoue, S., Hori, Y., Hirano, Y., and Tabata, Y. (2004). Effect of culture substrates and fibroblast growth factor addition on the proliferation and differentiation of rat bone marrow stromal cells. Tissue engineering *10*, 995–1005.

284. Kimura, Y., Ozeki, M., Inamoto, T., and Tabata, Y. (2003). Adipose tissue engineering based on human preadipocytes combined with gelatin microspheres containing basic fibroblast growth factor. Biomaterials *24*, 2513–21.

285. Hauner, H., Röhrig, K., and Petruschke, T. (1995). Effects of epidermal growth factor (EGF), platelet-derived growth factor (PDGF) and fibroblast growth factor (FGF) on human adipocyte development and function. European journal of clinical investigation *25*, 90–6.

286. Baddoo, M., Hill, K., Wilkinson, R., Gaupp, D., Hughes, C., Kopen, G.C., and Phinney, D.G. (2003). Characterization of mesenchymal stem cells isolated from murine bone marrow by negative selection. Journal of cellular biochemistry *89*, 1235–49.

287. Le Blanc, S., Simann, M., Jakob, F., Schütze, N., and Schilling, T. (2015). Fibroblast growth factors 1 and 2 inhibit adipogenesis of human bone marrow stromal cells in 3D collagen gels. Experimental cell research *338*, 136–48.

288. Schilling, T., Küffner, R., Klein-Hitpass, L., Zimmer, R., Jakob, F., and Schütze, N. (2008). Microarray analyses of transdifferentiated mesenchymal stem cells. Journal of cellular biochemistry *103*, 413–33.

289. Suga, H., Eto, H., Shigeura, T., Inoue, K., Aoi, N., Kato, H., Nishimura, S., Manabe, I., Gonda, K., and Yoshimura, K. (2009). IFATS collection: Fibroblast growth factor-2-induced hepatocyte growth factor secretion by adipose-derived stromal cells inhibits postinjury fibrogenesis through a c-Jun N-terminal kinase-dependent mechanism. Stem cells *27*, 238–49.

290. Powers, C.J., McLeskey, S.W., and Wellstein, A. (2000). Fibroblast growth factors, their receptors and signaling. Endocrine-related cancer *7*, 165–97.

291. Yu, P.-J., Ferrari, G., Galloway, A.C., Mignatti, P., and Pintucci, G. (2007). Basic fibroblast growth factor (FGF-2): the high molecular weight forms come of age. Journal of cellular biochemistry *100*, 1100–8.

292. Lemmon, M.A., and Schlessinger, J. (1994). Regulation of signal transduction and signal diversity by receptor oligomerization. Trends in biochemical sciences *19*, 459–63.

293. Ornitz, D.M., and Itoh, N. (2015). The Fibroblast Growth Factor signaling pathway. Wiley interdisciplinary reviews. Developmental biology *4*, 215–66.

294. Gimble, J.M., Bunnell, B.A., Frazier, T., Rowan, B., Shah, F., Thomas-Porch, C., and Wu, X. (2013). Adipose-derived stromal/stem cells: a primer. Organogenesis *9*, 3–10.

295. Ratushnyy, A., Lobanova, M., and Buravkova, L.B. (2017). Expansion of adipose tissue-derived stromal cells at 'physiologic' hypoxia attenuates replicative senescence. Cell biochemistry and function *35*, 232–243.

296. Zhao, Y., Waldman, S.D., and Flynn, L.E. (2012). The effect of serial passaging on the proliferation and differentiation of bovine adipose-derived stem cells. Cells, tissues, organs *195*, 414–27.

297. Kim, W.-S., Han, J., Hwang, S.-J., and Sung, J.-H. (2014). An update on niche composition, signaling and functional regulation of the adipose-derived stem cells. Expert opinion on biological therapy *14*, 1091–102.

298. Guillot, P. V., Gotherstrom, C., Chan, J., Kurata, H., and Fisk, N.M. (2007). Human first-trimester fetal MSC express pluripotency markers and grow faster and have longer telomeres than adult MSC. Stem cells *25*, 646–54.

299. Kim, S., Ahn, C., Bong, N., Choe, S., and Lee, D.K. (2015). Biphasic effects of FGF2 on adipogenesis. PloS one *10*, e0120073.

300. Ahmed, T.A.E., Dare, E. V., and Hincke, M. (2008). Fibrin: a versatile scaffold for tissue engineering applications. Tissue engineering. Part B, Reviews *14*, 199–215.

301. Prusty, D., Park, B.-H., Davis, K.E., and Farmer, S.R. (2002). Activation of MEK/ERK signaling promotes adipogenesis by enhancing peroxisome proliferator-activated receptor gamma (PPARgamma) and C/EBPalpha gene expression during the differentiation of 3T3-L1 preadipocytes. The Journal of biological chemistry *277*, 46226–32.

302. Doble, B.W., and Kardami, E. (1995). Basic fibroblast growth factor stimulates connexin-43 expression and intercellular communication of cardiac fibroblasts. Molecular and cellular biochemistry *143*, 81–7.

303. Preda, M.B., Rosca, A.-M., Tutuianu, R., and Burlacu, A. (2015). Pre-stimulation with FGF-2 increases in vitro functional coupling of mesenchymal stem cells with cardiac cells. Biochemical and biophysical research communications *464*, 667–73.

304. Longchamp, A., Allagnat, F., Alonso, F., Kuppler, C., Dubuis, C., Ozaki, C.-K., Mitchell, J.R., Berceli, S., Corpataux, J.-M., Déglise, S., and Haefliger, J.-A. (2015). Connexin43 Inhibition Prevents Human Vein Grafts Intimal Hyperplasia. PloS one *10*, e0138847.

305. Evans, W.H., and Boitano, S. (2001). Connexin mimetic peptides: specific inhibitors of gap-junctional intercellular communication. Biochemical Society transactions *29*, 606–12.

306. Yanagiya, T., Tanabe, A., and Hotta, K. (2007). Gap-junctional communication is required for mitotic clonal expansion during adipogenesis. Obesity *15*, 572–82.

307. Nishikawa, Y., Akiyama, Y., Yamamoto, K., Kobayashi, M., Watanabe, E., Watanabe, N., Shimizu, N., Mikami, Y., and Komiyama, K. (2015). Osteocytes up-regulate the terminal differentiation of pre-osteoblasts via gap junctions. Biochemical and biophysical research communications *456*, 1–6.

308. Todorova, M.G., Soria, B., and Quesada, I. (2008). Gap junctional intercellular communication is required to maintain embryonic stem cells in a non-differentiated and proliferative state. Journal of cellular physiology *214*, 354–62.

309. Guan, X., Wilson, S., Schlender, K.K., and Ruch, R.J. (1996). Gap-junction disassembly and connexin 43 dephosphorylation induced by 18 beta-glycyrrhetinic acid. Molecular carcinogenesis *16*, 157–64.

310. Davidson, J.S., Baumgarten, I.M., and Harley, E.H. (1986). Reversible inhibition of intercellular junctional communication by glycyrrhetinic acid. Biochemical and biophysical research communications *134*, 29–36.

311. Chen, J., Li, L., Li, Y., Liang, X., Sun, Q., Yu, H., Zhong, J., Ni, Y., Chen, J., Zhao, Z., Gao, P., Wang, B., Liu, D., Zhu, Z., and Yan, Z. (2015). Activation of TRPV1 channel by dietary capsaicin improves visceral fat remodeling through connexin43-mediated Ca2+ influx. Cardiovascular diabetology *14*, 22.

312. Davidson, J.S., and Baumgarten, I.M. (1988). Glycyrrhetinic acid derivatives: a novel class of inhibitors of gap-junctional intercellular communication. Structure-activity relationships. The Journal of pharmacology and experimental therapeutics *246*, 1104–7.

313. Guo, Y., Martinez-Williams, C., Gilbert, K.A., and Rannels, D.E. (1999). Inhibition of gap junction communication in alveolar epithelial cells by 18alpha-glycyrrhetinic acid. The American journal of physiology *276*, L1018-26.

314. Schiller, P.C., D'Ippolito, G., Balkan, W., Roos, B.A., and Howard, G.A. (2001). Gap-junctional communication is required for the maturation process of osteoblastic cells in culture. Bone *28*, 362–9.

315. Plotkin, L.I., Manolagas, S.C., and Bellido, T. (2002). Transduction of cell survival signals by connexin-43 hemichannels. The Journal of biological chemistry *277*, 8648–57.

316. Tang, J., Peng, R., and Ding, J. (2010). The regulation of stem cell differentiation by cell-cell contact on micropatterned material surfaces. Biomaterials *31*, 2470–6.

317. Zong, L., Qu, Y., Xu, M.Y., Dong, Y.W., and Lu, L.G. (2013). 18α-glycyrrhetinic acid extracted from Glycyrrhiza radix inhibits proliferation and promotes apoptosis of the hepatic stellate cell line. Journal of digestive diseases *14*, 328–36.

318. Burke, S., Nagajyothi, F., Thi, M.M., Hanani, M., Scherer, P.E., Tanowitz, H.B., and Spray, D.C. (2014). Adipocytes in both brown and white adipose tissue of adult mice are functionally connected via gap junctions: implications for Chagas disease. Microbes and infection *16*, 893–901.

319. Cogliati, B., Maes, M., Pereira, I.V.A., Willebrords, J., Da Silva, T.C., Crespo Yanguas, S., and Vinken, M. (2016). Immunohisto- and Cytochemistry Analysis of Connexins. Methods in molecular biology *1437*, 55–70.

320. Dancker, P., Löw, I., Hasselbach, W., and Wieland, T. (1975). Interaction of actin with phalloidin: polymerization and stabilization of F-actin. Biochimica et biophysica acta *400*, 407–14.

321. Wang, J., and Richards, D.A. (2011). Spatial regulation of exocytic site and vesicle mobilization by the actin cytoskeleton. PloS one *6*, e29162.

322. Lemcke, H., Nittel, M.-L., Weiss, D.G., and Kuznetsov, S.A. (2013). Neuronal differentiation requires a biphasic modulation of gap junctional intercellular communication caused by dynamic changes of connexin43 expression. The European journal of neuroscience *38*, 2218–28.

323. Zanata, F., Shaik, S., Devireddy, R. V., Wu, X., Ferreira, L.M., and Gimble, J.M. (2016). Cryopreserved Adipose Tissue-Derived Stromal/Stem Cells: Potential for Applications in Clinic and Therapy. Advances in experimental medicine and biology *951*, 137–146.

324. Li, S., He, H., Zhang, G., Wang, F., Zhang, P., and Tan, Y. (2015). Connexin43-containing gap junctions potentiate extracellular Ca^{2+}-induced odontoblastic differentiation of human dental pulp stem cells via Erk1/2. Experimental cell research *338*, 1–9.

325. Kamijo, M., Haraguchi, T., Tonogi, M., and Yamane, G.-Y. (2006). The function of connexin 43 on the differentiation of rat bone marrow cells in culture. Biomedical research *27*, 289–95.

326. Rossello, R.A., Wang, Z., Kizana, E., Krebsbach, P.H., and Kohn, D.H. (2009). Connexin 43 as a signaling platform for increasing the volume and spatial distribution of regenerated tissue. Proceedings of the National Academy of Sciences of the United States of America *106*, 13219–24.

327. Wankhade, U.D., Shen, M., Kolhe, R., and Fulzele, S. (2016). Advances in Adipose-Derived Stem Cells Isolation, Characterization, and Application in Regenerative Tissue Engineering. Stem cells international *2016*, 3206807.

328. Cawthorn, W.P., Scheller, E.L., and MacDougald, O. a (2012). Adipose tissue stem cells meet preadipocyte commitment: going back to the future. Journal of lipid research *53*, 227–46.

329. Lee, J.-H., and Kemp, D.M. (2006). Human adipose-derived stem cells display myogenic potential and perturbed function in hypoxic conditions. Biochemical and biophysical research communications *341*, 882–8.

330. Liu, Y., Zhang, Z., Zhang, C., Deng, W., Lv, Q., Chen, X., Huang, T., and Pan, L. (2016). Adipose-derived stem cells undergo spontaneous osteogenic differentiation in vitro when passaged serially or seeded at low density. Biotechnic & histochemistry *91*, 369–76.

331. Kim, D.S., Lee, M.W., Yoo, K.H., Lee, T.-H., Kim, H.J., Jang, I.K., Chun, Y.H., Kim, H.J., Park, S.J., Lee, S.H., Son, M.H., Jung, H.L., Sung, K.W., and Koo, H.H. (2014). Gene expression profiles of human adipose tissue-derived mesenchymal stem cells are modified by cell culture density. PloS one *9*, e83363.

332. Zappitelli, T., Chen, F., and Aubin, J.E. (2015). Up-regulation of BMP2/4 signaling increases both osteoblast-specific marker expression and bone marrow adipogenesis in Gja1Jrt/+ stromal cell cultures. Molecular biology of the cell *26*, 832–42.

333. Gupta, A., Anderson, H., Buo, A.M., Moorer, M.C., Ren, M., and Stains, J.P. (2016). Communication of cAMP by connexin43 gap junctions regulates osteoblast signaling and gene expression. Cellular signalling *28*, 1048–57.

334. Jia, B., Madsen, L., Petersen, R.K., Techer, N., Kopperud, R., Ma, T., Døskeland, S.O., Ailhaud, G., Wang, J., Amri, E.-Z., and Kristiansen, K. (2012). Activation of protein kinase A and exchange protein directly activated by cAMP promotes adipocyte differentiation of human mesenchymal stem cells. PloS one *7*, e34114.

335. Tzameli, I., Fang, H., Ollero, M., Shi, H., Hamm, J.K., Kievit, P., Hollenberg, A.N., and Flier, J.S. (2004). Regulated production of a peroxisome proliferator-activated receptor-gamma ligand during an early phase of adipocyte differentiation in 3T3-L1 adipocytes. The Journal of biological chemistry *279*, 36093–102.

336. Lemcke, H., Steinhoff, G., and David, R. (2015). Gap junctional shuttling of miRNA--A novel pathway of intercellular gene regulation and its prospects in clinical application. Cellular signalling *27*, 2506–14.

337. Mittelbrunn, M., and Sánchez-Madrid, F. (2012). Intercellular communication: diverse structures for exchange of genetic information. Nature reviews. Molecular cell biology *13*, 328–35.

338. Zong, L., Zhu, Y., Liang, R., and Zhao, H.-B. (2016). Gap junction mediated miRNA intercellular transfer and gene regulation: A novel mechanism for intercellular genetic communication. Scientific reports *6*, 19884.

339. Kang, H., and Hata, A. (2015). The role of microRNAs in cell fate determination of mesenchymal stem cells: balancing adipogenesis and osteogenesis. BMB reports *48*, 319–23.

List of Figures

Figure 1.1: Adipogenic differentiation. 21
Figure 1.2: Core components of the adipogenic transcriptional cascade leading to the adipogenic phenotype. 22
Figure 1.3: Model of PPARγ and C/EBP transcriptional action during adipogenic differentiation. 23
Figure 1.4: Schematic illustration of the basement membrane (BM) of the adipocyte ECM. 29
Figure 1.5: Principle of adipose tissue engineering in cell-based approaches. 33
Figure 3.1: Custom-made bioreactor system. 60
Figure 4.1: Experimental setup – timeline of seeding and cultivation of the jejunal segment. 73
Figure 4.2: MTT staining for living cells on jejunal segments cultured in a custom-made bioreactor. 74
Figure 4.3: Investigation of adipogenesis in the jejunal construct. 75
Figure 4.4: Development of adipose-specific extracellular matrix in the jejunal construct. 77
Figure 4.5: Illustration of tissue development within the porcine jejunal segment. 79
Figure 4.6: Effect of different bFGF concentrations on cell growth of ASCs. 86
Figure 4.7: Schematic illustration of the experimental setup of bFGF supplementation during different periods of ASC culture. 87
Figure 4.8: Histological investigation of the influence of bFGF application at different time points of culture on adipogenic differentiation of ASCs. 89
Figure 4.9: Influence of bFGF application at different points of culture on adipogenic triglyceride accumulation on ASCs. 90
Figure 4.10: Schematic illustration of the experimental setup of bFGF preculture in conjunction with a 2-day proliferation phase on ASC differentiation capacity. 91
Figure 4.11: Impact of the standard 2-day preculture period before adipogenic induction in conjunction with a 0 and 3 ng/mL bFGF preculture (PC) 94
Figure 4.12: Survival and proliferation of ASCs in the 3D fibrin hydrogel constructs. 95
Figure 4.13: Impact of bFGF (3 ng/mL) preculture on the differentiation capacity of ASCs in 3D culture. 96
Figure 4.14: Influence of the initial seeding density and the bFGF PC on adipogenesis of ASCs. 98
Figure 4.15: Examination of the influence of different concentrations of AGA and GZA on ASC proliferation. 105
Figure 4.16: Analysis of adipogenesis under AGA and GZA influence. 108
Figure 4.17: Analysis of the inhibition of GJIC by different AGA concentrations during differentiation. 108
Figure 4.18: Analysis of cell viability under different AGA, GZA, and DMSO concentrations during adipogenesis. 109
Figure 4.19: I. Establishment of the immunohistochemical staining for Cx43. 111
Figure 4.20: II. Establishment of the immunohistochemical staining for Cx43. 113
Figure 4.21: III. Establishment of the immunohistochemical staining for Cx43. 113

Figure 4.22: Cx43 expression in ASCs cultured at different seeding densities in growth medium. 119
Figure 4.23: Functional examination of gap junctional intercellular communication (GJIC) in ASCs at different seeding densities. 122
Figure 4.24: Impact of seeding density on adipogenesis of ASCs. 123
Figure 4.25: Impact of seeding density on adipogenesis of ASCs – Flow cytometry analysis. 124
Figure 4.26: Impact of GJIC inhibition on adipogenesis of ASCs. 126
Figure 4.27: Impact of GJIC inhibition on adipogenesis of ASCs, flow cytometry analysis. 127
Figure 4.28: Analysis of Cx43 expression during adipogenic differentiation. 129

List of Tables

Table 2.1: Overview of instruments. 47
Table 2.2: Overview of used consumables. 48
Table 2.3: Overview of used chemicals. 49
Table 2.4: Overview of used antibodies. 51
Table 2.5: Overview of used primers. 52
Table 2.6: Overview of used cells. 52
Table 2.7: ASC medium. 53
Table 2.8: MVEC medium. 53
Table 2.9: Co-culture medium. 53
Table 2.10: Overview of used buffers and solutions. 54
Table 2.11: Overview of used software. 55
Table 3.1: Running gel recipe for an 8% polyacrylamide gel. 67
Table 3.2: Stacking gel recipe. 68
Table 4.1: Nile red flow cytometry analysis of adipogenically differentiated ASCs at different seeding densities. 125
Table 4.2: Nile red flow cytometry analysis of adipogenically differentiated ASCs treated with AGA. 127

List of Abbreviations

The specification of physical quantities is based on the guidelines of the international system of units. Special abbreviations for technical terms that are not included in the list are explained in the text.

Abbreviation	Prefix	Factor
p	pico-	10^{-12}
n	nano-	10^{-9}
µ	micro-	10^{-6}
m	milli-	10^{-3}
c	centi-	10^{-2}
k	kilo-	10^{3}

2D	two-dimensional
3D	three-dimensional
°C	degrees celsius
AGA	18α-glycyrrhetinic acid
ANOVA	analysis of variance
aP2	adipocyte protein 2/ fatty acid binding protein 4 (FABP4)
ASC	adipose-derived stem cell(s)
AT	adipose tissue
AV	arteriovenous
BAT	brown adipose tissue
BCA	bicinchoninic acid
bFGF	basic fibroblast growth factor / fibroblast growth factor 2
BM	basal membrane
BMI	body mass index
BMP 2/4	bone morphogenic protein 2/4
BMSC	bone marrow-derived mesenchymal stem cell(s)
BODIPY	4,4-difluoro-4-bora-3a,4a-diaza-s-indacene
BSA	bovine serum albumin
CAL	cell-assisted lipotransfer
cAMP	cyclic adenosine monophosphate

cDNA	coding deoxyribonucleic acid
C/EBPα,β,δ	CCAAT-enhancer-binding protein alpha, beta, delta
CETP	cholesteryl ester transfer protein
cGMP	cyclic guanosine monophosphate
CO_2	carbon dioxide
CTLA-4	cytotoxic T lymphocyte-associated protein 4
Cx	connexin protein(s)
DAT	decellularized adipose tissue
dH_2O	distilled water
DAPI	4',6-diamidino-2-phenylindole
DMEM/F-12	Dulbecco's Modified Eagle's Medium/Ham's F-12
DMSO	dimethyl sulfoxide
DNA	deoxyribonucleic acid
DNase	deoxyribonuclease
EBM-2	endothelial cell basal medium 2
EDTA	ethylenediaminetetraacetic acid
EC	endothelial cell(s)
ECM	extracellular matrix
EF1α	elongation factor-1 alpha
e.g.	exempli gratia (Latin "for example")
EGF	epidermal growth factor
FACS	flow cytometry
FBS	fetal bovine serum
FDA	Food and Drug Administration
FFA	free fatty acid(s)
FGF 2	fibroblast growth factor 2
ESC	embryonic stem cell(s)
EthD-III	ethidium bromide homodimer III
g	gram
GAPDH	glyceraldehyde-3-phosphate dehydrogenase
GF	growth factor
GJ	gap junction
GJIC	gap junctional intercellular communication

GLUT4	glucose transporter 4
GPDH	glycerol-3-phosphate dehydrogenase
GZA	glycyrrhizic acid
HEPES	4-(2-hydroxyethyl)-1-piperazineethanesulfonic acid
HGF	hepatocyte growth factor
HIF-1α	hypoxia-inducible factor 1 α
HRP	horseradish peroxidase
HUVEC	human umbilical vein endothelial cell(s)
IBMX	3-isobutyl-1-methylxanthine
i.e.	id est (Latin “that is”)
IGF-1	insulin-like growth factor 1
IgG	immunoglobulin G
IHC	immunohistochemistry
IL	interleukin(s)
IP_3	Inositol trisphosphate
iPSC	induced pluripotent stem cell(s)
KIU	kallikrein inhibitory unit(s)
KLF	kruepple-like factor(s)
L	liter
LPL	lipoprotein lipase
M	molarity
m	meter
MAPK/ERK	mitogen-activated protein kinase/extracellular signal-regulated kinase
mmHg	millimeter of mercury
MMP	matrix metalloproteinase(s)
mRNA	messenger ribonucleic acid
MSC	mesenchymal stem cell(s)
MTT	3-(4,5-dimethylthiazol-2-yl)-2,5-diphenyltetrazoliumbromid
MVEC	microvascular endothelial cell(s)
ORO	Oil Red O
PBM-2	preadipocyte basal medium 2
PBS	phosphate-buffered saline
PCR	polymerase chain reaction

pCREB	phosphorylated cAMP response element-binding protein
PFGF	platelet-derived growth factor
PEG	poly(ethylene glycol)
PEGDA	PEG-diacrylate
PGA	poly(glycolic acid)
PLA	poly(lactic acid)
PLGA	poly(lactic-co-glycolic acid)
PPAR γ	peroxisome proliferator-activated receptor gamma
Pref-1	preadipocyte factor-1;
PU	polyurethane
qRT-PCR	quantitative reverse transcription-polymerase chain reaction
RNA	ribonucleic acid
RNase	ribonuclease
rpm	revolutions per minute
SD	standard deviation
SDF-1	stem cell-derived factor 1
SREBP-1/ADD-1	sterol regulatory element binding protein 1/adipocyte determination and differentiation-dependent factor 1
SVF	stromal-vascular fraction
TE	tissue engineering
TG	triglyceride(s)
TGF-β	transforming growth factor-betta
TIMP	tissue inhibitors of MMP(s)
TNF- α	tumor-necrosis factor-alpha
U	unit
v/v	volume/volume %
VEGF	vascular endothelial growth factor
WAT	white adipose tissue
WB	western blot
WMS	whole mount staining
w/o	without
w/v	weight/volume %
x g	fold gravitational acceleration (g = 9.81 m/s^2)

Affidavit

I hereby confirm that my thesis entitled ‘‘Stem cell-based adipose tissue engineering: Engineering of prevascularized adipose tissue constructs *in vitro* & investigation on gap junctional intercellular communication in adipose-derived stem cells’’ is the result of my own work. I did not receive any help or support from commercial consultants. All sources and/or materials applied are listed and specified in the thesis.

Furthermore, I confirm that this thesis has not been submitted as part of another examination process neither in identical nor in similar form.

Place, date

Signature

Eidesstattliche Erklärung

Hiermit erkläre ich an Eides statt, die Dissertation „Stammzellbasiertes Tissue Engineering von Fettgewebe: Entwicklung eines prävaskularisierten Fettgewebekonstrukts *in vitro* & Untersuchung der interzellulären Kommunikation über Gap Junctions in Stammzellen aus dem Fettgewebe“ eigenständig, d.h. insbesondere selbständig und ohne Hilfe eines kommerziellen Promotionsberaters, angefertigt und keine anderen als die von mir angegebenen Quellen und Hilfsmittel verwendet zu haben.

Ich erkläre außerdem, dass die Dissertation weder in gleicher noch in ähnlicher Form bereits in einem anderen Prüfungsverfahren vorgelegen hat.

Ort, Datum

Unterschrift

Statement on Copyright and Self-plagiarism

The data presented in this thesis have been partially published in the Journal of Cellular Physiology as an original article entitled “Gap junctional Intercellular communication in adipose-derived stromal/stem cells is cell density-dependent and positively impacts adipogenic differentiation”. In accordance with the regulations of the parent publisher Wiley, data, text passages and illustrations from the manuscript were used in identical or modified form in this thesis.

Statement of individual author contributions and of legal second publication rights

Wiesner, M., Berberich, O., Hoefner, C., Blunk, T., and Bauer-Kreisel, P. (2018). Gap junctional intercellular communication in adipose-derived stromal/stem cells is cell density-dependent and positively impacts adipogenic differentiation. Journal of Cellular Physiology 233, 3315-3329.

Participated in	**Authors** - Responsibility decreasing from left to right		
Study Design	M. Wiesner	P. Bauer-Kreisel	T. Blunk
Methods Development	M. Wiesner	O. Berberich	C. Hoefner
Data Collection	M. Wiesner	O. Berberich	C. Hoefner
Data Analysis and Interpretation	M. Wiesner	O. Berberich	
Manuscript Writing	M. Wiesner	P. Bauer-Kreisel	T. Blunk

Explanations

I, M. Wiesner, planned the study, carried out the experiments, evaluated and interpreted the data and wrote the manuscript. P. Bauer-Kreisel contributed to the study design and revised the manuscript together with me. Oliver Berberich mainly helped me with the FACS analyses within the study. Christiane Hoefner helped me establishing the western blot method. T. Blunk is the principal investigator and was involved in the study design, writing of the manuscript, and did the proofreading.

Acknowledgement

Curriculum Vitae